On the design of aluminum-based complex hydride systems for chemical hydrogen storage

To the Faculty of Chemistry and Physics,
Institute of Physical Chemistry
of the Technische Universität Bergakademie Freiberg
approved

DISSERTATION

to attain the academic degree of
doctor rerum naturalium
(Dr.rer.nat.)

by

Lesia Sandig-Predzymirska
born on the 18.10.1989 in Lviv, Ukraine

Reviewers: Prof. Dr. Florian Mertens, TU Bergakademie Freiberg
Prof. Dr. Roman Gumeniuk, TU Bergakademie Freiberg

Date of the defense: Freiberg, 19th of May 2021

"Take nothing on its looks; take everything on evidence."

— Charles Dickens

DECLARATION

I hereby declare that I completed this work without any improper help from a third party and without using any aids other than those cited. All ideas derived directly or indirectly from other sources are identified as such. In the selection and use of materials and in the writing of the manuscript I received support from the following persons:

Prof. Dr. Florian Mertens
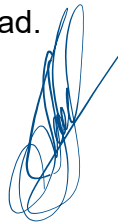
Prof. Dr. Klaus Bohmhammel

Dr. Jürgen Seidel

Dr. Erika Brendler

Dr. Jörg Wagler

Persons other than those above did not contribute to the writing of this thesis. I did not seek the help of a professional doctorate-consultant. Only those persons identified as having done so received any financial payment from me for any work done for me.

This thesis has not previously been published in the same or a similar form in Germany or abroad.

Freiberg, 04.01.2021

ACKNOWLEDGEMENTS

DEFINITIONS AND ABBREVIATIONS

CALPHAD	Calculation of phase diagrams
CMH	Complex metal hydride
COF	Covalent-organic framework
COSY	Correlated spectroscopy
DFT	Density functional theory
DIBAH	Diisobutylaluminum hydride
DOE	US Department of energy
DSC	Differential scanning calorimetry
EXSY	Exchange spectroscopy
FCTO	Fuel cell technologies office
HP-DSC	High-pressure differential scanning calorimetry
HSQC	Heteronuclear single quantum coherence
LOHC	Liquid organic hydrogen carrier
MOF	Metal-organic framework
NMR	Nuclear magnetic resonance
NOESY	Nuclear Overhauser effect spectroscopy
TEDA	Triethylenediamine, 1,4-Diazabicyclo[2.2.2]octan
TM	Transition metal
TMAL	Trimethylaluminum
XRPD	X-ray powder diffraction
G [kJ mol^{-1}]	Gibbs free energy
H [kJ mol^{-1}]	Enthalpy
E_a [J mol^{-1}]	Activation energy
P_{eq} [bar]	Equilibrium pressure
pipH	Piperidine
PTFE	Polytetrafluoroethylene
R [J mol^{-1} K^{-1}]	Universal gas constant (8.314 J mol^{-1} K^{-1})
S [kJ mol^{-1} K^{-1}]	Entropy
δ	Chemical shift in ppm
Hz	Hertz
χ_r	Pauling electronegativity
$^x J$	Coupling constant over x bonds

ABSTRACT

The development of suitable methods of hydrogen storage has been the subject of intensified research over the last two decades. Systems with light elements such as Li, Na, Mg, Al, B, N have attracted considerable attention due to their high gravimetric and volumetric density of hydrogen. Among other liquid and solid hydrogen storage materials, metal hydrides and complex hydrides are nowadays of the main interest. However, these materials suffer from unfavorable operating conditions and scarce cycling ability. These challenges are associated with materials properties and strongly depend on thermodynamics. The possible solution to this problem could come from the improvement of already existing systems or designing new materials with desirable properties. Therefore, the present study focuses on both directions: development of new Al-N-based systems and their examination as a medium for hydrogen storage; and modification of the hydrogen sorption properties of the well-known sodium alanate-based system.

The first part of this thesis is dedicated to the chemistry and properties of Al-N-based materials. The main effort was focused on the synthesis and characterization of so-called "aminoalanes" - the organic-metal hydrides, where the Lewis acid (aluminum hydride) is stabilized by the Lewis base (amine). In order to find suitable aminoalanes for hydrogen storage, several heterocyclic amines were examined. As the solid-state hydrogenation of the synthesized aminoalanes was not successful, other methods needed to be developed. The existing triethylenediamine-aluminum system was taken as the model for establishing the main principles for the alane formation from aluminum in solution. As a result, this approach was improved (in the term of the product yield) by applying other transition metal compounds as additives for producing activated aluminum. Furthermore, the prospective concept employing Zr-activated aluminum and piperidine has been developed. The synthesis, characterization, and detailed thermal decomposition studies of the formed piperidinoalanes have been described. Single-crystal X-ray diffraction analyses revealed two new crystal structures of piperidinoalanes [pip$_2$AlH]$_2$ and [pip$_3$Al]$_2$ (pip= 1-piperidinyl, C$_5$H$_{10}$N). In addition, the perspective approach for hydrogen uptake/release in piperidinoalane has been established.

The second part of this work was focused on the modification of the properties of the sodium alanate-based system to obtain the material suitable for high-pressure tank technologies. Sodium alanate has been considered as the most promising complex

metal hydride for practical applications, thanks to its reversibility in exchanging hydrogen at moderate conditions in the presence of a small amount of dopants. In order to provide the material with the high dissociation pressure, sodium alanate was doped with the high level of Ti-additive. The performed experiments showed, that with the increase of the doping level the increase of the dissociation pressure was observed. However, this effect was found to be connected to the lack of aluminum in the system due to the formation of Al-Ti-phases. Considerable progress has been achieved in improving the hydrogen sorption properties of sodium alanate-based system by adding extra aluminum powder in addition to the catalyst. As the result, the improved kinetics and increased gravimetric hydrogen storage capacity of the Ti-doped sodium alanate system were observed. Furthermore, the change of the thermodynamics of sodium alanate-based system upon addition of $TiCl_3$ and Al was investigated with the help of high-pressure DSC. An additional thermal signal was detected during HP-DSC measurements upon adding the high amount of Al to Ti-doped sodium alanate. Based on the performed experiments the formation of an unknown Na-Al-hydride has been suggested. The fact that the Al addition can influence the hydrogen properties of the sodium alanate system is of significant importance for other alanate-based systems. Thus, the present study contributes to the understanding of the hydrogenation and dehydrogenation behavior of doped sodium alanate with perspectives being applicable to other related materials.

CONTENTS

LIST OF TABLES

LIST OF FIGURES

MOTIVATION AND GOALS

In one of the famous Jules Verne's novels "The Mysterious Island" an engineer informs his colleagues "I believe that water will one day be employed as fuel, that hydrogen and oxygen which constitute it, used singly or together, will furnish an inexhaustible source of heat and light, of an intensity of which coal is not capable. … Water will be the coal of the future."[1] This fantastic far-sighting view, published in 1874, predicted the coming of the hydrogen economy. In the present time, nobody can be surprised that hydrogen can be used as fuel.

Hydrogen has been recognized as an environmentally friendly energy carrier, which can be produced from renewable energy resources. The most challenging task for its extensive commercial applications is the development of efficient storage materials, which can satisfy the established gravimetric and volumetric storage requirements. Unfortunately, until now, none of the existing hydrogen storage materials meets all targets established by the US Department of Energy (DOE). The current challenges in developing a suitable system are as follows:

• Low cost of the hydrogen storage material.

• Favorable storage properties of the material: high hydrogen storage capacity, fast kinetics, and favorable thermodynamics.

• Environmentally friendly combustion products.

The efforts, which we make today, will strongly influence how fast the hydrogen economy will emerge at the dawn of the hydrogen age. The search for a safe and techno-economically viable hydrogen storage method is a crucial material challenge for moving towards the hydrogen-based economy. This work is preferably dedicated to the development of the new pathways for hydrogen storage in liquid and solid state. It is hoped, that this research can provide new inspiration to solve this challenge and can help to create new materials and approaches for the efficient storage of hydrogen.

This basic research was a part of the RevAl project founded by the German Federal Ministry of Education and Research (BMBF, Proj. No. 03SF0481A) and was aimed at the application of Al-N-based compounds for designing efficient systems for reversible hydrogen storage. The main efforts of this work were focused on the development and optimization of suitable aminoalanes for hydrogen storage. So far, this class of material was only partly investigated. In the past, the main research focus was on alane separation from formed amine-alane adducts. However, aminoalanes by themselves were never considered as hydrogen storage materials.

Aminoalanes are interesting both from the point of view of their hydrogen storage content and their physicochemical properties. The synthesis and characterization of novel materials based on Al-N bonds have been a major task of this work. The investigation of aminoalanes as potential hydrogen materials requires several steps. First, the synthesis, purification, and characterization of their properties should be performed. Testing of the hydrogen sorption properties of the synthesized aminoalanes should be the next step.

The specific goals and objectives pursued in this thesis are:

1. Development and optimization of the synthesis procedure for crystalline aminoalanes.

2. Testing of synthesized aminoalanes for hydrogen uptake in liquid and solid state.

3. Improvement of properties of the aminoalane-based system by applying doping agents.

4. Development of the efficient method for hydrogen cycling in aminoalanes.

5. Investigation of the absorption/desorption properties of sodium alanate doped with a high catalyst amount.

6. Kinetic and thermodynamic optimization of doped sodium alanate system by doping with suitable destabilization agent.

7. Determination of thermodynamic parameters of doped sodium alanate system with help of high-pressure DSC.

1 INTRODUCTION

The introduction chapter of this thesis will give an overview of the different hydrogen storage possibilities. The advantages and drawbacks of the various storage systems will be discussed and evaluated in terms of their viability for practical applications. The lightweight Al-, B-, N-based materials, which have made the most significant progress in energy storage in recent years will be discussed in detail. The main focus will be on the achievements made in hydrogen storage, particularly in complex hydride systems, which are of particular interest for this work.

1.1 The prospects for hydrogen-based energy systems

The development of energy storage systems as enablers for various energy technologies has become the subject of intensive research to overcome negative consequences from the depletion of fossil energy resources and anthropogenic climate change. In many respects, hydrogen-based technologies appear to be a promising solution for the replacement of the current carbon-based energy systems. However, the lack of practical hydrogen storage systems is currently a crucial obstacle for the implementation of hydrogen-based energy.

Generally, hydrogen can be generated by applying different methods[2–4]:

1. Renewable (electrolysis, biomass, thermochemical, thermophysical, photo-electrochemical, photo-biological)
2. Non-renewable (steam reformation, coal gasification, nuclear power)

On the other hand, the only hydrogen produced from renewable energy sources (solar radiation, wind, falling water, tides, etc.) can be truly sustainable. Thus, renewably produced energy is the way into a safe, environmentally friendly, and economically successful future. The main drawback of renewable energy sources versus fossil energy sources is that they are capable of producing, mostly, one energy carrier: electricity. However, modern society cannot operate effectively with energy provided only in the form of electricity, as they also need chemical fuels and feedstocks. For example, airplanes cannot economically fly using electricity. Therefore, one of the major challenges is to develop a system for the utilization of electricity. Hydrogen has great potential as an energy carrier for storing and supplying the electricity generated from renewable energies and additionally can be used as fuel in the transport sector. For example, the energy from renewable resources can be used to generate hydrogen through water electrolysis[5] and then can be utilized for

smoothing fluctuation of renewable energy or as a fuel. However, this technology faces certain limitations such as thermal management, low efficiency of the cycle (up to 40%), and cost of the electrolyzer. If a more efficient method will be developed, hydrogen could replace fossil fuel in the future.

The variety of the production methods make hydrogen independent from the producing source. The other advantages of hydrogen as an energy carrier are[3,6–8]:

- *Available.* The most abundant element on Earth.
- *Producible.* The clean way to produce hydrogen from the water.
- *Utilizable.* The transport and power sectors have the potential to use hydrogen.
- *Storable.* Hydrogen can be stored in a variety of forms and in large quantities.
- *Transportable.* Hydrogen can be transported in many ways (e.g. road, rail, ship).
- *Environmentally friendly.* Hydrogen does not produce harmful emissions, which deplete the ozone layer.
- *Recyclable.* Hydrogen can be separated from oxygen by the electrolysis of water.
- *High gravimetric energy density.* The gravimetric energy density of hydrogen (120 MJ/kg) is approximately three times that of gasoline (46.4 MJ/kg).

Despite these potential benefits, there is a need to focus equally on the positive features of hydrogen and technical and economic obstacles to overcome its negative aspects. The major technical barriers and challenges in the use of hydrogen as a fuel are[6,8,9]:

- *Low volumetric energy density.* The low volumetric energy density of hydrogen (8.4 MJ/L) compared to gasoline (31.1 MJ/L) is the reason for the increased package volume required for a hydrogen storage system.
- *Purity.* For the application of hydrogen in fuel cells, high purity of hydrogen is required (99.99 %).
- *The cost of production.* Hydrogen is not naturally available, thus the cost for hydrogen production is higher compare to natural gas.
- *Safety.* Great care is needed to avoid problems during hydrogen operations.

It might be the simplest way to store compressed hydrogen in a pressure vessel. However, the low energy density of hydrogen in such systems cannot satisfy the fuel demand of most current vehicles. In order to carry enough fuel (about 5–6 kg of H_2) for achieving the standard car driving range of about 500 km, hydrogen needs to be stored in special containers with pressures up to 70 MPa[10,11]. Consequently, this leads to

several technical problems like adiabatic effects during refueling, design, and safety of storage containers. To overcome these issues much attention is currently being given to find material for solid-state hydrogen storage.

1.2 Requirements for the hydrogen storage system

The development of practical hydrogen storage systems is a challenging task as requirements of storage capacity, refueling rates and weight must be met. These are often taken to be the targets specified by the United States Department of Energy (DOE) in (Table 1.1).

Table 1.1 Summary of DOE technical system targets for on-board hydrogen storage for light-duty fuel cell vehicles[12].

Storage parameter	2020	2025	Ultimate
System gravimetric capacity, wt.-%	4.5	5.5	6.5
System volumetric capacity, g H_2/L	30	40	50
Fuel cost, $/gge* at pump	4	4	4
Min/max delivery temperature, C°	-40/85	-40/85	-40/85
Operational cycle life (1/4 tank to full), cycles	1500	1500	1500
Min/max delivery pressure from storage system, bar	5/12	5/12	5/12
System fill time (5 kg), min	3-5	3-5	3-5

* 1 kg H_2 ≈ 1 gal gasoline equivalent (gge) on energy basis.

Following these targets the practical hydrogen storage system must satisfy a number of requirements[13]:

- High-energy storage capacity.
- Favorable thermodynamics (moderate temperature and pressure range).
- Fast kinetics (rapid rate for desorption <1–2 wt.-%/min).
- Reversibility.
- Good thermal conductivity.
- Cheap and available.
- High stability against oxygen and moisture, long lifetime.
- No environmental, health, or safety issues (environmentally friendly by-products).
- Lightweight (minimal weight and volume increment to overall vehicle).

In order to accomplish these objectives, the Fuel Cell Technologies Office (FCTO) carried out extensive research on a wide range of hydrogen storage materials (Fig. 1.1).
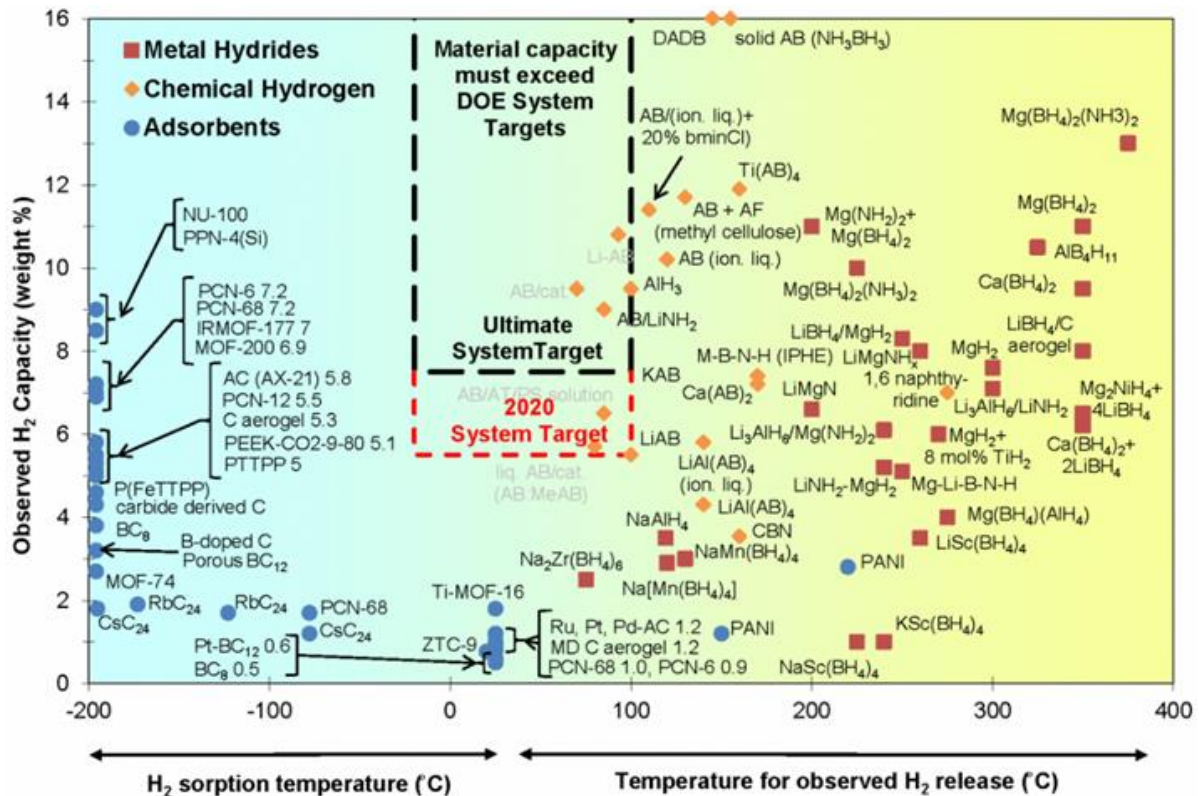
Figure 1.1 Hydrogen capacity of hydrogen storage materials investigated by FCTO as a function of operating temperature[14].

The study showed (Fig. 1.1), that most of the investigated materials with high storage capacity cannot fully satisfy the DOE targets due to the disadvantages associated with low hydrogen storage capacity or unfavorable thermodynamics. The materials with fast kinetics have issues with low storage capacity or complete irreversibility. A compromise between high storage capacity and slow kinetics may be accepted, since in that case material loading to the full capacity may not be required. The other compromise could be achieved by the combination of a high-pressure cylinder and a solid-state hydride[15,16]; thus the driving range of a vehicle could be extended significantly or the tank volume could be reduced for the same driving range. Therefore, the nowadays research direction is to find solid-state materials for hybrid tank systems that can work at elevated pressure of $p(H_2) = 300–700$ bar.

1.3 An overview of hydrogen storage strategies

The storage of hydrogen is a major challenge for its practical application as an energy carrier. Hydrogen storage technologies can be generally categorized into physical and chemical ones (Fig. 1.2). The common physical methods include compression, liquefaction, cryo-compression, physisorption by adsorbents. Typical chemical hydrogen storage materials include metal hydrides, complex metal hydrides,

and other hydrogen-containing compounds. Additionally, chemical storage materials can be classified in regard to their "reversibility" - ability to be rehydrogenated under moderate temperatures and pressures, as reversible (e.g. intermetallic alloys, sodium alanate, liquid organic carriers) and irreversible (e.g. borohydrides, aluminum hydride). Irreversible systems can release hydrogen by thermal decomposition or by hydrolysis reaction.
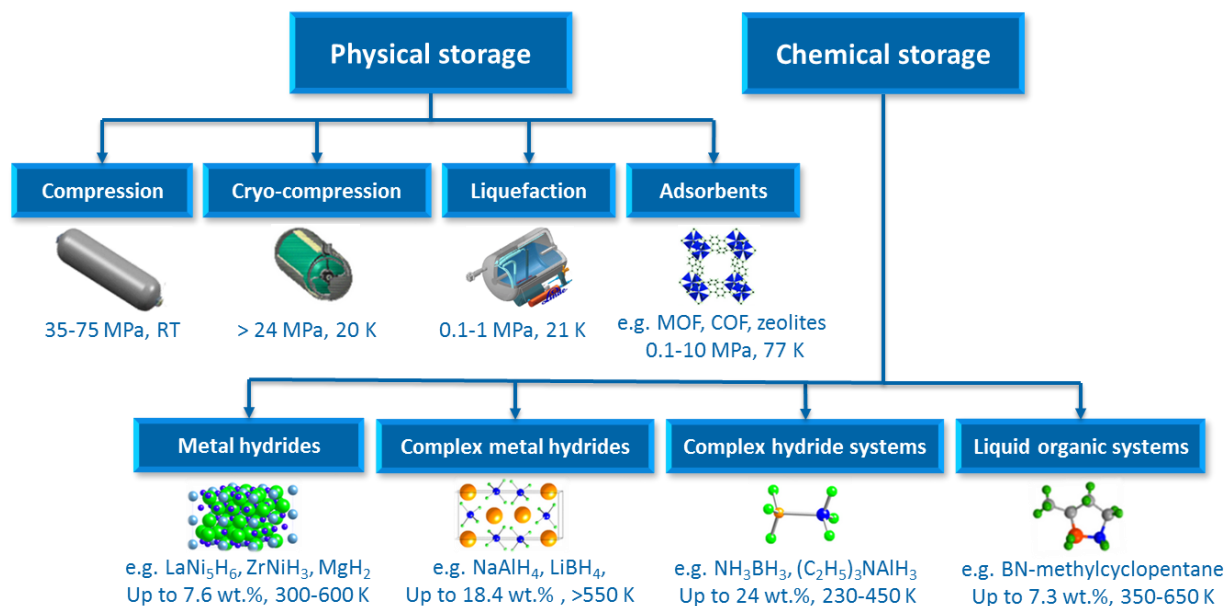
Figure 1.2 *Schematic illustration for hydrogen storage methods. Modified from*[17].

Each storage principle has its own prospects and constraints and the energy required to store hydrogen in each storage method is quite different. For instance, the necessary cooling energy for liquefying hydrogen is about 30 % of the stored chemical energy of hydrogen. The energy input of 12 % for pressurizing hydrogen up to 200 bar and 9 % for storing it at 100 bar in a hydride (e.g. $NaAlH_4$) will be required[18].

Compressed hydrogen gas requires highly pressurized vessels, made from strong, lightweight, and highly resistant materials. The advantage of liquefied hydrogen over pressurized is its high volumetric density at low pressure and its favorable transportation characteristics. However, this method faces two challenges: the efficiency of the liquefaction process and the costs for the thermal isolation of the storage containers from boil-off gas[11]. Cryo-compressed hydrogen storage systems operate at high pressures (24 MPa or higher) and cryogenic temperatures (20 K)[6]. The storage tanks are compatible with compressed and liquefied hydrogen refueling infrastructures. However, the cryo-compressed hydrogen storage system has the same challenging problems of design, operation, safety, cost, and maintenance, as

systems for liquefied hydrogen. Despite all above-mentioned limitations, physical storage technologies show up to date the best overall technical performance in automotive applications. The combination of pressurized or cryogenic tanks with other technologies such as fuel cells is the current solution for a variety of existing zero-emission vehicles.

In contrast, hydrogen storage in solid materials has reduced volumetric constraints; however, the main challenge is the gravimetric hydrogen storage capacity. In solid-state storage, hydrogen can be bonded either by weak physical forces on highly porous solids (Fig 1.3, a) or by chemical forces (Fig. 1.3, b and c) in hydrides.
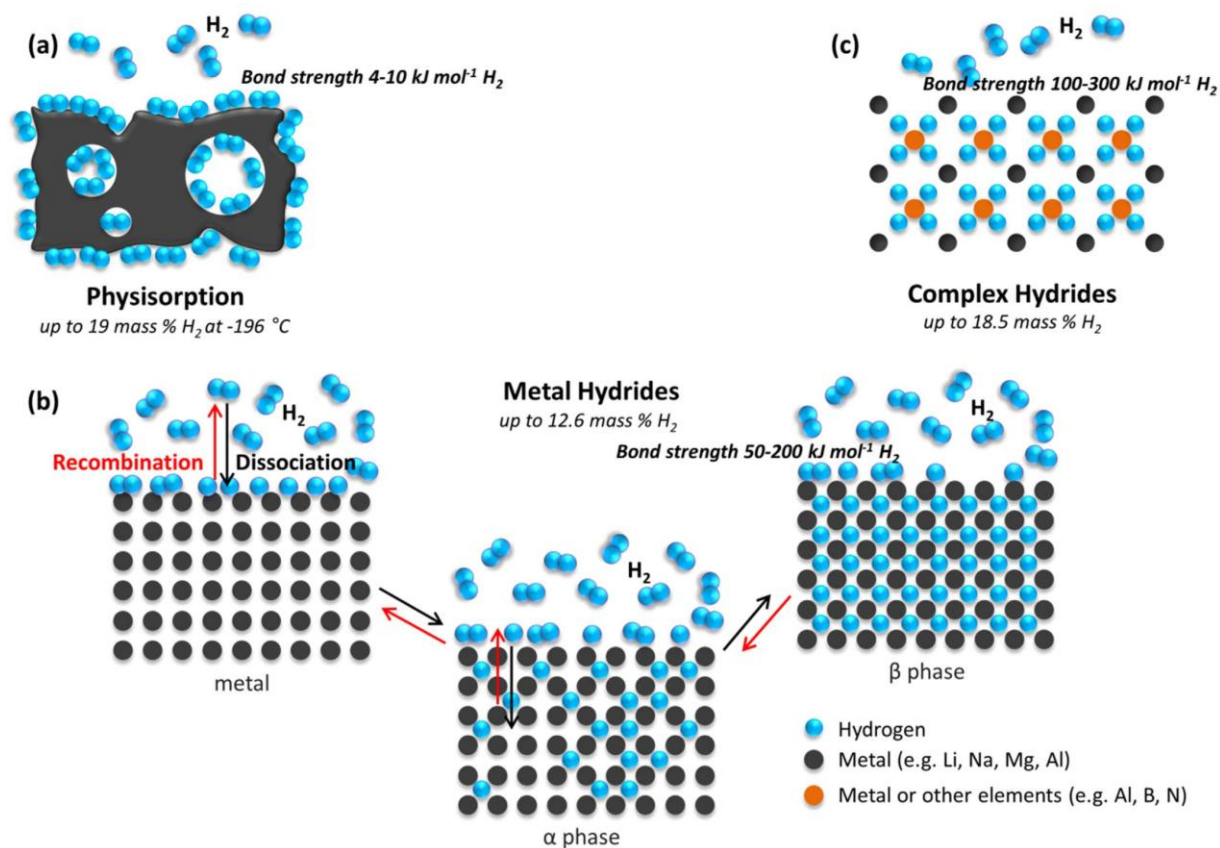
Figure 1.3 *The scheme of the physical and chemical bonding of the hydrogen in solid materials*[19].

Adsorption of hydrogen on high surface area materials

Physisorption is caused by weak intermolecular forces (van der Waals forces) between hydrogen molecules and the surface of the material. The maximum amount of hydrogen which can be adsorbed on the solid depends on the surface area, pore volume, and enthalpy of adsorption. The most widely studied materials are carbon-based materials (activated carbon, fullerenes, nanotubes, nanofibers and graphene)[20–23], zeolites[24–26], metal organic frameworks (MOFs)[27,28], covalent organic frameworks (COFs)[29–32], and clathrates[33–35].

Hydrogen storage by physical sorption is a very promising research path since it provides fast kinetics and reversibility, thus refueling time is short and safe. Since physisorption is nonactivating process, the only low heat effects during hydrogen uptake and release are involved. The low temperatures needed to store significant amounts of hydrogen, limit at present the practical application of adsorbents. To overcome the drawbacks of these systems several strategies have been suggested: increasing surface area and pore volume, designing a framework consisting of light elements, avoidance of nonessential free space in the structure, optimization of the adsorption energy, creating unsaturated metal sites, doping of frameworks with metal centers and particles to increase hydrogen uptake via a spillover mechanism. The porous materials can be also used as scaffolds for other hydrogen storage materials such as metal/complex hydrides to enhance the kinetics, thermodynamics, and reversibility of hydrogen sorption due to the defects and specific interactions between the Me-H bond and the nanoporous walls, and making the materials more attractive for practical applications.

Chemical storage of hydrogen in metal hydrides

Chemical hydrogen storage, wherein hydrogen is stored in a chemical compound and released via a chemical reaction, is a promising strategy for providing high volumetric and gravimetric hydrogen storage capacities. However, there is always the need to split or recombine the hydrogen molecules, to integrate the hydrogen atoms into the lattice of the metal, and to form a new chemical compound. This is a process that inherently involves large enthalpy changes, which have to be handled in technical applications. The formation and stability of such materials highly depend on the pressure and temperature.

In the past decade, systems consisting of light elements (e.g. Li, K, Na, Mg, B, Al, and N) have been under development. As the main interest of this work is related to complex metal hydrides and multi-cations hydrides, a short description of the conventional metal hydrides will be given here. In the next section, an extended overview of the most promising complex hydride systems will be presented.

Metals can combine with hydrogen by three different bond types: ionic, covalent, and metallic. Based on the strength of the bonds, metal hydrides are broadly classified into two categories: reversible and irreversible. In the metallic hydrides, the hydrogen typically occupies interstitial sites, which may lead to wide ranges of non-stoichiometry. The chemical hydrogen storage in transition metals and alloys is the common concept proposed in the late 1960´s. The first examples are Mg-based compounds (Mg_2Cu and

Mg$_2$Ni) and LiNi$_5$ which absorb hydrogen already at room temperature[6]. In the meantime, many **interstitial metal hydrides** have been reported[15,36]. Even though these hydrides are reversible and have excellent kinetics, theirs gravimetric hydrogen density (up to 3 wt.-%) is inherently low due to the high atomic weight of the metal. The high price of intermetallic hydrides and low hydrogen equilibrium pressures at room temperature also prevent the practical use of these materials. Nevertheless, they can be useful for special applications such as submarines or forklift trucks, where heavyweight is essential.

Among all the light metal hydrides, **magnesium hydride (MgH$_2$)** has been the one most studied because of its relatively large theoretical hydrogen density (7.6 wt.- %) and low costs. Mg-based hydrides possess good-quality functional properties, such as heat-resistance, reversibility, and recyclability. The reaction of hydrogen with Mg is exothermic with an enthalpy of reaction of -74.5 kJ/mol H$_2$ which means that a temperature of about 300 °C is required to release hydrogen from β-MgH$_2$ at a pressure of 1 bar[37]. Unfavorable thermodynamic properties, slow desorption kinetics, and high reactivity of MgH$_2$ toward air and oxygen limit its practical use. Numerous attempts have been made to overcome the unfavorable kinetic barriers and to decrease the desorption temperature of MgH$_2$. A commonly successful method to improve the hydrogenation rate is to introduce structural defects by alloying MgH$_2$ with various elements and/or compounds by the high-energy ball milling[19]. To improve the hydrogen exchange kinetics, the series of composite materials were prepared by ball milling of Mg with transition metals which either absorb hydrogen (e.g. Ti, V, Nb)[38,39], or not (e.g. Fe, Ni, Cu, Co)[39–41]. The metals and composites which do not alloy with Mg (e.g. V, Nb, Pd, NiB)[42] are supposed to act as gateways for the hydrogen into/from the magnesium matrix. On the other hand, the high desorption temperature makes magnesium hydride a favorable material, for instance, for thermal and solar-thermal applications.

Remarkable hydrogen content of about 10 wt.-% has promoted extensive studies on **aluminum hydride (AlH$_3$)** as a material for hydrogen storage applications. Considerable efforts have been made to characterize the thermodynamic and crystal structure of different alane polymorphs (α, α´, β, γ, δ, ε and ζ) in order to understand the hydrogen storage properties of this material[43–46]. Aluminum hydride decomposes in a single endothermic step with the release of hydrogen and aluminum metal, with the enthalpy of the dehydrogenation reaction of 6.0 ± 1.5 kJ/mol H$_2$, $-3 \sim -5$ kJ/mol H$_2$, and 1.0 ± 0.5 kJ/mol H$_2$[47] for the α-, β-and γ-phases, respectively. The main

drawback of alane is unfavorable hydrogenation conditions. While the dehydrogenation of AlH_3 occurs at 170 ºC (at a heating rate of 10 ºC/min)[45], a minimum of 7 kbar of H_2 pressure at room temperature is necessary for hydride formation[48]. This high hydrogenation pressure has precluded alane from being considered as a reversible hydrogen storage material. Thus, much research has been done in order to develop more economically and thermodynamically cost-effective synthetic routes to produce alane, such as the conventional organometallic (ethereal) reaction[43], direct high-pressure hydrogenation[49], electrochemical charging[50], and low-pressure hydrogenation using stabilizing ligands (e.g. amines)[51]. However, the ethereal reaction of lithium alanate with aluminum chloride[43] remains the preferred synthesis method.

1.4 Complex hydrides as a promising hydrogen storage materials

The chemistry of complex hydrides is extremely diverse and a wide range of novel hydrides have been discovered during the past decades. In contrast to intermetallic hydrides, in complex hydrides, hydrogen atoms are covalently bonded to a complex-forming element (e.g. B, Al or N) in an anionic complex (e.g. $[BH_4]^-$, $[AlH_4]^-$, $[NH_2]^-$) and stabilized by the cation, typically an alkali metal (e.g. $LiAlH_4$, $LiBH_4$, $LiNH_2$) or alkaline earth metal (e.g. $Mg(AlH_4)_2$, $Mg(BH_4)_2$)[10,11]. Most light metal complex hydrides often have very large hydrogen densities (Table 1.2).

Table 1.2 *Selected properties of complex metal hydrides.*

Material	ρ_m wt.-% H_2	ρ_V, g H_2/L	ΔH_{dec} (kJ/mol)	T_{dec}, ºC	Ref.
$LiBH_4$	18.4	122.5	74	400	[52]
$NaBH_4$	10.7	115.6	-108	500	[53]
$Ca(BH_4)_2$	11.6		32	527	[54]
α-$Mg(BH_4)_2$	14.9	117	67	280	[55]
$Al(BH_4)_3$	16.9	132	-	80	[56]
$LiAlH_4$	10.6	97.5	-10 (1st step) 25 (2nd step)	160–180 (1st step) 180–220 (2nd step)	[57]
$NaAlH_4$	7.5	93.5	37 (1st step) 47 (2nd step)	220 (1st step) 275 (2nd step)	[13,58]
$KAlH_4$	5.7	53.2	55 (1st step) 70 (2nd step)	290 (1st step) 330 (2nd step)	[59,60]
$Ca(AlH_4)_2$	7.9	70.4	-7 (1st step) 31 (2nd step)	127 (1st step) 250 (2nd step)	[61]
$Mg(AlH_4)_2$	9.3	72.3	1.7 (1st step) 48.8 (2nd step)	150–170 (1st step) 310–320 (2nd step)	[61]

LiNH$_2$	8.8	103.6	67 (1st step)	285	[62–64]
NaNH$_2$	5.1	71.9	-	400	[65,66]
Mg(NH$_2$)$_2$	7.2	97.3	-	200	[67]

ρ_m - gravimetric hydrogen density; ρ_V - volumetric hydrogen density; ΔH_{dec}- desorption enthalpy; T_{dec} - decomposition temperature

Generally, the hydrogen storage capacity of complex metal hydrides depends on the weight of the metal atoms and the number of possible bound hydrogen atoms in the complex anion. In many cases, the hydrogen release pathway from complex metal hydrides is complicated compared to metallic and ionic hydrides, and thus remains not fully understood. For having the potential for practical usage the reversible hydride system should have an absolute value of heat of hydrogenation and dehydrogenation between 20 - 30 kJ/mol H$_2$[15]. However, most of the complex hydrides are not suitable for practical applications due to their poor thermodynamic and kinetic properties or limited reversibility.

1.4.1 Metal borohydride systems

Metal borohydrides have received significant interest, as hydrogen storage materials, initiated by investigations of hydrogen storage properties of LiBH$_4$[68]. Since then a wide range of novel metal borohydrides have been discovered and tested, due to the great coordination flexibility of the complex [BH$_4$]$^-$ anion, and thus an extensive verity of possible compositions[69].

Lithium borohydride (LiBH$_4$) has a high gravimetric hydrogen density (18.4 wt.- %), which is the highest gravimetric storage capacity among the complex hydrides (Table 1.2). However, it exhibits high thermodynamic stability due to the strong B-H bond, and thus the dehydrogenation/hydrogenation temperatures and pressures are too high for practical applications. LiBH$_4$ starts to thermally decompose above 320 ºC, and the major decomposition process occurs at the temperature range of 400-600 ºC. Furthermore, LiBH$_4$ can be only rehydrogenated under extreme conditions, such as p(H$_2$) = 70-350 bar and T = 600-650 ºC[70]. The addition of different compounds to LiBH$_4$ has a positive influence on its rehydrogenation properties. For instance, lithium borohydride destabilized with MgH$_2$ and small quantitates of TiCl$_3$, showed reversible hydrogen storage of 8-10 wt.-% at 315-400 ºC[71]. With the MgH$_2$ addition, the hydrogenation/dehydrogenation enthalpy was lowered by 25 kJ/(mol H$_2$) compared to pure LiBH$_4$ (Table 1.2).

Sodium borohydride (NaBH$_4$) is widely used as a reducing agent and has a high potential to be used as a hydrogen storage material. The practical application has

been hindered by its high stability, leading to desorption temperatures above 500 ºC[53]. Considerable progress has been reached with many additives (Co-, Pt-, Ru- -based catalysts) for the initiation of the hydrolysis of $NaBH_4$[72]. However, the low-cost regeneration pathway of $NaBO_2$ formed during the hydrolysis reaction remains a critical issue.

Magnesium borohydride ($Mg(BH_4)_2$) has a high gravimetric hydrogen density and also favorable thermodynamics (Table 1.2) that permit reversible hydrogen release under moderate pressure and temperature[55,73]. However, the extremely slow kinetics of the reversible hydrogen release and hydrogenation conditions (950 bar at 400 ºC for 108 h)[74] are daunting challenges. Many attempts were made in order to lower the temperature required for the hydrogenation reaction through catalytic enhancement. Bardaji et al.[75] have shown that small amounts of transition metal (TM) additives ($PdCl_2$, $TiCl_3$, VCl_3, $MoCl_3$, $RuCl_3$, $CeCl_3$, and $NbCl_5$) decrease the decomposition temperature of $Mg(BH_4)_2$ by more than 100 ºC. However, no hydrogenation was observed for discharged material MgB_2 mechanical milled with 2 mol% of a variety of additives ($NiCl_2$, $RuCl_3$, Pd, $FeCl_3$, $CuCl_2$, and $TiCl_3$)[74]. In contrast, by mechanical milling of MgB_2 with MgH_2 or Mg, the formation of magnesium borohydride at 300 ºC under 700 bar was achieved[76]. Another Mg-based system (LiH-MgB_2) can be hydrogenated even at lower pressure 50 bar H_2 at 350 ºC, with the addition of Ti-containing compounds (TiF_4, TiO_2, TiN, and TiC)[77].

Up to now, for most of the metal borohydrides, the reversibility under moderate conditions has not been yet achieved. Moreover, boron hydrides suffer from the disadvantage that volatile boranes are possible decomposition products, which lead to a reduction of hydrogen capacity and are fatal for the fuel cell system. For the mentioned reasons, many research groups have been focused on complex aluminum hydrides.

1.4.2 Alanate-based systems

Light complex aluminum hydrides, such as $NaAlH_4$, $LiAlH_4$, $KAlH_4$, etc., have been intensively investigated as potential candidates for solid-state hydrogen storage due to their relatively high capacity, moderate absorption/desorption conditions, and good reversibility in the presence of catalysts. In general, the alkali metal alanates are less stable than the alkali metal borohydrides with decomposition temperatures of 60 to 300 ºC, however, they have low gravimetric hydrogen storage capacity (Table 1.2).

The attractive feature of alanates is related to their easy accessibility. Aluminum is cheap, plentiful, and widely used metal in 21st century technologies. For example, sodium alanate can be prepared starting from cheap industrial chemicals via ball-milling with the doping agent under a hydrogen pressure[78]:

$$NaH + Al \xrightarrow[\substack{8\ MPa\ H_2 \\ ball\ milling}]{dopant} NaAlH_4 \qquad (1.1)$$

Sodium alanate (NaAlH₄) is amongst the most advanced and intensely investigated materials for hydrogen storage, with a theoretical gravimetric capacity of 7.5 wt.-% H_2. However, in practice, only about 5.0 wt.-% of hydrogen release was reached so far. The dissociation of NaH, responsible for the release of 1.9 wt.-% H_2, takes place above 450 ºC, making this step unsuitable for practical applications. Even if it seems evident that its performance will be not useful for on-board applications, it is considered promising for stationary purposes.

In 1997, Bogdanovic et al.[79] demonstrated that the kinetics of the sodium alanate system could be strongly improved by adding a few molar percent of Ti-based compounds. It was the first indication that Ti worked catalytically for dry materials and that the system could be reversibly operated under practical conditions. This fundamental study created an entirely new prospect for lightweight hydrogen storage.

Despite catalytic enhancement, the dehydrogenation kinetics of sodium alanate still remains a huge obstacle. Different C-based materials[80–82] and metal halides[83–86] were claimed to be able to destabilize NaAlH₄, significantly reducing dehydrogenation temperature of the different steps. The role of the additive during the hydrogenation/dehydrogenation reaction remained unclear mainly due to difficult analytical problems. Moreover, most of the catalysts were found to react with the hydride, decreasing the gravimetric capacity of the system and its whole storage performance.

Lithium alanate (LiAlH₄) was synthesized in the late 1940s and was widely used as a reducing agent in organic chemistry, but attained increased attention as a hydrogen storage material after the discovery of the Ti-catalyzed sodium alanate systems. LiAlH₄ has a theoretical gravimetric capacity of 10.5 wt.-% H_2 and releases hydrogen in the following three steps[87]:

$$3LiAlH_4 \xrightarrow{150\text{-}175\ ^\circ C} Li_3AlH_6 + 2Al + 3H_2 \quad (5.3\ wt.\text{-}\%\ H_2) \tag{1.2}$$

$$Li_3AlH_6 \xrightarrow{180\text{-}220\ ^\circ C} 3LiH + Al + 3/2H_2 \quad (2.6\ wt.\text{-}\%\ H_2) \tag{1.3}$$

$$3LiH + 3Al \xrightarrow{\sim 400\ ^\circ C} 3LiAl + 3/2H_2 \quad (2.6\ wt.\text{-}\%\ H_2) \tag{1.4}$$
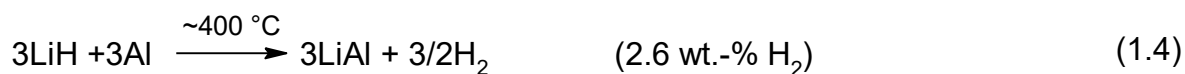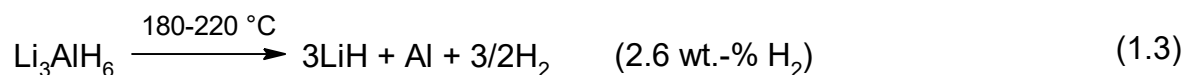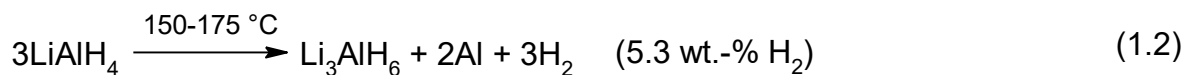
The working temperatures for the first two steps could be attractive for practical applications, but the desorption kinetics is still far from the practical targets. Several strategies have been applied in the last few years to overcome these limits. For example, ball milling[88] and catalysts addition (e.g. $TiCl_3$, $ZrCl_4$, VCl_3, $NiCl_2$, etc.)[89,90] tend to lower the decomposition temperature and to improve the dehydrogenation kinetics, but does not enable rehydrogenation. A way to overcome the energy barrier preventing rehydrogenation of $LiAlH_4$ is to use a solvent-mediated synthesis route by applying hydrogen pressure to slurries of LiH and Al in THF[91] or Me_2O[92].

The known alanates of metals from other groups of the periodic table are considerably less stable than those previously described. The several thermodynamically unstable **transition metal aluminum hydrides** with a high hydrogen content like $Ti(AlH_4)_4$ (9.3 wt.-% H_2)[93], $Fe(AlH_4)_2$ (6.8 wt.-% H_2)[94], $Zr(AlH_4)_4$ (7.5 wt.-% H_2)[95] or $In(AlH_4)_3$ (5.8 wt.-%)[96] are described. The general synthesis of transition metal complex aluminum hydrides $M(AlH_4)_n$ (M= Ti, V, Co, Mn, Fe, Cu, Zr, Nb, Ag, Ce, Ta, etc.) is carried out at very low temperatures, between -110 and -80 ºC, due to their very low decomposition temperature[94,96,97]. For instance, $Ti(AlH_4)_4$ and $Fe(AlH_4)_2$ start to decompose slowly above -110 ºC[94], $In(AlH_4)_3$ at -40 ºC[96], and further release hydrogen while heated to room temperature. Among these transition metal alanates **yttrium tetrahydroaluminate** (**$Y(AlH_4)_3$**, 6.6 wt.-% H_2), is exceptionally stable and starts slowly to decompose at room temperature[95]. Upon heating, this alanate decomposes via a four-stage dehydrogenation process[97]:

$$Y(AlH_4)_3 \xrightarrow{80\text{-}170\ ^\circ C} YAlH_6 + 2Al + 3H_2 \tag{1.5}$$

$$YAlH_6 \xrightarrow{170\text{-}250\ ^\circ C} YH_3 + Al + 3/2H_2 \tag{1.6}$$

$$YH_3 \xrightarrow{250\text{-}300\ ^\circ C} YH_2 + 1/2H_2 \tag{1.7}$$

$$YH_2 + 3Al \xrightarrow{>350\ ^\circ C} YAl_3 + H_2 \tag{1.8}$$

The recent study[97] confirmed that yttrium alanate can store hydrogen reversibly at about 140 ºC, which holds promise for low-temperature applications. An amount of 3.4 wt.-% H_2 can be released at 140 ºC from the first dehydrogenation step of $Y(AlH_4)_3$,

and reversibly absorbed at 145 ºC and 100 bar H_2. In contrast, yttrium borohydride, $Y(BH_4)_3$ (9.1 wt.-% H_2), starts to release hydrogen at about 190 ºC and the dehydrogenated material can be rehydrogenated at 250 ºC and p (H_2) = 350 bar[98].

A number of different experimental approaches can be applied to improve the storage properties of alanates, for example, by tailoring the physical properties of the materials by anion substitution or chemical reaction with other compounds[99]. These strategies are of the main interest of this work and will be discussed in detail in this section and the chapter related to solid-state hydrogen storage.

1.4.3 Nitrogen-containing complex hydrides

The chemistry of N-containing complex hydrides is very rich. Ammonia has a high hydrogen content (17.3 wt.-%) and can catalytically split into H_2 and N_2, however, the decomposition of NH_3 and subsequent hydrogen separation and purification from toxic NH_3 hampered the commercialization of this material[100]. The simplest ammonia-based compounds (BH_4NH_4, BH_3NH_3, AlH_3NH_3) have very high hydrogen content, which can be delivered by heating via a multistep decomposition process. Up to date, ammonium borohydride (NH_4BH_4) has the highest hydrogen content of solid-state materials (24.5 wt.-% H_2) reported so far. The release of about 20 wt.-% hydrogen from NH_4BH_4 at temperatures <160 ºC was reported[101]. However, its short lifetime at room temperature hampered its application for hydrogen storage. Ammonia borane (NH_3BH_3) releases about 19.6 wt.-% of hydrogen in three decomposition steps forming polymeric products $[NH_2BH_2]_n$ (90–120 ºC), $[NHBH]_n$ (120–200 ºC) and finally boron nitride BN (>500 ºC)[102,103]. However, the direct hydrogenation of the spent material would require substantial energy input[104]. Alternatively, Sutton et al.[105] has demonstrated that polyborazylene (BNH) can be converted back to ammonia borane (NH_3BN_3) with hydrazine (N_2H_4) in liquid ammonia at 40 ºC within 24 h (Scheme 1.1).
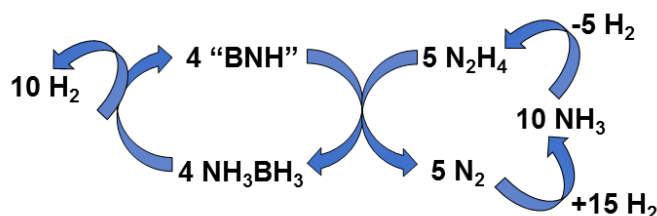
Scheme 1.1 *The overall reaction mechanism for the ammonia borane regeneration from polyborazylene using hydrazine. Modified from[105].*

Ammonia borane can be also regenerated from the dehydrogenated BNH-waste via regenerative procedure applying hydrochloric acid, amine, and molecular hydrogen[106].

Numerous combinations between B-N-H-based compounds and alkali or alkaline earth metal have been investigated, for example, metal hydrazinoborane ($MN_2H_3BH_3$), metal borohydride ammoniates ($M-BH_4-NH_3$), metal borohydride amides ($M-BH_4-NH_2$), metal borohydride-ammonia borane complexes ($M-BH_4-NH_3BH_3$), metal amidoborane ammoniates ($M(NH_2BH_3)_n xNH_3$), and metal amidoboranes ($M(NH_2BH_3)_n$)[107,108]. Generally, these hydrides show high gravimetrical and volumetrical hydrogen storage capacities and release hydrogen below 150 ºC[108]. The main drawbacks that hamper the widespread utilization of B-N-containing composites are the possible evaporation of toxic ammonia and boranes during the hydrogen evolution and the limited cyclability of the spent material.

In recent years, the strategy of using double-metal cations to adjust the temperature and purity of dehydrogenation of ammine borohydrides was reported[109,110]. Introducing another complex-forming element allows to tune the stability of bimetallic complexes and to obtain the material with the desired properties. Interestingly, the complex-forming metal, possessing higher electronegativity, is determining the stability of the bimetal borohydride. The relationship between the Pauling electronegativity of the metal cation which coordinates to the [BH_4]- group and the thermal stability of the metal and bimetal borohydrides has been established[108]. The higher the electronegativity of the metal the lower is the decomposition temperature of the complex (Figure 1.4).
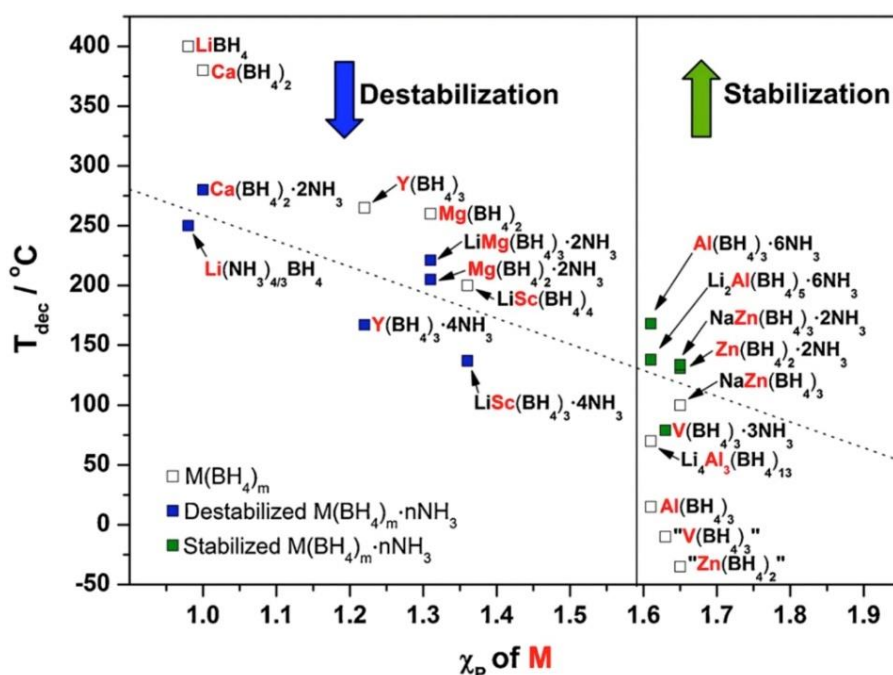
Figure 1.4 *Thermal decomposition temperature of metal borohydrides and metal borohydride ammoniates plotted as a function of the central metal electronegativity[108].*

In addition, ammonia has a destabilizing effect on metal borohydrides (Fig. 5) with low metal electronegativity ($\chi_p < 1.6$), while metal borohydrides with high electronegativity ($\chi_p > 1.6$) are generally stabilized[107,111]. For example, the highly unstable borohydrides $Al(BH_4)_3$ and $Zn(BH_4)_2$ are stabilized by the complexation with ammonia (Figure 1.4). In contrast, lithium borohydride is destabilized when ammonia is introduced into the complex. The destabilization is likely caused by dihydrogen elimination from protic and hydridic hydrogen in $N-H^{\sigma+}\cdots H^{\sigma-}-B$ dihydrogen bonds. Thus, the introduced metal cation plays a crucial role in the destabilization of N-B/B-H bonds and in the suppression of ammonia release in metal borohydride ammoniates[112]. Several of these metal borohydride ammoniates have been considered as potential hydrogen storage materials, for example, $LiSc(BH_4)_4\cdot4NH_3$ and $V(BH_4)_3\cdot3NH_3$[110] can release 15.1 and 14.3 wt.-% high-purity hydrogen, respectively, below 300 °C.

Aluminum complexes with B- and N-based hydrides have also been widely investigated in recent years, e.g. metal aluminum amides $M[Al(NH_2)_4]_n$[113], aluminum amidoboranes $M[Al(NH_2BH_3)_4]$[114], aluminum ammine borohydrides $Al(BH_4)_3\cdot nNH_3$[115,116], and metal aluminum ammine borohydrides $M[Al(BH_4)]_m\cdot nNH_3$[109]. The partial reversibility was demonstrated for $Na[Al(NH_2BH_3)_4]$[114], which can release up to 9 wt.-% of pure hydrogen at about 70 ºC. The dehydrogenated material can reversibly absorb about 27 % of the released hydrogen at 250 ºC and $p(H_2) = 150$ bar. The novel $Al(BH_4)_3\cdot NH_3BH_3$ complex (17.7 wt.- %) releases hydrogen (Scheme 1.2) at temperatures below 100 °C[117], which is considerably lower compared to pure NH_3BH_3[103].
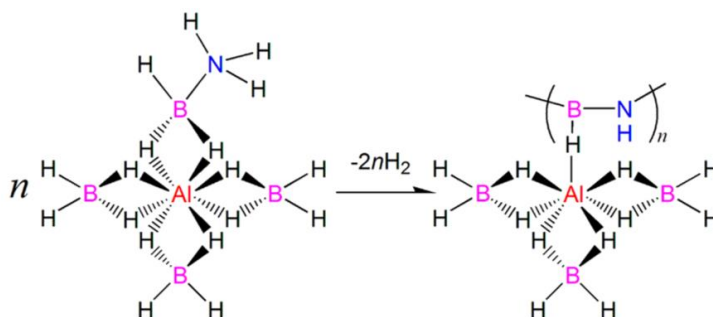
Scheme 1.2 *The first decomposition step of $Al(BH_4)_3\cdot NH_3BH_3$[117].*

Interesting studies were reported regarding the interactions between some alanates and ammonia borane composites $NH_3BH_3-MAlH_4$ (M = Na, Li)[118,119]. The novel mixed-metal (Li, Al) amidoborane compound can release up to 9 wt.-% H_2 at a temperature of 130 ºC within 200 min. However, the regeneration yield was only 35%

based on the post-milled material[118]. The amino-alanate-borane based system could overcome the barrier of by-product gas emission, which was observed in metal borohydride or amino-borane systems.

Quite recently, the **lithium-amide-hydride (LiNH$_2$-LiH)** composite system has been investigated as a possible candidate for hydrogen storage[62,64,120]. Chen et al.[64] illustrated the absorption of about 10.5 wt.-% of hydrogen by Li$_3$N at 285 ºC. The following reaction path for the reversible hydrogen storage in this system was suggested:

$$\text{LiNH}_2 + 2\text{LiH} \longleftrightarrow \text{Li}_2\text{NH} + \text{LiH} + \text{H}_2 \longleftrightarrow \text{Li}_3\text{N} + 2\text{H}_2 \qquad (1.9)$$
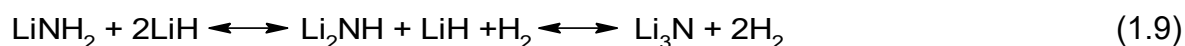
The decomposition reaction starts at T = 180 ºC, which is lower than the temperatures of the individual reactants, i.e. 300 ºC for LiNH$_2$[121] and 370 ºC for LiH[57]. Generally, the dehydrogenation of the amide-hydride system suffers from sluggish kinetics that might be caused by interface reactions, nucleation, and diffusion processes. Small amounts of TiCl$_3$ as dopant were found to have a strong accelerating effect on this reaction and might act as a transfer agent for the intermediate NH$_3$ to LiH. The product desorbs 5.5 wt.- % of hydrogen in the temperature range from 150 to 250 ºC upon heating without the emission of ammonia[62].

The partial cation substitution of Li with more electronegative elements (e.g. Mg) would weaken the Li-N and N-H bonds, thus decreases the dehydrogenation temperatures of the complex[122]. The thermodynamic destabilization can be achieved by the optimization of the composition of the system. The Mg(NH$_2$)$_2$ and LiH mixture decomposes at a lower temperature compared to the LiNH$_2$ system[67,123]. The overall reaction, with the hydrogen release of about 6.9 wt.-%, may take the following reaction path[67]:

$$3\text{Mg(NH}_2)_2 + 8\text{LiH} \longleftrightarrow \text{Mg}_3\text{N}_2 + 4\text{Li}_2\text{NH} + 8\text{H}_2 \qquad (1.10)$$
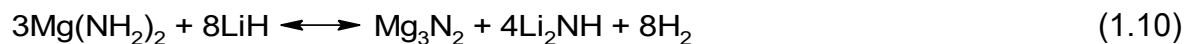
The hydrogenation of the obtained mixture takes place at 200 °C under 30 bar of H$_2$[67] with the transformation into the original mixture of Mg(NH$_2$)$_2$ and LiH (eq. 1.10). Very recently, it was published, that small quantities of K-containing compounds (0.08 mol% of KCl and KOH) reduce the dehydrogenation temperature down to 154 °C, with the reversible absorption/desorption of 4.6 wt.-% of hydrogen with improved kinetics[124].

There are a lot of other possible combinations of complex hydrides, which have high hydrogen content and good reversibility at moderate conditions. Nowadays, the main research is focused on the development of an N-based system with fast

dehydrogenation/hydrogenation kinetics and without the evolution of ammonia during hydrogen release.

Summarizing, some hydrides can meet the DOE target for H_2 storage capacity, however, their high discharge temperature and poor cycle performance remain roadblocks to their successful implementation in real-world systems. The possible applications could be the stationary hydrogen storage or combination of complex hydride with a high-temperature fuel cell (HT-PEM)[18], to provide energy for example for continuous operation for telecommunication satellites.

1.5 Summary

The latest advancements that have been made on different hydrogen storage materials and technologies have been highlighted in this chapter. Among gravimetric and volumetric hydrogen storage capacities, other factors such as reversibility, thermodynamic stability, kinetics of absorption and desorption, etc., need to be considered for developing a practical hydrogen storage system.

The recent research efforts in hydrogen storage materials have been predominantly devoted to light metal-based hydrides. The progress in the reversibility of the hydrogen release reaction and the effect of additives on the dehydrogenation/rehydrogenation reactions of potential hydrogen storage materials have been summarized. In addition, the advantages and drawbacks of the promising solid-state hydrogen storage systems have been outlined.

The potential of Al- and B-based material for hydrogen storage applications have been emphasized. However, there are many problems associated with their use, including unfavorable kinetics requiring heating and susceptibility to contamination by released impurities. Borohydrides systems exhibit limitations such as the high temperature of dehydrogenation, lack of reversibility, slow kinetics of dehydrogenation and hydrogenation, the evolution of diborane during hydrogen release.

Since the discovery of the doped alanate in 1997, this chemical system is probably the most widely studied type of hydrogen storage materials. However, until now the temperature required to release hydrogen at usable pressures is still too high for practical applications of this system. A class of metastable (kinetically stabilized) hydrides (e.g. $Y(AlH_4)_3$) offers some new hope with high volumetric and gravimetric energy densities and low decomposition temperatures (<150 ºC).

The combination of the different systems is now the new approach to overcome the drawbacks of each system alone. For thermodynamic tailoring, a second or even

third component is added to a hydrogen storage material, which can open up new reaction pathways with different thermodynamics. It may be a prospective way to stabilize or destabilize the decomposition reaction. In this respect, the materials based on Al/B and N are assumed to hold the best promise as hydrogen carriers, and further research in this field may significantly support the implementation of a hydrogen-based economy.

2 GENERAL CHARACTERIZATION METHODS

This chapter presents the description of the physical processes characteristic and applied measuring techniques used in this work.

2.1 X-ray crystallography

2.1.1 X-ray powder diffraction (XRPD)

XRPD patterns were recorded on a BRUKER D2 Phaser X-ray diffractometer with a Lynxeye® detector (CuKα radiation: 1.5406 Å). The X-ray tube is operated at 30 kV and 10 mA. Measurements were performed with a step size of 0.05° and 1s dwell time. Samples for XRPD analysis were prepared on an iron sample disk inside the glove box and were covered with polyethylene foil to protect the material from contact with air or moisture during the measurements. The polyethylene foil shows two diffraction peaks (2θ = 21.5 and 23.7°) and the iron sample holder at 43 and 44° 2θ.

2.1.2 Single-crystal structure analysis

The obtained crystals were transferred from the Schlenk flask into a drop of hydrocarbon oil. A suitable crystal was attached to a glass fibre, and immediately placed in the low-temperature nitrogen stream. Single-crystal X-ray diffraction data sets were collected with ω-scans on an 'IPDS-2(T)' diffractometer (STOE, Darmstadt, Germany) at 160(2) K using Mo K$_\alpha$-radiation (λ 0.71073 Å). Absorption correction was performed with XShape using integration correction type. Structures were solved by direct methods with ShelXS[125] and all non-hydrogen atoms were anisotropically refined in full-matrix least-squares cycles against $|F^2|$ (ShelXL)[126]. C-bound hydrogen atoms were isotropically included in the refinement in idealized positions (riding model). The coordinates of Al-bound hydrogen atoms were (isotropically) refined using SADI restraints to stabilize refinement of adjacent H atom positions of disordered Al−H groups. Cif-files have been deposited with the Cambridge Crystallographic Data Center (CCDC) and can be obtained by quoting the following reference numbers: CCDC 2016259 (**2**) and 2016260 (**3**).

2.2 Thermal analysis

Thermal gravimetric analysis (TGA) and differential scanning calorimetry (DSC) measurements were performed using Sensys DSC (SETARAM, France). The 5-10 mg of powder sample was weighed and placed into the alumina or aluminum crucible

inside the glove box. For protecting very sensitive samples during transfer to the measuring equipment, the samples were covered with a layer of dry Al_2O_3 powder (dried at 900 °C). All measurements were performed under argon atmosphere with the heating rate of 5 ºC/min from room temperature (25 ºC) to a set point given to each compound individually. Data were collected and analyzed using the Calisto (AKTS, SETARAM) software. The obtained data were used for the determination of the melting point of the samples. Some data collection was also performed in the collaboration with the Max-Planck-Institut für Kohlenforschung (Mülheim) using a Mettler Toledo TGA/DSC 1 (heating rate: 1 ºC/min) with a gas flow controller GC 200 (argon flow: 50 mL/min) combined with a ThermoStar GSD 300 T2 MS gas analyzer for the detection of the released gas.

2.3 Quantitative chemical analysis

2.3.1 Elemental analysis

Determination of C, N, and H contents was performed using a Vario MICRO-cube analyzer. In a typical procedure, ~5 mg of the sample were tightly packed into a tin-foil inside the glove box and then moved outside for the analysis.

2.3.2 Inductively coupled plasma optical emission spectrometry (ICP-OES)

The determination of the Al-content was performed by ICP-OES and measured with iCAP 6500 (Thermo Scientific). For preparing the analyzing mixture, the sample (~40-60 mg) was dissolved in 5 ml of the deionized water and was treated with 3 ml of concentrated hydrochloride acid until the complete dissolution of the solid sample. The mixture was diluted with deionized water in a ratio of 1:150. The obtained Al-values were corrected by measuring "blank" solution prepared in the same manner.

2.4 Nuclear magnetic resonance spectroscopy (NMR)

^{1}H, ^{13}C, ^{27}Al NMR spectra were recorded on Bruker Avance III 500 MHz (^{1}H (500.13 MHz), ^{13}C (125.76 MHz), ^{27}Al (130.3 MHz)) or Bruker Avance Neo 700 MHz (^{1}H (700.13 MHz), ^{13}C (176.1 MHz)) at 20 ºC. The chemical shifts for ^{1}H and ^{13}C spectra are given in ppm (δ) relative to $SiMe_4$ as an internal standard or the residual signal of the deuterated solvent (C_6D_6, ^{1}H δ = 7.16 ppm, ^{13}C δ = 128.06 ppm) and for ^{27}Al externally referenced to $Al(NO_3)_3$ in D_2O (1.1 mol/L). In each case, the remaining solvent was removed from the sample before dissolving it in a deuterated solvent. The broad featureless ^{27}Al resonance at $\delta \sim 65$ ppm is due to the NMR glass tube, found

in all ^{27}Al NMR spectra. NMR signal assignments are supported by additional 2D experiments.

2D ^{1}H−^{1}H COSY spectra were obtained with a phase sensitive pulse program including double quantum filtering (cosygpmfphpp) using the following parameters: 8.5 ppm spectral width, 16 dummy scans, 4 scans, 256 experiments for the indirect dimension, and zero filling to 1k data points in F2 and F1, respectively. 2D ^{1}H−^{13}C HSQC spectra were collected with a multiplicity edited pulse program (hsqcedetgpsisp2.3) experiment using the following acquisition parameters: sweep width for ^{1}H = 16 ppm, ^{13}C = 160 ppm, 4 scans, 32 dummy scans, 256 experiments for the indirect dimension, and zero filling to 1k data points in F2 and F1, respectively.

Typically, 20-30 mg of the sample were diluted in 0.7 ml of deuterated solvent, stored in a glove box. After filtering with a 2 mm PTFE filter, the obtained transparent solution was transferred into a 5 mm NMR tube. NMR spectra were analyzed by using the TopSpin software.

3 LIQUID-STATE HYDROGEN STORAGE

In this chapter, the important goal was to acquire a fundamental understanding of reversible hydrogen storage in an Al-N-based system. So far, only a few systems have been studied in this field, and only liquid hydrogenation has been successfully shown. The primary goal of this work was to develop the Al-N-based system that may store hydrogen reversibly in the solid state.

The introduction part of this chapter highlights the recent progress made in the development of liquid-phase organic and organometallic systems for chemical hydrogen storage, along with their advantages and drawbacks, with particular emphasis on the development of heterocyclic compounds. A number of N-based compounds as potential materials for hydrogen storage systems have been described. In addition, this chapter highlights the main achievement in the field of hydrogen storage in Al-N-based systems, as well as other liquid carriers that are capable to store hydrogen.

The present contribution has been focused on the exploration of Al-N-based compounds as possible hydrogen storage materials. In order to search for a practical system, several amine-alane complexes and aminoalanes have been synthesized and tested for their ability to store hydrogen. The systems, which showed the hydrogen uptake, in the tested pressure and temperature ranges, have been further developed, and their properties have been investigated in detail.

3.1 State of the art

3.1.1 Liquid-state hydrogen storage materials

An auspicious alternative to a conventional approach of hydrogen storage is to use unsaturated organic compounds that have a high capacity to bind hydrogen covalently. Hydrogen storage in these materials is achieved by catalytic hydrogenation and subsequent dehydrogenation of the organic compounds. In such a reversible process, the material is not consumed and can be reused for hydrogen storage. In contrast to the physical trapping of hydrogen gas in porous materials, the systems appear as high-boiling liquids that do not require compression or cryogenic procedures.

One of the possible solutions for liquid hydrogen storage is to use liquid organic hydrogen carriers (LOHC) which are also referred to as "liquid organic hydrides". Early research on liquid organic hydrides for chemical hydrogen storage has been focused

on hydrocarbons, using a catalytic reaction pair through the dehydrogenation of cycloalkanes and hydrogenation of the corresponding aromatics. Various organic liquids with potentially commercially applicable properties have been considered as hydrogen storage materials[36,127–136]:

➢ Cyclohexane/benzene, 7.2 wt.-% H_2, ΔH= 68 kJ/mol H_2

➢ Methylcyclohexane/toluene, 6.2 wt.-% H_2, ΔH= 73 kJ/mol H_2

➢ N-heptane/toluene, 8 wt.-% H_2, ΔH= 63 kJ/mol H_2

➢ Decalin or tetralin/naphthalene, 7.3 wt.-% H_2, ΔH= 66 kJ/mol H_2

➢ Bicyclohexyl/biphenyl, 7.3 wt.-% H_2, ΔH= 67 kJ/mol H_2

➢ Perhydroterphenyl/terphenyl, 7.3 wt.-% H_2

➢ Methanol or formic acid/CO_2, 12.1 or 4.3 wt.-% H_2, ΔH= 32 kJ/mol H_2

The hydrogenation of aromatic compounds is usually exothermic and the reaction rate is determined mainly by the efficiency of the catalysts, which generally include supported noble metals (Ru, Rh, Ir, Pd, or Pt). However, the reverse can be conducted only at elevated temperatures (200-400 ºC). Thus, the target application of cyclic hydrocarbons is not on-board hydrogen storage. The organic chemical hydrides can be useful as storage media to buffer seasonal changes in demand and supply of renewable energy or for long-term storage and long-distance transportation of hydrogen to fulfill the producer-to-customer chain[137].

For the tailoring of dehydrogenation enthalpy of hydrocarbons, several strategies can be applied, such as fused ring compound, heteroatom replacement, and electron-donating substitution (Fig. 3.1).
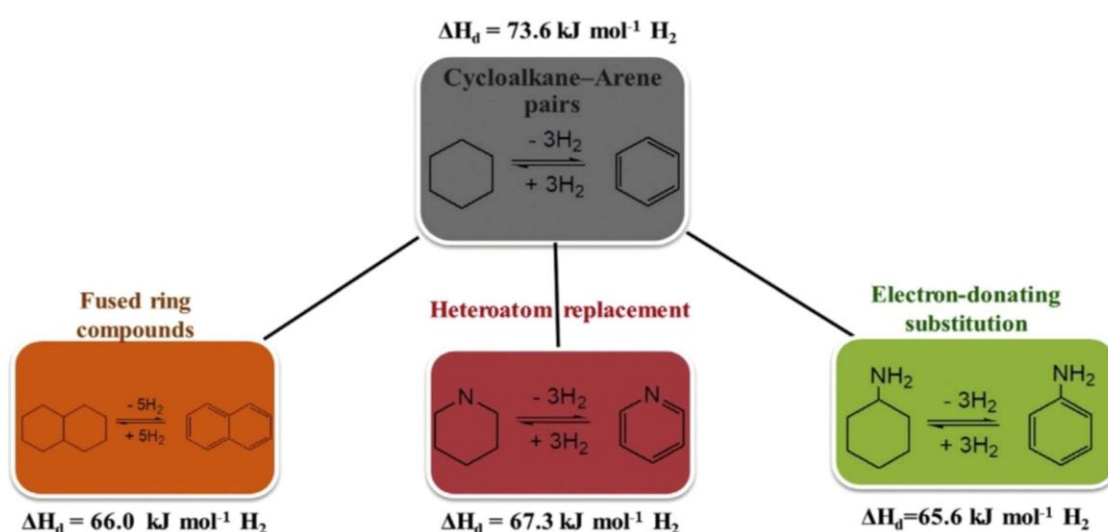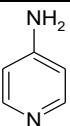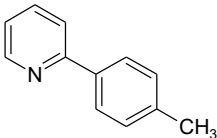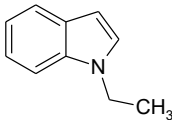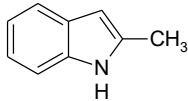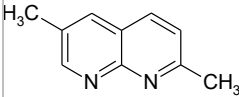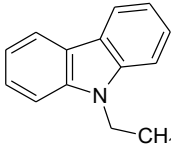
Figure 3.1 *The possible strategies to tune the dehydrogenation enthalpy of cycloalkane[138].*

Numerous theoretical[139,140] and experimental[141,142] studies have validated that the partial substitution of carbon atoms in the ring by the heteroatom could help substantially decrease the enthalpy of dehydrogenation and therefore improve hydrogen release at low temperature. Organic aromatic compounds containing the heteroatoms (e.g. O, N, B) have attracted the most interest because of their thermal stability, high storage capacity, and reasonable hydrogenation/dehydrogenation conditions[143–146].

A wide range of N-heterocyclic compounds was investigated as liquid hydrogen storage carriers[147–149]. The catalytic dehydrogenation rates of these compounds were increased by incorporating electron-donating or conjugated unsaturated substituents. The hydrogen stored in these systems (Table 3.1), can be facilely released for use by catalytic dehydrogenation of the latter in the presence of supported heterogeneous catalysts at less than 250 ºC[141,142].

Table 3.1 *Comparison of hydrogenation/dehydrogenation conditions for N-substituted heterocycles.*

Storage media	Dehydrogenated form	Hydrogen capacity	Operating conditions			Ref.
			T_H/T_D, ºC	P_H, bar	Catalyst for hydrog./dehydrog.	
4-aminopyridine		6.0 wt.-%	160 / 170	70	Rh-C / Pd-SiO$_2$	[147]
2-(N-methylbenzyl)-pyridine		6.15 wt.-%	150 / 230-270	50	1 or 5 wt.-% Ru-Al$_2$O$_3$ / 1 wt.-% Pd-C	[150]
N-ethylindole		5.23 wt.-%	160-190	90	5 wt.-% Ru-Al$_2$O$_3$ / 5 wt.-% Pd-Al$_2$O$_3$	[151]
2-Methylindole		5.7 wt.-%	120-170 / 160-200	70	5 wt.-% Ru-Al$_2$O$_3$ / 5 wt.-% Pd-Al$_2$O$_3$	[152]
2,6-dimethyl-1,5-naphthyridine		6.0 wt.-%	110 or 130 / 138	70	Cp*Ir- complex (Cp* - pentamethylcyclopentadienyl)	[153]
N-ethylcarbazole		5.8 wt.-%	130-150 / 150-170	70	Ru / Pt or Pd	[141,142,154]

* T_H – hydrogenation temperature, T_D – dehydrogenation temperature, P_H – hydrogenation pressure

Among other N-heterocycles, N-ethylcarbazole (5.8 wt.-% H_2)[154,155] has been considered as one of the most promising liquid organic hydrogen carriers in a view of good reversibility and mild dehydrogenation temperature. Recent studies have also demonstrated the potential of indole and pyridine derivatives[147,151,152,156] as alternative hydrogen storage materials. The hydrogenation of N-heterocyclic systems usually proceeds under pressure lower than 100 bar in the temperature range 110-190 ºC over Ru-supported catalyst. The dehydrogenation usually takes place at a slightly higher temperature over Pt or Pd-based catalyst.

Recently, boron-nitrogen-based hydrides, a new class of liquid hydrogen storage materials, was recognized as one of the most promising material to store and transport hydrogen[127,157]. B,N-heterocycles (e.g. 1,2-B,N-cyclohexane, 3-Methyl-1,2-B,N-cyclopentane), linear B-alkylsubstituted ammonia borane derivatives (e.g. methylamine-borane, diethylamine-borane), might be excellent candidates for hydrogen storage, owing to their higher hydrogen capacities[145,146,158]. Luo et al.[146] demonstrated that B,N-methylcyclopentane releases hydrogen (4.7 wt.-%) to form a trimer by both catalytic (in toluene at 80 °C for 20 min, in presence of 5 mol% $FeCl_2$) and thermal (without solvent at 150 ºC for 1 h) pathways. The regeneration of the spent fuel was performed by treatment of the dehydrogenated product with methanol and lithium alanate:
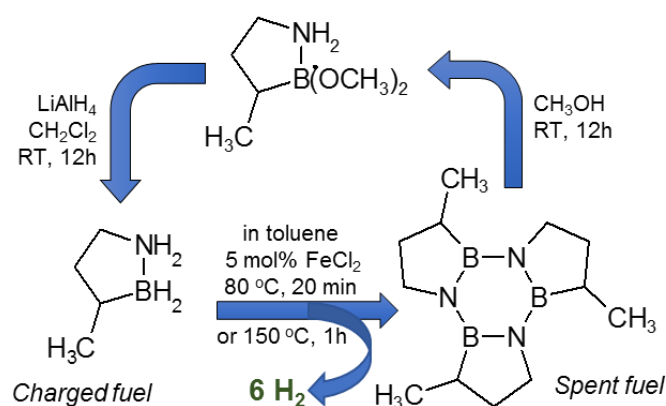
Scheme 3.1 Hydrogen storage cycle in B,N-methylcyclopentane. Modified from[146].

Very recently, Winner et al.[159] have reported the partial rehydrogenation of B,N-substituted aminoborane and has shown the mechanism of H^+/H^- exchange between ammonia borane and iminoborane:
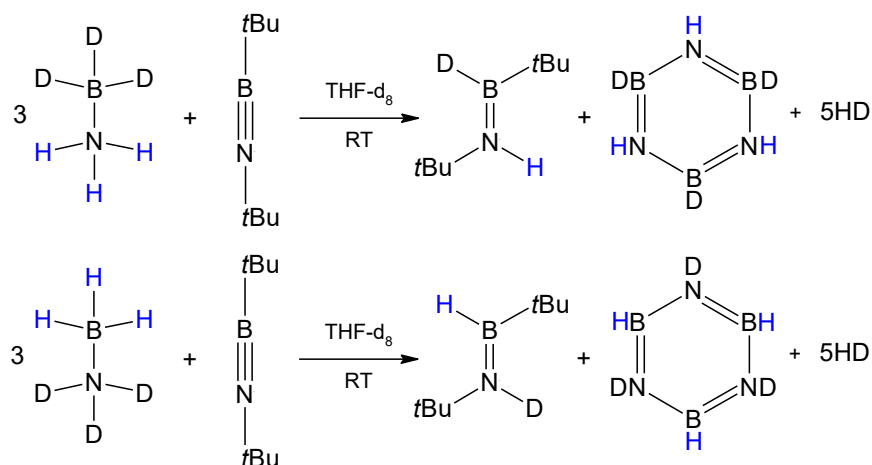
Scheme 3.2 *Hydrogen transfer from ammonia borane to iminoborane. Modified from*[159].

In the last years, there was observed a tendency for hydrogenation of the materials in a liquid state, which was not possible in the solid-state. For example, up to date, there are no reports of the use of $LiAlH_4$ for reversible solid-state hydrogen storage. However, the unfavorable thermodynamics of the reversible reaction may be altered by carrying out the hydrogenation in the solvent, which plays the role of stabilizing agent for lithium alanate formation. In early 1963 Ashby et al.[160] produced $LiAlH_4$ from the mixture of LiH and activated Al in THF or diglyme at 350 bar of H_2 and temperature 120 °C. Recently, this synthesis has been improved by using Ti-doped aluminum to significantly lower the required hydrogenation pressure and temperature[91]. The Ti-doped $LiAlH_4$ system can operate as a reversible hydrogen storage media that can release up to 7 wt.-% at 80 °C and can be recharged almost quantitatively by employing dimethyl ether as a solvent[92].

In summary, it is worth emphasizing the main advantages which offer liquid carrier as the hydrogen storage system[161,162]:

- The supply of CO_x free hydrogen.
- Easy transportation using conventional methods for liquids (pipelines, railcars, tanker trucks).
- High compatibility with the existing fuel station infrastructures.
- There are no high requirements on the liquid carrier tank compared to the gas tank.
- The long-time storage of large quantities of material under ambient conditions without detectable losses.
- The exhaust heat of an internal combustion engine can be used as input for the endothermic onboard dehydrogenation reaction.

Thus, the use of the liquid organic hydrides in the hydrogen economy could be envisaged as a transition step from the existing fuel infrastructure to the one based on hydrogen.

3.1.2 Al-N-based compounds as potential materials for hydrogen storage

It has been already mentioned in the introduction chapter (section 1.3) that the direct hydrogenation of aluminum to alane requires extremely high pressure, and therefore has been considered not useful for hydrogen storage purposes. This barrier can be substantially reduced by the addition of Lewis bases (lone pair donors) to form ligand-stabilized adducts. For example, aluminum hydride can easily react with X–H bonds (X being various heteroatoms[163–171]) with X = nitrogen being particularly interesting for this study, to generate Al-N compounds[172–174], often referred to as aminoalanes.

In general, aminoalanes display a wide variety of interesting structures (Fig. 3.2) by a marked tendency to oligomerize through the formation of Al-H or Al-N bridges. The substituents on the nitrogen or aluminum atoms substantially affect the structural nature of aminoalanes, which usually may be monomers, dimers, trimers, or tetramers similar to aminogallanes and aminoboranes[175–181].
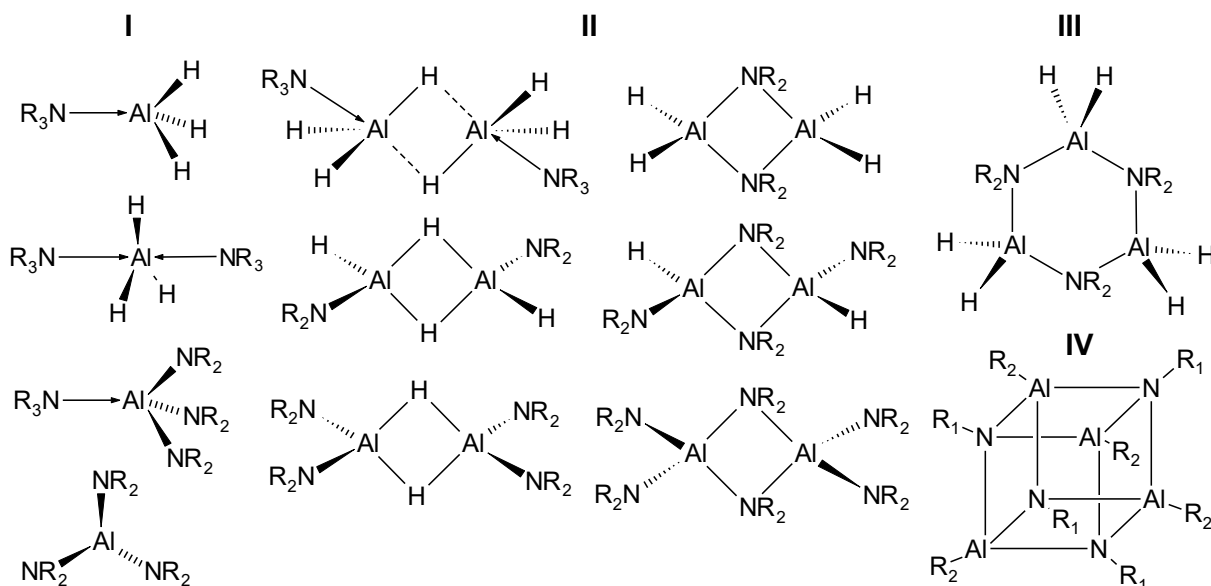
Figure 3.2 *Structure types of alane derivatives of amines with R = H or alkyl moieties: I) monomers; II) dimers; III) trimers; IV) hexamers.*

Very few monomeric alane adducts (**I**) with several structural differences for (L·AlH$_3$), (L$_2$·AlH$_3$), and (L$_3$·AlH$_3$) have been reported. The monomeric molecules, in which both Al and N are four coordinated (e.g. (quin)·AlH$_3$ (quin – quinuclidine)[164], TEA·AlH$_3$ (TEA – triethylamine)[182]), normally gain extra stability by augmenting the

coordination of the Al center with the tertiary amino ligand. The less common five-fold coordinated alane adducts ($L_2 \cdot AlH_3$) adopt a trigonal bipyramidal arrangement at the Al center with three equatorial hydrides and two axial donor ligands (e.g. $(NMe_3)_2 \cdot AlH_3$[183,184], $(quin)_2 \cdot AlH_3$[185]). The formation of a dimer through Al–H–Al bridges between two alane moieties (e.g. $[(mtp) \cdot AlH_3]_2$ (mtp – 1-methyltetrahydropyridine)[186], $[TAA \cdot AlH_3]$ (TAA – triallylalmine)[187]) helps to stabilize the complex when the amine donor cannot fully satisfy the Lewis-acidic aluminum center.

Secondary amines usually favor the dimeric (**II**) or trimeric (**III**) structures depending on the substituents R, with an exception of the only one structurally characterized example of the monomeric species $Al[N(i-Pr)_2]_3$[180]. The dimeric structure either with a cyclic Al_2H_2 (e.g. $[(tmp)_2AlH]_2$ (tmp – 2,2,6,6-tetramethylpiperidine)[188]) or an Al_2N_2 core (e.g. $[(dmp)_2AlH]_2$ (dmp – 2,6-dimethylpiperidine)[188], $[Et_2NAlH_2]_2$[189]) are preferred. However, when R is relatively compact, the trimeric structure (**III**) is preferred, as in $[Me_2NAlH_2]_3$[190], usually with a chair like conformation for the six-membered Al_3N_3 ring. The tetramers (**IV**) are usually formed by the thermolysis of the dimers with the more hindering R groups ($[MeAl(mes)]_4$ (mes – 2,4,6-trimethylphenyl)[191]) and possesses the cubic Al_4N_4 core.

The preparation of aminoalanes can be achieved by several approaches applying the suitable aluminum hydride source. The original method was developed in 1952 by Wiberg et al.[192] and involved the freshly prepared alane-diethyl ether solution, followed by replacement of coordinated ether by amine:

$$AlCl_3 + 3LiAlH_4 \longrightarrow 4AlH_3 * Et_2O + 3LiCl \tag{3.1}$$

$$AlH_3 * Et_2O + NR_3 \xrightarrow{Et_2O} AlH_3NR_3 \tag{3.2}$$
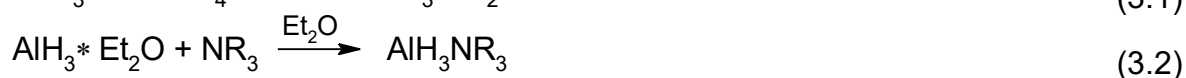
Later, the direct reaction between lithium alanate[172] (or sodium alanate[193]) and the hydrochloride salt of amine in diethyl ether was proposed:

$$3LiAlH_4 + R_3NHCl \longrightarrow AlH_3NR_3 + 3LiCl \tag{3.3}$$

The exchange reaction is also possible if the amine in the amine-alane complex can be substituted by the more basic ligand[174,194,195]:

$$AlH_3NR_3 + NR'_3 \longrightarrow AlH_3NR'_3 + NR_3 \tag{3.4}$$
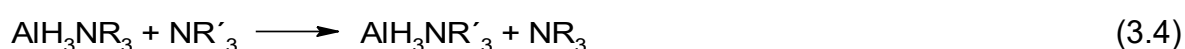
Some aminoalanes can be prepared by the direct hydrogenation of catalyzed aluminum and amine in a liquid medium[196,197]. The general reaction can be written:

$$Al^* + NR_3 + 3/2H_2 \longrightarrow AlH_3NR_3 \hspace{3cm} (3.5)$$

Great interest in numerous of these complexes arises from their applications in diverse fields, i.e. their use as hydroalumination agents[168], as precursors or intermediates for the deposition of aluminum films[198–201], as reducing agents for organic functional groups[202,203] and others. In recent years, aminoalanes have attracted significant interest as potential hydrogen storage materials, owing to their relatively high volume/mass hydrogen density. The simplest amine-alane adduct of AlH_3 and NH_3[204] can liberate in total 12.9 wt.-% of hydrogen by stepwise decomposition by forming the polymeric species:

$$AlH_3NH_3 \xrightarrow[3.9\ wt.-\%\ H_2]{-40\ °C} AlH_2NR_2 \xrightarrow[4.3\ wt.-\%\ H_2]{-20\ °C} -\big[AlHNH\big]- \xrightarrow[4.7\ wt.-\%\ H_2]{150\ °C} -\big[AlN\big]-$$
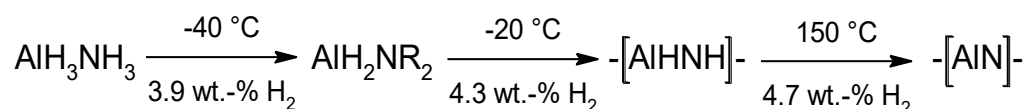
Scheme 3.3 *Hydrogen release from ammonium alane. Adapted from*[204].

The existence of protic N-bound and hydridic Al-bound hydrogen facilitates the release of hydrogen from aminoalanes already at low temperatures, however, a viable rehydrogenation approach of the "spent fuel" was not yet proposed. Recyclability is critical to the success of any hydrogen storage system. To obtain a room temperature stable amine-alane adduct, substituted amines need to be used for an enhanced stabilization effect.

Graetz et al.[205–208] discovered the perspective approach for AlH_3 regeneration from amine-alane complexes. This pathway involves a three-step procedure in order to obtain the alane (Scheme 3.4).
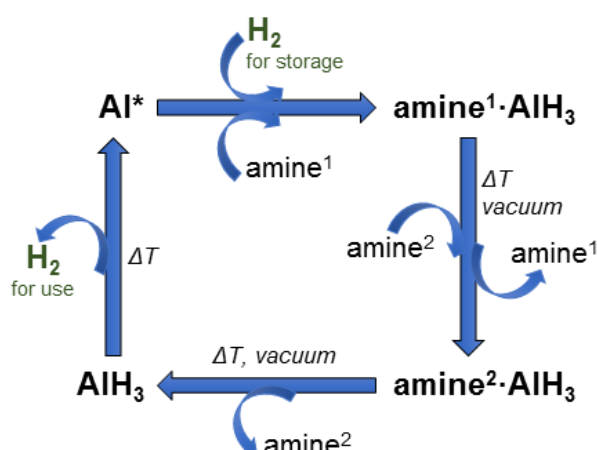
Scheme 3.4 *The pathway for alane regeneration applying amines and Ti-activated aluminum. Modified from*[207].

In the first stage, the stable amine-alane adduct (i.e. trimethylamine alane $(CH_3)_3NAlH_3$, dimethylethylamine alane $(CH_3)_2NC_2H_5AlH_3$) is formed by the direct

hydrogenation of Ti-activated aluminum powder with the corresponding amine. As the Al−N bond in the formed amine-alane complex is usually very strong, the alane recovery is impossible, because the complex decomposes at higher temperatures with the release of hydrogen before the Al−N bond is cleaved. Therefore, this approach requires the second step, transamination reaction with another amine to form a less stable adduct (usually triethylamine alane $(C_2H_5)_3NAlH_3$). Triethylamine alane cannot be formed by the direct hydrogenation of aluminum, but it can decompose at mild conditions. Thus, the last step involves the removal of the stabilizing agent at 75 ºC under a nitrogen sweep and the final recovery of the alane.

Murib and Horvitz[197] demonstrated a similar three-step process involving trimethylamine for alane stabilization and triethylamine as a transamination agent, in the presence of the complex catalyst based on the Group IA or Group IIA metals. The major concern with this strategy is the large energy investment required for the heating, as well as for the removal of the solvent and alane separation. Furthermore, while three steps are involved, the low yield of alane being produced[209], thus the efficiency of the whole regeneration process can reach only about 24.2% (well-to-tank efficiency) which can be improved to ~42.1% by using the waste heat from industrial sources[210].

Several other tertiary amines are also effective for stabilizing the alane, including triethylenediamine, quinuclidine, hexamine, and others are shown in Table 3.2. In almost all cases the ($L_2·AlH_3$) adduct is the most stable form. Thus, the total hydrogen content in this complex is decreased compared to monomer or dimer (e.g. dimethylethylamine).

Table 3.2 *Hydrogenation/dehydrogenation properties of several amine-alane complexes synthesized from Ti-activated aluminum.*

Amine	Amine-alane adduct type	Theor. H_2 capacity, wt.-%	Operating conditions		Ref.
			P_H, bar (t_H, h)	T_D, ºC (t_D, h)	
Triethylenediamine $C_6H_{12}N_2$	(1:1)	2.11	34.5 bar (80 h)	120 ºC (10 h)	[51]
Trimethylamine $(CH_3)_3N$	(2:1)	2.02	117.9 bar (24 h)	100 ºC (2 h)	[206]
Dimethylethylamine $(CH_3)_2NC_2H_5$	(1:1)	2.91	72.4 bar (56 h)	22 ºC (10 h)	[205]
N-methylpyrrolidine $C_5H_{11}N$	(2:1)	1.5	69 bar (20 h)	100 ºC (1 h)	[211]
Quinuclidine $C_7H_{13}N$	(2:1)	1.19	64 bar (24 h)	120 ºC (3 h)	[212]
Hexamine $C_6H_{12}N_4$	(2:1)	0.97	65.7 bar (48 h)	80 ºC (3 h)	[209]

The alane recovery from most of these amine-alane complexes is impossible since the temperature required for alane separation is higher than the alane decomposition temperature. Thus, for these adducts only the direct decomposition to aluminum and hydrogen is possible. The general feasibility of this idea was previously demonstrated using Ti-activated aluminum[51,212]:

$$AlH_3NR_3 \rightleftharpoons Al^* + NR_3 + 3/2H_2 \tag{3.6}$$

In this organic-metal system, hydrogen can reversibly be absorbed/desorbed simply by changing the pressure during cycling. The hydrogenation reaction is completely reversible (Fig. 3.3) with a plateau pressure of about 2 bar at 88 ºC[51] (in sharp contrast to the direct aluminum hydride formation from the elements at hydrogen pressure higher than 7 kbar at 27 ºC[48]). The Gibbs energy was calculated to be equal ΔG_{f298K} = -4.63 kJ/mol H_2 compared to α-AlH₃ ΔG_{f298} = 32.3 kJ/mol H_2[51].
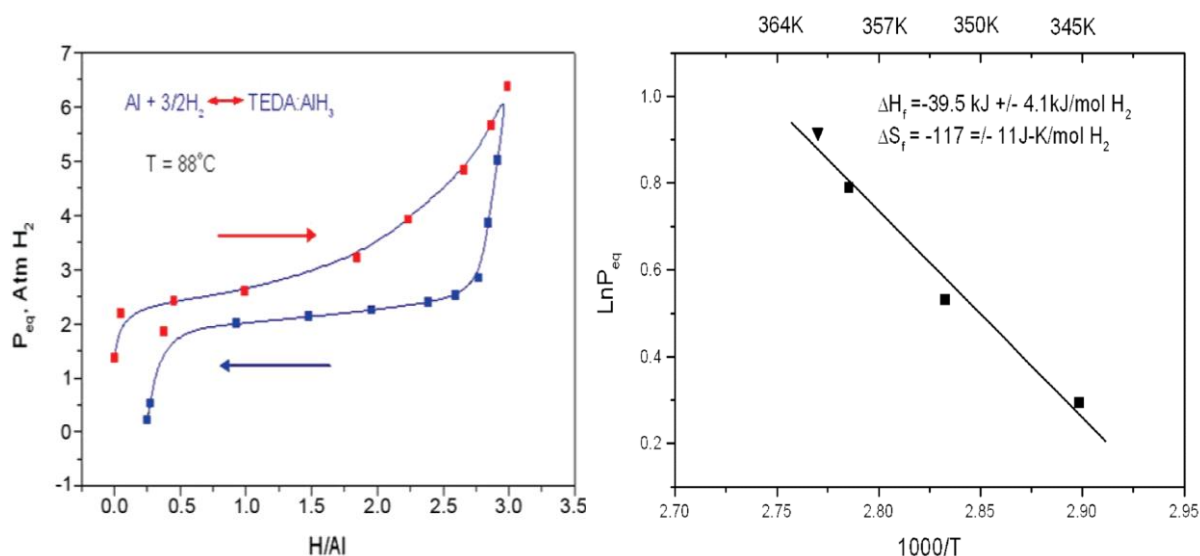
Figure 3.3 *The pressure composition isotherm for TEDA-AlH₃ system in n-undecane (left), the van´t Hoff plot of the equilibrium plateau pressure measured at 72, 80, 86, and 88 ºC (■ - in THF,▼ - in n-undecane)[51].*

However, several drawbacks are connected to this option, which are low reversible storage capacity, low reaction rate, and low yield of the amine-alane complex. Despite these disadvantages, it was shown that aluminum hydrogenation was possible at low temperatures and pressures. In this process, the activated aluminum plays a crucial role, which is neither understood nor sufficiently explored yet. Thus, these examples are very complex and require more detailed study for further improvement of this regeneration concept.

Very recently, with the help of NMR measurement under deuterium gas, Hatnean et al.[213] monitored the reversible transfer of hydrogen into Al–N bonds, i.e. the

reversible transformation of an aminoalane into an amine-alane adduct at 100 ºC in toluene. The general example of this procedure is as follows:

$$R_2Al{-}NR'_2 \underset{-H_2}{\overset{+H_2}{\rightleftharpoons}} R_2HAl{-}NHR'_2 \tag{3.7}$$

This method was originally used as an alternative approach for imine reduction and at the same time evidenced the reversible hydrogen transfer in aminoalanes without the breaking of the Al-N bond. Despite the huge potential of this pathway, the formed amines have large substituted groups such as phenyl and butyl, giving in total very low gravimetric hydrogen storage capacities.

Since this area is still emerging, a basic study of the hydrogen release and uptake by other aminoalanes should first be performed. The new concepts of reversible hydrogen uptake in aminoalanes should be proposed in order to make them attractive for practical applications.

3.1.3 Summary

A brief survey of the research progress in the development of diverse liquid-phase chemical hydrogen storage materials, including organic and organometallic chemical hydrides, with the emphasis on Al-N bond-containing compounds, was presented. Storing hydrogen in the form of a liquid hydride is a perspective approach for the soft transfer of the industry from fossil fuels to the hydrogen-based economy. In the past, liquid organic hydrogen storage materials did not attract much attention because the dehydrogenation step requires temperatures (up to 400 ºC) that are too high for the practical hydrogen storage system. The investigations of organic molecules with heteroatom opened up new possibilities in this field. The experimental and theoretical studies have indicated that the dehydrogenation of N-substituted heterocycles is more favorable compared to that of cycloalkanes, due to the decreased enthalpy of the dehydrogenation, making heterocycles more appealing for reversible hydrogen storage applications. Thus, heteroaromatic systems can offer a practical solution for the generation, storage, and transportation of hydrogen. The main disadvantage of organic hydride systems is associated with the usage of expensive noble metal catalysts.

In recent years, the interest in Al-N-based compounds has been intensively growing. It was showed, that in the presence of a stabilizing agent (i.e. amine, ether), the thermodynamic barrier of aluminum hydrogenation is substantially reduced and rehydrogenation can occur under mild conditions. The divers Al-N-based compounds

and their derivatives have been extensively investigated. The dual hydridic/protic nature of Al–H/N–H bonds can be harnessed for chemical hydrogen storage. However, the issue of the "spent fuel" regeneration is complicated and requires more attention.

Several strategies have been suggested and employed to a range of different amine-alane systems with varied results, but a real long-term solution for the regeneration problem is not a present reality. The most successful attempts were performed by using Ti-activated aluminum in the organometallic approach, where tertiary amines can be converted to AlH_3 and amine in a stepwise hydrogenation/dehydrogenation procedure. Besides the low hydrogenation pressure and low dehydrogenation temperature, the overall hydrogen regeneration path is not energy efficient. Thus, it is hoped, that further investigation in this direction could open the promising solution for hydrogen uptake by Al-N-based systems.

3.2 Materials preparation and experimental details

In this chapter, the preparation methods of aminoalanes, along with the short description of starting materials and sample handling are presented.

3.2.1 Chemicals and sample handling

All materials handled in this study are extremely air- and moisture-sensitive, requiring all manipulations (reactions, sample handling, transfer, and storage) to be performed using the standard Schlenk technique or employing an MBraun glove box (H_2O and $O_2 < 0.1$ ppm). The chemicals used for the synthesis are listed in Table 3.3.

Table 3.3 The list of chemicals including the purity and producer.

Compound	Formula	Purity	Producer
Aluminum chloride	$AlCl_3$	99%	Acros Organics
Aniline	$C_6H_5NH_2$	98%	TCI
Benzene	C_6H_6	99.5%	Roth
3,5-Diamino-1,2,4-triazole	$C_2H_5N_5$	98%	Sigma-Aldrich
Diethyl ether	$(C_2H_5)_2O$	99.7%	CHEMSOLUTE
Diisobutylaluminum hydride solution	$C_8H_{18}AlH$	1.0 M in hexane	Sigma-Aldrich
3,5-Dimethylaniline	$(CH_3)_2C_6H_3NH_2$	98%	Sigma-Aldrich
Hafnium (IV) chloride	$HfCl_4$	98%	Alfa Aesar
n-Hexane	C_6H_{14}	98.2%	VWR PROLABO CHEMICALS
Lithium aluminum hydride	$LiAlH_4$	reagent grade 95%	Sigma-Aldrich
n-Pentane	C_5H_{12}	99%	CHEMSOLUTE
2-Picolylamine	$C_6H_8N_2$	99%	Sigma-Aldrich
3-Picolylamine	$C_6H_8N_2$	≥99%	Sigma-Aldrich
Piperazine	$C_4H_{10}N_2$	99%	Alfa Aesar
Piperidine	$C_5H_{11}N$	99%	Alfa Aesar
Pyrazine	$C_4H_4N_2$	98%	Alfa Aesar
Pyridine	C_5H_5N	99+%	Alfa Aesar
Pyrrole	C_4H_5N	99%	TCI
Pyrrolidine	C_4H_9N	99%	Alfa Aesar
Tetrahydrofuran	C_4H_8O	99.9%	VWR PROLABO CHEMICALS
2,2,6,6-Tetramethylpiperidine	$C_9H_{19}N$	>99%	Sigma-Aldrich
Titanium (IV) butoxide	$Ti(OBu)_4$	99%	Acros Organics
Toluene	C_7H_8	>99.5%	VWR PROLABO CHEMICALS

Trimethylaluminum solution	$(CH_3)_3Al$	2.0 M in hexane	Sigma-Aldrich
2,4,6-Tris(chloroamino)-1,3,5-triazine	$C_3H_3Cl_3N_6$	>95.0%	TCI
2,4,6-Triaminopyrimidine	$C_4H_7N_5$	98+%	Alfa Aesar
2,4,6-Triamino-1,3,5-triazine	$C_3H_6N_6$	99%	Merck
1,3,5-Triazine	$C_3H_3N_3$	97%	Sigma-Aldrich
1,2,4-Triazole	$C_2H_3N_3$	98%	Sigma-Aldrich
Triethylenediamine	$C_6H_{12}N_2$	>99%	Sigma-Aldrich
Yttrium (III) chloride	YCl_3	99.99%	Alfa Aesar
Zirconium (IV) chloride	$ZrCl_4$	99.5%	Alfa Aesar

All solvents were dried and were distilled by refluxing over Na/Al_2O_3 (SOLVONA Bilger GmbH) and stored under argon atmosphere in the solvent reservoirs that contained 4 Å molecular sieves. Amines were used without further purification. Lithium aluminum hydride ($LiAlH_4$) was dissolved in diethyl ether and then the solution was filtered. Subsequently, the solvent was removed in vacuum and the residue was dried at 60 °C for 3 h under high vacuum. Hafnium (IV) chloride was dried and purified by sublimation at 240 °C (for a detailed description see the bachelor thesis of F. Habermann[214]).

3.2.2 Synthesis of aminoalane in diethyl ether solution with aluminum hydride

Preparation of triethylenediamine alane adduct (TEDA·AlH₃)

For the preparation of 0.266 g (8.9 mmol) ethereal solution of AlH_3, 0.296 g (2.2 mmol) of $AlCl_3$ was dissolved in 5 mL of diethyl ether and added to 0.253 g of $LiAlH_4$ (6.7 mmol) in 15 mL Et_2O. This suspension was filtered to remove precipitated LiCl. Triethylenediamine (TEDA) 1 g (8.9 mmol) was mixed with 20 mL of Et_2O for a few minutes and cooled in an isopropanol/dry ice bath before adding AlH_3 ethereal solution. The reaction mixture was then allowed to warm up to room temperature and stirred for ~20 h. The resulting solution was filtered, affording a white powder. After drying in a high vacuum the yield of TEDA·AlH₃ was about 1 g (79 %).

Preparation of piperidinoalanes

The three complexes of piperidine (pipH) with alane, [pipAlH₂]₂ (**1**), [pip₂AlH]₂ (**2**) and [pip₂Al]₂ (**3**) were formed upon adding 1 mL (10.1 mmol, 1 : 1 / AlH₃ : pipH), 2 mL (20.2 mmol, 1 : 2 / AlH₃ : pipH) or 3.5 mL (35.4 mmol, 1 : 3.5 / AlH₃ : pipH) of piperidine in diethyl ether (20 mL), respectively, to the solution of 0.304 g (10.1 mmol) of AlH_3 in diethyl ether (20 mL). For AlH_3 solution preparation, 0.337 g (2.5 mmol) of $AlCl_3$ in 5 mL

diethyl ether and 0.288 g (7.6 mmol) of LiAlH$_4$ in 15 mL diethyl ether were dissolved separately and then mixed by adding AlCl$_3$ solution to the LiAlH$_4$ solution. The resulting suspension was stirred for several minutes and precipitated LiCl was removed by filtration. Before adding the piperidine solution, the AlH$_3$ solution was pre-cooled in a dry ice/isopropanol bath. The reaction flask was allowed to reach room temperature and was stirred until gas evolution had ceased. The soluble piperidinoalane was recovered from diethyl ether under a dynamic vacuum at room temperature in each case. Compound **1** was purified by sublimation at 45 °C giving colorless crystals. Purification of **2** and **3** was performed by recrystallization in pentane at -30 °C to afford colorless crystals after a few days in both cases.

3.2.3 Preparation of activated aluminum

Preparation of activated aluminum powder by the liquid procedure

The synthesis route of Ti-activated aluminum (henceforth denoted as Al*(Ti)) followed the procedure developed by Graetz et al.[51], which is based on mixing LiAlH$_4$ and AlCl$_3$ with 2 mol % of TiCl$_3$ or Ti(OBu)$_4$. The solution of the additive in diethyl ether was added to LiAlH$_4$ and AlCl$_3$ mixture in diethyl ether and then filtered to remove precipitated LiCl. The solvent was evaporated from the filtrate and the remaining solid was dried and then was decomposed under vacuum at 80 °C. Additionally, this synthesis was modified by changing the transition metal (TM) additive to ZrCl$_4$, HfCl$_4$, or YCl$_3$ (henceforth denoted as Al*(Zr), Al*(Hf), Al*(Y)).

The uncatalyzed Al powder (for the control experiment) was prepared in the same way, except no additive was included in the synthesis. The decomposition of alane was performed at a higher temperature (150 °C).

Preparation of activated aluminum powder by ball milling approach

Aluminum powder and TM additive at a molar ratio of 1:0.02 were added to a ball milling jar made of tungsten carbide. The ball-to-powder weight ratio was fixed at 20:1 with balls also made of tungsten carbide (balls: 2 x 8 g). The milling process was carried out on a Fritsch Pulverisette 6 planetary ball mill at a speed of 400 rpm for 2 h. After the milling process, the product was collected as a fine dark grey powder.

3.2.4 Direct hydrogenation of activated aluminum supported by amine

The hydrogenation experiments were conducted in the autoclave reactor, the general setup is depicted in Figure 3.4. As all of the used reactants were oxygen and

moisture sensitive, the reactor was transferred into the glove box for filling and removing the reaction mixture.
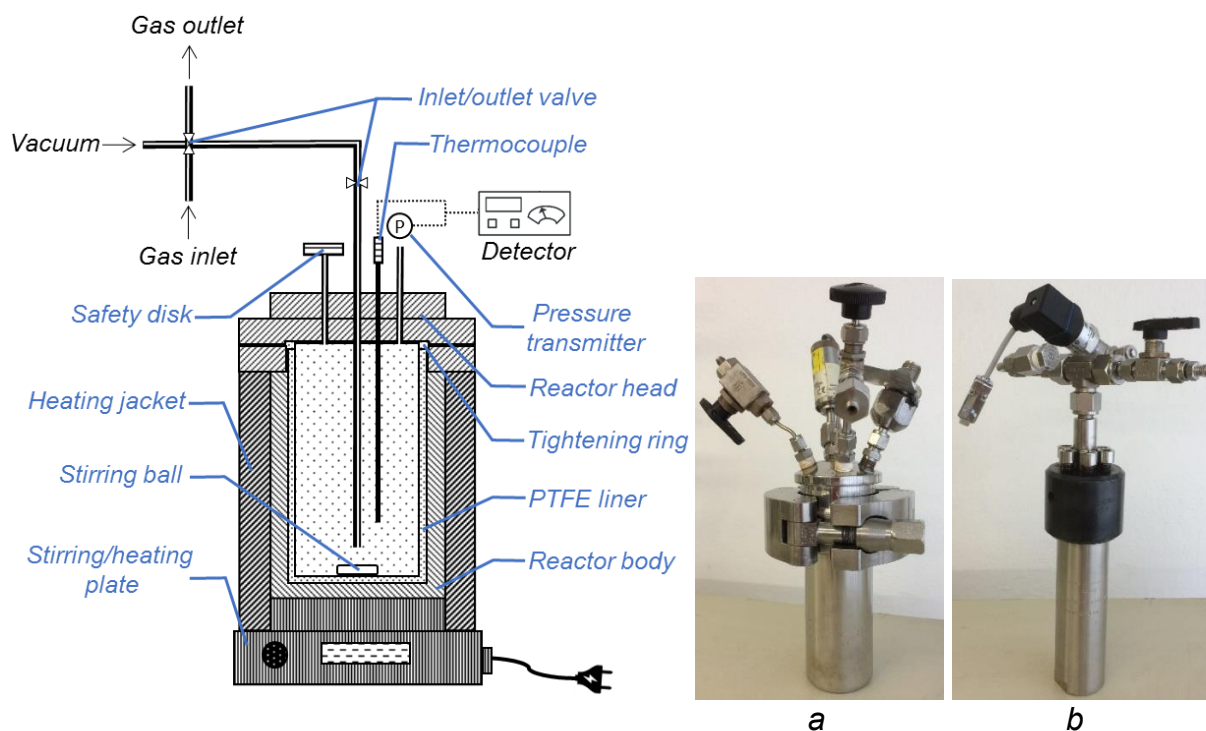
Figure 3.4 *Laboratory setup with the autoclave reactor (a – Berghof reactor (150 ml); b – Parr reactor (75 ml)) used for the direct hydrogenation of aluminum and amine.*

Autoclave reaction with activated aluminum and triethylenediamine

The hydrogenation reactions were carried out in the 150 mL stainless steel reactor (Berghof; Figure 3.4, a) with a PTFE liner (100 ml) and equipped with a 200 bar pressure transmitter (MKS). The direct hydrogenation experiment was carried out using the following protocol: the reactor was loaded in a glove box with 0.317 g (11.8 mmol) of Al*(TM), 3.6 g (32.1 mmol) of TEDA, and 21 mL of THF under the inert atmosphere. The rest of the inert gas was removed by evacuating the reactor, after placing it outside of the glove box. Next, hydrogen gas was added to the reactor. After 92 h of stirring at room temperature, the reaction was stopped. The hydrogen pressure was released and the reactor was placed in the glove box for removing and filtrating the reaction mixture. A blank experiment with non-activated aluminum powder was performed in the same manner.

Direct synthesis with activated aluminum and piperidine

Hydrogenation and dehydrogenation reactions were carried out in a 75 mL stainless steel reactor (Parr Instruments; Figure 3.4, b) with a PTFE liner (40 ml) and equipped with the 250 bar pressure transmitter (Wika). Under an inert atmosphere, the

reactor was loaded with 0.55 g (20.3 mmol) of activated aluminum, 2 mL (20.2 mmol) of piperidine, and 25 mL of THF. The reactor was sealed and then evacuated to remove the inert gas phase. Afterward, the reactor was pressurized with hydrogen gas and heated if it was necessary. Before releasing hydrogen, the reactor was cooled with ice to prevent the release of the solvent. The unreacted Al*(TM) was removed from the soluble product by filtration. The solvent was evaporated under reduced pressure and the residue was dried under vacuum at room temperature resulting in a grey crystalline powder. A blank experiment using aluminum without any TM additive was carried out under the same conditions.

3.3 Results and discussion

The main effort of this work was focused on the synthesis of aminoalanes and the development of Al-N-based systems suitable for reversible hydrogen uptake. For this reason, several aminoalanes were synthesized and their hydrogen storage properties were tested. In order to define the optimal conditions for aminoalane preparation, several reaction approaches were investigated and modified. The importance of aluminum activation for the reversible hydrogenation in aminoalanes was highlighted. Using a variety of transition metal compounds, a suitable additive for the reversible piperidinoalane system has been found. The structure and the thermal properties of three piperidinoalanes have been investigated. The crystallographic analysis revealed two new crystal structures of piperidinoalanes.

One of the main techniques used in this work was NMR spectroscopy to obtain information about the structure of aminoalanes and the kinetics of the hydrogenation/dehydrogenation processes. As a result of this work, the hydrogenation cycle of the aminoalane system employing activated aluminum and piperidine was proposed.

3.3.1 Is the solid-state hydrogen storage in aminoalanes possible?
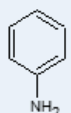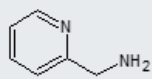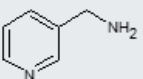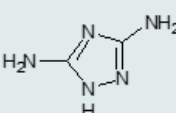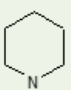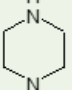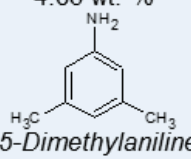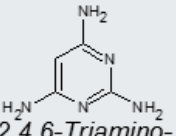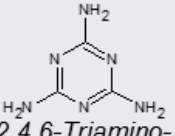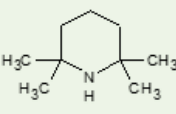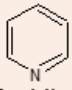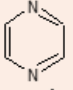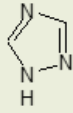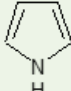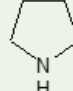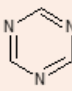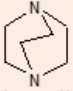
In the past, the reversible hydrogen uptake in aminoalanes was shown only in the presence of solvents. However, to the best of our knowledge, no hydrogen uptake was achieved in purely solid systems. In addition, complexes of AlH_3 with aliphatic amines have been more intensively studied compared to heterocyclic amines. As a result, many of these complexes are yet unexplored and their properties are unknown. Therefore, in the present study, mainly heterocyclic amines were examined. Systematic investigations of these systems may reveal the material that matches simultaneously the thermodynamic and hydrogen storage capacity requirements. The complexation of alane with heterocyclic amines has several advantages, in respect to hydrogen storage, compared to aliphatic amines. First, the bulkiness of the amine could prevent the alane from polymerization. Second, the boiling points of heterocyclic amines are usually higher than the ones of the corresponding aliphatic amines; and in addition, the formed aminoalanes do not sublimate, and thus the resulting aminoalanes can be used even at high temperatures.

In order to find the suitable aminoalanes for reversible hydrogenation several specific tasks were defined:

➢ To investigate the capability of primary, secondary, and tertiary cyclic amines to form aminoalanes.

➢ To develop and optimize the synthesis procedure for crystalline aminoalanes.

➢ To build the equipment for testing hydrogen sorption properties of synthesized materials ($P(H_2)_{max}$ = 1000 bar, T = 0 - 250 ºC).

➢ Hydrogen release/uptake tests and determination of the stability and long-term behavior of synthesized aminoalanes.

In the first stage, systematic investigations of the several five- and six-membered ring heterocyclic and aromatic amines were performed in order to synthesize aminoalanes with desired properties (stability, crystallinity, high hydrogen content, and fast hydrogen release). Depending on the substituents on the N-atom and the number of N-atoms in the molecule (Table 3.4), the formed aminoalanes can offer a comparably high gravimetric storage capacity.

Table 3.4 *The selected amines considered for the synthesis of aminoalanes.*

*the gravimetric hydrogen storage capacity that can be achieved by the in the corresponding amine-alane complex

In the course of this work, to obtain the desired crystalline aminoalanes, several synthesis routes were applied:

1. *Direct reaction between aluminum hydride and amine (all amines showed in Table 3.4 were tried in this synthesis approach):*

   - with alane and amine in THF
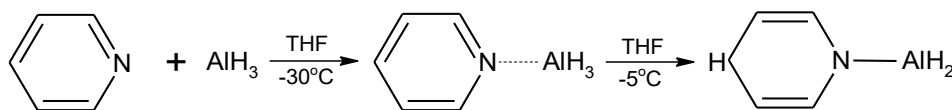
Scheme 3.5 *The proposed reaction of pyridine with aluminum hydride in THF solution.*

Advantages: simple synthesis procedure; no additional by-products.

Disadvantages: possible polymerization of the alane during preparation; strong coordination of alane by THF; time-consuming procedure for alane preparation; passivation of the surface during storage of alane; a short lifetime of alane (up to 7 days); amorphous product (in most cases).

   - with a diethyl ether solution of alane and amine
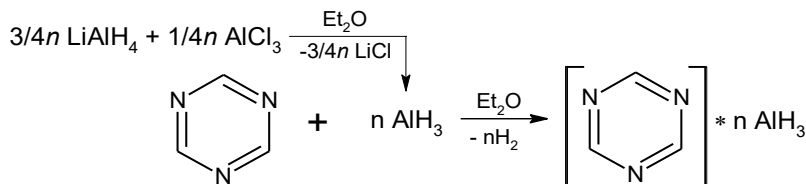
Scheme 3.6 *The proposed reaction path for the synthesis of triazine alane from AlH$_3$ ethereal solution and triazine.*

Advantages: fast preparation of alane; no additional by-products.

Disadvantages: possible polymerization of the alane during preparation; highly pyrophoric/explosive aminoalanes are formed; amorphous product (in most cases); low solubility of some amines in diethyl ether.

2. *Direct reaction between alkyl aluminum and amine (aniline, 2-picolylamine, 3-picolylamine, 2,4,6-triaminopyrimidine, 2,4,6-triamino-1,3,5-triazine, pyrazine, pyrrole)*
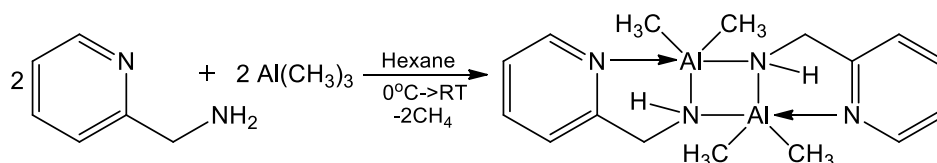
Scheme 3.7 *The formation of dimeric aminoalane by the reaction between 2-picolylamine and trimethylaluminum[215].*

Advantages: DIBAL, TMAL are known as efficient hydrogenation catalysts; the large substituent on Al can prevent the polymerization, thus a crystalline aminoalane may be formed; usage of non-coordinating solvents (pentane, hexane, toluene).

Disadvantages: low theoretical hydrogen content of the formed aminoalanes; difficult work up due to insolubility of some amines.

3.   *Synthesis via chloramine (trichlormelamine)*
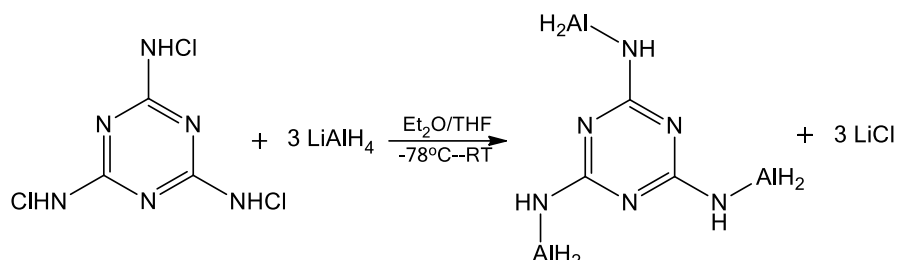
Scheme 3.8 *The proposed reaction of trichlormelamine with lithium aluminum hydride in ethereal solution.*

Advantages: new alternative synthesis route; simple removal of the by-product; soluble reactants.

Disadvantages: possible unknown side reactions; amorphous product.

4.   *Cascade reaction with aluminum chloride, lithium alanate and amine (2,4,6-triaminopyrimidine, 2,4,6-triamino-1,3,5-triazine)*
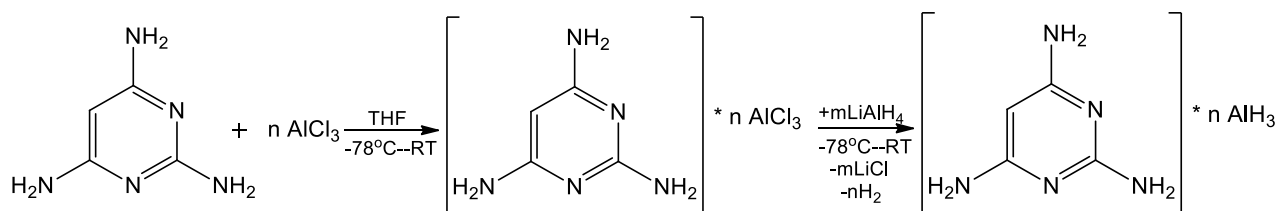
Scheme 3.9 *The stepwise reaction of 2,4,6-triaminopyrimidine with aluminum chloride and lithium alanate.*

Advantages: formation of soluble intermediates, *in situ* production of AlH$_3$.

Disadvantages: possible unknown side reactions; amorphous products.

5.   *Salt reaction between lithium alanate and amine hydrochloride (piperidine hydrochloride)*
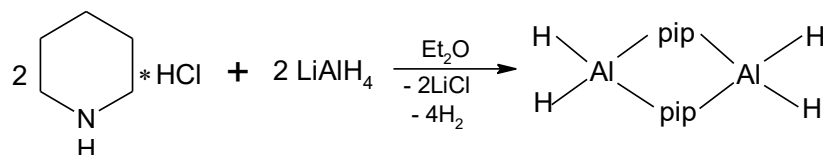
Scheme 3.10 *The reaction between piperidine hydrochloride and lithium alanate (pip = piperidinyl)[216].*

Advantages: simple procedure, soluble reactants.

Disadvantages: not all amines are commercially available as hydrochlorides; the purification of the product is necessary.

6. *Transamination reaction (aniline, 3,5-dimethylaniline, 3-picolylamine, 2,4,6-triamino-1,3,5-triazine, 2,2,6,6-tetramethylpiperidine)*
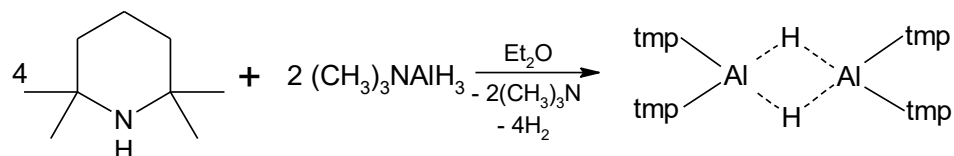
Scheme 3.11 *Transamination reaction between trimethylamine alane and 2,2,6,6-tetramethylpiperidine (tmp = 2,2,6,6-tetramethylpiperidinyl)[188].*

Advantages: soft reaction conditions; possible suppression of the oligomerization.

Disadvantages: requirement of an additional step for the preparation of starting aminoalane; the exchange reaction cannot be conducted with all amines.

7. *Direct hydrogenation of activated aluminum and amine (pyridine, pyrazine, pyrrole, pyrrolidine, piperidine, 2,2,6,6-tetramethylpiperidine, triethylenediamine)*
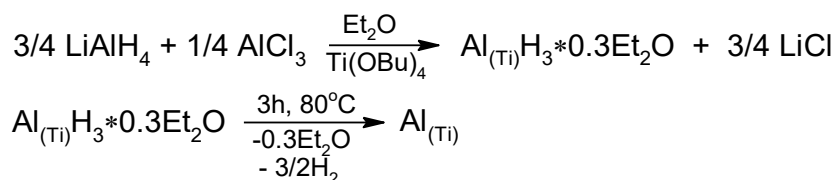
Scheme 3.12 *Preparation of Ti-activated aluminum according to the approach developed by Graetz et al.[51].*
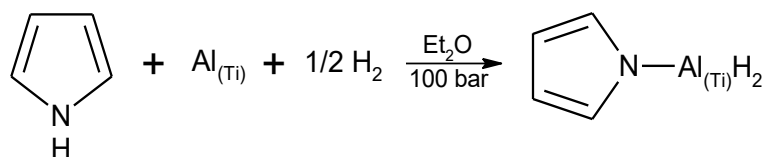
Scheme 3.13 *Formation of pyrroloalane via direct hydrogenation of Ti-activated aluminum supported by pyrrole.*

Advantages: cheap reactants are used; reversible hydrogenation is possible.

Disadvantages: the activation of aluminum is needed; the proceeding of the reaction depends on substituents bound to the nitrogen atom.

Numerous modifications of the original procedure for the preparation of aminoalanes have been studied, to make the formation of crystalline aminoalanes possible. Most of the modifications involved the use of different reactants. As a reaction medium, tetrahydrofuran was mainly used, but other solvents were also tested, these included diethyl ether, hexane, pentane, benzene, and toluene. However, none of these solvents, except Et₂O, proved to be superior to THF. In hexane, pentane, benzene, and toluene amines and alane appear to be insoluble, and as result, no reaction was observed. The low solubility of amines determines the reaction rate and decreases the yields and purity of the product (Appendix A, Table A.1). In some cases,

the use of THF or Et$_2$O leads to the formation of gelatinous deposits, which made filtration difficult and sometimes even impossible. Another reason why aminoalane was not observed may be the slow reaction kinetics of its formation. Because of that aluminum hydride may be formed, polymerized, and precipitated out of the solution before it can react with the amine species.

In order to avoid the disadvantages of the known syntheses, several alternative approaches for producing aminoalanes were developed in this work. Based on the performed experiments, it can be concluded that the stability of the formed aminoalanes highly depends on the type of amine. For example, the heteroaromatic amines (e.g. 2,4,6-triaminopyrimidine, 2,4,6-triamino-1,3,5-triazine, pyrrole, pyridine, pyrazine) result in unstable (in the case of triazine and 2-picolylamine – explosive) amorphous compounds with an unknown composition (Appendix A, Table A.2 and A.3, Figure A.1 and A.2). In general, the formation of amorphous compounds could occur because of several reasons. Aluminum hydride is a strong reducing agent, thus the aromatic ring of an amine can be easily hydrogenated forming mixtures of different isomers[217]. Alane can also lead to the reductive cleavage of the solvent[218,219] and its further interaction with the amine and incorporation into the structure of the formed aminoalane (Appendix A, Fig. A.3). Therefore, the hydrogenation of these materials is arguably due to the complicated and undefined nature of the formed products. In contrast, heterocyclic nonaromatic amines (e.g. pyrrolidine, piperidine, 2,2,6,6-tetramethylpiperidine) release hydrogen during the reaction with alane and form partly dehydrogenated crystalline aminoalanes.

The aminoalanes, which were obtained in good yields, were systematically investigated under hydrogen pressure up to P(H$_2$)$_{max}$ = 1000 bar in a temperature range T = 0 - 100 ºC, for their hydrogen uptake (Appendix A, Table A.4). The equipment for measuring hydrogen absorption based on the volumetric method was constructed and modified (Appendix A, Fig. A.5). Unfortunately, none of the investigated aminoalanes showed hydrogen uptake in solid-state. It was concluded that the reaction of primary or tertiary amines (e.g. 2,4,6-triaminopyrimidine, 2,4,6-triamino-1,3,5-triazine, pyridine, pyrazine) with alane produces polymerized products. The hydrogenation of whose is hampered by the high stability of the formed polymer. Secondary amines tend to form strong dimers or trimers with alane, the products of which have been proven to be too thermodynamically stable to allow hydrogenation. Even bulky groups on N or Al atoms (e.g. 3,5-dimethylaniline, 2,2,6,6-tetramethylpiperidine, reactions with DIBAL or TMAL) did not prevent the dimerization

of aminoalane. Therefore, another strategy, described in the next section, has been developed to overtake these obstacles and to achieve the main goal of this work.

3.3.2 Optimization of the direct hydrogenation of activated aluminum supported by amine

In recent years, it was established in the literature that aluminum can be hydrogenated in the presents of stabilizing agents (e.g. amine, ether). Depending on the stability of the formed adduct, hydrogen can be reversibly released through different pathways (Section 3.1.2). It was shown that the direct hydrogenation of aluminum can only take place in the presence of strong coordinating solvents, like dioxane or THF[51,209], that can stabilize the alane during the formation of the amine-alane complex. Another important issue is that hydrogenation can only proceed with activated aluminum. That said, from all transition metals, only Ti was examined for aluminum activation thus far. However, it has also been demonstrated that other TMs are useful to achieve reversibility in alanate systems[83,89]. It was therefore of interest to investigate whether or not it would be possible to synthesize amine-alane complexes or Al-H functionalized aminoalanes, potentially more efficiently, by activating aluminum with other TM activating agents. Furthermore, the optimization of the existing method and the development of a new pathway for reversible hydrogen storage in aminoalane systems have been discussed.

3.3.2.1 Synthesis and characterization of triethylenediamine alane complex

Triethylenediamine alane complex (TEDA·AlH$_3$) can be synthesized in several ways (Scheme 3.14). In this section, the direct hydrogenation of activated aluminum in the presence of TEDA will be discussed in detail.

The first synthesis of the triethylenediamine alane adduct was originally performed in 1964 by Ashby[196]. The reaction took place in a THF solution of TEDA with activated aluminum at a hydrogen pressure of 350 bar and temperature of 70 ºC. The activation procedure was carried out by treating aluminum powder with triethylaluminum[220]. This approach did not attract much attention until the discovery by Graetz et al.[51], that this system can be reversibly hydrogenated at much milder conditions (35 bar and room temperature) by using titanium doped aluminum (Scheme 3.14, first row).
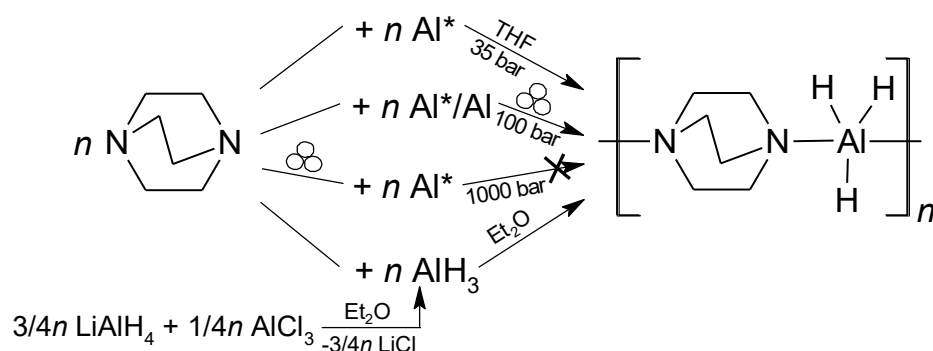
Scheme 3.14 *Possible pathways for the synthesis of the TEDA·AlH₃ adduct.*

Recently, we have published the mechanochemical synthesis of the TEDA·AlH₃ adduct starting from Al powder and TEDA under 100 bar of hydrogen pressure[221]. Initially, it was assumed that a catalyst would be necessary for the hydrogenation of aluminum. Therefore, this synthesis (Scheme 3.14, second row) was first tested with aluminum activated by the catalyst, resulting in conversion as low as 19 % after 6 h of milling time. Surprisingly, by using metallic aluminum, the conversion of Al has reached 43 % after 6 h and was increased up to 90 % with the prolonged milling time (72 h) even without the addition of an activation agent or solvent. However, the prior ball milling of TEDA with Al and the subsequent exposure of this solid mixture to hydrogen pressure up to 1000 bar did not lead to the TEDA·AlH₃ complex (Scheme 3.14, third row), signifying the importance of the processes (e.g. the increased temperature and the close contact of the reactants) that occur during milling under the hydrogen pressure.

Another commonly used synthesis for the preparation of aminoalanes involves two steps procedure shown in Scheme 3.14 (fourth row). The first stage of the synthesis is the preparation of an ethereal solution of aluminum hydride. This solution is generated by mixing LiAlH₄ with AlCl₃ in Et₂O. In the second step, by adding the TEDA solution in the AlH₃ ethereal solution the TEDA· AlH₃ complex is formed. However, the formed TEDA·AlH₃ adduct by this approach is not recoverable (the dehydrogenated material cannot be recharged, since aluminum in alane is not activated), and will be further used only for the preparation of the reference material.

The mechanochemical approach (Scheme 3.14, second row) is a convenient method for the preparation of the TEDA·AlH₃ adduct, however, the dehydrogenation step requires heating above 200 ºC, and as a result, TEDA is evaporated and contaminates the released hydrogen. In contrast, in the organometallic method (Scheme 3.14, first row), which involves the THF slurry of TEDA and Ti-activated

aluminum, the dehydrogenation occurs already at 120 ºC. Nevertheless, the efficiency of the hydrogen regeneration pathway is highly dependent on the yield of the product, which was only 60 %[209]. Therefore, in order to improve the yield of the TEDA·AlH$_3$ complex, other TM additives as activating agents for aluminum were tested in this work.

Following the original procedure for the TEDA·AlH$_3$ synthesis developed by Graetz[51] (Scheme 3.14, first row), the reaction was performed in an autoclave reactor with Ti-activated Al and TEDA in THF. Hydrogen gas was added to the reactor at pressures of 41.6 bar at room temperature. The hydrogen uptake during the hydrogenation of Ti-activated Al and TEDA is shown in Fig. 3.5. The hydrogenation occurred over 90 h, reaching a final pressure of 30.3 bar. The pressure drop was ~11.3 bar from which ~2.8 bar due to dissolution of H$_2$ in the reaction mixture (tested with non-activated aluminum). The long hydrogenation time may be attributed to the heterogeneous solid-liquid-gas reaction which takes place in the reactor and requires the interaction between solid Al*(Ti), dissolved TEDA, and hydrogen gas. Thus, the slow reaction kinetics is not surprising.
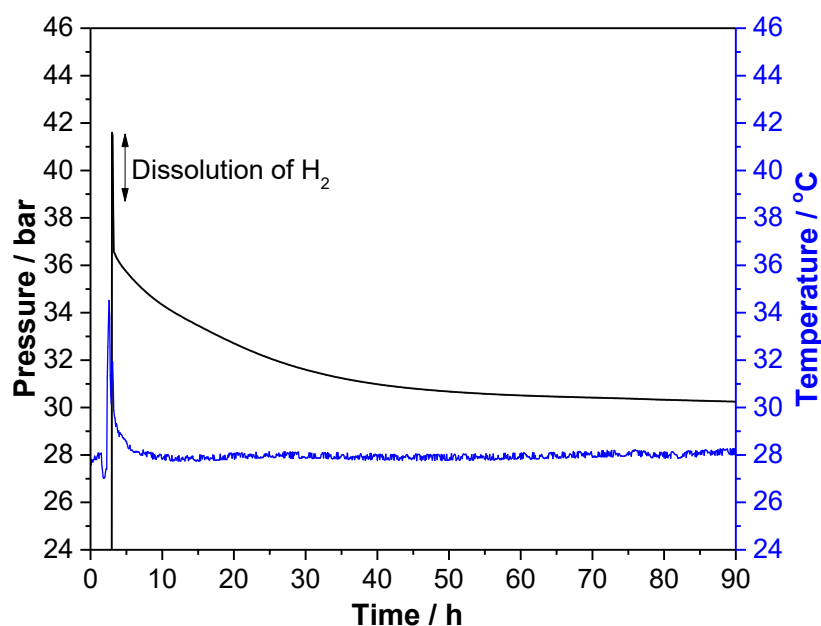
Figure 3.5 *Reactor pressure during the direct hydrogenation of Ti-activated aluminum and TEDA in THF solution.*

After hydrogenation, the solid amine-alane complex was recovered by filtration. Data obtained from the elemental analysis showed a good agreement with theoretically calculated values and values obtained from the reference material formed by the wet chemical method (Table 3.5).

Table 3.5 *Elemental analysis and ICP-OES of the product formed by different synthesis methods.*

		N	**C**	**H**	**Al**
Calculated	TEDA·AlH$_3$	19.70	50.69	10.63	18.98
Found	TEDA·AlH$_3$	18.71	49.51	10.97	18.95
Found	TEDA·Al$_{(Ti)}$H$_3$	19.00	47.69	10.49	21.34*

*for the direct synthesis the Al content is slightly higher due to the unreacted aluminum left after reaction, which cannot be separated

The XRPD patterns of the reference product and product formed from Al*(Ti) in this work were compared (Fig. 3.6). The XRPD pattern of the reference product formed from ether solution displays broader reflections compared to the pattern of the product from the direct hydrogenation, most probably resulting from the low degree of order in the crystal structure caused by the short reaction time (~20 h), the elongated reaction time can improve the intensities significantly[221].
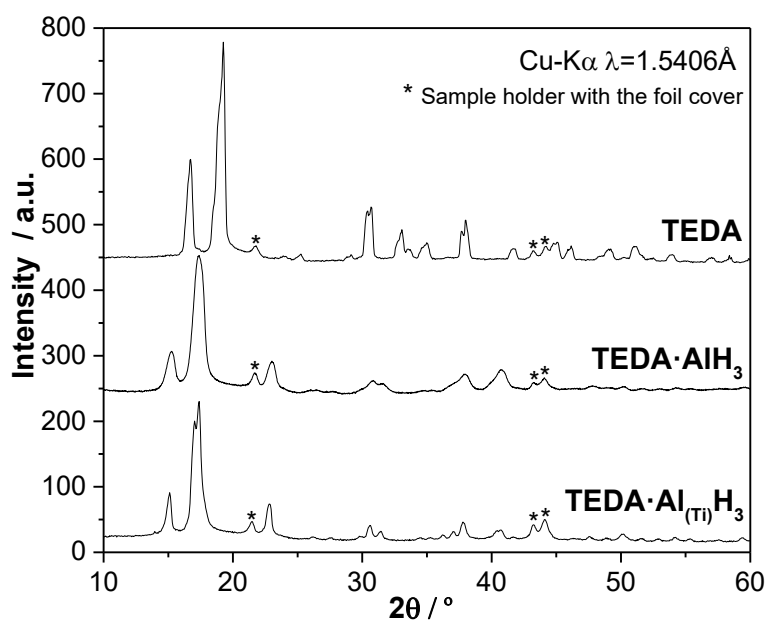
Figure 3.6 *Comparison of XRPD patterns: pure TEDA (top), product received via the wet chemical method (middle), product obtained from the direct hydrogenation of Ti-activated Al* and TEDA in THF solution (bottom).*

The XRPD data of the TEDA·AlH$_3$ complex was previously presented by Graetz[51], however, its crystal structure was not described. The synthesis and the structure determination of the TEDA·AlH$_3$ adduct were performed by the project partner group in the Max-Planck-Institut für Kohlenforschung, Department of Heterogeneous Catalysis (Mülheim) and revealed the structure of an 1-D-coordination polymer[221] shown in Figure 3.7.
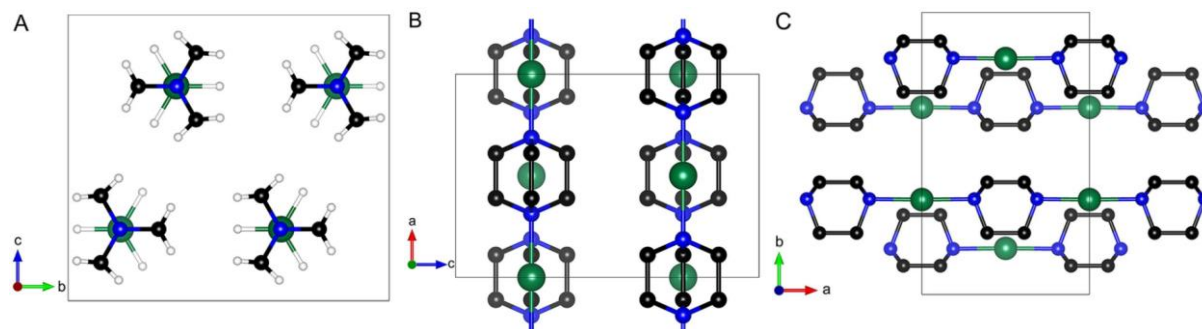
Figure 3.7 *The structure of polymeric [TEDA-AlH₃]ₙ (white: H, green: Al, blue: N, black: C atoms) depicted along a axis (A), b axis (B, H atoms omitted), and c axis (C, H atoms omitted)*[221].

The crystal structure is described in the orthorhombic centrosymmetric space group *Cmcm* (63). The aluminum atom is penta-coordinated by three hydrogen atoms in the basal plane and two equivalent nitrogen atoms in capping positions to form a nearly ideal trigonal bipyramid. Both nitrogen atoms of the TEDA ligand are coordinating to equivalent AlH_3 to form polymeric chains along the *a* axis (Fig. 3.7). The polymeric chains are shifted by ½ *a* to achieve dense packing. The hydrogen atoms connected to aluminum are orientated staggered to the TEDA ligand[221].

For the investigation of transition metals activity for the direct formation of TEDA·AlH_3 from activated aluminum, a series of additives were applied ($ZrCl_4$, $HfCl_4$, YCl_3). In section 3.2.3, the synthesis route for introducing the transition metal into aluminum was described. A typical hydrogenation experiment was carried out in the same way as with Ti-doped aluminum mention above, just the type of activated aluminum was varied. After the synthesis, the yield of TEDA-AlH_3 was in agreement with the literature, determined to be 60 %[209] in the case of $Ti(OBu)_4$ as an additive, approximately 95 % for $ZrCl_4$, and 91 % for $HfCl_4$ (Table 3.6). No product was observed after synthesis with aluminum activated by YCl_3. These results demonstrated the advantage to use Zr or Hf as the activation agent instead of Ti.

Table 3.6 *The yield and desorption temperature of TEDA·AlH_3 complex formed from Al activated with the different additives.*

Additive	Yield, %	T_{des}, °C
$ZrCl_4$	95	237
$HfCl_4$	91	256
$Ti(OBu)_4$	60	238
YCl_3	-	-

It is noteworthy, that activation of metallic Al was also possible by ball milling TM salt with Al powder. However, aluminum prepared by ball milling (section 3.2.3) showed

a lower hydrogenation activity (74 %, yield of TEDA-AlH$_3$ by using mechanochemical activation of Al with ZrCl$_4$) than the Al activated by the liquid procedure (95 %) and therefore the former one was not further used.

The decomposition behavior of TEDA·AlH$_3$ complexes formed by the different synthesis procedures was investigated by simultaneous thermal analysis (TG-DSC). An endothermal process was observed at 269 °C (Fig. 3.8), accompanied by a mass loss of 55 %, and corresponding to the decomposition of the polymeric complex. In comparison, the complex formed by the direct hydrogenation of Al*(Zr) has a slightly lower decomposition temperature of 237 °C, compared to the standard TEDA·AlH$_3$ complex prepared without activated aluminum. This effect can be attributed to the introduction of the atoms of TM-additive into the complex structure, and as a result, could have lowered the decomposition temperature of the complex.
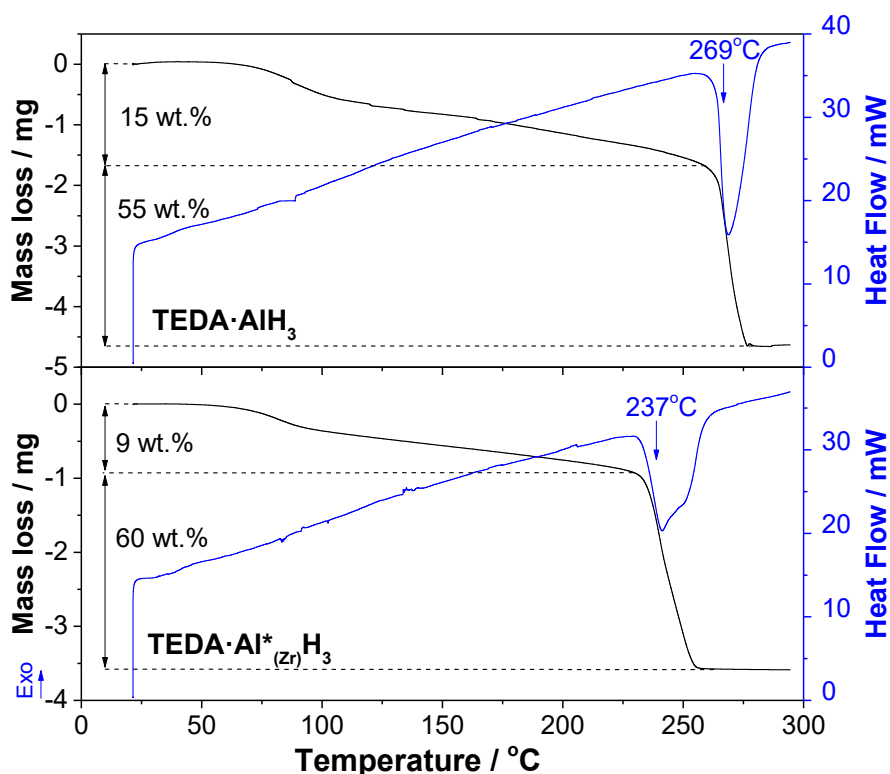
Figure 3.8 *TG-DSC data of the TEDA·AlH$_3$ complex obtained via the wet chemical synthesis (top) and the product formed by the direct hydrogenation of Zr-activated aluminum supported by TEDA (bottom).*

Starting from ~80°C, a mass loss occurred in both cases, which can be explained by the removal of the residual solvent traces, due to the absence of an additional effect before the decomposition signal.

Summarizing, the described herein hydrogen absorption by the TEDA-Al*-slurry occurs readily at temperature and pressures well within the range for hydrogen storage applications in high yield. Unfortunately, this system suffers from a high

dehydrogenation temperature above 200 °C. Nevertheless, this procedure can be applied for the stabilization of AlH_3 via complexation with TEDA and the long-term storage of alane. The search for suitable amines for the formation of aminoalanes with desired properties may help to avoid the drawbacks of this system.

3.3.2.2 Synthesis of aminoalanes via direct hydrogenation of activated aluminum and N-heterocyclic amine

The simplicity of the direct hydrogenation of aluminum in the presence of amine makes it suitable for the preparation of other aminoalanes. Since Graetz and coworkers[209] used several tertiary amines for the synthesis of amine-alane complexes, it was of interest to investigate, if the synthesis can be conducted also with the secondary amines. As the focus of this work was on the heterocyclic amines, the hydrogenation tests were performed using six aromatic and non-aromatic heterocyclic amines (pyrrole, pyrrolidine, pyrididne, pyrazine, piperidine, 2,2,6,6-tetramethylpiperidine), in order to establish a criterion for the formation of aminoalanes from aluminum and corresponding amines (Appendix A, Table A.5). No product was detected after synthesis with pyridine, pyrazine, or tetramethylpiperidine. The obtained results indicate that several factors may play a role in the direct synthesis of aminoalane. The first important criterion is the base strength differences of the amines. Usually, secondary amines are stronger bases than tertiary amines, thus, a more basic amine is able to satisfy the electrons deficiency of the Lewis-acidic Al center and the formation of a stable complex is encouraged. The basicity of the tested amines increases in the order pyrrole < pyridine < pyrazine < tetramethylpiperidine < piperidine < pyrrolidine. Hence, the formation of pyridinoalane (pyridine pK_b = 8.75) is less favorable than the formation of piperidinoalane (piperidine pK_b = 2.88).

The steric effect of the amine ligand is also an important factor for the complex formation[222]. In particular, tertiary amine-alane complexes with alkyl substituents are usually less stable than complexes with the corresponding primary and secondary amines[209]. In sterically crowded amines, the close approach of the AlH_3 species to the Lewis base electron pair on the N atom is hindered. Consequently, from tetramethylpiperidine and piperidine, which have nearly the same base strength (pK_b 2.94 and 2.88, respectively), only piperidine forms complexes with alane.

The other tested amines (pyrrole and pyrrolidine) were also able to form complexes with aluminum, however, the investigation of the formed products revealed only the dehydrogenated forms of the corresponding aminoalanes (Appendix A,

Fig. A.8). Therefore, the investigation of these systems for hydrogen storage purposes was not performed. From all six investigated amines only piperidine holds the potential for the reversible hydrogenation of its aminoalane and will be further discussed in detail.

Based on these results, the following trends were observed:

1. Tertiary amine-alane complexes have lower stability than corresponding complexes with secondary amines.

2. With the increase of the base strength of the amines, the capability to form complexes with AlH_3 is increasing.

3. The increase of steric substituent on nitrogen atom hampers the aminoalane formation.

It should be also noted, that tertiary amines are desirable for the reversible splitting of AlH_3 from amine-alane complexes, in contrast, secondary amines resulting in the stable partly dehydrogenated aminoalane compounds (e.g. $C_5H_{10}NAlH_2$), where only Al-H splitting would be possible.

3.3.3 Investigation of piperidinoalanes for reversible hydrogen uptake

The theoretical hydrogen storage capacity of the piperidine-alane complex is about 3.47 wt.- %, which is high compared to the other known reversible amino-alane systems (Section 3.1.2, Table 3.2). In order to fully investigate the potential of piperidinoalane as a hydrogen storage material, the hydrogenation mechanism of aluminum in presence of piperidine needs to be understood. Therefore, the properties of the formed piperidinoalanes should be investigated first.

3.3.3.1 Crystal structure determination of piperidinoalanes

Piperidinoalanes $[(pip)_nAlH_{3-n}]_2$ (n = 1 (**1**), 2 (**2**), 3 (**3**)) have been know before[195,216,223], but no crystallographic studies on $[(pip)_2AlH]_2$ (**2**) and $[(pip)_3Al]_2$ (**3**) have been published. Therefore, in the present study, the crystal structure investigations of these piperidinoalanes were conducted.

In this work, three piperidinoalanes were synthesized from freshly prepared alane solution in diethyl ether and piperidine (pipH), by varying the ratio between the reactants according to the following reaction scheme:

$$^3/_2 \text{ LiAlH}_4 + \,^1/_2 \text{ AlCl}_3 \xrightarrow[-\,^3/_2 \text{ LiCl}]{\text{Et}_2\text{O}}$$

$$2 \text{ AlH}_3 + 2n \text{ pipH} \xrightarrow[-2n \text{ H}_2]{\text{Et}_2\text{O}} \left[\text{pip}_n\text{AlH}_{(3-n)}\right]_2$$

$$n = 1, 2, 3$$
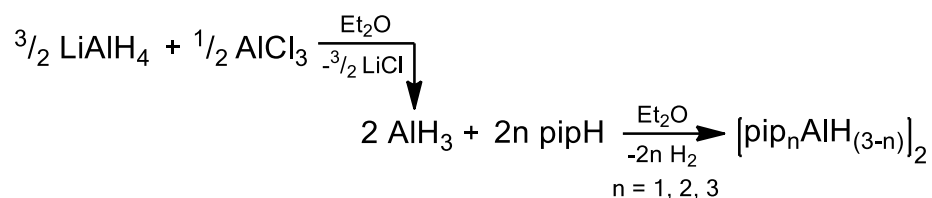
Scheme 3.15 *Synthesis of piperidinoalanes via dehydrogenative substitution of aluminum hydride with piperidine.*

The crystals of **1** obtained by sublimation were in agreement with the crystal structure earlier described[216]. It consists of a dimeric structure based on a cyclic [AlN]$_2$ core (Fig. 3.9). The compound crystallizes in the monoclinic space group $P2_1/c$ with Z = 2. The molecule is located on a center of inversion and the asymmetric unit is comprised of the one-half dimer. The molecular structure of **1** is similar to those of 2,6-dimethylpiperidinoalane[188] and diethylaminoalane[189], which are confirmed to be also dimeric. This situation contrasts with 2,2,6,6-tetramethylpiperidinoalane[188], in which cyclization via the Al–H bonds occurs due to steric crowding of the methyl groups leading to the formation of a trimer.
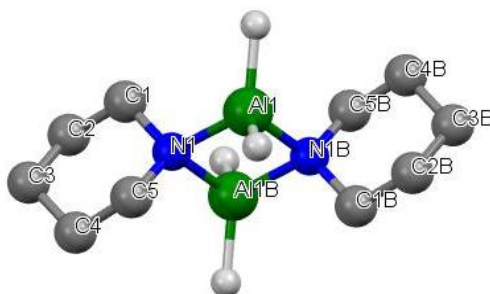
Figure 3.9 *Molecular structure of [(pip)AlH$_2$]$_2$ (**1**)[216].*

The results of single-crystal studies, performed in this work, showed that **2** and **3** are composed of dimers, as illustrated in Fig. 3.10 and 3.11. Table 3.7 shows the crystallographic data and gives information on data collection and structure refinement. The full crystal data information is presented in Appendix B (Table B.1 and B.2).

Table 3.7 *Data of crystal, data collection and structure refinement for [pip$_2$AlH]$_2$ (**2**) and [pip$_3$Al]$_2$ (**3**).*

Compound	2	3
Empirical formula	$C_{20}H_{42}Al_2N_4$	$C_{30}H_{60}Al_2N_6$
Formula weight	392.53	558.80
T, K	160(2)	160(2)
λ, Å	0.71073	0.71073
Crystal system	Orthorhombic	Triclinic
Space group	$Pbca$	$P\bar{1}$

a, Å	12.5724(5)	8.6112(9)
b, Å	17.8509(8)	8.8513(9)
c, Å	20.6212(10)	10.9777(10)
α, °	90	95.138(8)
β, °	90	90.659(8)
γ, °	90	108.065(8)
Z/D_c, g cm^{-3}	8/1.127	1/1.172
μ, mm^{-1}	0.137	0.121
$F(000)$	1728	308
Crystal size, mm	0.5 × 0.3 × 0.1	0.3 × 0.2 × 0.1
Θ range for data collection	2.8–26.0	2.9–27.0
Reflections collected	28952	10488
Independent reflections/ R(int)	4533/0.0453	3419/0.0387
Completeness to Θ max	99.8 %	99.5 %
Refinement	Full-matrix least-squares on F^2	
Data/restraints/ parameters	4533/42/478	3419/0/172
Goodness-of-fit on F^2	1.102	1.050
R_1/wR_2 [$I > 2\sigma(I)$]	0.0473/0.1129	0.0417/0.1006
R_1/wR_2 (all data)	0.0681/0.1216	0.0638/0.1124
Largest diff. peak/ hole, e Å^{-3}	0.196/–0.227	0.304/–0.264

Compound **2** was found to crystallize in the orthorhombic space group *Pbca* with $Z = 8$.
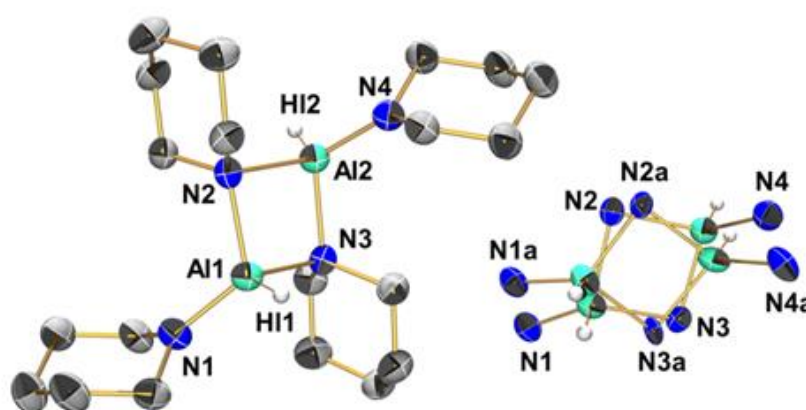
Figure 3.10 *Molecular structure of [pip$_2$AlH]$_2$ (**2**), C-bound hydrogen atoms are omitted for clarity. Thermal displacement ellipsoids show 50 % probability, only the predominant part of the disorder is shown as a full molecule, the disorder is shown for the Al$_2$N$_4$H$_2$ core.*

The association through bridging via the piperidinyl ligands in the dimeric structure of **2** (Fig. 3.10) contrasts to the dimeric structure of bis-2,2,6,6-

tetramethylpiperidinoalane[188] where dimerization occurs via Al–H bridges, possibly favored because of steric reasons. Even though the molecule almost adheres to inversion symmetry, it is not located on a special crystallographic position, and the crystallographic asymmetric unit consists of a whole molecule. This molecule exhibits severe positional disorder, which can be described as the two states achieved by mutual flipping of the chair conformations of the four piperidine rings. While the corresponding γ-CH_2 groups rest in related positions (and thus establish essentially the same intermolecular packing interactions), the four N atoms are flipped into one direction, and so is the entire $Al_2N_4H_2$ core (in Fig. 3.10, top right, this means a clockwise turn toward the alternative disorder positions indicated with "a"). Site occupancies of the two disordered parts refined to 0.682(2) and 0.318(2). It is not clear why disorder in the molecule appears. The possible reasons may be the pureness of the compound, the speed of crystal growth, and the conditions during crystallization, that can favor or disfavor the building of the long-range order. One way of getting hints on the nature of the disorder is to try to collect data at different temperatures. While a dynamic disorder problem should become less pronounced with temperature decrease, a static disorder will mostly be not influenced by temperature changes. For the initial data collection the crystal of compound **2** was mounted at 200 K and rapidly cooled to 160 K, but the further thermal treatment of this crystal (heating to 260 K and cooling to 160 K at a rate of 80 K h^{-1}) did not change the site occupancy ratio of the two disordered parts. Thus, it is unlikely that the two disorder positions occur as a dynamic disorder in the crystal.

In the structure of **3,** the dimeric molecule is located around a crystallographically imposed center of inversion which generates the whole molecule (Fig. 3.11), similar to the structure of **1**. The asymmetric unit contains one pip$_3$Al moiety. The dimeric compound **3** features a four-membered ring of aluminum and nitrogen atoms analogous to [pyr$_3$Al]$_2$[223] (pyr = pyrrolidinyl, C_4H_8N). However, the packing of the molecules in their corresponding crystal structures differs significantly from each other. Compound **3** crystallizes in the triclinic space group $P\bar{1}$ (Table 3.7), while [pyr$_3$Al]$_2$ crystallizes in the monoclinic space group $P2_1/c$. In sharp contrast, the more bulky substituted compound (N(i-Pr)$_2$)$_3$Al[180] does not form dimers but crystallizes in the triclinic space group $P\bar{1}$ with two crystallographically independent monomeric molecules in the asymmetric unit. The structure of **3** is very similar to the one of the related compound [(pip)$_2$AlN$_3$]$_2$[224] which is also dimeric by virtue of bridging piperidinyl

ligands, except that the non-bridging positions are occupied by piperidinyl and azide ligands.
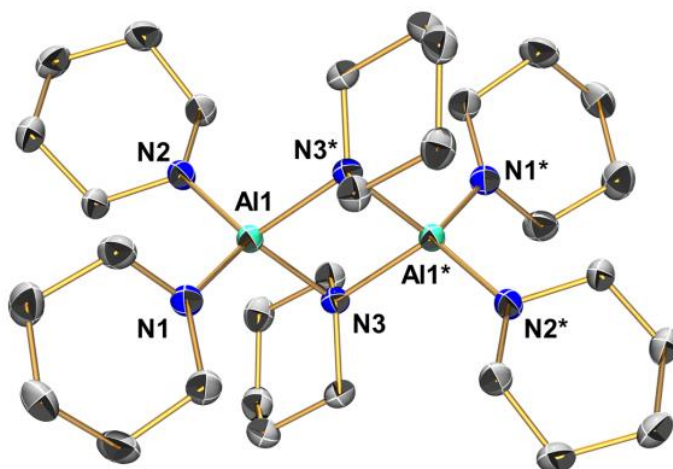
Figure 3.11 *Molecular structure of [pip₃Al]₂ (**3**), C-bound hydrogen atoms are omitted for clarity. Thermal displacement ellipsoids show 50 % probability.*

The crystal contained a small twin contribution. However, refinement as a singly crystal gave a better result than twin integration of the whole data set and refinement against HKLF5 format data. Therefore, data integration and refinement were carried out for a single crystal, and merely the 15 most disagreeable reflections were omitted from the refinement.

In Table 3.8 selected bond lengths and angles are presented and compared with corresponding parameters of **1**.

Table 3.8 *Comparison of selected bond lengths (Å) and angles (°) of [pipAlH₂]₂ (**1**)[216], [pip₂AlH]₂ (**2**) and [pip₃Al]₂ (**3**).*

1		2		3	
Defining atoms	**Bond lengths (Å)**	**Defining atoms**	**Bond lengths (Å)**	**Defining atoms**	**Bond lengths (Å)**
Al1–N1	1.9449(14)	Al1–N2	1.961(4)	Al1–N3	1.9684(16)
		Al2–N2	1.983(3)		
Al1–N1*	1.9410(14)	Al1–N3	1.965(4)	Al1–N3*	1.9920(15)
		Al2–N3	1.970(4)		
		Al1–N1	1.792(3)	Al1–N1	1.8135(15)
		Al2–N4	1.789(3)	Al1–N2	1.8095(15)
Al1···Al1*	2.7599(10)	Al1···Al2	2.822(2)	Al1···Al1*	2.8519(10)
	Angles (°)		**Angles (°)**		**Angles (°)**
N1–Al1–N1*	89.49(6)	N2–Al1–N3	88.32(15)	N3–Al1–N3*	87.87(6)
		N1–Al1–N2	117.36(15)	N1–Al1–N3	117.02(7)
		N1–Al1–N3	120.32(16)	N2–Al1–N3	114.27(7)
				N2–Al1–N1	110.84(7)

*The asterisk denotes a symmetry equivalent atomic position generated by a center of inversion, as it is shown for compound **3** in Fig. 3.11.

As expected, for compound **3**, the Al–N bonds to the bridging piperidinyl groups are noticeably longer (by almost 0.2 Å) than those to the terminal piperidinyl groups, also observed for other similar aminoalanes containing [AlN]$_2$ units[178,223,224]. The Al–N–Al bridges are almost symmetric, bond length differences are smaller or only marginally greater than the experimental error. Along the series of compounds **1**, **2**, and **3** the average bridging Al–N bond lengths increase (from 1.94 via 1.97 to 1.98 Å) as a result of the increasing steric bulk about the Al coordination sphere. A similar trend is reflected by the average terminal Al–N bond lengths of compounds **2** and **3** (1.79 and 1.81 Å, respectively). As expected, lowering the steric bulk for compounds with related substitution patterns results in somewhat shorter bond lengths (compare 1.98 and 1.81 Å for bridging and terminal Al–N bonds, respectively, in compound **3** with the corresponding bond lengths of 1.96 and 1.80 Å, respectively, in its pyrrolidinyl analog[223]). Replacing rather covalently bound substituents by rather ionic groups, however, has some more severe effect of bond shortening, as the bridging and terminal (Al-pip) Al–N bonds of compound [pip$_2$AlN$_3$]$_2$ confirm (1.93 and 1.77 Å, respectively)[224], in which a terminal piperidinyl group of **3** or likewise the sterically less demanding hydride of **2** is replaced by an azide group.

Structure elucidation of piperidinoalanes by NMR spectroscopy

In the NMR spectra, ^{1}H chemical shifts determined for **1** mainly agree with those previously reported (α-CH$_2$ at δ = 2.74 ppm, β and γ-CH$_2$ at δ = 2.26 ppm)[177,196]. However, the higher resolution of the obtained spectra for **1** allowed to distinguish between the β and γ methylene protons at δ = 1.36 and 1.14 ppm, respectively**.** The ^{1}H NMR spectra of compounds **2** and **3** show distinct signals for bridging and terminal piperidinyl groups (Fig. 3.12, left). The not assigned signals (at δ = 2.61 and 1.4 ppm) correspond to free piperidine.

(**1**) m.p. 97 °C; **^{1}H NMR** (700.13 MHz, C$_6$D$_6$): δ = 1.14 (4 H, m, γ-CH$_2$), 1.36 (8 H, qnt, ^3J = 5.6 Hz, β-CH$_2$), 2.74 (8 H, t, α-CH$_2$(N)), 4.17 (4 H, br. s, Al-H) ppm. **^{13}C NMR** (176.1 MHz, C$_6$D$_6$): δ = 23.7 (γ-CH$_2$), 26.6 (β-CH$_2$), 51.3 (α-CH$_2$(N)) ppm. **^{27}Al NMR** (130.3 MHz, C$_6$D$_6$): δ = 152 ppm.

(**2**) m.p. 121 °C; **^{1}H NMR** (700.13 MHz, C6D6): δ = 1.34 (4 H, m, γ-CH$_2$ bridg.), 1.51 (8 H, m, β-CH$_2$ term.), 1.53 (8 H, m, β-CH$_2$ bridg.), 1.69 (4 H, m, γ-CH$_2$ term.), 2.78 and 2.88 (8 H, m, α-CH$_2$ bridg.), 3.18 (8 H, m, α-CH$_2$(N) term.), 3.85 (2 H, br. s, Al-H) ppm. **^{13}C NMR** (176.1 MHz, C$_6$D$_6$): δ = 24.5 (γ-CH$_2$ bridg.), 26.3 (β-CH$_2$ bridg.)

26.7 (γ-CH$_2$ term.), 29.7 (β-CH$_2$ term.), 48.2 (α-CH$_2$(N) bridg.), 49.6 (α-CH$_2$(N) bridg.), 49.8 (α-CH$_2$(N) term.) ppm. **^{27}Al NMR** (130.3 MHz, C$_6$D$_6$): δ = 128 ppm.

(**3**) m.p. 77 °C; **^{1}H NMR** (700.13 MHz, C$_6$D$_6$): δ = 0.62 and 1.11 (8 H, m, β-CH$_2$ bridg.), 0.82 and 1.17 (4 H, m, γ-CH$_2$ bridg.), 1.50 (2 H, m, α-CH$_2$ bridg.), 1.60 (16 H, m, β-CH$_2$ term.), 1.81 (8 H, m, γ-CH$_2$ term.), 2.31 and 2.93 (8 H, m, α-CH$_2$ bridg.), 3.15 (16 H, m, α-CH$_2$(N) term.) ppm. **^{13}C NMR** (176.1 MHz, C$_6$D$_6$): δ = 23.5 (γ-CH$_2$ bridg.), 26.1 (β-CH$_2$ bridg.), 27.3 (γ-CH$_2$ term.), 30.1 (β-CH$_2$ term.), 46.4 (α-CH$_2$(N) bridg.), 50.2 (α-CH$_2$(N) term.) ppm. **^{27}Al NMR** (130.3 MHz, C$_6$D$_6$): δ = 106 ppm.

The ^{27}Al resonance for **2** (at δ = 128 ppm) is shifted upfield compared to **1** (δ = 152 ppm). Similar behavior was also observed for other aminoalanes with [L$_2$AlH]$_2$ substitution pattern compared to [LAlH$_2$]$_2$ species[188,225,226]. Substituting all hydrogen atoms at Al by piperidine shifts the ^{27}Al resonance for **3** to even lower frequency (δ = 106 ppm) resulting in a value typical for an AlN$_4$ motif (Fig. 3.12, right).
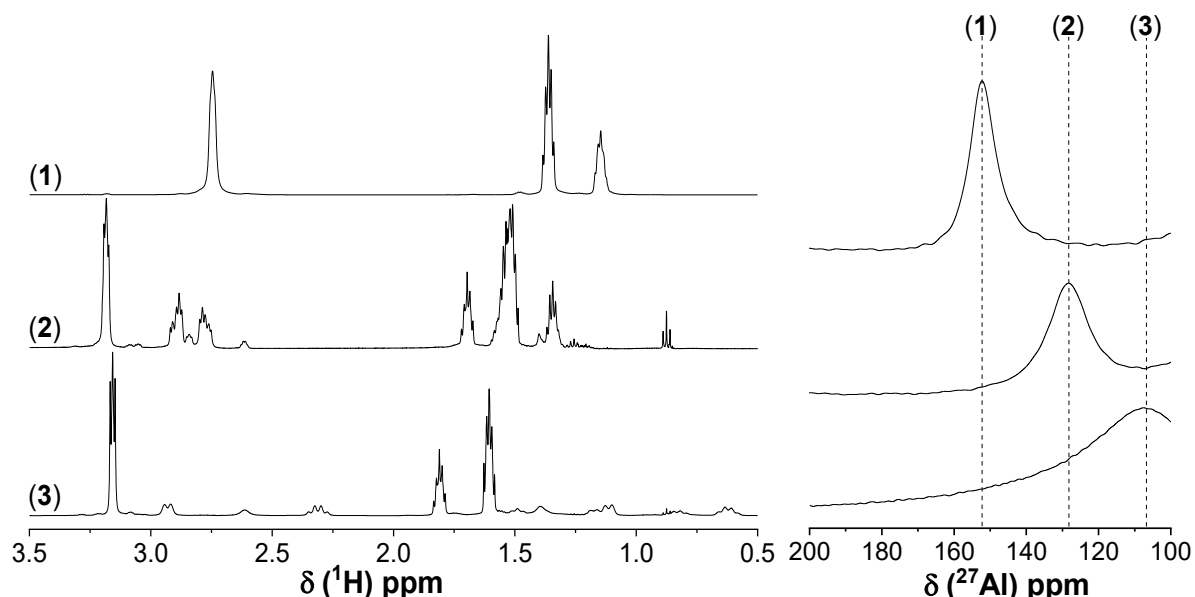
Figure 3.12 *^{1}H and ^{27}Al NMR spectra of piperidinoalanes in benzene-d6: top – [pipAlH$_2$]$_2$ (**1**); middle – [pip$_2$AlH]$_2$ (**2**); bottom – [pip$_3$Al]$_2$ (**3**).*

While the ^{27}Al chemical shifts confirm retention of the Al atoms´ tetracoordination in solution, 2D NMR measurements (Fig. 3.13 and 3.14) confirmed the presence of terminal and bridging piperidinyl ligands for **2** and **3** in solution, which is of particular interest with compound **2**, for which it indicates retention of the bridging mode which was also found in the solid-state (and rules out transformation into an Al–H–Al bridged isomer).

The two-dimensional ^{1}H spectrum of **2** and **3** in benzene-d$_6$ solution showed signals of terminal (higher intensity) and bridging (lower intensity) piperidinyl groups,

with corresponding assignments mentioned above. Scalar couplings between nuclei are indicated by the cross-peaks in Fig. 3.13 (left) and 3.14 (left). Thus, the correlation between α-CH$_2$(N) with β-CH$_2$ can be detected and in the same way between β-CH$_2$ with γ-CH$_2$.
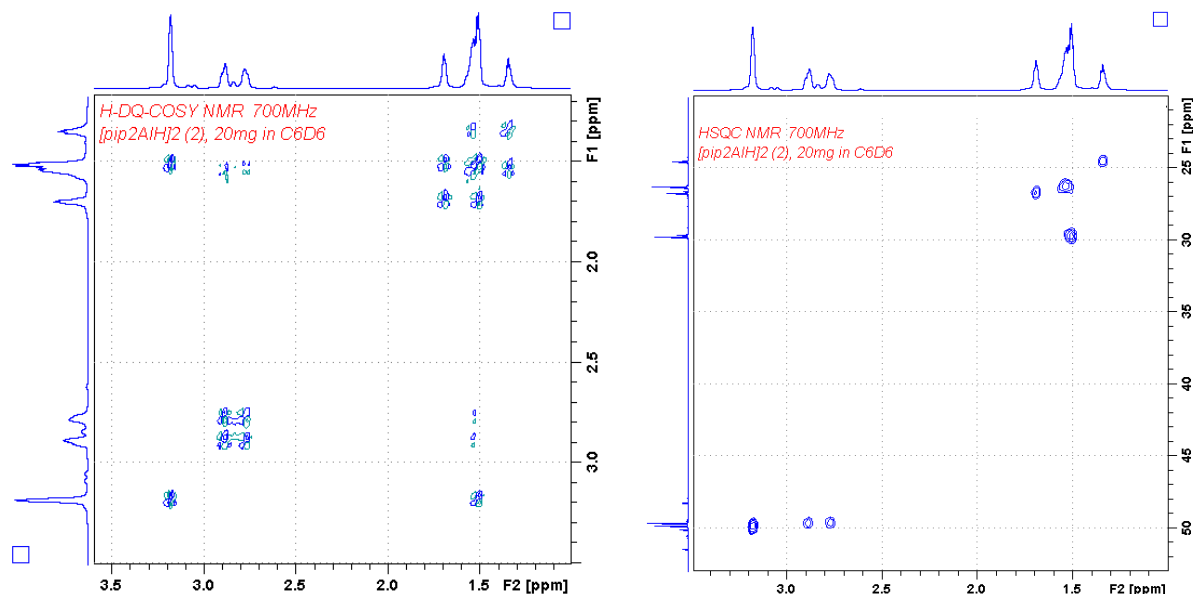
Figure 3.13 *2D NMR spectra: ^{1}H–^{1}H COSY (left) and ^{1}H–^{13}C HSQC (right) for [pip$_2$AlH]$_2$ (**2**) in benzene-d6.*

The signals between 2.77–2.89 ppm for **2** (Fig. 3.13, left) correspond to α-CH$_2$ bridging protons of bridging piperidinyl groups, the presence of axial and equatorial protons was confirmed by scalar coupling between dissimilar nuclei ^{1}H–^{13}C which indicated one signal at 48.2 ppm in proton/carbon cross-peak (Fig. 3.13, right). The complex multiplets between 1.45 and 1.60 ppm originate from β-CH$_2$ of terminal and bridging piperidinyl groups. However, severe signal overlap in ^{1}H NMR spectra hinders accurate assignment. Extension of ^{1}H to ^{1}H–^{13}C HSQC leads to the dispersion of peaks along the ^{13}C dimension and greatly alleviates peak overlapping, thus, terminal (at 1.50 ppm) and bridging (at 1.53 ppm) proton piperidinyl group resonances by the different carbon resonances (at 29.7 and 26.3 ppm, respectively) can be well distinguished.

Proton chemical shifts in ^{1}H spectra for **3** were also identified from the positions of 2D ^{1}H–^{13}C HSQC cross-peaks (Fig. 3.14, right). The 0.62 and 1.11 ppm, 0.82 and 1.17 ppm, 2.31 and 2.93 ppm resonances in ^{1}H spectra are attributed to β, γ, and α bridging methylene groups of piperidinyl ligands and correspond to 26.1, 23.5, and 46.4 ppm in ^{13}C spectra, respectively.
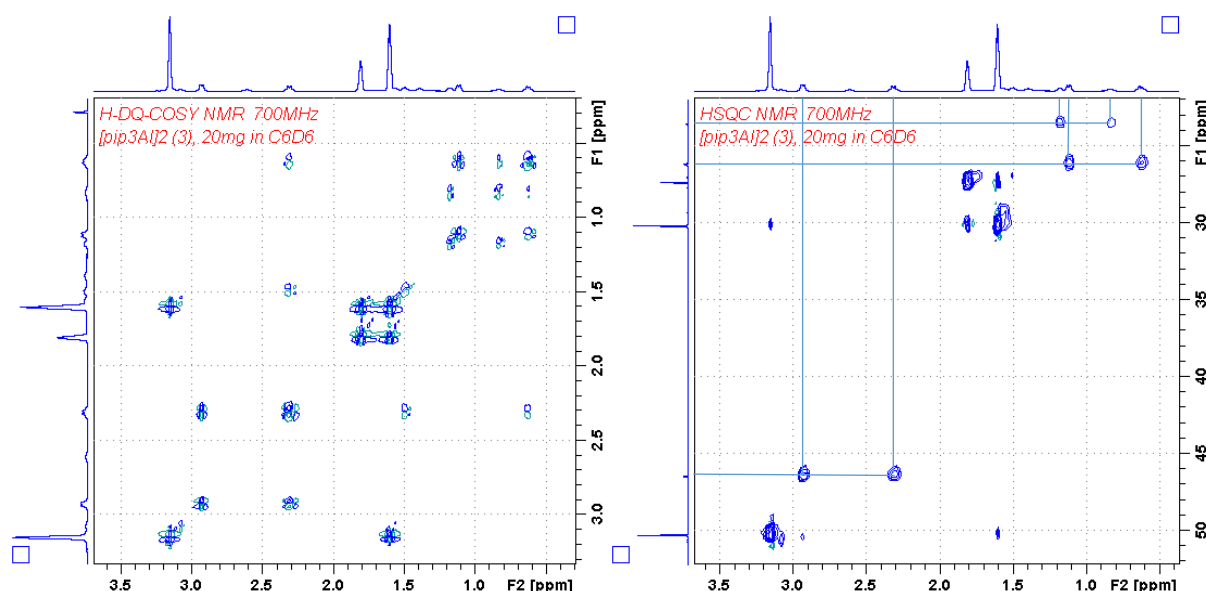
Figure 3.14 *2D NMR spectra: ^1H–^1H COSY (left) and ^1H–^{13}C HSQC (right) for [pip$_3$Al]$_2$ (3) in benzene-d6.*

The integration of the ^1H spectra for compound **3** showed a lower ratio (3:1) between the bridging and terminal piperidinyl groups than expected (2:2). A possible explanation could be the formation of the monomeric species in the solution. Steric relief would therefore provide a driving force to overcome increased ring strain in the dimer[227]; large piperidinyl groups would probably cause the conversion from dimer to monomer. Thus, dimer-monomer equilibrium for compound **3** was assumed:
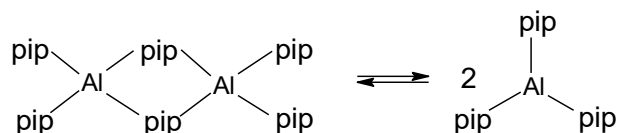
Scheme 3.16 *Possible equilibration between monomeric and dimeric species of compound 3 in solution.*

Another uncertainty was related to the proton signal with small intensity at δ = 1.5 ppm in benzene-d6, which was not observed for compound **3** in the previous report[223]. Therefore, the NMR measurements were performed in toluene-d8 instead of benzene-d6 yielding essentially the same results compared to earlier published data[223]. Dissolution in toluene-d8 revealed no evidence for an additional signal. Only the small shoulder was observed at δ = 1.56 ppm (terminal piperidinyl group), which is the possible reason why it was not identified in earlier published data.

(3) ^{1}**H NMR** (500.13 MHz, C$_6$D$_5$CD$_3$): δ = 0.71 and 1.20 (8 H, m, β-CH$_2$ bridg.), 0.91 and 1.25 (4 H, m, γ-CH$_2$ bridg.), 1.56 (16 H, m, β-CH$_2$ term.), 1.78 (8 H, m, γ-CH$_2$ term.), 2.34 and 2.95 (8 H, m, α-CH$_2$ bridg.), 3.09 (16 H, m, α-CH$_2$(N) term.) ppm. ^{13}**C NMR** (125.8 MHz, C$_6$D$_5$CD$_3$): δ = 23.7 (γ-CH$_2$ bridg.), 26.2 (β-CH$_2$ bridg.), 27.3 (γ-CH$_2$

term.), 30.1 (β-CH$_2$ term.), 46.5 (α-CH$_2$(N) bridg.), 50.2 (α-CH$_2$(N) term.) ppm. **^{27}Al NMR** (130.3 MHz, C$_6$D$_5$CD$_3$): δ = 106 ppm.

For a more detailed study of compound **3**, the temperature dependent NMR measurements in toluene-d8 were carried out (Fig. 3.15). The spectra revealed the signals shift of terminal piperidinyl groups to a lower field in toluene-d8 and the appearance of the signal at δ = 1.5 ppm. Therefore, it was concluded the signal at δ = 1.5 ppm cannot be detected in toluene-d8 at room temperature due to the overlapping with the signal of the terminal piperidinyl group. The unidentified signal at about 1.5 – 1.7 ppm (depending on the temperature) is present over the whole temperature range, confirmed by a two-dimensional NMR study. An evaluation of H,H-COSY spectra measured in toluene-d8 at low temperature showed that the undefined signal was shifted to be nearly coincident with the signal at δ = 1.56 ppm, but has the correlation to the bridging piperidinyl group of compound **3**.
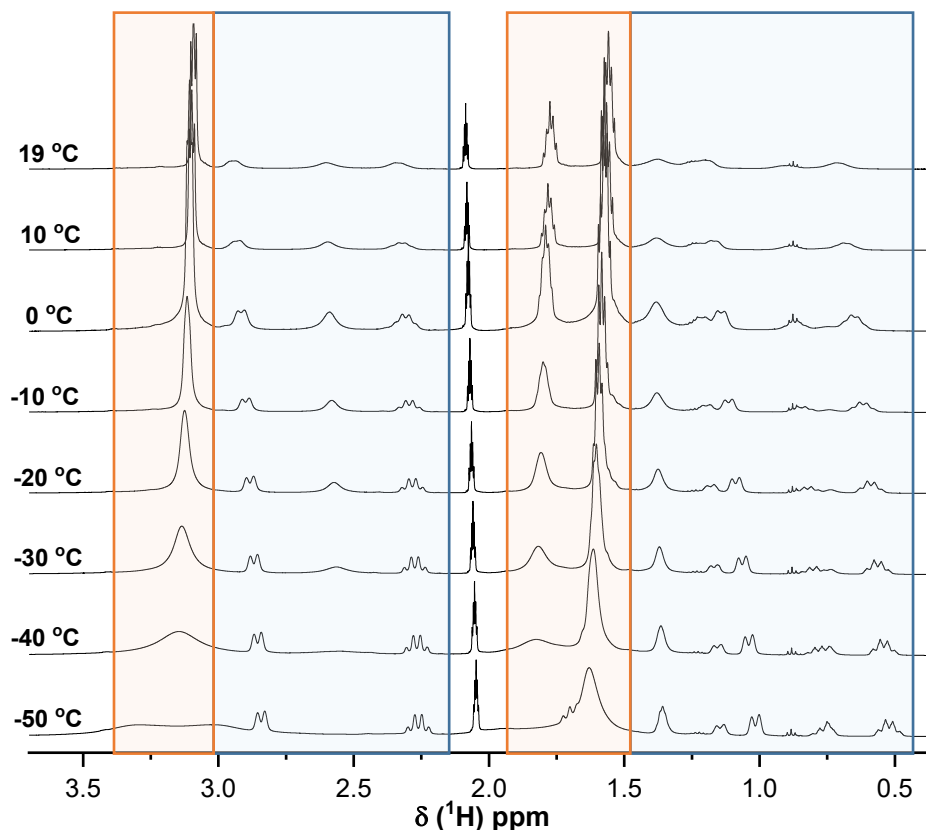
Figure 3.15 *Temperature dependent ^{1}H NMR spectra of 3 in toluene-d8 (marked in orange – signals for terminal piperidinyl ligands; in blue – bridging piperidinyl ligands).*

The temperature-dependent NMR measurements also clarified the discrepancy in the integration values of the spectra for compound **3** obtained at room temperature. The broad signals for piperidine and bridging piperidinyl ligand of **3** at room temperature getting narrower at a lower temperature, indicating the exchange with

each other, which is significantly reduced at a lower temperature. With the further decrease of the temperature, free piperidine signals become broader due to slow down of conformational exchange and seam to disappear (because of broadening) at the lowest measure temperature (-50 ºC). At the same time, the signals of the terminal piperidinyl ligand become broader due to the reduced mobility to change conformation at low temperature and finally the α-CH$_2$ signal splits at -50 ºC. Additionally, at a lower temperature, the signals shift to lowfield for terminal and highfield for bridging piperidinyl ligands was observed, resulting in a better separation of the signals. Generally, there are two exchange phenomena present: exchange of piperidine with the (mainly) bridging piperidinyl ligand and conformational exchange. When the temperature decreased to 0 ºC the signals of piperidine become narrower due to a slowdown of (pip$_3$Al↔piperidine) exchange, but the conformational exchange is still fast. Furthermore, when the temperature decreases to -50 ºC the signal broadening can be observed before the signal splits into two due to the limited interconversion of the piperidine chair conformations.

Compound **3** is not stable in solution but decomposes to pipH and some polymeric species, which were observed during the dissolution of **3** in the solvent. The intensity of free piperidine signals was increasing with time. All piperidinoalanes are extremely sensitive to traces of moisture or hydroxyl groups of another origin (e.g. remaining Si-OH groups at the glass surface) resulting in the formation of piperidine. As could be shown by 2D EXSY NMR (Fig. 3.16), already small amounts of piperidine are in fast exchange on the NMR timescale with the piperidinyl ligands of the alane.
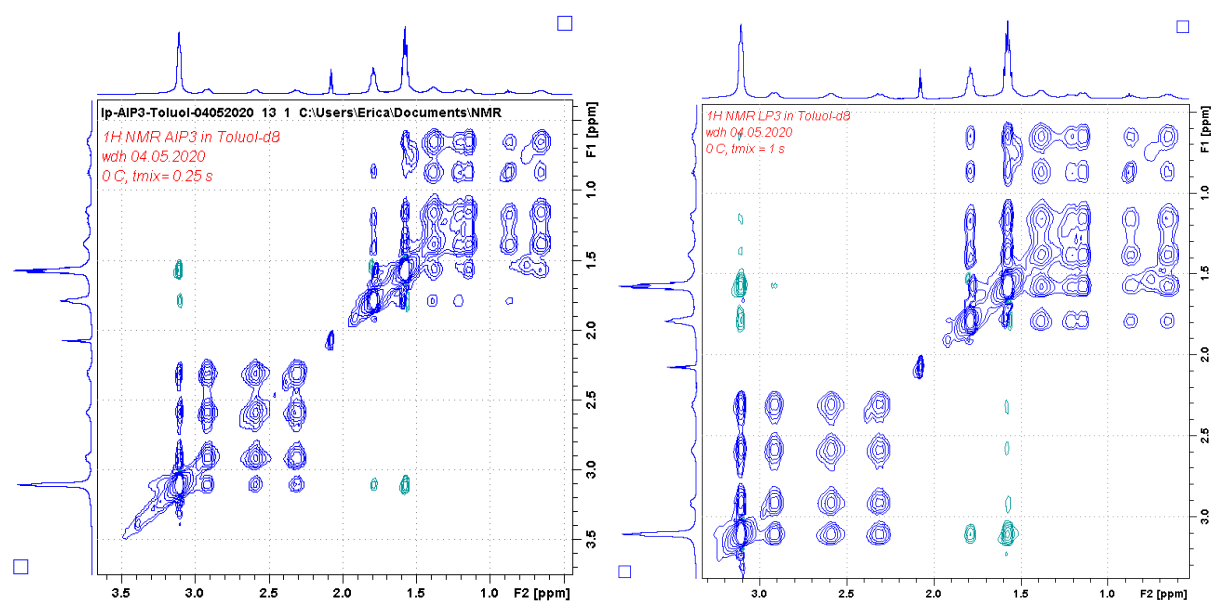
Figure 3.16 ^{1}H-^{1}H NOESY/EXSY spectra of 3 in toluene-d8, t_{mix} = 0.25 s (left) and 1 s (right). Cross peaks: green: NOESY, blue: exchange.

At short mixing times, the cross-peaks pipH ↔ bridg. pip have higher intensity compared to the cross-peaks of terminal pip (although their signal intensity is much higher!), thus the former exchange is probably the faster one.

3.3.3.2 Influence of the initial reaction parameters on the piperidinoalane formation

Kovar and Ashby[195] reported a direct synthesis of piperidinoalanes at harsh conditions 110 ºC and 205-275 bar in benzene suspension of activated aluminum and piperidine. In the present work, by activating aluminum with TM additives the direct synthesis of piperidinoalanes became possible at much milder conditions. The direct hydrogenation using activated aluminum prepared in the course of this work (Al*(Ti), Al*(Zr), Al*(Hf) or Al*(Y)), and its stabilization by piperidine was carried out in THF under the hydrogen pressure 100 bar at room temperature. The main efforts were made in order to evaluate the critical parameters influencing the direct hydrogenation of aluminum supported by piperidine.

Effect of dopants on the direct hydrogenation of aluminum with piperidine

To learn about the nature of the reaction products, formed by using these different types of activated aluminum, their ^{27}Al NMR spectra were recorded (Table 3.9). The conversion values of activated aluminum were calculated based on the initial amount of Al* and unreacted metal recovered after the reaction.

Table 3.9 *Conversion values of aluminum activated by different TM additives and the corresponding ^{27}Al NMR shifts (**1**: 152, **2**: 128, and **3**: 106 ppm) of the piperidinoalanes formed at 100 bar and room temperature within 24 h.*

Additive	Unreac. Al*, g	Al* convers., %	δ(^{27}Al), ppm
ZrCl$_4$	0.09	84	152, 129
HfCl$_4$	0.13	76	152, 129
Ti(OBu)$_4$	0.16	71	128
YCl$_3$	0.46	16	107

The ^{27}Al NMR spectra of the various products (Fig. 3.17) revealed that for the Zr-activated aluminum, the formation of **1** is preferred, indicated by the dominant signal at δ = 152 ppm. Similar behavior was observed for Hf-activated Al with the difference that the content of **1** was lower. For the synthesis based on Ti-activated Al, only one signal was detected at δ = 128 ppm corresponding to compound **2**.
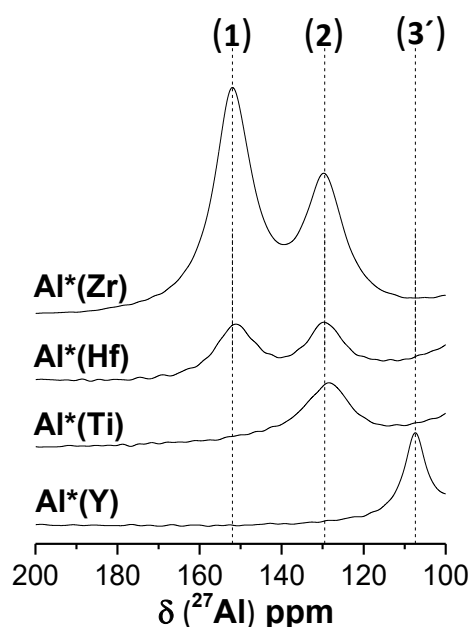
Figure 3.17 ^{27}*Al NMR spectra of products (i.e. piperidinoalanes **1**, **2**, and **3′**) obtained by hydrogenation of TM activated aluminum Al*(TM) supported by piperidine at 100 bar and room temperature within 24 h.*

In order to interpret these findings, it is also important to note that the type of complex formed correlates with the amount of aluminum that has reacted (Table 3.9). The conversion of Zr-activated Al was approximately 84 %, which is higher than the conversion values of the Hf-activated Al (76 %) and Ti-activated Al (71 %). In the case of Y-activated Al, the amount of converted aluminum was the lowest (16 %). In addition, ^{27}Al NMR revealed the sharp signal at δ = 107 ppm that slightly differs from **3** (at δ = 106 ppm), formed by the direct reaction of piperidine with aluminum hydride.

^{1}H NMR of **3′** spectra clearly showed two different piperidine moieties surrounding the aluminum center (Fig 3.18).
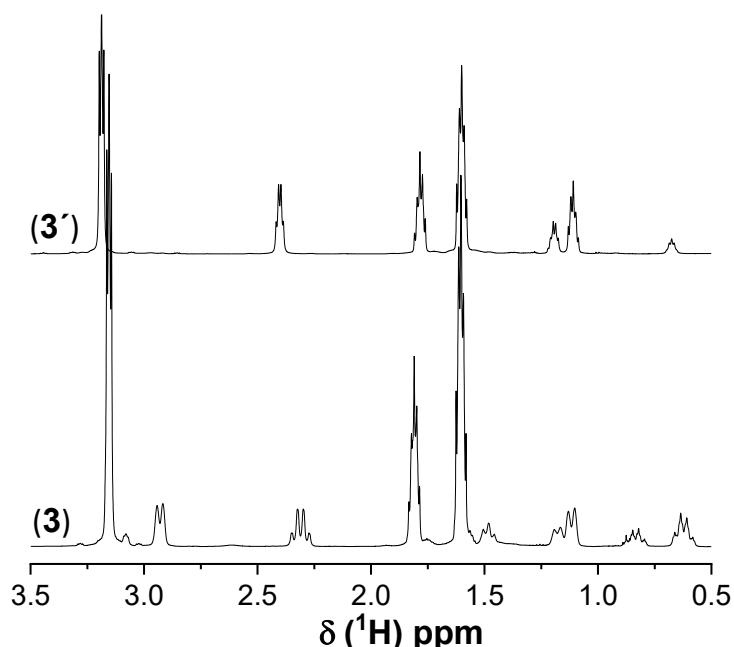
Figure 3.18 ^{1}*H NMR spectra of **3** and **3′** (formed from Al*(Y) synthesis).*

(**3′**) **^{1}H NMR** (500.13 MHz, C$_6$D$_6$): δ = 0.68 (1 H, m, N-H, pipH), 1.11 (4 H, qnt, ^{3}J=5.5, β-CH$_2$, pipH), 1.20 (2 H, m, γ-CH$_2$, pipH), 1.60 (12 H, m, β-CH$_2$, pip), 1.78 (6 H, m, γ-CH$_2$, pip), 2.40 (4 H, m, α-CH$_2$, pipH), 3.19 (12 H, t, α-CH$_2$(N), pip) ppm. **^{13}C**

NMR (125.7 MHz, C_6D_6): δ = 24.5 (γ-CH_2, pipH), 26.0 (β-CH_2, pipH), 27.2 (γ-CH_2, pip), 30.0 (β-CH_2, pip), 47.1(α-CH_2(N), pipH), 50.4 (α-CH_2(N), pip) ppm. **^{27}Al NMR** (130.3 MHz, C_6D_6): δ = 107 ppm.

Based on NMR signal integration, the ratio (3:1) between these two groups was obtained. The signals corresponding to terminal piperidinyl groups for **3′** are slightly shifted compared to **3**. Besides signals ascribed to terminal piperidinyl groups, just three additional signals were assigned to α-, β- and γ-protons of the piperidine group, respectively. The signal at 0.68 ppm was assigned to the N-H group for **3′**. The more precise investigation of this complex was hindered by its instability. Efforts to crystalize the new species failed.

The simplest explanation could be that the dimeric structure of compound **3** was broken. After integration of the ^{1}H spectra, the composition of **3′** - $pip_3AlpipH$, was expected. It was suggested that this complex was formed due to the presence of extra piperidine in the reaction mixture:
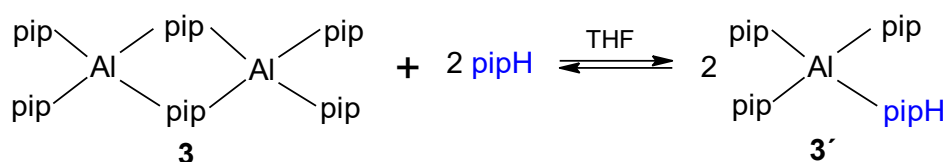
Scheme 3.17 *Cleavage of dimeric structure of 3 in the presence of the excessive amount of piperidine.*

In order to confirm this suggestion the NMR measurements with **3** and piperidine addition were performed (Fig. 3.19).
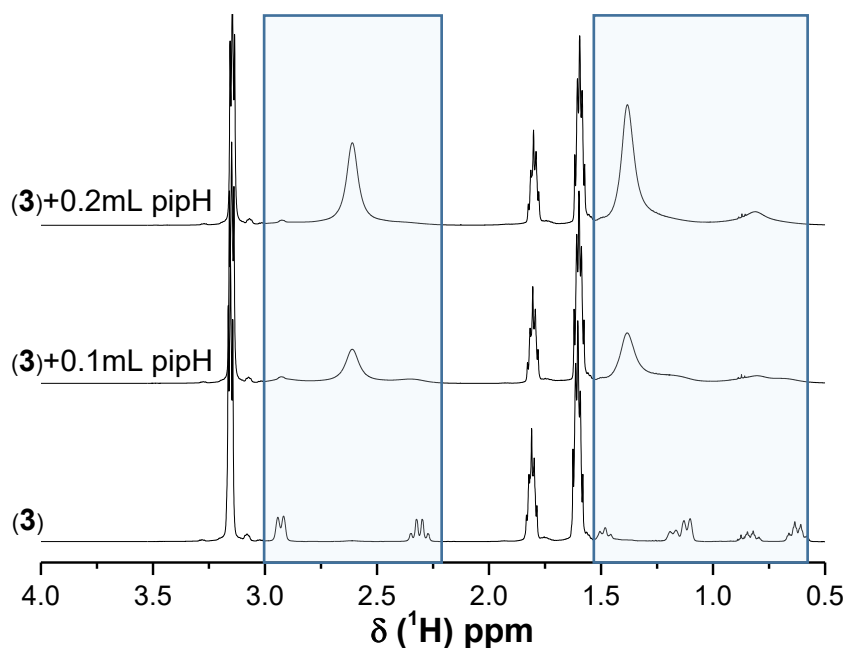
Figure 3.19 *^{1}H NMR spectra of pure 3 and with the addition of piperidine (in 0.5 mL benzene-d6).*

The solution of piperidine (pipH, 0.1 or 0.2 mL) in 0.5 mL benzene-d_6 was added to pure **3** dissolved in 0.7 mL benzene-d_6. With increasing pipH concentration the bridging piperidinyl groups disappeared, however terminal ligands were not influenced. The observed effect is possibly due to the rapid exchange of piperidine with piperidinyl ligand in molecule **3**, which resulted in the formation of **3´**.

The existence of **3´** was confirmed by the addition of piperidine to the product formed by the direct hydrogenation of Al*(Zr) (**1** and **2**). After the hydrogenation reaction in the autoclave reactor was completed, 0.5 mL of piperidine was added to 1 mL of the filtered reaction mixture. The NMR spectra recorded for both samples detected the change from **1** and **2** to **3´** in the sample with piperidine addition (Fig. 3.20).
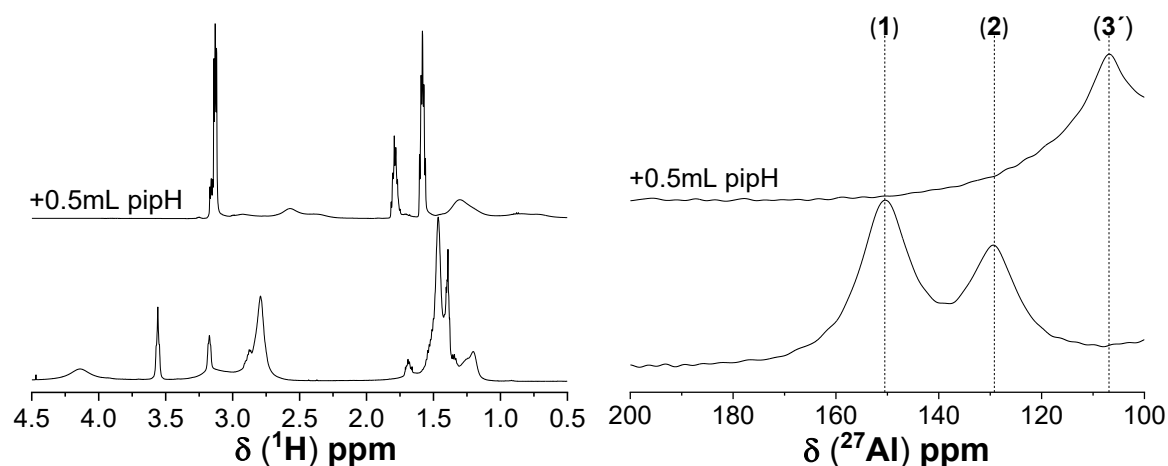
Figure 3.20 ^{1}H and ^{27}Al NMR spectra of product formed by direct hydrogenation of Al*(Zr) supported by piperidine (bottom) and with the further addition of 0.5 mL of piperidine (top).

Based on the NMR data (Fig. 3.18 - 3.20), it was concluded, that complex **3´** was formed only when an excessive amount of piperidine is present in the reaction mixture. This conclusion also correlates with the amount of converted Al*(Zr) (Table 3.10) and products formed within different reaction times.

Table 3.10 Influence of the reaction time on the conversion of Zr-activated aluminum supported by piperidine and corresponding ^{27}Al NMR shifts (**1**: 152, **2**: 128, and **3**: 106 ppm) for the piperidinoalanes formed at 100 bar and room temperature.

Reaction time, h	Unreac. Al*, g	Al* convers., %	$\delta(^{27}$Al), ppm
6	0.44	20	107
18	0.27	51	129, 107
24	0.09	84	152, 129
48	0.03	95	152, 129

The performed experiments showed (Fig. 3.21), that at a short reaction time (6 h or 18 h) **1** was not detected at all. The extension of the reaction time to 24 h leads to the formation of **1** and **2**, however, after 48 h only the ratio between **1** and **2** changes, and the Al* conversion was increased by 11 % (Table 3.10). From this finding and the one that with larger alane content in solution the coordination pattern shifts from **3´** via **3** to **2** and from **2** to **1**, it can be concluded that **1** is only formed if there is no free piperidine available in the reaction mixture.
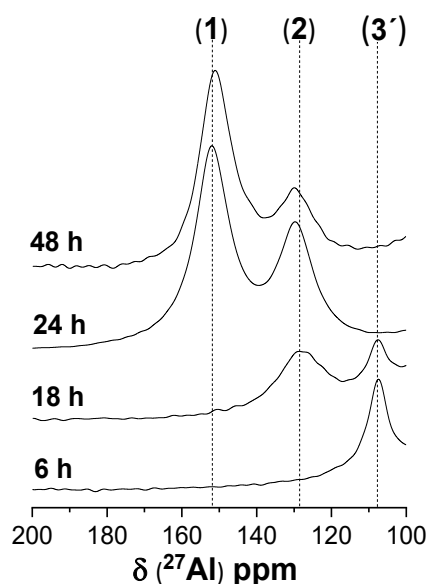
Figure 3.21 ^{27}Al NMR spectra of products obtained by hydrogenation of Zr-activated aluminum supported by piperidine within different reaction times.

Based on these observations the overall reaction pathway for the direct hydrogenation of activated aluminum Al* supported by piperidine is proposed in Scheme 3.18.
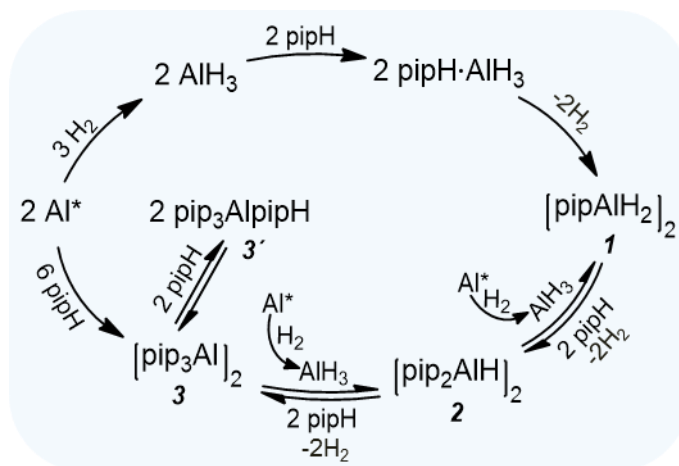
Scheme 3.18 *Proposed pathway of activated aluminum hydrogenation in the presence of piperidine.*

The role of the TM for hydrogen sorption/desorption in aluminum systems was intensively discussed in doped sodium alanate[228,229]. However, the exact mechanism is not yet well understood. It is assumed that the dopant lowers the activation energy barrier and can act as a conduit for the splitting of H–H bonds on the aluminum surface and leads to the intermediate formation of alane[230–233]. In the case of aminoalanes, the formed alane can then be stabilized by the N-donor ligand[51,195], for the secondary

amine (pipH) the intermediate amine-alane complex (pipH·AlH$_3$) can be formed. Since pipH·AlH$_3$ is unstable and eliminates hydrogen below room temperature[195], the first stable product is [pipAlH$_2$]$_2$ (**1**). In the presence of additional piperidine, **1** reacts further to form [pip$_2$AlH]$_2$ (**2**) and with higher excess of piperidine to [pip$_3$Al]$_2$ (**3**) or even pip$_3$AlpipH (**3´**). Amine can also play an essential role in the surface reaction by removing alane from the aluminum surface and keeping it in solution. It is important to note that the formation of piperidinoalane from activated aluminum and piperidine is also feasible without the supply of hydrogen gas (Appendix B, Fig. B.1). Therefore, the formation of **3** (or **3´**) from activated Al and piperidine and its further reaction with alane to **2** and **1** can take place parallel to the formation of alane (Scheme 3.18). The importance of amines in catalyzed hydrogenation reactions was also emphasized by work regarding catalytic hydrodechlorination of BCl$_3$ using a nickel boride catalyst[234,235].

Summarizing, it was demonstrated that piperidinoalanes can be prepared by using aluminum activated by any of four TM additives. The TM activity for the piperidinoalane formation decreases in the order of Zr > Hf > Ti > Y. It is important to note, that piperidinoalane did not form when Al was used without any TM compound, signifying the role of the additive in the aminoalane formation. Activation of metal with the TM additive is one of the key factors for reversible hydrogenation. The Ti-based catalysts were reported by being unusually very efficient catalysts for the dehydrogenation of complex hydrides[79,89,236]. For example, the TM catalytic activity order defined for sodium alanate[83,237,238]: Ti > Zr > Hf > Y, differs from the one obtained in this work. The enhanced kinetics for H$_2$ desorption by doping with titanium could be explained by the larger electronegativity compared to other TM additives (Table 3.11), hence, contributing to the distortion of the structure by the reduction of the anionic charge of the complex adjacent to a Ti dopant.

Table 3.11 *Relevant properties of the selected metals*[239,240].

Metal	Pauling electronegativity (χ_r)	Electron configuration	Effective ionic radii, Å
Al	1.61	$3s^2 3p^1$	0.53
Ti	1.54	$3d^2 4s^2$	0.74
Zr	1.33	$4d^2 5s^2$	0.84
Hf	1.30	$5d^2 6s^2$	0.83
Y	1.22	$4d^1 5s^2$	1.02

In the case of aminoalanes, the additive should lower the hydrogenation energy barrier of aluminum and lead to the formation of intermediate AlH_3. Thus, Ti additive is promoting both the alane formation and the aminoalane destabilization, consequently leading to the formation of the more thermodynamically stable species **2**. Zirconium and hafnium have similar properties, and, thus, showed a similar trend (Fig. 3.17), both additives led to the formation of **1** and **2**.

The dependence of the ionic radius and the catalytic activity is also apparent. Very low catalytic activity for yttrium was observed, which has an ionic radius significantly larger than that for aluminum (0.53 Å[240]). As smaller the ionic radius as easier the ion can substitute into the aluminum lattice[83] and create defects in the structure.

The mentioned above assumptions are only attempts to explain why some TMs have higher or lower catalytic activity compared to others. Future work should focus on *in situ* experiments (NMR, IR) to understand the role of the TM additive in enabling the hydrogenation reaction.

Influence of the solvent

The media in which hydrogenation takes place is the other important parameter, which can influence the efficiency of aluminum hydrogenation. The results of the attempts on the direct hydrogenation of Zr-activated aluminum supported by piperidine performed in THF, diethyl ether, and benzene are summarized in Table 3.12. These syntheses were performed in collaboration with F. Habermann in terms of her bachelor thesis[214].

It was experimentally confirmed that replacing THF with another solvent (diethyl ether or benzene) has led to the lowering of the Al*(Zr) conversion value (Table 3.12).

Table 3.12 *The conversion values of Zr-activated aluminum supported by piperidine and the corresponding ^{27}Al NMR shifts (**1**: 152, **2**: 128, and **3**: 106 ppm) for the products formed at 100 bar and room temperature within 24 h by using different solvents.*

Solvent	Unreac. Al*, g	Al* convers., %	$\delta(^{27}Al)$, ppm
THF	0.09	84	152, 129
Et$_2$O	0.21	62	152, 129
Benzene	0.31	44	129, 106

The ^{27}Al NMR analysis of the products formed from Zr-activated aluminum supported by piperidine in the various solvents is shown in Figure 3.22.

When benzene was used as a solvent, compounds **2** and **3** were formed, only. In diethyl ether compounds **1** and **2** were detected as hydrogenation products, with a lower concentration of **1** compared to **2**. Only THF favored the formation of **1** and smaller quantities of **2**. The higher efficiency of THF instead of Et_2O was also confirmed for the direct formation of $LiAlH_4$ from LiH and Al[91]. In that case, the better performance of THF was explained by the differences in the formation enthalpy for the concentration dependent solvent-separated ions (in THF) over the solvent-separated contact ions (in Et_2O).
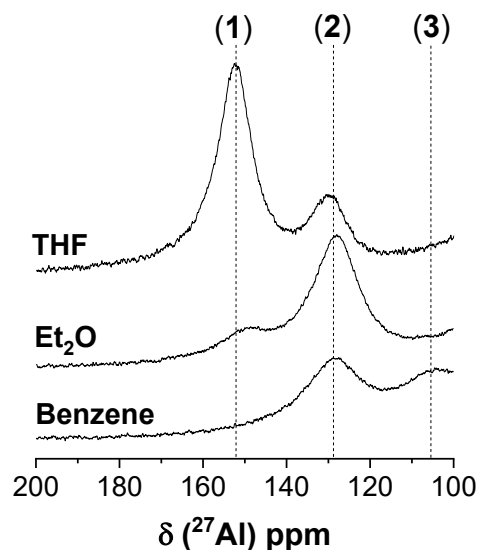
Figure 3.22 *Comparison of the ^{27}Al NMR spectra of the products from the direct hydrogenation reactions made in different solvents at 100 bar and room temperature.*

The high dipole moment of THF (1.63 D) for which exceeds that of Et_2O (1.15 D) (given values for the gas-phase molecules)[92] may play an important role in the stabilization of the amine-alane complex. The interaction between THF and Al is clearly stronger than for Et_2O and Al, which is a too feeble solvent to stabilize the formation of the intermediate AlH_3. The complexation with the solvent is the possible reason why activated aluminum can be hydrogenated in the solution by leveling the thermodynamic playing field that is otherwise dominated in the solid state. Thus, it can be concluded that the stability of the alane-solvent complexes decreases in the following order: tetrahydrofuran-alane > diethyl ether-alane > benzene-alane. The variation in the stability of the formed alane-solvent complexes parallels the coordinating ability of the solvents. Since the alane-tetrahydrofuran solvate species is more stable it is unlikely to improve the hydrogenation of aluminum with the weaker bound solvents like diethyl ether or benzene.

Temperature and pressure influence

In order to increase the yield of the product, the main reaction parameters (temperature and pressure) were investigated in this section. The reaction temperature was varied in the range from 0 ºC to 60 ºC (Fig. 3.23), keeping the other conditions in the reactor constant.

The syntheses at 0 ºC and 40 ºC were performed in collaboration with F. Habermann in terms of her bachelor thesis[214].

It was shown that with increasing the temperature from 0 ºC to 40 ºC the pattern shifts from **3´** to **1**. Further increase of the reaction temperature from 40 ºC to 60 ºC leads to the shifting from **1** to **2**. On the one hand, the high reaction temperature can promote aluminum hydrogenation, on the other hand, it can lead to the decomposition of alane, therefore there is an optimal temperature to achieve the maximum conversion of aluminum. Based on these results it is also assumed that compound **2** is the most stable of piperidinoalanes.
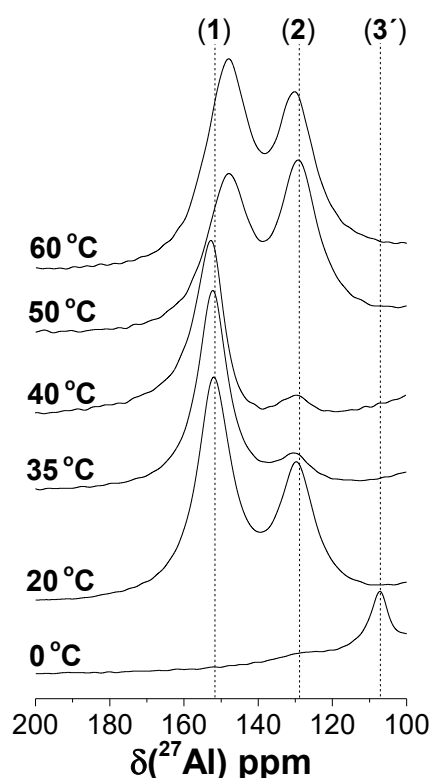
Figure 3.23 ^{27}Al *NMR spectra of the products from the direct hydrogenation of Al*(Zr) supported by piperidine performed at different temperatures.*

Table 3.13 shows the Al*(Zr) conversion values depending on the reaction temperature. The obvious maximum of the aluminum conversion was observed by differing the reaction temperature, in the temperature range 0 – 35 ºC the conversion increased by 67 %, with further increasing the temperature to 60 ºC, the conversion of aluminum decreased by 25 %.

Table 3.13 *The influence of the temperature on the conversion of aluminum supported by piperidine and the corresponding* ^{27}Al *NMR shifts (**1**: 152, **2**: 128, and **3**: 106 ppm) for the products formed at 100 bar within 24 h.*

T, ºC	Unreac. Al*, g	Al* convers., %	δ(^{27}Al), ppm
0	0.38	31	106, 128
20	0.09	84	128, 152
35	0.01	98	128, 152
40	0.02	96	128, 152
50	0.06	89	129, 150
60	0.15	73	129, 150

In order to investigate the influence of the pressure on the piperidinoalane formation, the syntheses were performed in steps of 20 bar from 20 bar to 100 bar. Table 3.14 shows the dependence of the conversion values of the aluminum powder

on the change of pressure. Surprisingly, the hydrogenation of Zr-activated aluminum was realized already at 20 bar with the high conversion value for aluminum – 84 %. With the further increase of the hydrogen partial pressure, the conversion of Al* did not change significantly (± 2 %), however, the proportion of the obtained products **1** and **2** in the reaction mixture was varied (Appendix B, Fig. B.2). In order to determine the correlation between compounds **1** and **2**, the program for the deconvolution of the ^{27}Al NMR spectra (dmfit) was used (Appendix B, Fig. B.3). After the performed simulation, the presumable proportion of each compound in the reaction mixture, depending on the area under the absorption curve, was calculated (Table 3.14). There was observed no strong dependence in the ratio between **1** and **2**, even when the pressure was varied over the wide range. However, at the hydrogen pressure of 80 bar, the predominant formation of compound **1** in the product mixture was detected.

Table 3.14 *The influence of the pressure on the conversion of Zr-activated aluminum supported by piperidine and the corresponding ^{27}Al NMR shifts (1: 152, 2: 128) for the formed products at room temperature within 24 h.*

P, bar	Unreac. Al*, g	Al* convers., %	δ(^{27}Al), ppm	(1), %	(2), %
20	0.09	84	129, 148	58	42
40	0.10	82	129, 151	63	37
60	0.08	86	129, 152	61	39
80	0.09	84	129, 149	76	24
100	0.09	84	128, 152	63	37

Summarizing, the positive effect of the hydrogen partial pressure on Al* conversion was expected, as the higher hydrogen pressure allows the reaction to proceed at higher reaction rates. Despite that, the hydrogen partial pressure of 20 bar was sufficient to obtain the high conversion value of Al*, whereas at 80 bar the enhanced formation of desired compound **1** was observed. The results of this study indicated that the optimal reaction parameters for the hydrogenation of Zr-activated aluminum were the temperature of 35 ºC and the hydrogen pressure of 80 bar.

3.3.3.3 Reversible hydrogenation in piperidinoalane system

In order to test [pipAlH$_2$]$_2$ as a model for Al-N-H based hydrogen storage applications, it is of interest to study its dehydrogenation/rehydrogenation cyclability. The thermal behavior of **1** was investigated by simultaneous TG-DSC-MS analysis (Fig. 3.24). The obtained data showed that the first endothermal signal at 97 °C corresponds to the melting point of [pipAlH$_2$]$_2$. The first mass loss is connected to the

hydrogen release and finishes with an endothermal process at 206 °C which probably corresponds to the decomposition of **1** into **2** with the release of hydrogen and aluminum[195]. The observed partial sublimation of **1** may explain the fluctuations of the heat flow signal and the higher mass loss (22.4 %) compared to the calculated ones (1.33 %) that assume hydrogen release, only. The next endothermic effect at 310 °C is assigned to the decomposition of **2** with the release of hydrogen and piperidine.
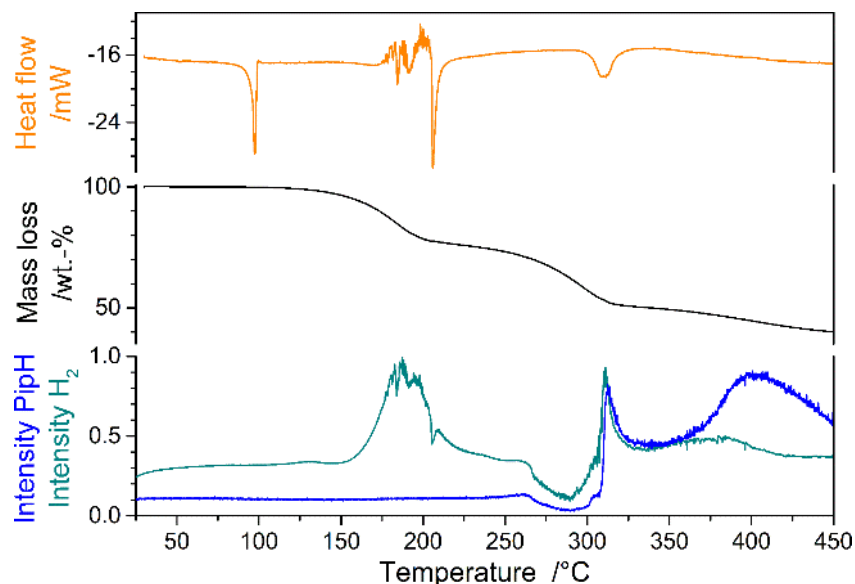
Figure 3.24 *Simultaneous DSC (top), TGA (middle), and MS (bottom) measurement of [pipAlH₂]₂ (1) (performed in MPI, Mülheim).*
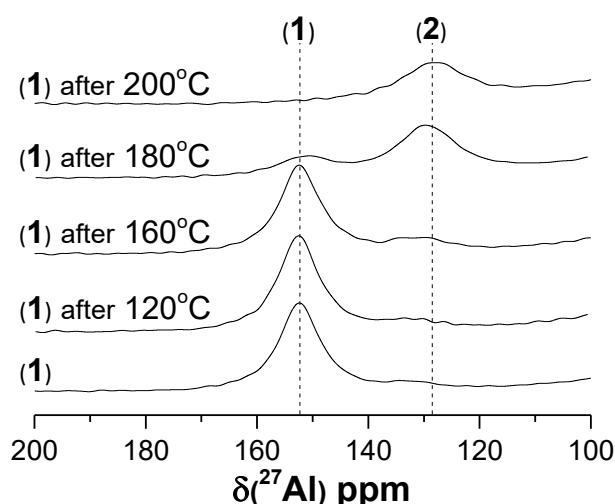
Figure 3.25 *Stepwise thermal decomposition of [pipAlH₂]₂ (1).*

The pyrolysis experiment of **1** confirmed that the solid obtained after decomposition at 200 °C is identical to **2** (Fig. 3.25). Decomposition of **1** was performed in steps of 20 °C from 100 °C until 200 °C. After 2 h at the desired temperature, the sample was cooled and the part of the solid was taken for NMR analysis, afterwards, the sample was heated until the next desired temperature. NMR analysis of the sample after 200 °C revealed the presence of only **2**.

Figure 3.25 shows that the decomposition of **1** to **2** commences at around 160 ⁰C, with increasing temperature the **1** : **2** ratio decreases. In addition, starting from 160 ⁰C, partial sublimation was observed on the cold part of the flask and a grey precipitate on the bottom, confirming the suggestions made from TG-DSC measurement.

TG-DSC-MS analysis of compound **2** showed the small and weak endothermic signal at 121 °C (Fig. 3.26), corresponding to the melting point, reproduced by several measurements. The second event starts at 275 °C, assigned to the decomposition of **2**, and is followed by the vigorous release of piperidine and hydrogen, which caused the fluctuations of the heat flow signal. This endothermic event finished at 306 °C with a mass loss of 68.8 %. The same event was observed for compound **1** confirming the suggestion about the decomposition of **1** via **2**.
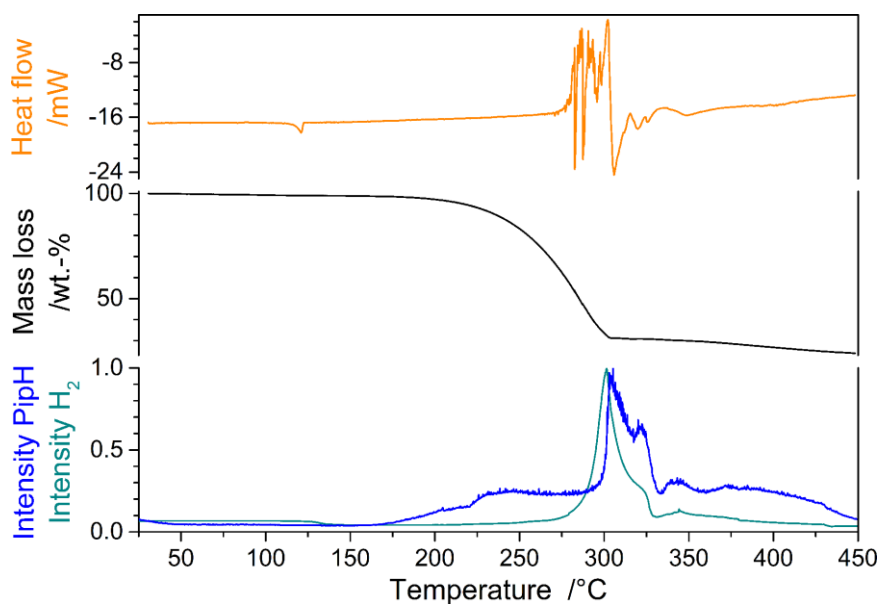
Figure 3.26 *Simultaneous DSC (top), TGA (middle), and MS (bottom) measurement of [pip$_2$AlH]$_2$ (**2**) (performed in MPI, Mülheim).*

A similar trend was observed for compound **3** at 291 °C, corresponding to the decomposition of the final compound and piperidine by itself (Fig. 3.27).
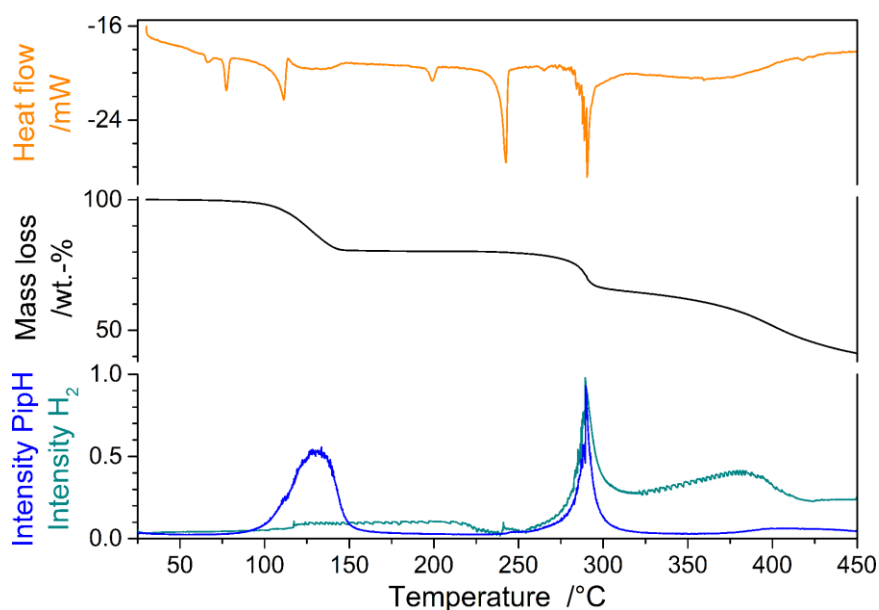
Figure 3.27 *Simultaneous DSC (top), TGA (middle), and MS (bottom) measurement of [pip$_3$Al]$_2$ (**3**) (performed in MPI, Mülheim).*

The decomposition analysis of compound **3** shows several thermal events (Fig. 3.27). The sharp endothermic signal at 77 °C is attributed to the melting point. The next endothermic signal is considered to be the first decomposition step of **3** supported by intensive piperidine release with a mass loss of 19.4 %. The cause for two endothermic events at 199 °C and 243 °C is not clear. The mass loss of 33.8 % was observed after the last endothermic event at 291 °C. The vaporized products detected by MS, hydrogen and piperidine, confirmed the second decomposition step of compound **3**.

The formation of **1** by direct hydrogenation and its continued reaction, more precisely its decomposition, to **2** may be an important step for hydrogen storage in this system:

$$4 \text{ Al}^* + 4 \text{ pipH} + 2 \text{ H}_2 \xrightarrow{\Delta} 2 \quad \mathbf{1} \quad \rightleftharpoons^{\Delta} \quad \mathbf{2} \quad + 2 \text{ Al}^* + 3 \text{ H}_2$$
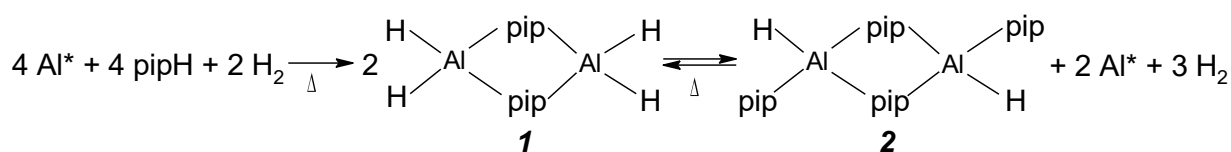
Scheme 3.19 *Proposed pathway for the formation of **1** from activated aluminum with piperidine, and its subsequent dehydrogenation.*

It must be noted, that the thermal decomposition of [pipAlH$_2$]$_2$ does not allow to simply revert to the amine but to [pip$_2$AlH]$_2$, as the first reaction step in Scheme 3.19 is considered as being largely irreversible. Thus, the reversible hydrogen storage cycle can only be based on the second step if it is found to be reversible. To test the reversibility of this step, the product formed by direct hydrogenation of Zr-activated aluminum supported by piperidine was decomposed in THF and then reformed in the reactor, according to Scheme 3.19. After optimization of the procedure (hydrogenation step: 21 h at 80 bar of H$_2$ pressure and a temperature of 35 $^\circ$C with 10 % excess of Al*, dehydrogenation step: 6 h at 120 °C) the conversion of the Zr-activated Al reached 98 %. The hydrogen pressure change during one cycle is displayed in Fig. 3.28. The hydrogen uptake due to the H$_2$ dissolution and the hydrogenation of activated aluminum stabilized by piperidine led to the pressure change of 13.1 bar. In contrast, a pressure change of 8.4 bar due to H$_2$ dissolution was observed for the experiment performed only with THF. The right graph of Fig. 3.28 shows the decomposition of the product formed in THF upon heating to 120 °C and the control experiment performed only with THF. The gas released after heating was vented from a pressure level of 5.8 bar to bring the reactor down to atmospheric pressure. In the blank experiment, only 2.3 bar of residual pressure was released.
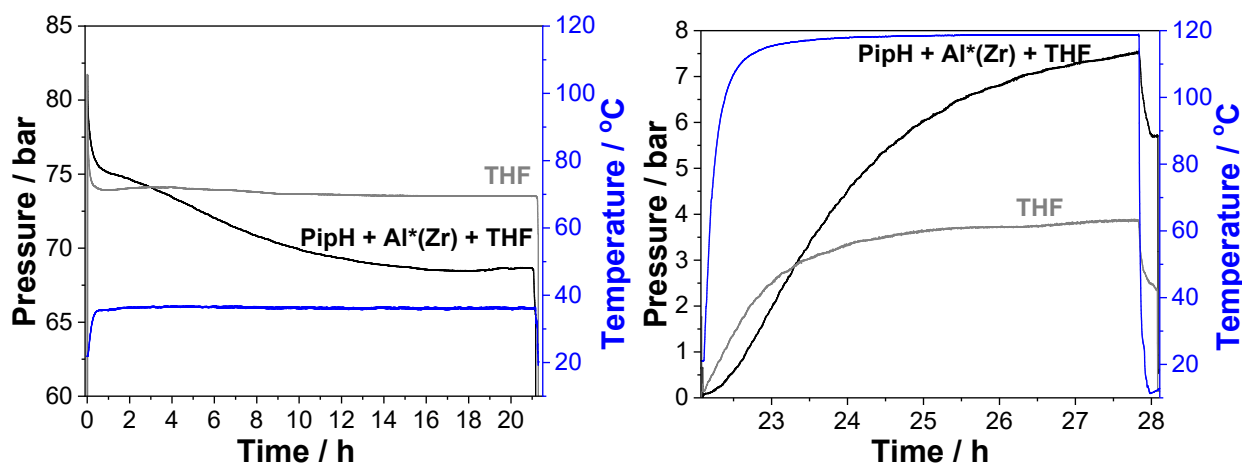
Figure 3.28 *Reactor pressure during hydrogenation of Zr-activated aluminum and piperidine in THF slurry (80 bar/35 °C, left) and decomposition of the formed product (120 °C, right).*

After each hydrogenation and dehydrogenation step, samples for NMR measurements were taken (Fig. 3.29, right).
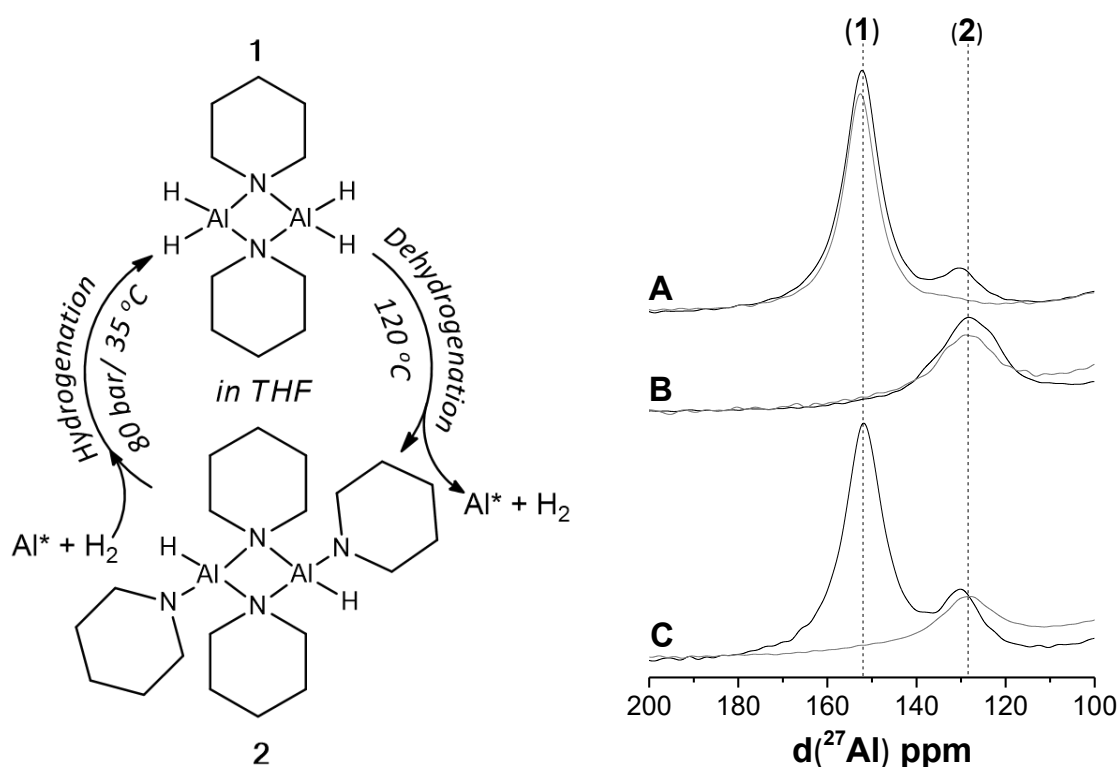
Figure 3.29 *The proposed hydrogenation/dehydrogenation cycle applying piperidinoalanes (left). ^{27}Al NMR spectral study of reversible hydrogenation of [pip$_2$AlH]$_2$: A – spectrum after first hydrogenation (80 bar/35 °C); B – spectrum after thermal decomposition (120 °C); C - spectrum of second hydrogenation (80 bar/35 °C), grey: A – spectrum of pure **1**; B – spectrum after thermal decomposition (200 °C); C - spectrum after hydrogenation (100 bar/RT) (right).*

The signals at δ = 152 and 129 ppm, which belong to **1** and **2**, respectively, resulting from the measurement that was recorded after the first hydrogenation step (Fig. 3.29, A). After the decomposition of **1** upon heating to 120 °C, only a signal at

$\delta = 129$ ppm remains and indicates the formation of **2** (Fig. 3.29, B). Thus, the observed scenario of the dehydrogenation of **1** appears to follow the proposed route (Fig. 3.29, left). In the second hydrogenation step, **2** was hydrogenated to **1**, however not completely. Two signals were recorded at $\delta = 152$ and 129 ppm (Fig. 3.29, C) demonstrating that **1** can be synthesized reversibly by direct hydrogenation from **2**.

It must be also noted that the reversibility was not successful when starting from pure **1** in THF (Fig. 3.29, grey). Whereas the decomposition of **1** to **2** still occurred (Fig. 3.29, grey B), the hydrogenation from **2** to **1** failed. A higher temperature was needed for the decomposition of pure **1** (200 °C), compared to the product obtained from Zr-activated Al* (120 °C). Therefore, it can be concluded, that the TM can catalyze, as expected, both directions: it supports the hydrogenation of activated Al in the presence of piperidine, and decreases the dehydrogenation temperature of the formed compound.

In order to gain more understanding about the mechanism of the reversible hydrogenation cycle, two additional experiments applying compound **2** (differently prepared) were carried out in an autoclave reactor:

1) Compound **2*** (formed from activated Al*(Zr) and piperidine) with additionally added non-activated Al.

2) Compound **2** (formed from AlH$_3$ and piperidine) and additionally added activated Al*(Zr).
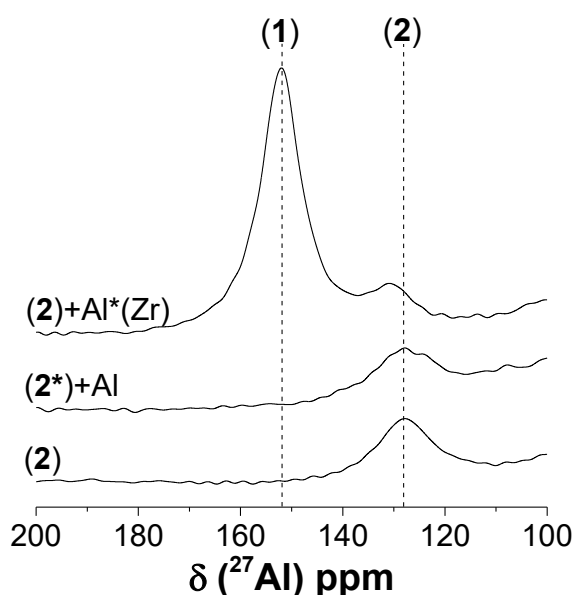
Figure 3.30 ^{27}Al NMR spectra of compound **2** (bottom) and products obtained after hydrogenation of compound **2*** with metallic Al (middle), compound **2** and Al*(Zr) (top).

Both syntheses were carried out in THF solution at the same conditions (hydrogen pressure of 100 bar, room temperature, reaction time 24 h). After the reaction, the sample for NMR analysis was taken in both cases. In the first case, after the hydrogenation of compound **2*** and non-activated aluminum, the ^{27}Al NMR spectra showed only one signal at 128 ppm, which corresponds to starting compound **2** (Fig. 3.30). The reversible hydrogenation was not realized, even so, the compound **2*** was formed (previously) from activated aluminum.

In the second case, ^{27}Al NMR revealed the intense signal at 152 ppm and a smaller signal at 129 ppm, corresponding to compounds **1** and **2**, respectively. The hydrogenation of compound **2**, in the second case, was realized. Thus, it was confirmed that compound **1** can be formed from **2**, even if it consists of non-activated aluminum. Based on these observations, it became apparent that the driving force for the reversible hydrogenation has to be the activated aluminum. The attempt to explain the reaction mechanism is shown in Scheme 3.20.
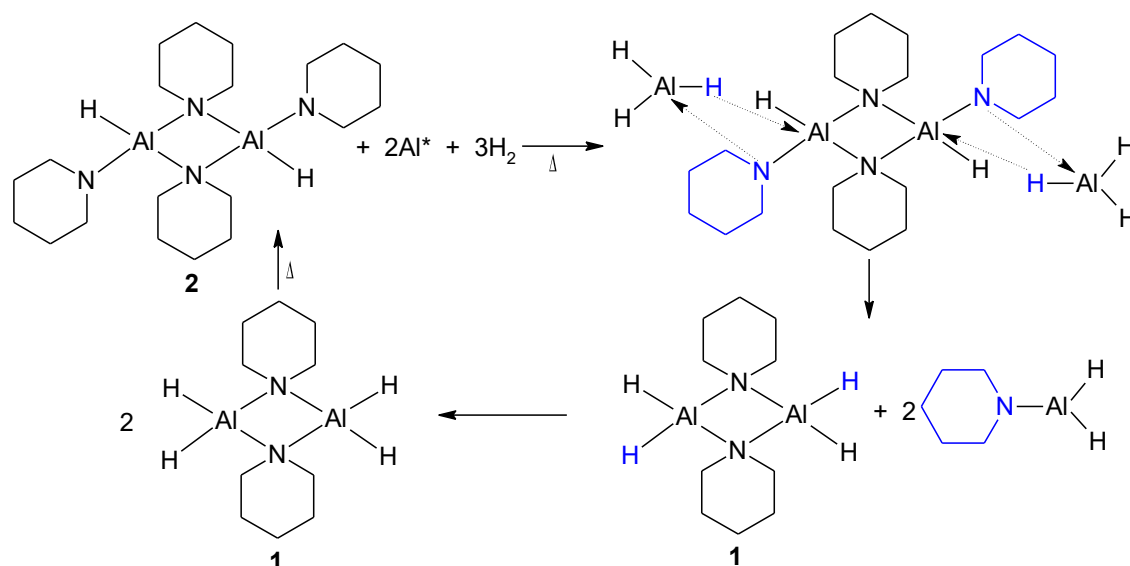
Scheme 3.20 *The proposed mechanism of the reversible hydrogenation cycle in piperidinoalane system.*

Initially, the intermediate formation of aluminum hydride from activated aluminum has been suggested. Further, aluminum hydride interacts with compound **2** and the hydrogen transfer from aluminum hydride to aluminum of compound **2** take place. In a similar manner, the terminal piperidinyl ligand of compound **2** transfers to aluminum of alane, resulting in the formation of monomeric piperidinoalane (pipAlH$_2$), which then further stabilizes by the formation of the dimeric compound **1**. As mentioned above, the thermolysis of compound **1** leads to the formation of compound **2,** with the release of hydrogen and aluminum, and the cycle can be started again. For a more detailed understanding of the hydrogenation/dehydrogenation mechanism, the *in situ* experiments with deuterium gas will be helpful.

3.3.4 Conclusions

A primary goal of this work was to explore the options for hydrogenation of aminoalanes, and to understand the factors that enable this reaction to proceed reversibly. While the majority of current research has been focused on the separation of hydrogen from amine-alane complexes or on the search for new Al-N-based

materials with favorable hydrogen release properties, in this work, it was showed that the development of the new method that establishes sustainable cycles for known material is an equally valid approach that could provide the solution for hydrogen storage when the properties of the material are well investigated.

In this study, the perspective approach for the reversible hydrogenation in aminoalane has been developed, which could provide a solution for hydrogen storage in other similar systems. After unsuccessful attempts to rehydrogenate aminoalanes in the solid state, the reversible hydrogenation of aminoalanes in the presence of solvent was performed. In this respect, the discovery of the reversibility in the piperidinoalane system is encouraging although the weight percentage of hydrogen stored is low. In order to fully exploit the potential of piperidinoalanes as hydrogen storage materials, the properties of the corresponding aminoalanes were investigated. As the result of the structural and spectroscopic characterization, two crystal structures, $[pip_2AlH]_2$ and $[pip_3Al]_2$, were revealed. Both structures possess dimers with $[AlN]_2$ units as central elements. Furthermore, the pathway to obtain hydrogen from $[pipAlH_2]_2$ by its controllable decomposition to $[pip_2AlH]_2$ which can then again be hydrogenated to $[pipAlH_2]_2$ was presented.

In order to optimize the developed aminoalane system, several reaction parameters (temperature, pressure, and solvent) were varied. It was established that the key aspect that enables hydrogenation of aluminum is the coordinating ability of the solvent that can sufficiently stabilize the intermediate alane and support the amine-alane formation.

The other significant results were obtained from the investigation of the ability of TM additives ($Ti(OBu)_4$, $ZrCl_4$, $HfCl_4$, YCl_3) for aluminum activation. It has been shown, that not only Ti, but also Zr and Hf can efficiently promote the activation of aluminum for its hydrogenation. The attempt to explain the TM activity order (Zr > Hf > Ti > Y) for the formation of aminoalanes has been done.

Future work should focus on *in situ* experiments (NMR, IR) to understand the role of the TM additive in enabling the reversibility of the hydrogenation reaction. The additional study on the additive amount for the aluminum activation may also be useful for improving the cycle performance.

4 SOLID-STATE HYDROGEN STORAGE

This chapter is organized in three sections that cover the theoretical, experimental, and practical aspects of the doped-NaAlH$_4$ system. The introduction part presents an overview of the recent developments that have been made in the field of doped-NaAlH$_4$ system, with the emphasis on selected catalyst materials, doping procedure, as well as thermodynamics and kinetics of the fundamental (de)hydrogenation reaction chemistry.

In the experimental part, the change of the hydrogen sorption/desorption behavior of sodium alanate upon doping with the different levels of the additive has been investigated. The aim of this work was to develop the hydride composite (based on sodium alanate) for hydrogen storage in high-pressure tanks. Therefore, it was of interest to investigate to which degree the high content of titanium additive does have a catalytic or thermodynamic impact on the (de)hydrogenation of sodium alanate. In the first instance, the improvements have been made with respect to the kinetics of (de)hydrogenation reactions by the addition of the high amount of TiCl$_3$ to NaAlH$_4$. Further improvements have been achieved regarding the gravimetric storage capacity by the addition of Al powder to Ti-doped NaAlH$_4$ samples.

The main instrumental techniques, used in this work, include high-pressure DSC for the study of thermal effects of doped sodium alanate, and Sievert's apparatus for the characterization of the hydrogen sorption properties of the materials. With the help of XRPD and TG-DSC, the state of the samples between the hydrogenated and dehydrogenated forms has been determined.

4.1 State of the art

Hydrogen storage in solids is considered to be an attractive method for the realization of hydrogen storage systems, where the safety, sustainability, and performance requirements may be met.

4.1.1 Thermodynamic tuning of the hydrides

Nowadays, there exist plenty of complex metal hydrides, but none of them can simultaneously satisfy suitable kinetic and thermodynamic properties with the high gravimetric storage capacity, necessary for a practical solid-state hydrogen storage system. While, in the past, kinetic limitations could be solved successfully by the addition of the doping agent, thermodynamic constraints still remained.

The reaction enthalpy has been a serious problem preventing the adoption of complex hydrides for hydrogen storage. For hydrogen sorption at useful temperature (below 100°C) and pressure (up to 10 bar), the potential hydrogen storage material should have a reaction enthalpy of about 20 - 30 kJ/(mol H_2)[15]. Unfortunately, the thermodynamic properties of most currently known hydrides fall outside this range. The materials with small values of reaction enthalpy are highly unstable and require high hydrogen pressure for rehydrogenation. The other part of the hydrides have rather high thermodynamic stability and require high temperature for hydrogen release.

One of the promising approaches to meet the thermodynamic target is to alter the thermodynamics of the complex hydrides[15,241]. In principle, there are two approaches possible, in order to adjust the reaction enthalpy of the hydrides. The first option is a substitution in the metal lattice and the formation of a new intermetallic single-phase hydride. In this case, in order to decrease the overall reaction enthalpy, the enthalpy of formation of the new hydride has to be smaller than the heat of formation of the intermetallic compound. This pathway was successfully demonstrated by Libowitz et al.[242], who could achieve a breakthrough in solid-state hydrogen storage by discovering the reversible intermetallic compound ZrNi. This alloy reacts reversibly with gaseous hydrogen to form the ternary hydride $ZrNiH_3$, which has thermodynamic stability in between the stable high-temperature hydride ZrH_2 and the rather unstable NiH. This work opened up a new research field which led to the discovery of hundreds of new interesting compositional types with different thermodynamic properties following Miedema´s rule of reversed stability[243]:

$$\Delta H(AB_nH_{2m}) = \Delta H(AH_m) + \Delta H(B_nH_m) - \Delta H(AB_n) \qquad (4.1)$$

Generally, these intermetallic alloys consist of a high-temperature hydride forming element A and a non-hydride forming element B shown in Table 4.1.

Table 4.1 *Hydrogen storage properties of typical intermetallic hydrides*[244,245].

Composition	A	B	Example	wt.-% H_2	P_{eq}, T
A_2B	Mg, Zr	Ni, Fe, Co	Mg_2Ni	3.6	1 bar, 555 K
AB	Ti, Zr	Ni, Fe	TiFe	1.9	5 bar, 303 K
AB_2	Zr, Ti, Y, La	V, Cr, Mn, Fe, Ni	ZrV_2	3.0	10-8 bar, 323 K
AB_3	La, Y, Mg	Ni, Co	$CaNi_3$	1.8	0.5 bar, 298 K
AB_5	Ca, La, Ce	Ni, Cu, Co, Pt, Fe	$LaNi_5$	1.4	2 bar, 298 K

This is a relatively straightforward process, which is mainly used for the metal hydrides, where the initial metal can be alloyed with a second metal to alter the hydride stability. Another example of Ni-composites is intermetallic Mg_2Ni, the reaction enthalpy of this alloy is reduced by about 11 kJ/(mol H_2) for Mg_2NiH_4[246], compared to pure MgH_2 (74 kJ/(mol H_2))[37]. However, the main drawbacks of this system are low storage capacity (3.6 wt.-%) and still too high desorption temperature (above 250 ºC).

The alloying with TM may significantly improve hydrogen release and uptake properties of metal hydrides[38,39,247]. The Mg-Ti[248] and Mg-V[249] hydride phases have lower desorption temperatures, 130 ºC and 160 ºC, respectively, than pure MgH_2 (above 300 ºC). Despite that, the reversibility and long-term stability of these systems are questionable. Other examples are the Mg-Cd[250], Mg-Ag[251,252] systems, which also result in a decrease in enthalpy change and desorption temperature compared to pure magnesium. The theoretical study[253] predicted, that the ability of the alloying atom for the destabilization of magnesium hydride decreases in the following order Cu > Ni > Al > Nb > Fe > Ti. Thus, the composition modification by the addition of the other metal is a viable option for reducing the thermodynamic barrier of the metal hydrides. However, it can become trickier for the complex hydrides, where the electronegativity of the cation and anion complexes determine the structure and bonding of the compound.

Different groups have searched for mixed alkaline or alkaline earth-based alanates and borohydrides[254–256]. A very prominent example for tuning of thermodynamic properties of complex metal hydrides is the $LiBH_4$/Al system[257–259]. Aluminum addition decreases the decomposition temperature of this system and $LiBH_4$ can be formed from LiH and AlB_2 at 450 ºC under a hydrogen pressure of 13 bar[257]:

$$2LiBH_4 + Al \rightleftharpoons 2LiH + AlB_2 + 3H_2 \qquad (4.2)$$

The interesting lithium-magnesium alanate[61] system has the dissociation enthalpy of 13.1 kJ/mol for the second endothermal step:

$$LiMg(AlH_4)_3 \xrightarrow{100\ °C} LiMgAlH_6 + 2Al + 3H_2 \qquad (4.3)$$

$$LiMgAlH_6 + 2Al \xrightarrow{150\ °C} MgH_2 + (LiH) + 3Al + 3/2H_2 \qquad (4.4)$$
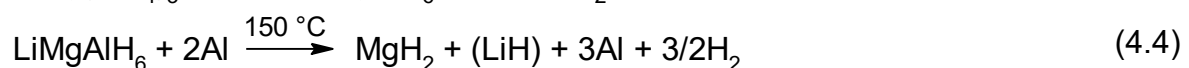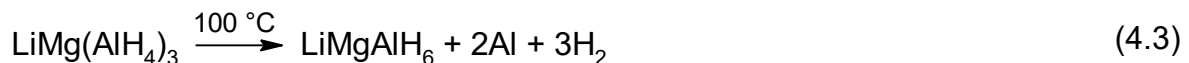
A positive effect on the thermodynamics was observed in the fluorine-modified Na-Al systems, which yields in the reduction of the overall reaction enthalpy to 35 kJ/mol H_2[256]. Theoretically, 3.3 wt.-% of hydrogen could release by the following reaction scheme:

$$1/2NaAlH_4 + 1/6Na_3AlF_6 \rightleftharpoons 1/3Na_3AlH_3F_3 + 1/3Al + 1/2H_2 \qquad (4.5)$$

$$1/3Na_3AlH_3F_3 + 1/3Al \rightleftharpoons NaF + 2/3Al + 1/2H_2 \qquad (4.6)$$
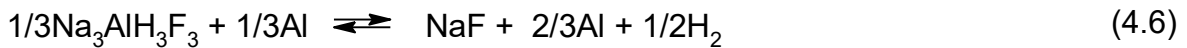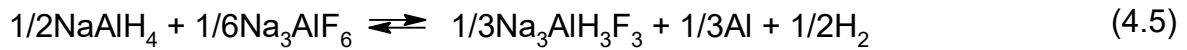
Generally, the alloying of the hydrides with the other non-hydrogen-containing element/compound can effectively decrease the operation temperature, but at the same time, it also reduces the total hydrogen storage capacity. To overcome this drawback, the second approach to alter the reaction enthalpy was developed. This concept is often referred to as the reactive hydride composite (RHC)[71,260]. In these systems, two high-capacity hydrides are combined and the reaction enthalpy of the hydride can be tailored very efficiently, if a new stable compound is formed. This approach is more successful, as the total hydrogen storage capacity of the composite is the sum of the added hydrides. Vajo et al.[71] were the first who demonstrated this approach by designing the MgH_2/$LiBH_4$ composite in order to lower the dehydrogenation temperature of $LiBH_4$. The formation of MgB_2 upon decomposition stabilizes the dehydrogenated state and, thereby, destabilizes $LiBH_4$:

$$LiBH_4 + 1/2MgH_2 \rightleftharpoons LiH + 1/2MgB_2 + 2H_2 \qquad (4.7)$$
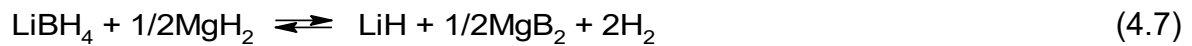
This composite shows a superior reversible hydrogen capacity of about 8 wt.-%, which is 70% of the theoretical value. The hydrogenation/dehydrogenation enthalpy was reduced by 25 kJ/(mol H_2) compared with pure $LiBH_4$ (74 kJ/(mol H_2)[52]).

Following this pioneering work, a large number of other metal hydrides (CaH_2[261], YH_3[262,263], CeH_2[261,262], SrH_2[264]) were investigated in order to obtain the reversible composites with $LiBH_4$. The remaining issue of these composites is to allow lower temperature applications.

The situation has been changed when high-pressure hydrogen storage was suggested for on-board application, due to the absence of the practical hydrogen storage concept. A possible solution could be a novel hybrid tank system, which combines a high-pressure tank with unstable metal hydrides. This system could show obvious advantages in terms of gravimetric and volumetric hydrogen density compared to high pressure, solid-state, or liquid hydrogen storage techniques.

The possible adjusting of the hydrogen pressure can be achieved by the combination of the stable and unstable hydrides or hydride forming compounds. The higher dissociation pressure was observed for Mg-Al phases[265,266] compared to pure Mg. The hydrogenation of Mg-Al intermetallic phases leads to the formation of MgH_2

and Al and a new phase is formed back upon dehydrogenation. The general hydrogenation/dehydrogenation reaction can be written as follows:

$$x\text{MgH}_2 + y\text{Al} \rightleftharpoons \text{Mg}_x\text{Al}_y + x\text{H}_2 \qquad (4.8)$$

However, the formation of AlH_3 or $\text{Mg(AlH}_4)_2$ could not occur during the hydrogenation of Mg-Al system, since severe conditions are needed[267].

The increase of the pressure plateau was also observed by adding a large amount of the dopant (TiCl_3) to NaAlH_4[268]. Such a change of properties of this system remains not completely clear. The possible explanation of this phenomenon could be the formation of AlTi-alloy, which then can alter the thermodynamic of the NaAlH_4 system.

To summarize, tremendous efforts have been made to overcome the thermodynamic barrier of the hydrides and to obtain the material with suitable dehydrogenation properties. Despite all the strategies mentioned above, there are still left many challenges to meet all requirements of the practical hydrogen storage system.

4.1.2 Features of the sodium alanate system

Among other solid materials, sodium alanate is one of the most thoroughly investigated hydrogen carriers due to its favorable gravimetric storage density, auspicious operating conditions, and reversibility in the presence of the additive. Moreover, sodium alanate is also significantly cheaper than classical interstitial metal hydrides making it the most practically viable solid system known. Despite the comprehensive knowledge in the field of hydrogen storage in sodium alanate, the practical approach to overcome the present drawbacks of this system has not been yet proposed. As will be shown in the following sections many attempts have been made to favorably modify the enthalpy of hydride formation. While the reaction kinetics could be optimized significantly by the addition of the additive, the desorption enthalpies of NaAlH_4 and Na_3AlH_6 (37 kJ/(mol H_2 and 47 kJ/(mol H_2)[58]) are still too large for many applications.

The presented in the literature contradictory observations and statements on the hydrogen absorption/desorption pathways hindered the understanding of the fundamental processes that appear during hydrogen sorption in sodium alanate, which is of key importance toward modification and design of materials for hydrogen storage. Thus, the next part will point out the fundamentals of the reversible hydrogenation of

the sodium alanate system and will present an overview of the recently discovered methods for the catalytic enhancement of this process.

Decomposition and hydrogenation processes

A brief description of sodium alanate formation and decomposition was mentioned already in 1955 by Finholt et al.[269]. The formed salt by the reaction of sodium hydride with aluminum chloride/bromide started to melt at around 183 ºC and was decomposed at 230-240 ºC. The more detailed studies of the sodium alanate properties were made several years later by different groups[87,270–272]. In general, $NaAlH_4$ can release hydrogen in the following three steps:

$$3NaAlH_4 \xrightarrow{220\,°C} Na_3AlH_6 + 2Al + 3H_2 \quad (3.7\ wt.-\%\ H_2) \qquad (4.9)$$

$$Na_3AlH_6 \xrightarrow{250\,°C} 3NaH + Al + 3/2H_2 \quad (1.9\ wt.-\%\ H_2) \qquad (4.10)$$

$$3NaH \xrightarrow{>450\,°C} 3Na + 3/2H_2 \quad (1.9\ wt.-\%\ H_2) \qquad (4.11)$$
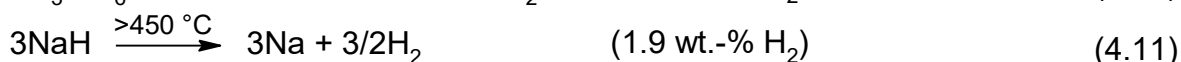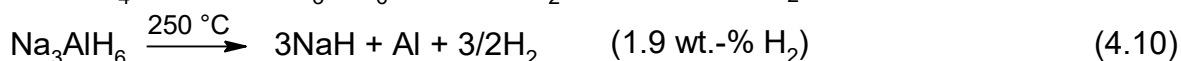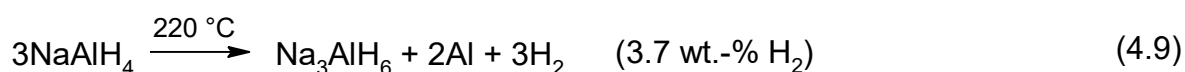
The final decomposition of NaH (eq. 4.11), which would give the total storage capacity of 7.5 wt.-% H_2, requires a temperature (above 450 ºC) that is too high for most applications. The occurrence of these dehydrogenation reactions has been verified during studies of the thermal behavior of $NaAlH_4$ by a variety of techniques including thermal analysis[87], *in-situ* X-ray-diffraction[230], solid-state NMR spectroscopy[273], and others.

The direct formation of $NaAlH_4$ from the elements was first reported independently by Clasen[270] and Ashby et al.[160]. It was found that $NaAlH_4$ can be formed from sodium or sodium hydride, activated aluminum powder, and a hydrogen pressure of about 150 bar at 150 ºC in the tetrahydrofuran solution. The later study by Dymova et al.[274] revealed that this reaction could be carried out without solvent by melting the reactants for 2-3 h at 270 ºC under 175 bar of hydrogen pressure.

The first equilibrium-pressure studies of sodium alanate were reported in 1975 by Dymova et al.[275]. Two plateaus at hydrogen pressures of 154 and 21 bar were observed at 210 ºC corresponding to the first (4.9) and second (4.10) reactions. Due to the high kinetic barriers of the hydrogenation/dehydrogenation reactions, the potential of sodium alanate as a practical onboard hydrogen storage material was obscured for many years until the discovery in 1997 by Bogdanović and Schwickardi[79], that the addition of small amounts of Ti-based catalysts significantly enhances the kinetics of these reactions. In addition, the conditions required for rehydrogenation were reduced to 170 °C at 152 bar of hydrogen pressure.

Structural properties

Sodium aluminum hydride (or hexahydride) is composed of a "complex anion" $[AlH_4]^-$ (or $[AlH_6]^{3-}$) and the Na^+ cation. The bond between the hydrogen atoms and aluminum can be regarded as covalent with a strong ionic character, the bond to the sodium is ionic[276]. Sodium alanate crystallizes in a body-centered tetragonal structure having the $I4_1/a$ space group[277]. The aluminum atom is surrounded by four hydrogen atoms in $NaAlH_4$ and six in α-Na_3AlH_6, forming the $[AlH_4]^-$ tetrahedral and $[AlH_6]^{3-}$ octahedral complexes (Fig. 4.1).
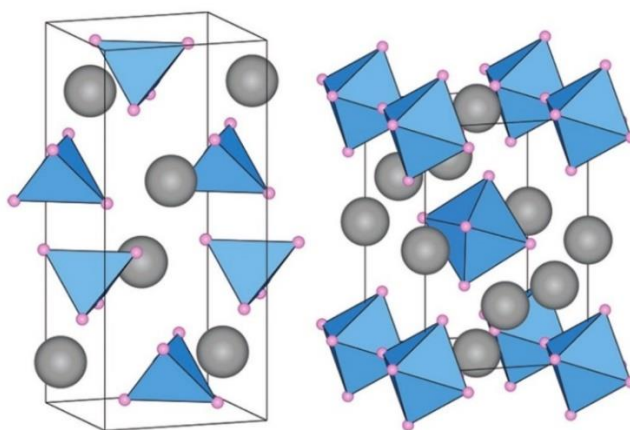
Figure 4.1 *The crystal structures of NaAlH$_4$ and α-Na$_3$AlH$_6$: grey balls – sodium cations; blue polyhedral – aluminum hydride anions[278].*

The structure of Na_3AlH_6 was determined for the low-temperature phase α-Na_3AlH_6 to be monoclinic with the $P2_1/n$ space group symmetry[279]. At about 252 ºC the monoclinic α-Na_3AlH_6 phase transforms to a cubic β-Na_3AlH_6 phase[280].

Thermodynamic parameters

In the literature, a large amount of information on thermodynamic properties of $NaAlH_4$, Na_3AlH_6, and NaH is available from the experimental studies[58,281–285] and also from the theoretical calculations[286–290]. Usually, calorimetric methods, pressure-composition-isotherm (PCI) measurements, or thermodynamic modeling (CALPHAD method, DFT calculation) have been used to obtain the thermodynamic information about the sodium alanate system. The relevant literature data about the formation and decomposition enthalpy of sodium alanate is summarized in Figure 4.2. Thermodynamic data from various research groups show a scattering depending on the applied method. Several groups performed detailed measurements of dehydrogenation enthalpies of $NaAlH_4$. The combination of the heat of fusion (23.2 kJ/mol) and heat of phase transition (1.8 kJ/mol), determined by calorimetric

studies[283], with the dehydrogenation enthalpy of liquid NaAlH$_4$ to Na$_3$AlH$_6$, determined from the PCI measurements[275], gives the dehydrogenation enthalpy (from NaAlH$_4$ to Na$_3$AlH$_6$) of 36.7 kJ/mol. This value is in good agreement with the data obtained by Bogdanović et al.[58] from PCI measurements (37 kJ/mol). The pressure-equilibrium measurements give the average enthalpy value between the desorption and absorption step, thus the deviation of the data is not surprising.

Na+Al+2H$_2$

ΔH_f^o,kJ/mol
-112 [290]
-113 [282]
-116.3 [289]
-117 [283]
-117 [287]

Na+1/2H$_2$

ΔH_f^o(NaH),kJ/mol
-56.4 [282,289]
-56.9 [281]
-56.98 [290]

NaH+Al+2H$_2$

ΔH_{des},kJ/mol
13.8 [283]

1/3 β-Na$_3$AlH$_6$ +2/3Al+H$_2$

ΔH_{struc},kJ/mol
1.8 [283]

1/3 α-Na$_3$AlH$_6$ +2/3Al+H$_2$

ΔH_{des},kJ/mol
12.8 [275]

ΔH_{des},kJ/mol
37 [58]

ΔH_{des},kJ/mol
53 [58]
56.5 [282,287]

NaAlH$_4$(l)

ΔH_{fus},kJ/mol
23.2 [283]
28 [58]
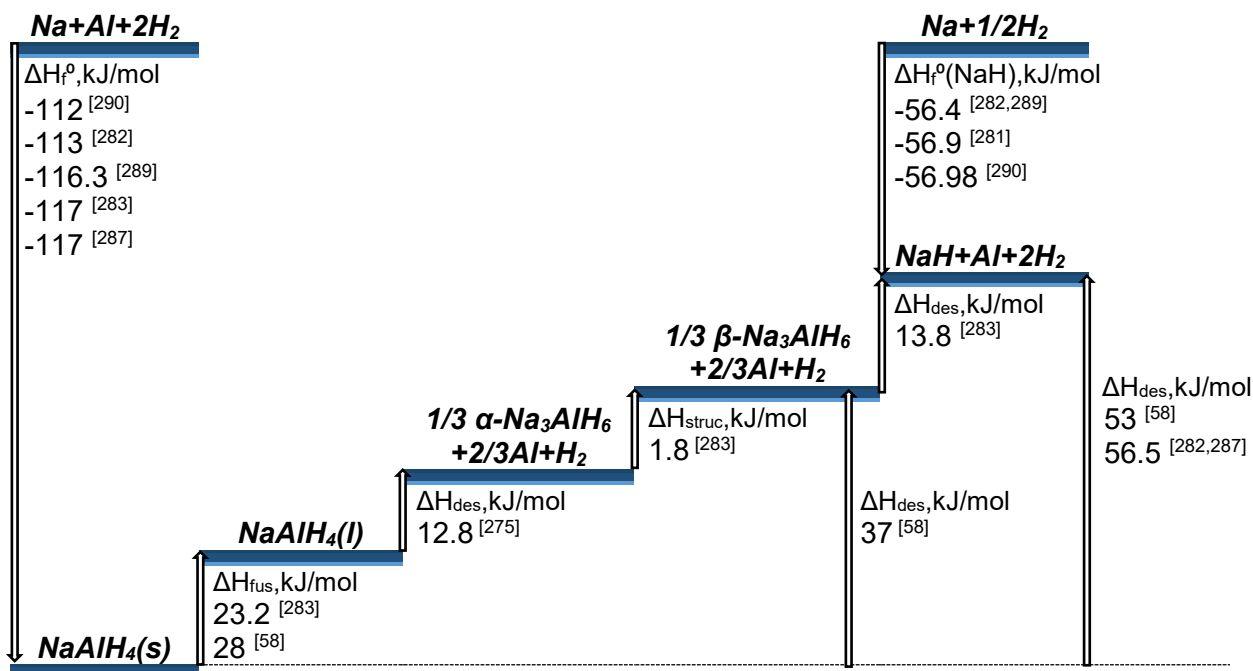
NaAlH$_4$(s)

Figure 4.2 *Schematic enthalpy diagram of the phases and intermediate products of 1 mol NaAlH$_4$.*

The equilibrium relationship in the metal-hydrogen system by means of pressure-composition isotherm schematically presented in Figure 4.3 (left). A PCI diagram indicates the maximum attainable storage capacity and thermodynamic conditions for the reversible reaction. When hydrogen gas is introduced into the system, it dissolves in the lattice of the metal and forms a solid solution, which takes place in the region AB[6]. The concentration of hydrogen in the metal increases with increasing of the hydrogen pressure in the system, thus the interactions between hydrogen atoms become locally important, and the nucleation and growth of the hydride phase are started. For the given temperature, the hydrogen equilibrium pressure is constant in the two-phase region (a solid solution phase and hydride phase), shown as plateau section BC. When the solid solution phase has been converted to the hydride phase, the equilibrium pressure changes with the amount of solute hydrogen in the hydride phase (region CD). Typically, metal hydrides exist in two or more solid phases, thus the conversions between them may exhibit hysteresis. The hydride metallic phase is

assumed to be both disordered and strained, giving rise to a greater plateau pressure for hydride formation than for the hydride decomposition: $p_{des} < p_{abs}$.
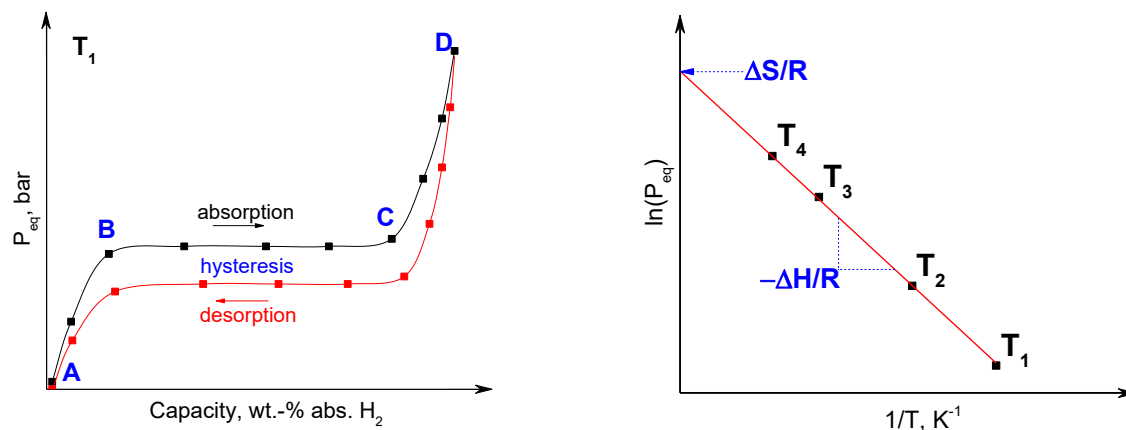
Figure 4.3 *Schematic diagram of pressure-composition isotherm (left) and the Van´t Hoff plot (right). Adapted from*[6,291]

At a given temperature, the plateau pressure represents one point on a Van't Hoff plot, usually plotted as the logarithm of pressure versus reciprocal temperature, shown in Fig 4.3 (right). Under the reference state, the Gibbs free energy is:

$$\Delta G^o = \Delta H^o - T\Delta S^o \tag{4.12}$$

with $\Delta G^o = -RT \ln K_{eq}$ (4.13)

For the hydrogenation reaction:

$$K_{eq} = p^o / p_{eq} \tag{4.14}$$

Then the Van't Hoff equation takes the form:

$$\ln p_{eq}/p^o = \Delta H^o/ RT - \Delta S^o/R \tag{4.15}$$

Based on this equation, the reaction entropy can be obtained from the y-intercept of the linear fit in the Van´t Hoff plot, and the reaction enthalpy from the slope (Fig. 4.3, right). Generally, the entropy change corresponds to the change from molecular hydrogen gas to dissolved hydrogen and has to be roughly -130 J/(K·mol H$_2$)[292].

The temperature at which the hydrogen dissociation pressure of a metal hydride reaches 1 bar, is used for the classification of the reversible metal hydrides as low temperature (LT - below 50 ⁰C), medium temperature (MT - between 50 and 200 ⁰C), and high-temperature metal hydrides (HT - above 200 ⁰C). There are only a few metal hydrides that show equilibrium pressure about 1 bar at above room temperature (Fig. 4.4), which can be suitable for hydrogen storage in fuel cell applications.
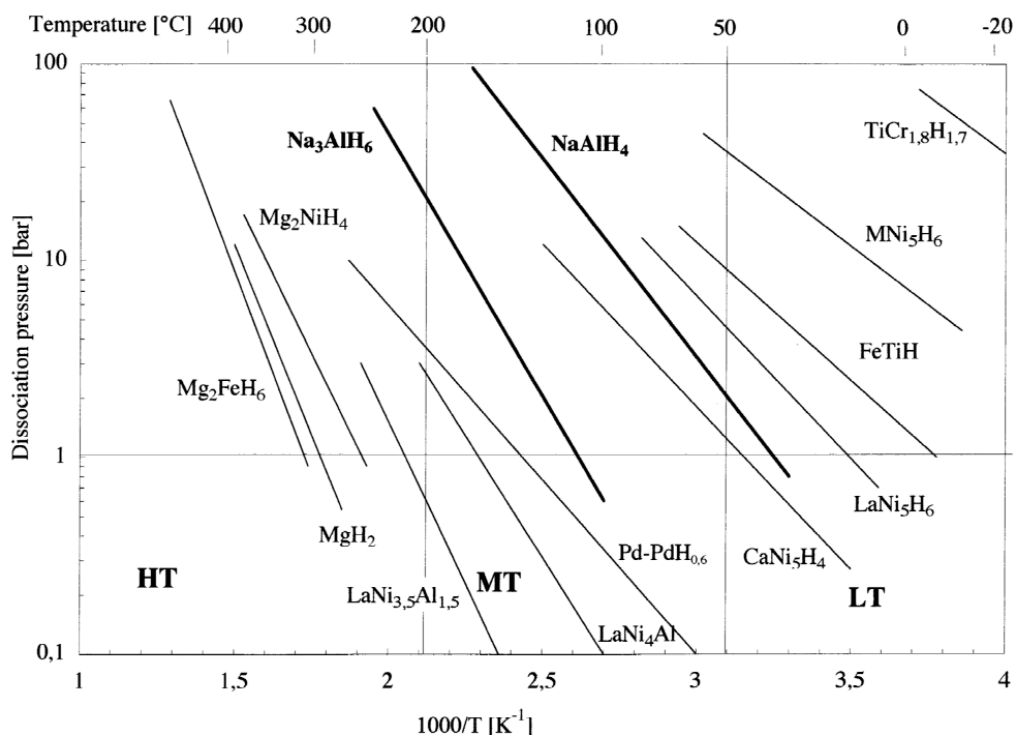
Figure 4.4 *Comparison of the Van´t Hoff plot for the various metal hydrides[58].*

The first decomposition step for $NaAlH_4$ has an equilibrium pressure of 1 bar at around 30 ºC, thus belongs to low-temperature complex metal hydrides. The equilibrium pressure of 1 bar for the second decomposition step (Na_3AlH_6) appears about 100 ºC, and it is thus one of few known medium temperature complex metal hydrides[36].

Kinetics

For the hydrogen storage system, a fast reaction rate at near-ambient temperatures and pressures is an important property and corresponds to fast recharging. The kinetics is usually represented by the activation energy (E_a) of the reaction. The activation energy of sorption reactions can be determined by the Arrhenius equation (4.16) and Kissinger equation (4,17) as follows:

$$K = A \ exp(-E_a/RT) \tag{4.16}$$

$$ln(\beta/T_p^2) = ln(AR/E_a) - E_a/(RT_p) \tag{4.17}$$

where K - rate constant, A - frequency factor, β - heating rate, and T_p - peak temperature.

Generally, the reaction kinetics of complex metal hydrides depends on the occurrence of phase transition, the surface area of the material, the dimensions and homogeneity of the microstructure, type of the additives, etc.[36]. In the reaction between sodium alanate and hydrogen, the grain boundaries, crystal defects, or

impurities may play the role of the nuclei where the reaction usually starts. The hydride formation process is composed of several intermediate partial processes[6,293,294]:

1.   Physisorption of hydrogen on the surface of the material.

2.   Chemisorption of the hydrogen molecule.

3.   Dissociation of the hydrogen molecule into atoms.

4.   Diffusion of hydrogen atoms through the surface/formed hydride layer.

5.   Chemical reaction on the metal/hydride interface.

The desorption reaction follows the same steps but in a reverse direction: de-bonding from metal atoms, diffusion to the surface, the formation of the molecular hydrogen, and dissociation from the surface of the material (Fig. 4.5).

Figure 4.5 *The illustration of the hydrogen absorption/desorption process in the metal particle. Adapted from[19].*

The hydrogen absorption kinetics depends on the activation barrier involved with the chemisorption of hydrogen atoms on the metal surface, diffusion of hydrogen atoms, and nucleation of the hydride phase. During the hydrogenation step, the nucleation of the hydride phase may control the reaction rate in the early stages, and the hydrogen diffusion through the product layer may control the rate in the latter stages[295].

Pure sodium alanate has very slow hydrogen desorption rates and re-hydrogenation is only possible under harsh conditions. The method of preparation and activation procedure can significantly influence the reaction kinetics. In principle, the doped sodium alanate material can be prepared, by applying following methods:

1.   Doping of pre-synthesized $NaAlH_4$ by reaction (ball milling or wet chemical reaction) with catalytic amounts of additive[58,296].

2.   Direct synthesis – the reaction (ball milling or wet chemical synthesis) of NaH (or Na) and Al in the presence of doping agents, and subsequent hydrogenation of doped mixtures under pressure[297,298].

3.   One-step direct synthesis - ball milling of NaH, Al powder, and doping agent mixtures under hydrogen pressure[78,299].

4.   Hydrogenation of aluminum-dopant alloys together with NaH (or Na)[300,301].

Significant progress has been made in enhancing the hydrogen sorption kinetics by preparing the samples via ball milling[302]. Fine microstructures, created by this method, provide fast diffusion pathways and a high number of nucleation sites for the phase transformation in the solid-state reaction[303]. It is also possible to achieve a more close mixing of the additive and NaAlH$_4$ with high homogeneity, but the chemical reactions involved are not necessarily the same as in solution[83,304].

By reducing the particle size, the thermodynamic material properties may be changed to a point where the surface free energy can govern the reaction[305]. Thus, nanoconfinement of NaAlH$_4$-based system can display improved (de)hydrogenation kinetics, can enable reversibility under milder conditions and may lead to an improvement of the thermodynamic properties, compared to bulk NaAlH$_4$, by to the introduction of a substantial level of relatively stable structural defects or phase change.

However, nanosizing is not easy to apply on an industrial level. Another important issue is that the material agglomerates during hydrogen sorption cycling, and loses the benefits of nanosizing. Thus, the approach of using a catalyst to enhance the sorption rate is preferable over nanoscaling.

4.1.3 Catalytic enhancement of reversible hydrogenation in sodium alanate

The discovery of Bogdanovic et al.[79], that the addition of small amounts of Ti-based compounds considerably improve the hydrogen sorption properties of sodium alanate-based systems, urges a widespread search for more efficient dopants. A screening of a large number of transition and non-transition metals that are commonly effective in catalyzing a wide range of chemical processes has been tested as an alternative to titanium. The same research group performed a comprehensive analysis of the different doping materials and showed the rehydrogenation ability of doped NaAlH$_4$ at a temperature as low as 120 °C at 130-150 bar of H$_2$[237]. Surprisingly, the traditional hydrogenation catalysts (Pt, Pd, Ir, Rh, and others) were found to be not nearly as effective for reversible hydrogenation of NaAlH$_4$ as Ti[83,278].

So far, most research has been focused on Ti-additives (Ti powder, TiCl$_2$, TiH$_2$, TiO$_2$, TiB$_2$, TiCl$_3$, TiF$_3$, TiCl$_4$, TiBr$_4$, Ti(OBu)$_4$)[306–309] and Zr-containing compounds (ZrCl$_4$, Zr(OPr)$_4$)[306,310,311] or on combination of these dopants[230,310,312,313] for enhancing hydrogen sorption/desorption behavior of sodium alanate. Zidan et al.[310] found that Ti is a catalyst superior for catalyzing the first dehydrogenation reaction (NaAlH$_4$ → Na$_3$AlH$_6$) compared to Zr which is catalyzing the second dehydrogenation

step (Na$_3$AlH$_6$ → NaH) more efficiently. Thus, the combination of both titanium and zirconium additives optimizes the dehydrogenation behavior of NaAlH$_4$ and leads to a reversible hydrogen uptake of about 4 wt.-% at temperatures below 100 ºC. Anton[83] has performed a comprehensive study on different transition metal additives and showed the dependence of the dehydrogenation rates of doped NaAlH$_4$-system on the radius of the TM ions in the catalyst. The optimal radius of the TM ions in the catalyst was identified between those of Al^{3+} (0.51 Å) and Na$^+$ (0.97 Å).

Later, Bogdanovic et al.[314] reported that the salts of the rare earth elements such as CeCl$_3$, PrCl$_3$, or ScCl$_3$ have even better catalytic activity than TiCl$_3$. Pukazhselvan et al.[315] concluded that the Ce rich mischmetal catalyzed NaAlH$_4$ can store hydrogen up to 4.2 wt.-% at a temperature of 120 ºC. Moreover, CeAl$_2$-doped NaAlH$_4$ exhibited rapid kinetics (recharge 4.9 wt.-% of hydrogen in 20 min), and the materials could release about 70% of the hydrogen capacity in the first 6 min[316]. However, it should be noted that these materials are expensive and may not be the best option for practical applications.

In order to find a more inexpensive additive, different C-based materials were tried as dopants for accelerating the (de)hydrogenation kinetics of sodium alanate. Incorporating carbon[80,81,317], carbon aerogel[82], single-walled carbon nanotubes[85], carbon nanofibers[318] into NaAlH$_4$ by ball milling can improve the kinetics of dehydrogenation and cycling of NaAlH$_4$ even in the absence of a transition metal catalyst. The improvements are probably related to the enhancement of the hydrogen transport between the solid and the gas phase resulting from the increase of the surface area of the material.

For the general overview of the influence of the different additives on the sorption properties of sodium alanate, the hydrogen storage capacity as a function of operating temperature is presented in Figure 4.6. Much attention has been devoted to metal halides as a catalyst for NaAlH$_4$. However, for the metal halides or oxides, the greatest problem remains the formation of by-products (e.g. NaCl, NaOH), which contribute to a dead weight and also consume the active Na element, and evolve gas impurities. Therefore, to minimize the loss of available hydrogen capacity, pure metals, metal hydrides, or other Me-Ti species have also been directly introduced by ball milling to NaAlH$_4$.
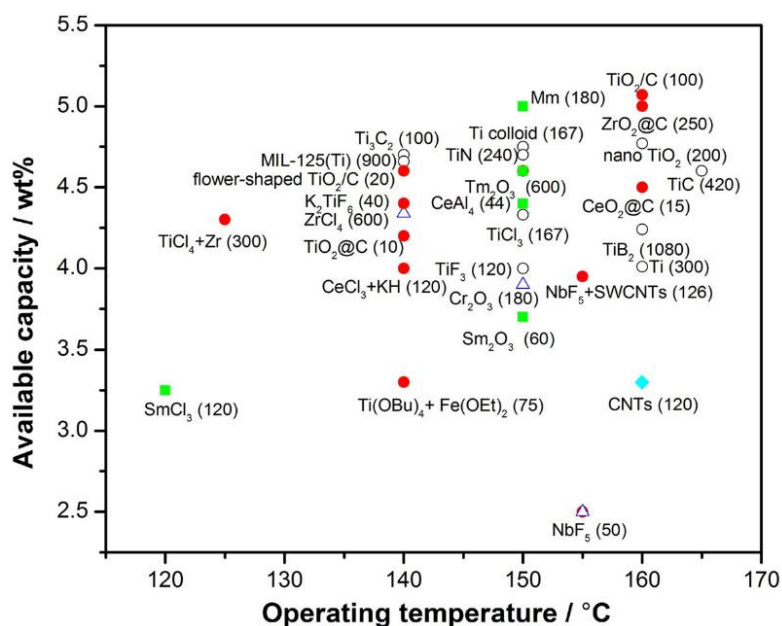
Figure 4.6 *Comparison of isothermal dehydrogenation capacities of NaAlH₄ doped with the different additives (discharge time, min)*[319].

Mechanism of the hydrogen absorption/desorption

The hydrogen sorption/desorption in complex metal hydrides involves relatively complex multi-step mechanisms. A wide variety of catalytic mechanisms has been proposed in order to explain the dopant action in the $NaAlH_4$ system. Frankcombe[228] presented a detailed review of the existing mechanisms for the catalytic activity of Ti-doped $NaAlH_4$. The main and the most often proposed mechanisms in the literature are:

1. Hydrogen pump/spillover mechanism[41,293]. According to this mechanism, the dopant works like an excellent bridge for breaking and forming the H-H bond with substantially lower activation energy than at the sites of the other constituents. However, the main difficulty with this idea is to explain why the metals with the high dissociation activity (e.g. Pt, Pd) do not act in a similar manner as Ti-compounds. Overall, this mechanism can explain the role of the dopant in providing the low energy routes between molecular hydrogen and the hydride, but it is not sufficient to explain the catalytic effect of the particular additive.

2. Mobile species[230,320–322]. In this mechanism, the proposed action of the dopant is to promote the mobility of species in order to facilitate the phase separation of the products. Several mobile species have been detected during alanate (de)hydrogenation (AlH_3, AlH_x ions, Al_xH_y phases, clusters, and others) that may act as shuttles for the transport of Al to solid NaH. Nevertheless, the transport of these species and the role of the catalyst are not completely clear.

3. Vacancy-mediated mechanism[321,323–325]. This mechanism suggests the formation of the H-, Na-, AlH3-based vacancies and their dynamics via a long-range from trapping site to trapping site. For this model, the diffusion of the mobile species occurs due to the presence of the charged vacancies. On the other hand, the reason why dopant favors the formation of the vacancies has not been explained.

4. Zipper model[326]. In this model, the catalytically active Ti species displace Na ions from the bulk, moving the Na ions and other species to the surface, where they can easily react. Thus, Ti works as a slider of a zip, destabilizing the surface, and during decomposition, Ti returns to the surface. However, this model only specifically explains the decomposition process, leaving out the hydrogenation step.

5. Atomistic model[229]. In this mechanism the Ti dopant reduces the charge separation between the ions, to form the intermediate states $M^+\cdots Ti\cdots H^-$, NaH and AlH3. The catalyst acts as a bridge to transfer NaH or Na$^+$ and H$^-$ from NaAlH4 forming Na3AlH6 and finally isolated NaH, leaving AlH3 behind, which spontaneously releases hydrogen and aluminum. However, the intermediate formation of AlH3 cannot be proven, as these species are very unstable.

In general, these models include the steps, which are necessary for the overall transformation process. Nevertheless, only the atomistic mechanisms could explain the catalytic effect of the dopant for both hydrogenation and dehydrogenation reactions.

Role of the dopant

Many studies have confirmed the extraordinary effect of dopants on the accelerating hydrogen sorption kinetics of catalyzed sodium alanate. In general, several suggestions were made to explain the role of the dopant:

➤ It supports the dissociation of hydrogen and its activation for the exchange with the solid[293,321,327].

➤ It supports the formation/splitting of intermediates (e.g. AlH3)[230,233,327].

➤ It supports the diffusion of hydrogen in the corresponding phases[328].

➤ It supports the formation and diffusion of the highly mobile species (AlH$_x$, NaH molecules, or Na, Al, H ions)[230,329].

➤ It reduces the nucleation barrier of new phases[328,330].

➤ It interferes with the anion-cation charge transfer; reduces the charge separation by forming the metal-hydrogen bridge[229,327].

> ➤ It may lead to the metastable state of the system by the distortion or substitution of Al or Na in the lattice[325,331,332].

> ➤ It takes part in the formation of catalytically active species (solid solution, clusters, alloys, amorphous or crystalline phases) on the surface or in bulk[307,308,333].

So far, the knowledge about the effects of the dopant for reversible hydrogenation of NaAlH$_4$ is indirect and mostly based on the differently prepared samples starting from freshly doped, cycled, or dehydrogenated samples. These differences in initial materials, preparation methods, and sample manipulations make the situation complicated and extend the information obtained from the dehydrogenation to the hydrogenation.

Influence of the dopant content

Using a low content of Ti-based additive is highly desirable from a gravimetric perspective, particularly for TiCl$_3$, which consumes a part of NaAlH$_4$ to form NaCl, and adds dead weight to the system. In general, the lower the dopant content the higher the storage capacity of the system. However, the low content of the additive is also one of the main reasons why it is complicated to justify its role.

The early studies of TiCl$_3$-doped NaAlH$_4$ demonstrated a strong nonlinear dependence of hydrogenation/dehydrogenation rates as a function of the TiCl$_3$ content[297,334]. It was not completely clear why the sorption kinetics improves significantly with increasing the level of the Ti-additive (Fig. 4.7, left).
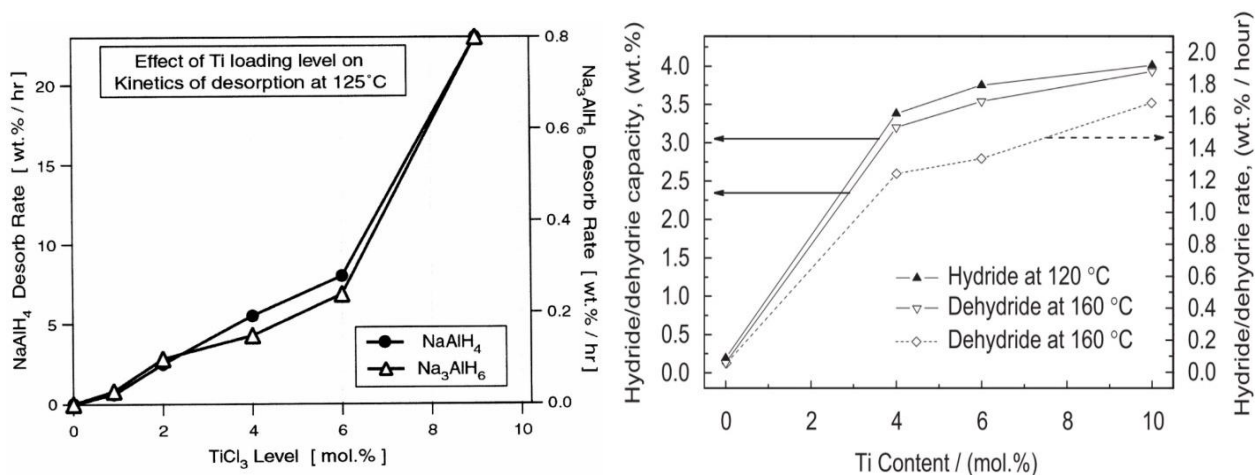
Figure 4.7 *Desorption rates for NaAlH$_4$ and Na$_3$AlH$_6$ as a function of added TiCl$_3$ (left)[297] and the hydrogen storage capacity and sorption rates of NaAlH$_4$ as a function of Ti content (right)[309].*

These findings differ partly from that of Xiao et al.[309] which showed similar results, that dehydrogenation/hydrogenation rates increase with the increase of Ti

content (Fig. 4.7, right). The difference could arise from the various Ti additives applied for doping: pure metallic Ti powder used by Xiao et al.[309] does not produce inactive by-product NaCl, unlike TiCl$_3$ dopant used by Gross et al.[297]. Furthermore, it was suggested that Ti introduced into the composite finally reacts to the titanium hydride and a Ti-Al phase, which are catalytically active materials for the hydrogenation/dehydrogenation of the NaAlH$_4$ system. These transformations may explain why the hydrogen storage characteristic is improved with the increase of the Ti content.

XRD studies of NaAlH$_4$ doped with titanium or zirconium revealed that significant changes occur in the lattice parameters upon doping[332]. This effect indicates that the remarkable enhancement of dehydrogenation kinetics may be due to the dopant-induced lattice distortions. Furthermore, Streukens et al.[268] observed the increase of the dissociation pressure, hysteresis, and the slope of the dissociation pressure plateaus with increasing doping level in Ti-doped NaAlH$_4$ (Fig. 4.8).
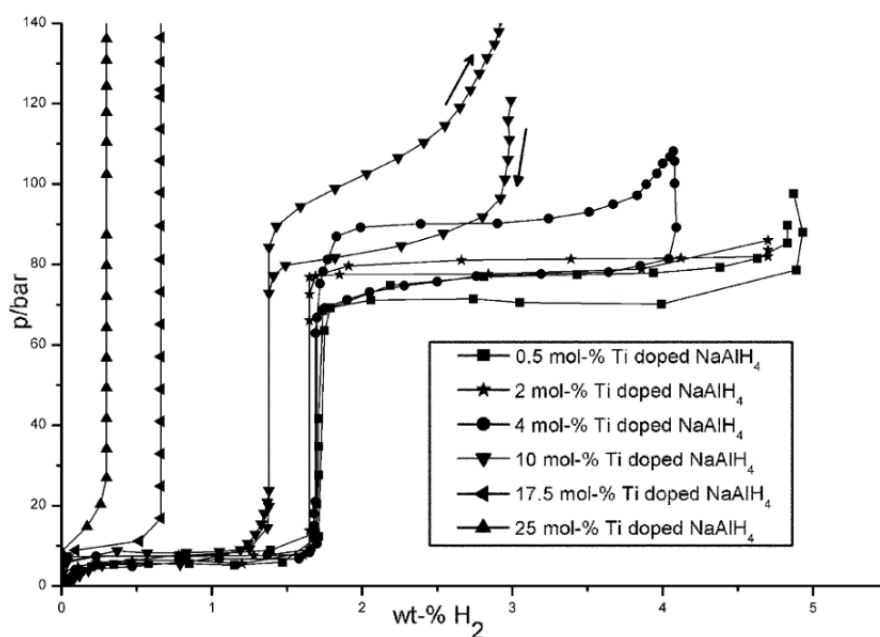
Figure 4.8 *PCI curves for Ti-doped NaAlH$_4$ with the different TiCl$_3$ levels measured at 160 °C*[268].

These results demonstrated that the titanium doping can influence not only the kinetics of the NaAlH$_4$ system, as expected for a catalyst, but also can change the thermodynamics. Based on the authors' suggestions, after doping reaction, a new Ti-Al-alloy is formed, which is thermodynamically more stable than the reactants, and leads to the increase of the dissociation pressure. During cycling of doped NaAlH$_4$, the Ti-Al-alloy changes the state between Ti-poor and Ti-rich, and contributes to the change of the hydrogen equilibrium pressure. However, the disappearance of the

plateau pressure for the first hydrogenation step (NaH $\rightarrow$ Na$_3$AlH$_6$) at high titanium content (Fig. 4.8) had no reasonable explanation.

The observation that the Al-Ti phase formation takes place during the decomposition of NaAlH$_4$ and can affect the thermodynamics, provides the possibility to adapt the hydrogen pressure, achieved at a certain temperature, to the requirements of specific applications. This holds great potential for thermodynamic tailoring of the complex hydride systems simultaneously with catalyzing the (de)hydrogenation reactions.

4.1.4 The relevance of the Al-TM species in doped sodium alanate

There are many suggestions about the nature and composition of the active component formed after the doping procedure of sodium alanate. The early reports suggested that for having the hydrogenation reaction reversible, titanium aluminide (or hydrides) may play a decisive role[307,309,333,335]. In addition, theoretical studies[331,336,337] revealed that Ti, as an amorphous or crystalline Al-Ti intermetallic phase, can modify the properties of Al surface and promote (de)hydrogenation reactions. These observations were supported by the high-resolution TEM experimental studies[338], which demonstrated that the TM-Al species were located at the surface of the grains. This hypothesis was further supported by the fact that Al-Ti-alloys, in the different composition range (Al$_{0.95}$Ti$_{0.05}$ to Al$_{0.75}$Ti$_{0.25}$), can be prepared by the mechanochemical procedure from elemental Ti and Al[301,339–341]. However, there exists no known stable phase in the Al-Ti binary phase diagram in the range between pure Al and Al$_3$Ti[342,343].

Numerous X-ray diffraction studies[344–346] showed a shoulder on the high angle side of the Al reflection, which has been ascribed to the presence of crystalline Al$_3$Ti or Al-Ti phases with the different compositions. The X-ray diffraction analysis of 10 mol% TiCl$_3$-doped NaAlH$_4$ showed that hcp-Ti(Al) solid solution has formed after milling, which transforms after cycling to an amorphous Al-Ti phase of unspecified composition[346]. The X-ray absorption near-edge structure analysis of Ti K-edge spectra for cycled 2 mol% and 4 mol% TiCl$_3$ doped NaAlH$_4$ proposed that Ti is bound in an amorphous Al$_3$Ti, which predominately occurs during the first decomposition process, where metallic Al is more abundant[333]. On the other hand, the Al$_3$Ti phase can also be obtained by milling stoichiometric amounts of NaAlH$_4$ and TiCl$_3$, which reduces completely to NaCl and Al$_3$Ti[307]. However, attempts to improve the kinetics by directly NaAlH$_4$ doping with Al$_3$Ti showed a drastically lower effect compared to TiCl$_3$ doping[347]. Thus, it was assumed that a long-range order of Ti-Al pairs, such as

bulk Al_3Ti, may lose its catalytic activity, and actually, the catalytically active species are Ti-Al clusters[308].

The formation of Al_2Ti, Al_3Ti, $Al_{82}Ti_{18}$ and $Al_{89}Ti_{11}$ phases was observed after the first hydrogenation cycle of 2 mol% $TiCl_3$ doped sample, and their further conversion into $Al_{85}Ti_{15}$ and Al_3Ti during cycling[348]. The recent high-resolution synchrotron X-ray diffraction and TEM compositional analysis of 10 mol% $TiCl_3$ doped samples demonstrated that the Al-Ti phases are in the composition range $Al_{86.5}Ti_{13.5}$ - $Al_{92}Ti_8$, and after thermal treatment, the $Al_{85}Ti_{15}$ phase is present in the majority[345,349].

The multiple numbers of Al-Ti phases (amorphous or crystalline), which are existing in doped or cycled samples have led to conflicting data, with wide interpretations regarding the Al-Ti phase composition. Much of the problem with the identification of the correct Al-Ti phase can be attributed to the fact that the observed phases always fall very close in d-spacing to the Al reflection, yielding a broad feature around Al (111) reflection (Fig. 4.9). The composition of the formed Ti-Al phases is also strongly dependent on the dopant content and hydrogen cycling conditions[345].
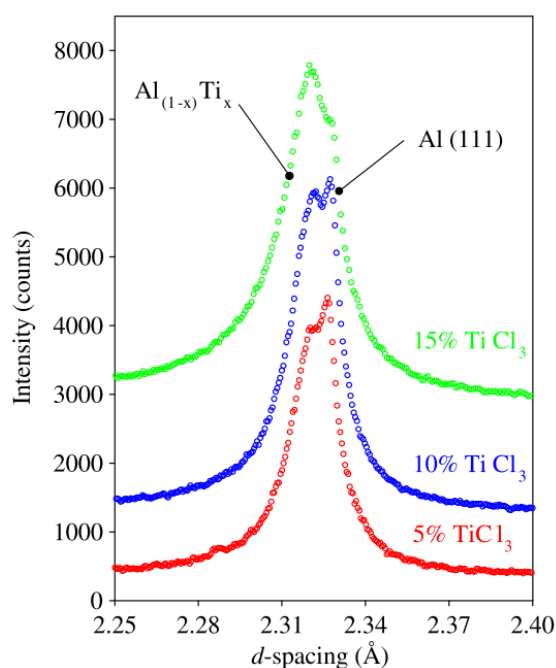
Figure 4.9 *The intensity of the Al-Ti phase as a function of the TiCl₃ content in doped NaAlH₄ (right)[345].*

During recent years, numerous transition metal-aluminum species, such as Ti-Al, Zr-Al, Hf-Al, V-Al, Fe-Al, La-Al, Ce-Al, Sc-Al[338,350–352], have been detected immediately after the doping processes or subsequent cycling of $NaAlH_4$. It has been generally ascertained that the transition metal will react with Al to form TM-Al species, which are quite likely relevant for the kinetics. These TM-Al phases most probably facilitate the dissociation and recombination of H-H bonds, which thereby reduce the working temperature and improve the hydrogen storage performance of $NaAlH_4$. However, the presence of a TM-Al phase alone cannot explain the enhancement of sorption kinetics of doped sodium alanate.

4.1.5 Summary

In principle, complex hydrides can meet the capacity requirement for hydrogen storage, however, the strong covalent/ionic bonds are related to unfavorable thermodynamics and sluggish kinetics of hydrogen sorption. Several methods to modify the properties of lightweight hydrogen storage materials were discussed. While the thermodynamic constraints could be resolved by alloying or by making reactive composites with other components, the kinetics could be improved by applying nanoscaling or catalysts.

After the discovery of reversibility in Ti-doped sodium alanate, enormous efforts have been made in order to further improve the hydrogen storage behavior of this material. However, the incomplete understanding of the mechanism of the dopant action hinders further improvement of the thermodynamics and kinetics of the sodium alanate system. A wide variety of experimental techniques and theoretical calculations has been employed to study the role of Ti in doped $NaAlH_4$. Several mechanisms have been proposed for Ti-catalyzed $NaAlH_4$ system, such as hydrogen pump/spillover mechanism, mobile species, zipper model, atomistic model, however, the exact role of the dopant stays elusive.

Numerous studies suggested that the high catalytic activity of $TiCl_3$ is due to the formation of the nano-crystalline Al-Ti phase obtained by the reaction between $TiCl_3$ and $NaAlH_4$ upon milling. The differently prepared samples and different states of the material caused confusion in distinguishing the effects of Ti species due to multi-steps of the hydrogenation/dehydrogenation processes. During cycling the state of the titanium can be changed between a low concentration in the aluminum phase $Al_{1-y}Ti_y$ (y<0.25) to the stable Al_3Ti phase. This suggestion was supported by the observation of different Al-Ti phases with the increase of the dopant content. Additionally, the content of the additive used for the doping procedure was found to have a strong influence not only on the kinetics but also on the thermodynamics of the sodium alanate system. Therefore, further work is necessary for the classification and understanding of the nature and role of Al-Ti-based species.

It is believed that the modification of the properties of the sodium alanate system can awake commercial interest in it. When the properties of the material can be adjusted to the need of the industry, this system could still hold promise for stationary applications.

4.2 Materials preparation and experimental details

4.2.1 Chemicals and purification procedure

All reactions, sample handling, transfer, and storage were performed under dry argon atmosphere using either standard Schlenk technique or employing an MBraun glove box (H_2O and O_2 < 0.1 ppm). All solvents were dried and were distilled by refluxing over Na/Al_2O_3 (SOLVONA Bilger GmbH) and stored under argon atmosphere in the solvent reservoirs that contained 4 Å molecular sieves. The used chemicals are listed in Table 4.2 and were also stored under inert conditions.

Table 4.2 *The list of the chemicals including the purity and producer.*

Compound	Formula	Purity	Producer
Sodium aluminum hydride	$NaAlH_4$	technical grade, 90%	Sigma Aldrich
Titanium (III) chloride	$TiCl_3$	99.999%	Sigma-Aldrich
Titanium (II) hydride	TiH_2	98+%	Sigma-Aldrich
Tetrahydrofuran	C_4H_8O	99.9%	VWR PROLABO CHEMICALS
Pentane	C_5H_{12}	99%	CHEMSOLUTE

Sodium aluminum hydride was purified according to the procedure developed by Bogdanović et al.[58]. First, sodium alanate was dissolved in THF and was then stirred for 3 h inside the glove box. The solution was filtered, then the filtrate was concentrated in vacuum to the volume when $NaAlH_4$ starts to separate from the solution. Under vigorous stirring, pentane was added to the THF solution causing the separation of $NaAlH_4$ as a fine precipitate. The suspension was then stirred for 1 h, and $NaAlH_4$ was filtered off and washed twice with pentane. After drying in vacuum, $NaAlH_4$ was obtained as a fine white powder.

4.2.2 Activation procedure of sodium alanate via mechanochemical treatment

Sodium alanate and TM-additive at different molar ratios (Table 4.3) were filled into a tungsten carbide ball milling jar (volume: 12 ml) in a glove box. The ball-to-powder weight ratio was fixed at 20:1 with balls also made of tungsten carbide (balls: 2 x 8 g). The milling process was carried out on a Fritsch Pulverisette 6 planetary ball mill with a maximum speed of 650 rpm. The mixture was milled for 3 hours according to Streukens[353] in order to obtain comparable results. Generally, one milling cycle included 30 minutes of milling and a 10 minutes break to avoid a destructive temperature increase inside the milling jar.

For the mixtures of sodium alanate with aluminum, the Al powder was first prepared from the decomposition of AlH_3 powder. Approximately three grams of sample were prepared each time as described in section 3.2.3 (for uncatalyzed aluminum). Afterward, the $NaAlH_4$, $TiCl_3$, and Al powders were weighed and then mixed in the designated molar ratio (Table 4.3). After the milling process, the product was collected as a fine dark gray powder.

Table 4.3 The amounts of the reactants for the mechanochemical synthesis.

Sample	m($NaAlH_4$) g	m(TM) g	m(Al) g	m(total) g	theor wt.-% H_2
$NaAlH_4$	1.000	-	-	1.000	5.60
$NaAlH_4$+2mol%$TiCl_3$	0.946	0.054	-	1.000	4.98
$NaAlH_4$+10mol%$TiCl_3$	0.778	0.222	-	1.000	3.05
$NaAlH_4$+15mol%$TiCl_3$	0.700	0.300	-	1.000	2.16
$NaAlH_4$+15mol%$TiCl_3$+40mol%Al	0.700	0.300	0.140	1.140	1.89
$NaAlH_4$+10mol%$TiCl_3$+27mol%Al	0.778	0.222	0.105	1.105	2.76
$NaAlH_4$+10mol%$TiCl_3$+51mol%Al	0.778	0.222	0.198	1.198	2.54
$NaAlH_4$+10mol%$TiCl_3$+66mol%Al	0.778	0.222	0.257	1.257	2.43
10mol%$TiCl_3$+66mol%Al	-	0.222	0.257	0.479	-
$NaAlH_4$+66mol%Al	0.778	-	0.257	1.035	4.21
$NaAlH_4$+10mol%TiH_2	0.915	0.085	-	1.000	5.13

4.2.3 Pressure-composition-isotherm measurements with a Sieverts-apparatus

The hydrogen sorption measurements were performed in a homemade Sieverts apparatus, which works based on a volumetric method and can be operated with pressure up to 200 bar and temperatures up to 600 °C. The milled material (~150-180 mg) was loaded in the sample cell inside a glove box. The sample cell was then connected to the Sieverts apparatus and was outgassed under a high vacuum (~10^{-6} bar).

The equipment (Fig. 4.10) is fully automated and controlled by a homemade software program. The experimental apparatus is shown schematically in Figure 4.10 (right) and consists of different volumes for the calibration with valves and pipes for adding hydrogen and helium, venting, and evacuating. Pressure regulators were installed to control the hydrogen pressure applied to the sample and to allow hydrogen to flow to or from the sample. The pressure was measured with a high-precision (±2.5 %) pressure transducers (MKS Instruments). The sample holder consists additionally of the manual valve, which can be opened when the whole equipment was

previously evacuated. The evacuation of the equipment was conducted by opening the appropriate valves to the turbo vacuum pump (V1-V3-V6-V9-V10) or to the helium gas (V1-V3-V6-V7). The amount of hydrogen added to the sample by opening the valves (V1-V3-V6-V8-V11) can be controlled by the pressure regulator.
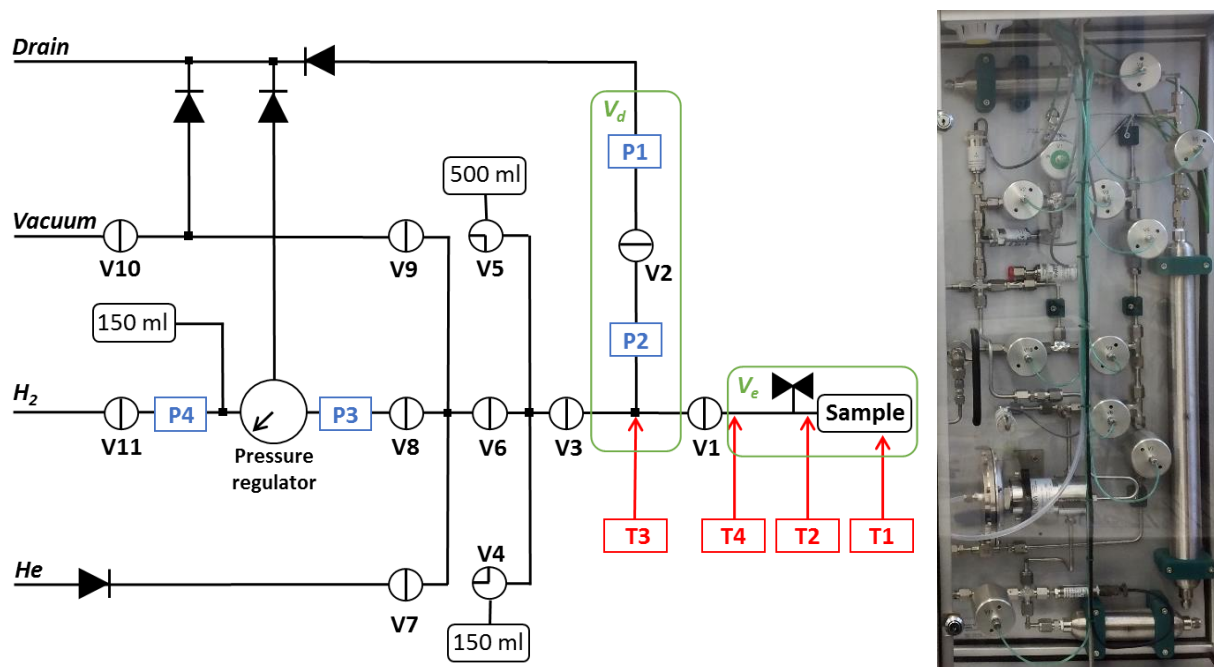
Figure 4.10 *The schematic depiction (left) and the view (right) of the Sieverts apparatus (V_d – dosage volume, V_e – effective volume, P1-P4 – pressure transducers, T1-T4 – thermoelements, V1-V11 – valves).*

For each new sample, the tightness of the equipment was tested at a pressure of 180 bar and room temperature. Next, the measurement with the helium was performed, to determine the effective volume (V_e), assuming negligibly small adsorption of helium on solid surfaces at room temperature. Afterward, the sample cell was heated with the oven controlled by PID-regulator (±0.2 °C) until the measuring temperature. Additionally, the external temperature on the wall of the sample holder was measured by a thermocouple (T1). Then, the material was hydrogenated under an initial hydrogen pressure of 180 bar for 4 h and dehydrogenated for 2 h (at ~10^{-6} bar). The sample was subjected to at least three such absorption/desorption cycles before analysis to achieve reasonably stable performance. The recording of the PCI curve was started from the desorbed sample heated to the measuring temperature. The hydrogenation capacity was calculated by the decrease in pressure caused by the hydrogen uptake by the sample. The volume (V_d) was measured before injection of the hydrogen gas to the sample (valve V1 is closed). After opening the valve V1 the hydrogen gas was injected to the sample and the equilibrium pressure (p_{eq}) was measured after reaching

the equilibration time fixed by the measuring program. This procedure was repeated with the various steps (that the region with absorption can be measured more precisely and the no-absorption region can be faster overtaken) until the chosen maximum pressure was reached. The desorption curve was measured in the same way by stepwise reducing the pressure. The absorbed amount of hydrogen was calculated based on the recorded equilibrium pressure from the following equation (4.18) in connection with the ideal gas law:

$$n_{abs} = n_1 - n_{eq} \tag{4.18}$$

$$n_{abs} = \frac{p_1 V_d}{RT} - \frac{p_{eq}(V_d - V_e)}{RT} \tag{4.19}$$

The necessary corrections were done in regard to the non-ideal gas behavior of hydrogen[354]. No doubt a variety of factors may contribute to errors (faulty valve closures, external or internal leaks, room temperature variation, barometric pressure variation, insufficient equilibration time), but the dominant error will most likely be due to the temperature variations of the sample[355].

4.2.4 High-pressure differential scanning calorimetry investigation of sodium alanate samples

High-pressure DSC measurements were carried out in a Sensys Evo (SETARAM, France) with a Calvet type DSC. The calorimeter was coupled with the high-pressure gas panel PVHP-50-100-V2 (SETARAM, France) with 1000 bar maximum operating pressure (Fig. 4.11). The hydrogen pressure can be adjusted by the pressure controller inside the gas panel and keep stable (±0.1 bar) during the isobaric measurements. The gas panel is equipped with a vacuum pump for the evacuation of the pipes.
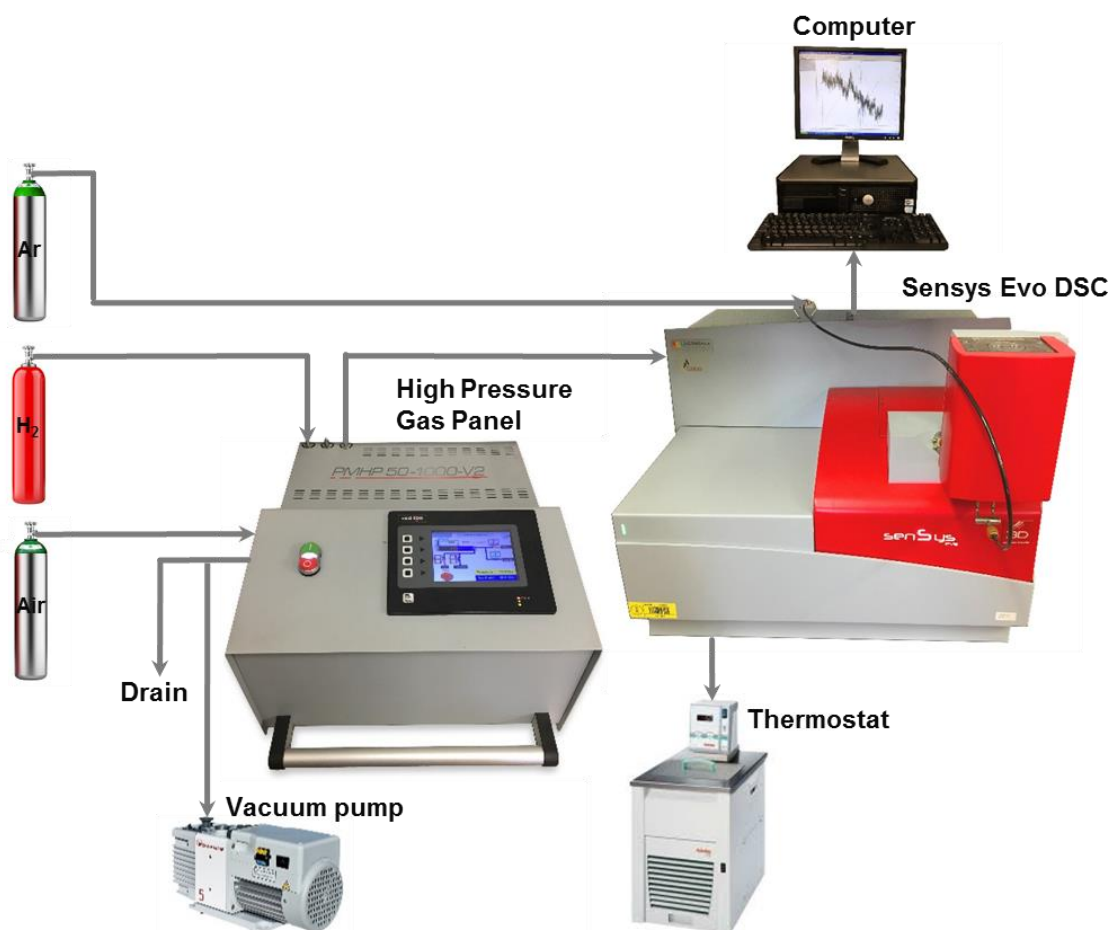
Figure 4.11 *The scheme of the experimental setup for the high-pressure DSC measurements.*

The calorimeter was equipped with a high-pressure cell (Fig. 4.12), which consists of the crucible, connecting part, safety disk, and connections to the pressure display and high-pressure gas panel. The sample cell can operate with a maximum temperature of 600 ºC and pressure up to 400 bar.

For the measurements, the sample cell was filled with 30-40 mg of the sample. The packing and tightening of the sample holder were carried out inside the glove box for protecting the sample from oxidation. Additionally, the sample cell was tightened outside of the glove box. After the sample cell was connected to the calorimeter, the equipment was evacuated three times. Then the sample cell was opened and hydrogen gas was pressurized/depressurized with exchanging the gas each time to remove residual argon. Afterward, the hydrogen pressure was adjusted to the desired level by the high-pressure gas panel.
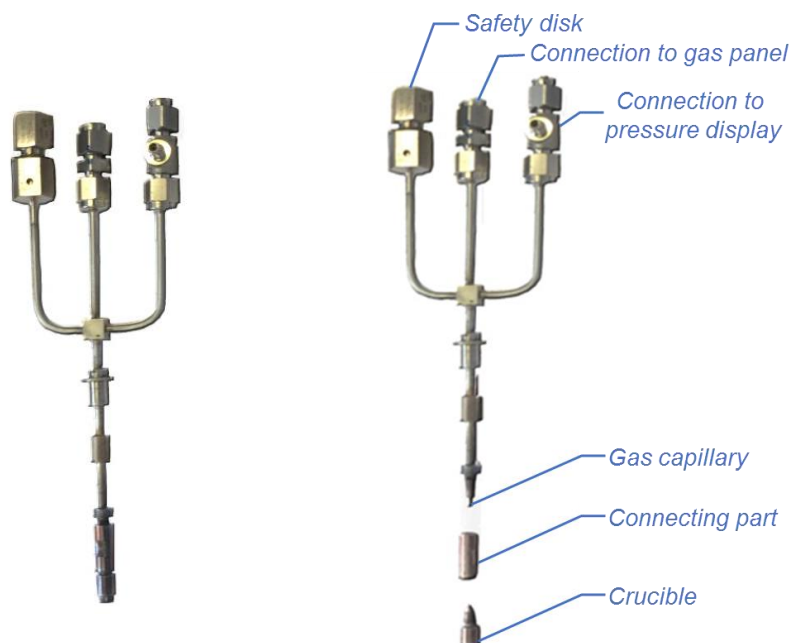
Figure 4.12 *High-pressure DSC cell with the crucible (left) and in a separated form (right).*

The measuring procedure was controlled by thermal analysis software (Calisto, SETARAM). The measurement was started only after the heat flow signal reached an appropriate stable level. In each case, the system was heated up to the measuring temperature and cooled down to room temperature with the constant heating/cooling rate. During the operation, the absorption and desorption characteristics of the sample were investigated. The thermal events were evaluated with the help of the software.

4.3 Results and discussion

One of the main goals of this work was associated with the development of the hydrogen storage material, which can be compatible with the hybrid tank system that combines a high-pressure tank with unstable metal hydrides. Thus, the following section describes the attempts to tailor the hydrogen sorption properties of sodium alanate-based system, in order to develop the material with favorable thermodynamics, kinetics, and the highest possible hydrogen storage capacity.

The first part of this chapter focuses on the hydrogen sorption behavior of doped sodium alanate. The factors that influence the hydrogen charging and discharging behavior of doped sodium alanate will be discussed. Additionally, the influence of the additive content on the thermodynamics and kinetics of sodium alanate will be investigated. Furthermore, the effect of the addition of aluminum on the sorption properties of sodium alanate doped with $TiCl_3$ will be studied in detail. This section concludes with the evaluation of the role of additional aluminum on the hydrogen sorption behavior of sodium alanate.

4.3.1 Tailoring the properties of sodium alanate-based system with the help of Ti-additive

The thermodynamic tuning of the reaction enthalpies by mixing of "stable" and "unstable" complex metal hydrides is the perspective approach for developing the composite suitable for a high-pressure hybrid tank. Therefore, in this work, the combination of "stable" sodium alanate with "unstable" titanium alanate was suggested. The high catalytic activity of Ti-based additives for achieving reversibility of sodium alanate hydrogenation/dehydrogenation, in addition to the high theoretic hydrogen storage capacity of titanium alanate (9.3 wt.-%), make Ti a very promising candidate to tailor the properties of Na-Al-H systems. In order to achieve the desired system, it is reasonable to alloy $NaAlH_4$ with elements that destabilize the hydride. This may be achieved by the addition of a high amount of dopant. The obtained composite should ideally show higher plateau pressure compared to $NaAlH_4$ doped with the small catalyst amount, and, thus, lower thermodynamic stability.

The first option for the tailoring of $NaAlH_4$ properties was connected to the application of TiH_2 as a destabilizing agent, and the development of a hydride composite, where an Al-Ti phase can be formed and potentially be hydrogenated. The following reaction path was expected:

$$NaAlH_4 + xTiH_2 \longrightarrow x/yAl_{(1-y)}Ti_y + (1-m)NaAlH_4 + mNaH + (x+3/2m)H_2 \rightleftharpoons$$

$$\overset{+xH_2}{\underset{-xH_2}{\rightleftharpoons}} xTi(AlH_4)_4 + (1-4x)NaAlH_4 + 4xNaH$$
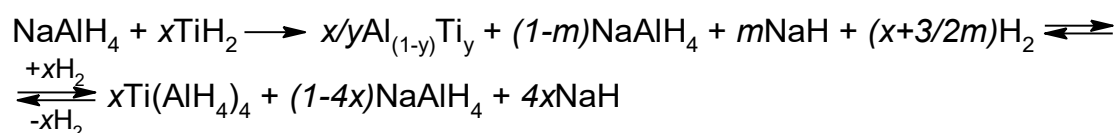
Scheme 4.1 *The proposed pathway for the hydride composite formation based on TiH_2 and $NaAlH_4$, where m = (1-y)x/y.*

Titanium hydride has the advantage compared to other Ti-additives (e.g. halides, oxides), that it does not form by-products (e.g. NaCl, NaOH), which lowers the total hydrogen storage capacity. However, based on the obtained results (Appendix C, Fig. C.1), it was concluded that, first, TiH_2 has quite low catalytic activity for the reversible hydrogenation of sodium alanate (even at high dopant level); second, no increased (or additional) hydrogen dissociation plateau was observed, indicating that TiH_2 does not influence the thermodynamics of sodium alanate (in the temperature range of 170-200 ºC and hydrogen pressure up to 180 bar). The previous investigation of Ti-doped $NaAlH_4$ showed that $TiCl_3$ does increase the hydrogen dissociation pressure[353]. Thus, it was of interest to investigate the influence of $TiCl_3$ on the thermodynamic properties of $NaAlH_4$ in detail.

First, the hydrogen sorption/desorption properties of $TiCl_3$-doped $NaAlH_4$ were investigated in order to gain a better understanding of the cycling behavior of a simple model system where sodium alanate is doped with only small amounts of the catalyst. Next, with the focus to develop the practical composite material, the additive content was increased. It is expected that the additive added in stoichiometric amount will play a double role: on one side it will act catalytically, and by using large quantities it will be able to change the thermodynamics, so it will influence both kinetics and thermodynamics of the sodium alanate system.

In Figure 4.13, a typical pressure composition isotherm (PCI) for the Ti-doped sodium alanate system displaying common features of hysteresis in respect to the plateau pressures for hydrogen absorption/desorption measurement is shown. The PCI diagram exhibits two distinctive plateaus, in accordance with the two-step decomposition/hydrogenation of the system, following the cycle:

$$NaAlH_4 \underset{2^{nd}\ \text{hydrogenation step}}{\overset{1^{st}\ \text{dehydrogenation step}}{\rightleftharpoons}} 1/3Na_3AlH_6 + 2/3Al + H_2 \underset{1^{st}\ \text{hydrogenation step}}{\overset{2^{nd}\ \text{dehydrogenation step}}{\rightleftharpoons}} NaH + Al + 3/2H_2$$
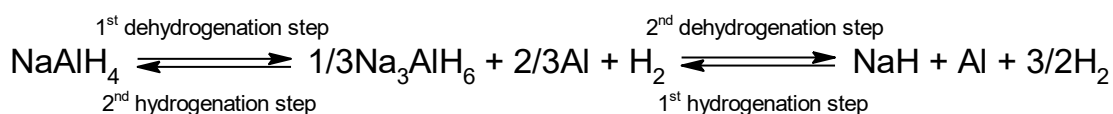
Scheme 4.2 *Two-step reversible hydrogenation cycle of $NaAlH_4$.*

The lower plateau corresponds to the first hydrogenation step (Fig. 4.13), the higher one - to the second hydrogenation step, and in reverse: higher pressure plateau - first dehydrogenation step, and lower plateau - second dehydrogenation step.
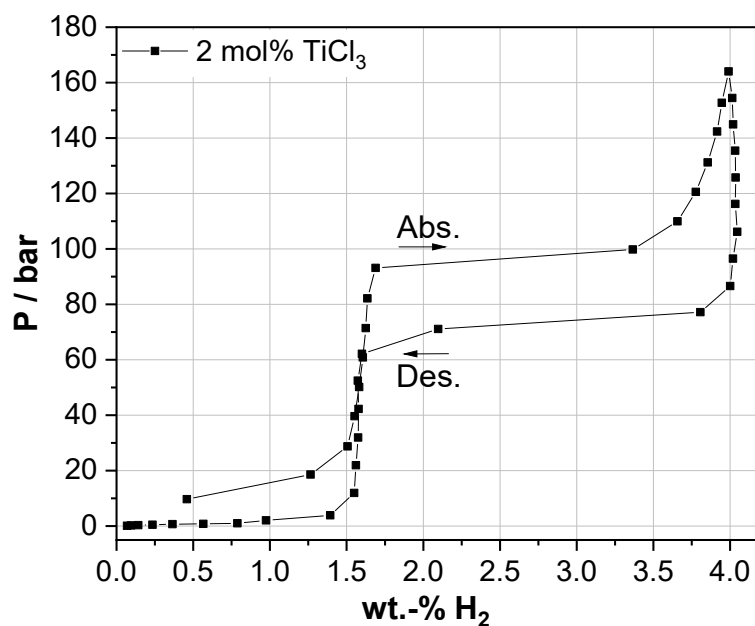
Figure 4.13 *Pressure composition isotherm for 2 mol% TiCl₃-doped NaAlH₄ measured at 160 ºC.*

The PCI measurements were conducted at 160 °C. This temperature was chosen as a compromise between high sorption rates, low operating temperature, and sufficient distance from the melting point of NaAlH₄. Melting can negatively affect the surface area of the particle as well as the catalyst activity, which leads to a decrease in the fraction of material that finally reacts. Thus, the measured hydrogen capacity of the material can decrease as well. The measurement was repeated several times to ensure the reproducibility of the recorded PCI curves. At this temperature, the difference between hydrogenation and dehydrogenation pressures was significant. The slow kinetics of hydrogenation/dehydrogenation reactions resulted in a long equilibration time and strong hysteresis. The hydrogen absorption was still observed when more time (5 h for each measuring point) was given to the system to equilibrate (Appendix C, Fig. C.2), therefore it was concluded that the equilibrium state was not reached. This could explain the obtained low measured hydrogen storage capacity (4.0 wt.-%) compared to the theoretical value (4.98 wt.-%). However, the time of 5 hours (for each measuring point) was chosen as a compromise between the long duration of the cycle (up to two weeks) and the equilibrium state of the system.

In order to follow the goal of this study, namely, to achieve the higher dissociation pressure plateau, the TiCl₃ content in NaAlH₄ was increased to 10 mol% and 15 mol%.

It can be seen (Figure 4.14) that increase of the dopant concentration results in significant changes.
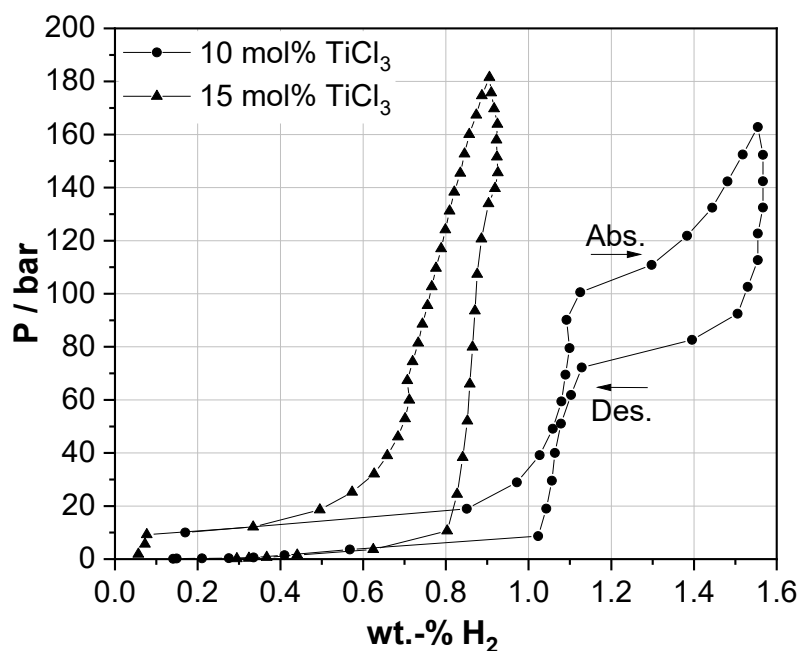
Figure 4.14 *Pressure composition isotherms for 10 mol% and 15 mol% TiCl₃-doped NaAlH₄ measured at 160 ºC.*

The individual PCI curves of freshly prepared Ti-doped $NaAlH_4$ samples have a number of distinctive features. First, the PCI curve for 10 mol% $TiCl_3$-doped $NaAlH_4$ has two pressure plateaus, in contrast, the one for 15 mol% $TiCl_3$ has only one. The first plateau at the lower pressure corresponds to the first hydrogenation step ($NaH \rightarrow Na_3AlH_6$), thus only 0.5 molecules of H_2 should be absorbed per mole of $NaAlH_4$; the higher plateau corresponds to the second hydrogenation stage ($Na_3AlH_6 \rightarrow NaAlH_4$) and one H_2 molecule should be absorbed. Therefore, the ratios of the capacities of the two plateaus correspond to the stoichiometry of the reaction. However, for 10 mol% $TiCl_3$ doped $NaAlH_4$, the second plateau at the higher pressure is significantly shorter compared to the first one, indicating incomplete hydrogenation of Na_3AlH_6. The hydrogen storage capacity of the 10 mol% doped $NaAlH_4$ sample reached 1.57 wt.-%, whereas with 15 mol% only 0.93 wt.-% was obtained. These values are about half of the theoretical values (3.05 and 2.15 wt.-% for 10 and 15 mol% of $TiCl_3$, respectively). The expected relationship between doping concentration and stored hydrogen is only clear for the first hydrogenation step. Different batches of $TiCl_3$-doped $NaAlH_4$ showed good reproducibility; thus, preclude the probability of an error occurring during sample preparation.

Furthermore, to evaluate the error resulting from the measuring process using Sieverts apparatus, a measurement with Pd powder as a reference sample was carried

out. The obtained value of stored hydrogen was in good agreement with the theoretical value (Appendix C, Fig. C.3). The possible error could also appear from the volume change during hydrogenation or dehydrogenation (theor. volume change 36.1% (Appendix C, Table C.2) based on the volume of $NaAlH_4$), however, in practice, only small volume change (<1%) was detected during the measurement.

In order to understand these results, the reaction of $TiCl_3$ with $NaAlH_4$ was studied in detail. It is obvious, if the Ti-halide doping level increases the total reversible hydrogen capacity decreases:

$$NaAlH_4 + xTiCl_3 \xrightarrow{BM} (1\text{-}3x)NaAlH_4 + 3xNaCl + xTi + 3xAl + 6xH_2 \quad (4.20)$$
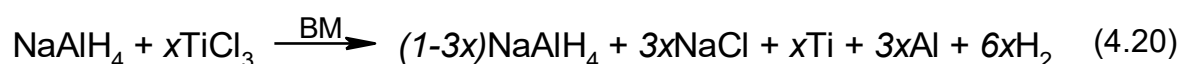
In the stoichiometric reaction between sodium alanate and titanium chloride, titanium probably is reduced to the zerovalent state[334]. In addition, the by-product NaCl is formed, which becomes a thermodynamic sink because of its stability. Theoretically, the $TiCl_3$ amount of ~33.3 mol% will completely convert $NaAlH_4$ into NaCl. In practice, the hydrogen storage capacity value differs significantly from the theoretically calculated one (Fig. 4.15).
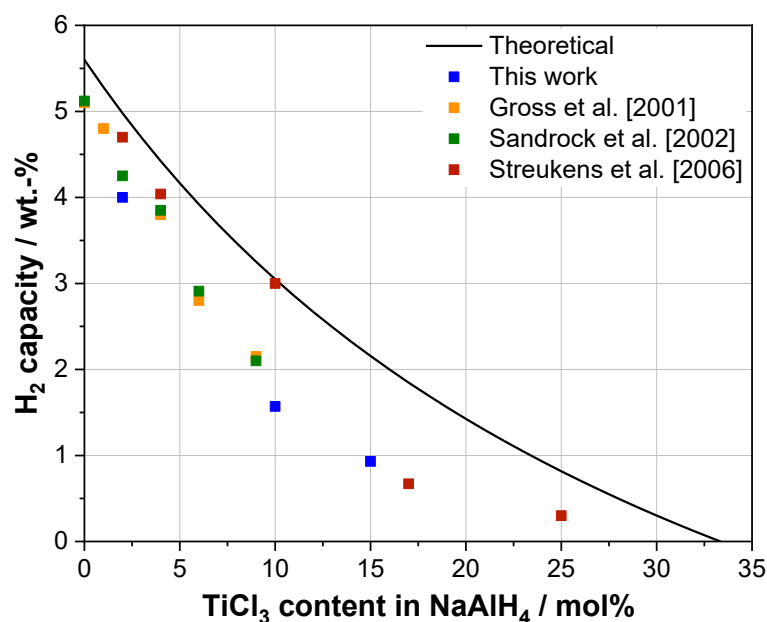
Figure 4.15 *Comparison of theoretically calculated hydrogen storage capacities of $NaAlH_4$ doped with the different $TiCl_3$ content with experimentally reached values in the literature[268,334,356] and in this work.*

Many studies (Fig. 4.15) showed significant differences (in the range of 10 – 60 %) between theoretical and practical storage capacities of $TiCl_3$-doped $NaAlH_4$. In contrast, Streukens et al.[268] showed, for 10 mol% $TiCl_3$ doped sodium alanate, the difference of 1.6 % between theoretical and practical value, this is quite unusual compared to the results obtained by the other groups. The reason for this discrepancy,

which becomes more pronounced at higher dopant contents, is not completely clear. However, one should keep in mind that the modification of material properties during ball-milling is highly dependent on various parameters, such as sample size, ball size, filling degree of the milling vessels, etc., which are not easily transferable between mills of the different types and could cause the difference in the properties of the prepared material. Partial oxidation during ball milling could also have occurred due to the long milling period of this air- and moisture-sensitive material. However, the trend of low experimentally obtained values of the hydrogen storage capacity compared to the theoretical value can be seen in all cases.

From the aspect of thermodynamic equilibrium, the formation of intermetallic Al_3Ti is most likely, and then reaction (4.20) will be transformed into:

$$NaAlH_4 + xTiCl_3 \xrightarrow{BM} (1\text{-}3x)NaAlH_4 + 3xNaCl + xAl_3Ti + 6xH_2 \qquad (4.21)$$
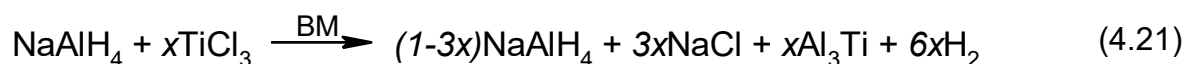
The often-described Al_3Ti phase is the most stable phase, which could appear after a long equilibration time[307]. This intermetallic compound is inert under the present hydrogenation/dehydrogenation conditions[357] and cannot explain the decrease of hydrogen storage capacity. Therefore, it was suggested that during the cycling of the material, the system is in a non-equilibrium state and as a result, the metastable Al-Ti phases with different compositions may be formed (Section 4.1.4).

Figure 4.16 shows the XRPD patterns for ball milled sodium alanate samples doped with 2, 10, or 15 mol% $TiCl_3$. Although the broad peaks were found at the expected for NaCl and Al positions, they nevertheless indicate their formation.
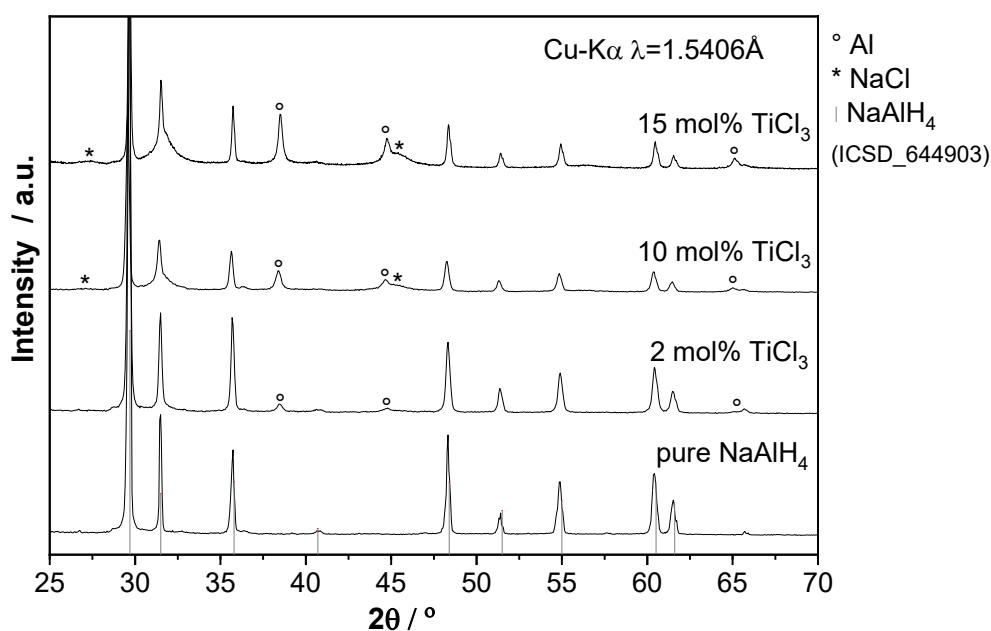
Figure 4.16 *XRPD patterns for milled sodium alanate samples with different TiCl₃ content.*

No crystalline or other Ti-containing phases were observed after ball milling of NaAlH4 with a high amount of additive. However, after cycling, a high-angle shoulder on the three strongest Al reflections was observed (Fig. 4.17). These shoulders may indicate that a relatively small fraction of Al, presumably on the surfaces, formed an Al-Ti phase during cycling. The stable Al3Ti phase appeared only after thermal treatment of the sample (Fig. 4.17). However, the intensity of the broad signal at about 46° 2θ is most probably the superposition of the reflection from Al, NaCl, and Al3Ti, thus the Al3Ti phase can be only well distinguished at 39° 2θ and 42 °2θ. These results correlate well with the previous X-ray diffraction studies[345,358] which confirmed that Al-Ti phases first appear after cycling or thermal treatment of the material. Furthermore, the heat treatment in the cycling process results in a considerable increase of the NaCl crystallite size.
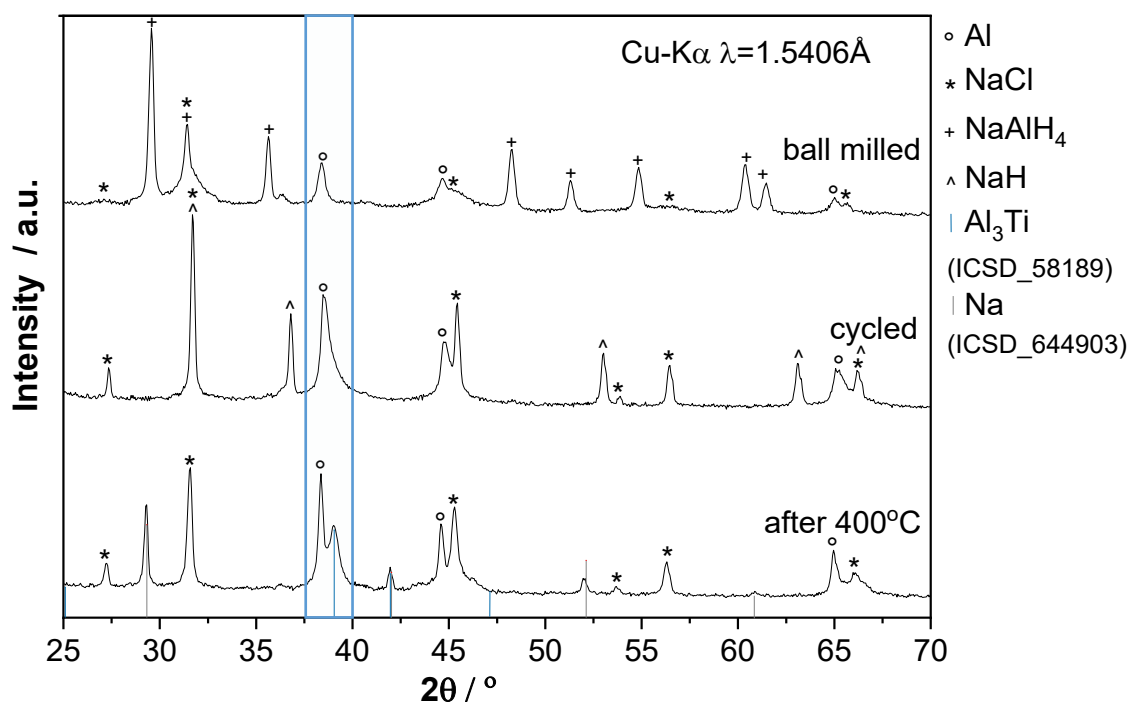
Figure 4.17 *XRPD patterns for 10 mol% TiCl₃-doped NaAlH₄ sample after ball milling (top), after cycling in dehydrogenated state (middle), and after thermal treatment at 400 ºC for 2 h (bottom).*

In the cycled material, the Ti-containing phase caused the shoulder near Al reflection, and therefore, it may contain less Ti than in the pure Al3Ti phase. Thus, it was suggested that aluminum is too strongly bound in this phase to react with Na3AlH6 and to form NaAlH4. Depending on the phase which can be formed, the reaction equation can be generally described as follows[359]:

$$NaAlH_4 + xTiCl_3 \longrightarrow (1\text{-}kx)NaAlH_4 + x/yAl_{(1\text{-}y)}Ti_y + lxNa_3AlH_6 + 3xNaCl + (2k\text{-}3l)xH_2$$
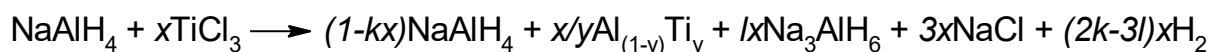
Scheme 4.3 *Formation of Al$_{(1-y)}$Ti$_y$ phase (y<0.25) in TiCl$_3$ doped NaAlH$_4$, where k = (3-6y)/2y, l = (1-4y)/2y.*

This equation is based on a complete consumption of Ti in order to form a homogeneous Al$_{(1-y)}$Ti$_y$ phase. The formation of this phase could be a simplification of the real situation, because in practice the range of compositions or solid solution may be formed. However, the formation of this phase may explain the reduction of capacity beyond the theoretical reduction from the dead weight of the additive and the formed by-product.

Many studies confirmed that the Al$_{(1-y)}$Ti$_y$ phase formed during cycling of NaAlH$_4$ doped with higher TiCl$_3$ content has a composition of Al$_{0.85}$Ti$_{0.15}$[304,344,345]. Therefore, in order to understand the effect of TiCl$_3$ addition, the formation of an Al$_{(1-y)}$Ti$_y$ phase with fixed stoichiometry (y = 0.15) was assumed. Figure 4.18 illustrates the consumption of NaAlH$_4$ due to the formation of an Al$_{0.85}$Ti$_{0.15}$ phase compared to the formation of the stable Al$_3$Ti phase.
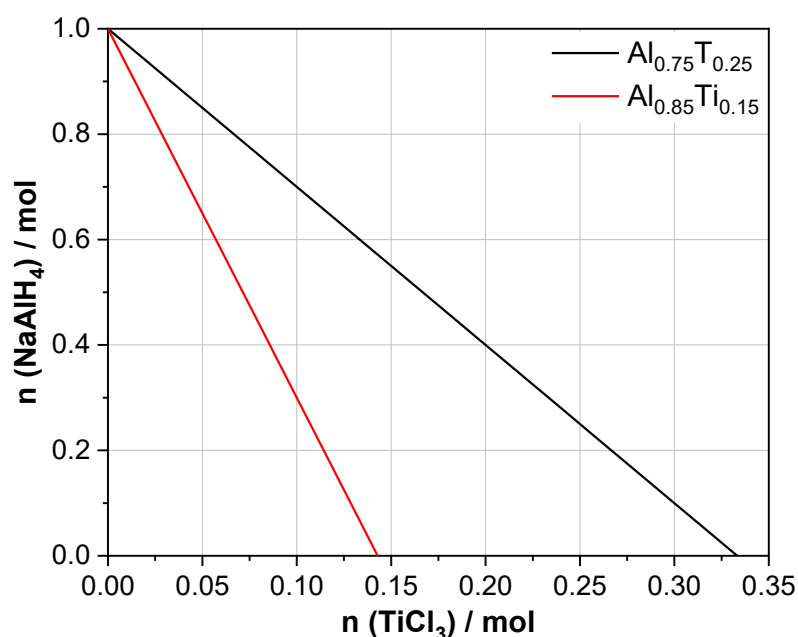
Figure 4.18 *The influence of the dopant content on the consumption of the NaAlH$_4$ depending on the Al-Ti phase composition.*

This example already can explain why the reversible hydrogen capacity drastically decreases with increasing a dopant content, and why a dopant concentration lower than ~33.3 mol% is needed for the complete consumption of NaAlH$_4$. It has been calculated, that for the hypothetical Al$_{0.85}$Ti$_{0.15}$ phase, at the critical amount of ~14.28 mol (TiCl$_3$) the second hydrogenation step (Na$_3$AlH$_6$ → NaAlH$_4$) will be completely suppressed. In the case when the dopant content will be further

increased, the formed Na_3AlH_6 will continue to react with the dopant until the remaining Na_3AlH_6 will be fully converted into NaH:

$$lxNa_3AlH_6 + dTiCl_3 \longrightarrow (lx-ad)Na_3AlH_6 + d/yAl_{(1-y)}Ti_y + bdNaH + 3dNaCl + (a-b)H_2$$
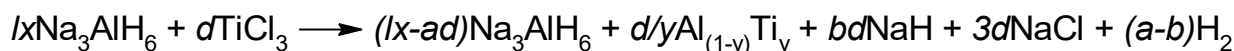
Scheme 4.4 *Consumption of Na_3AlH_6 by $TiCl_3$ addition (in a case of $Al_{(1-y)}Ti_y$ (y<0.25) phase formation), where d = x-(1/k), a = (1-y)/y, b = (3-6y)/y.*

The calculated critical amount for the suppression of both steps is ~18.68 mol% of $TiCl_3$. This example is the single case for the assumed $Al_{0.85}Ti_{0.15}$ phase, in cases when more Al-rich phases (lower y) are formed, then less $NaAlH_4$ will be regenerated. The generalization of this idea is illustrated in Figure 4.19, which presents how the critical amount of $TiCl_3$ dopant depends on the Ti content in Al-Ti phase.
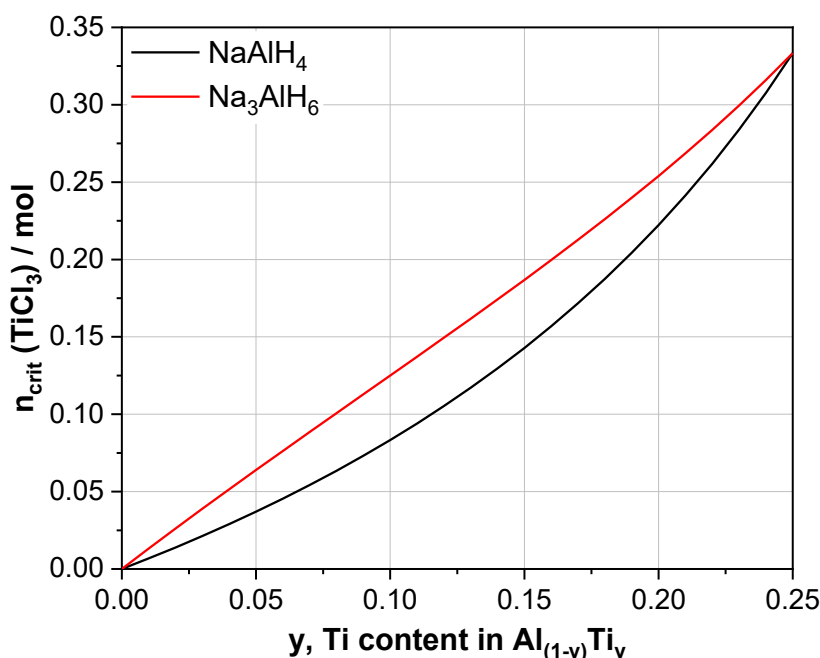
Figure 4.19 *The critical amount of the $TiCl_3$ additive needed for the complete consumption of $NaAlH_4$ and Na_3AlH_6 as the function of the $Al_{(1-y)}Ti_y$ phase composition.*

Thus, it is possible to estimate the critical amount of Ti-additive required for the suppression of the first and second hydrogenation step depending on the formed Al-Ti-phase, and in reverse to estimate the composition of the formed Al-Ti phase depending on the critical $TiCl_3$ concentration. However, one should keep in mind that the reduced capacity due to other reasons, then $Al_{(1-y)}Ti_y$ formation, will lead to an underestimation of Ti content in Al-Ti phase.

4.3.2 Influence of the aluminum addition on the sorption behavior of Ti-doped sodium alanate

The formation of metastable Al-Ti phases is consistent with many observations. XRPD analyzes reveal crystalline Al and the intermetallic Al_3Ti phase only if the sample was subjected to a high-temperature treatment (above 400 °C). The Al-Ti alloy formation is a positive aspect for the development of systems with high dissociation pressure if some of these alloys are able to absorb hydrogen at acceptable conditions[360]. In the case of y < 0.25 for $Al_{(1-y)}Ti_y$ some more aluminum is consumed for the formation of the Al-rich-Ti phase. Consequently, in the reverse reaction, Na_3AlH_6 will have an insufficient amount of available Al to form $NaAlH_4$, resulting in a decrease of reversible hydrogen storage capacity. This situation can be improved by the simple addition of Al powder to the reaction mixture during ball milling:

$$NaAlH_4 + xTiCl_3 + 2lxAl \longrightarrow (1\text{-}3x)NaAlH_4 + x/yAl_{(1-y)}Ti_y + 3xNaCl + 2kxH_2$$

Scheme 4.5 *The reaction pathway for the prevention of Al deficiency in TiCl$_3$ doped NaAlH$_4$.*

Brinks et al.[359] investigated the influence of the Al addition to 2 and 4 mol% $TiCl_3$ doped sodium alanate samples and suggested that 5.3 and 10.7 mol% of additional Al, respectively, are necessary to prevent Al deficiency for the reaction with Na_3AlH_6 to $NaAlH_4$ (for the assumed $Al_{0.85}Ti_{0.15}$ phase).

In the present work, in order to find the optimal amount of Al for 10 mol% Ti-doped $NaAlH_4$ sample, a set of experiments with the different amounts of Al was performed. Assuming the formation of the $Al_{0.85}Ti_{0.15}$ phase, the minimum added amount of Al was calculated to be 27 mol%. Normalized with respect to weight, additional aluminum will results in a lower overall storage capacity, if there will be no positive influence of it (Appendix C, Fig. C.4). In addition, supposing the formation of the more Al-rich Ti-phases (e.g. $Al_{0.89}Ti_{0.11}$ and $Al_{0.9}Ti_{0.1}$[349]), the addition of higher Al amounts (51 mol% and 66 mol%) was also investigated.

The generalization of this idea was illustrated in Figure 4.20 for the whole range (y < 0.25) of the possibly formed $Al_{1-y}Ti_y$ phases. The theoretical hydrogen storage capacities for $NaAlH_4$ with 2, 10, and 15 mol% $TiCl_3$ as a function of Ti content in $Al_{(1-y)}Ti_y$ phase were calculated. Based on the stored amount of hydrogen, it can be estimated which phase was formed, and thus it can be calculated which minimum amount of Al should be added to complete the hydrogenation of Na_3AlH_6 to $NaAlH_4$ (Fig.4.20, right).

The higher the dopant content, the more Ti will be available to form an Al-Ti phase. At the stage where no reversible hydrogen will be observed (0 wt.-% H_2; Fig. 4.20, left), all Al will be consumed for the formation of Al-Ti phase. In this case, the assumed Al-Ti phase will have the minimum possible Ti content. Therefore, it is possible to calculate the maximum amount of Al needed to compensate the deficiency of free Al in the system (Fig. 4.20, right), based on Scheme 4.5, which depends on the minimum possible Ti content in the assumed Al-Ti phase.
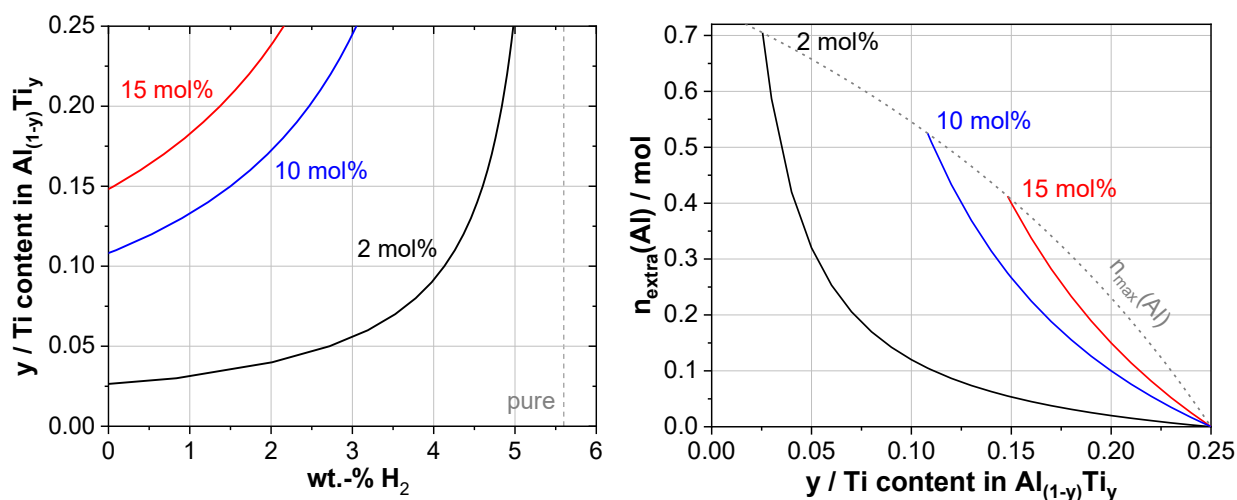
Figure 4.20 *The influence of the Ti content in Al-Ti phase on the theoretical storage capacity (left) and the required amount of extra aluminum (right) for TiCl₃ doped NaAlH₄.*

The PCI measurements of 10 mol% doped samples with extra aluminum confirmed the positive effect of Al addition (Fig. 4.21). The reversible hydrogen storage capacity was increased significantly compared to the sample without additional aluminum. The small decrease of the storage capacity for the first hydrogenation step was due to the increased mass of the sample when Al was added.

Moreover, the Al addition influences only the second hydrogenation step indicating that hydrogenation of Na_3AlH_6 due to the lack of Al was not completed. The absorption isotherms illustrate, that by the addition of 27 mol% of Al to 10 mol% TiCl₃ doped NaAlH₄ the reversible storage capacity increases to 2.14 wt.-% (by 0.57 wt.-%, compared to the sample with just 10 mol% TiCl₃). About 2.34 wt.-% of hydrogen can be absorbed by the sample with 51 mol% of Al in 10 mol% TiCl₃-doped NaAlH₄. With the addition of 66 mol% of Al, the storage capacity did not improve further and reached only 2.21 wt.-% (Appendix C, Fig. C.5). Therefore, 51 mol% of Al was chosen as the optimal amount for 10 mol% TiCl₃ doped NaAlH₄. Because the screening was quite coarse, the final optimization of the Al addition is still desired.
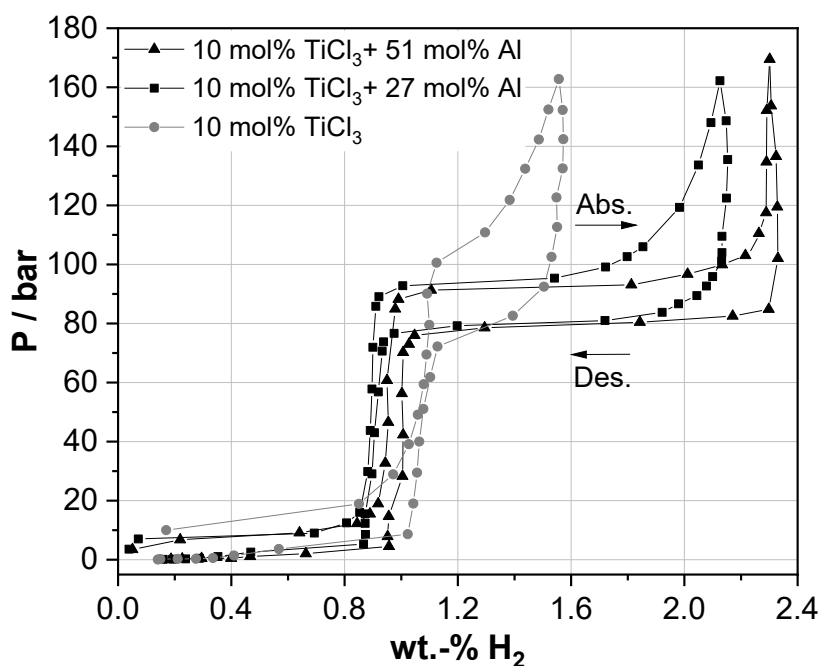
Figure 4.21 *The PCI curves for the sodium alanate samples with 10 mol% TiCl₃ and additional aluminum.*

It was also observed that with Al addition the pressure plateaus became more pronounced, compared to the sample without Al. Furthermore, the dissociation pressure is kept at the same level as for the sample with the low dopant content. Therefore, the formation of another hydride composite can be most likely excluded.

To facilitate the understanding of the composition changes during hydrogen absorption and desorption in the sodium alanate sample doped with $TiCl_3$ and Al, X-ray powder diffraction analysis was performed. XRPD pattern for the 10 mol% $TiCl_3$ doped sample (Fig. 4.22) showed that the hydrogenated sample is composed mainly of $NaAlH_4$ and Na_3AlH_6. There is certainly enough Al available for the reaction with Na_3AlH_6, however, the rehydrogenation was not completed.

To understand this ambiguity, several possible reasons why aluminum can not fully participate in the rehydration reaction, such as the mass transfer problem or the irreversible formation of the $Al_{(1-y)}Ti_y$ phase with $y < 0$, have been discussed. Generally, the mass transfer may be the reason for incomplete hydrogenation due to the long diffusion paths through the product layer[273]. During rehydrogenation, metallic aluminum particles would first react with NaH to Na_3AlH_6, and in parallel formed Na_3AlH_6 would react with the residual aluminum to $NaAlH_4$. The metallic aluminum particles would thus be coated by the $NaAlH_4$ layer. Those aluminum particles would after some period of rehydrogenation consist of an aluminum center coated with $NaAlH_4$. The aluminum in the particle cores will not be reached by the reactant Na_3AlH_6

formed in other parts of the sample so that the rehydrogenation process will be terminated.
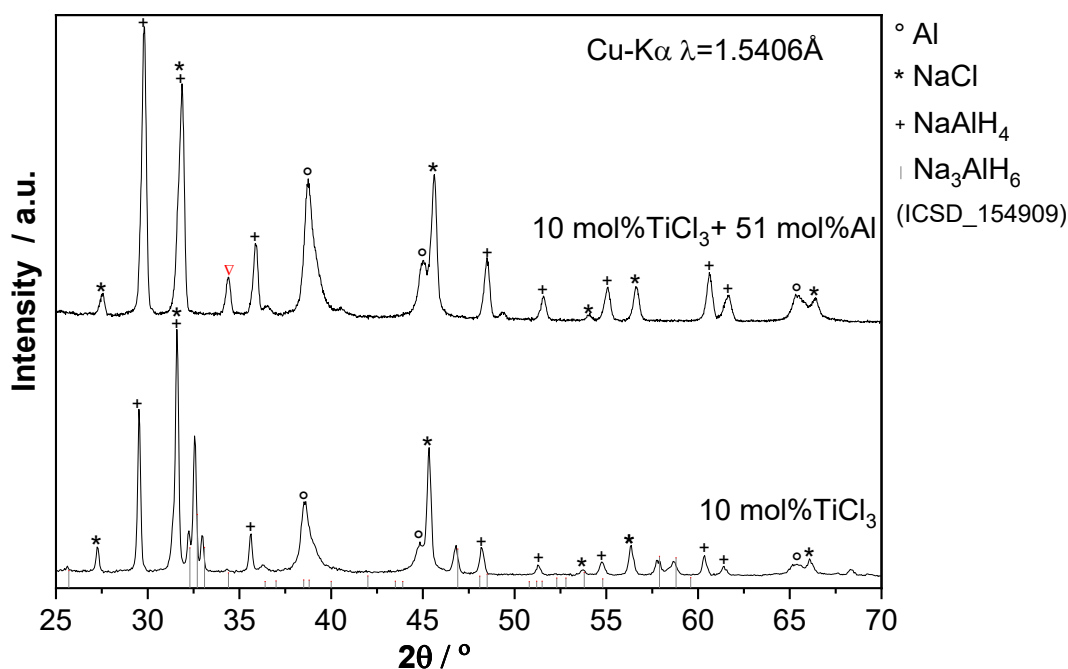
Figure 4.22 *XRPD patterns for cycled 10 mol% TiCl₃ doped sodium alanate sample with and without Al addition (hydrogenated state).*

However, a closer look at the Al reflections reveals that the mass transfer problem is probably not the main reason in this case. All aluminum reflections are broad, and this most probably indicates the presence of a non-identified Al-phase. After hydrogenation of the sample with additional aluminum, the Na_3AlH_6 reflections disappeared, suggesting that there was enough free Al present for Na_3AlH_6 to form $NaAlH_4$. Furthermore, in the sample with additional aluminum, a new reflection with an unclear origin at about 34.4º 2θ was observed. It worth noting that the reflection at 34.4º 2θ is present in the Na_3AlH_6 pattern; however, none of the other reflections of Na_3AlH_6 were present in the hydrogenated sample with extra aluminum.

A similar situation was observed with the sample doped with 15 mol% TiCl₃ (Fig. 4.23). After hydrogenation, only the reflections of Na_3AlH_6 and Al were present. This means that the rehydrogenation of NaH to Na_3AlH_6 was completed, while the hydrogenation of Na_3AlH_6 to $NaAlH_4$ did not take place. After the addition of 40 mol% of aluminum (based on the assumed $Al_{0.85}Ti_{0.15}$ phase) to 15 mol% TiCl₃ doped sodium alanate, the formation of $NaAlH_4$ was observed. The XRPD pattern of the sample with additional aluminum displays reflections that indicate the presence of $NaAlH_4$ and the unidentified structural element at 34.4º 2θ.
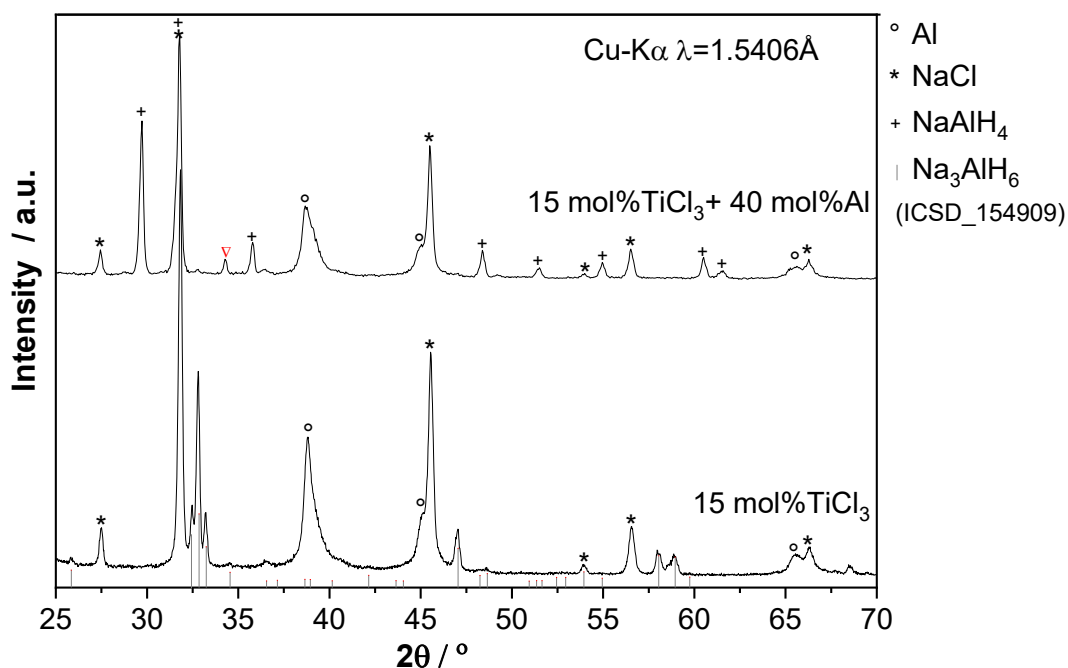
Figure 4.23 *XRPD patterns for cycled 15 mol% $TiCl_3$ doped sodium alanate sample with and without Al addition (hydrogenated state).*

The PCI measurements confirmed these observations (Fig. 4.24). Extra Al addition influences only the second hydrogenation step ($Na_3AlH_6 \rightarrow NaAlH_4$). Thus, in this case, two hydrogenation steps are present, compared to the sample with $TiCl_3$ addition, only.
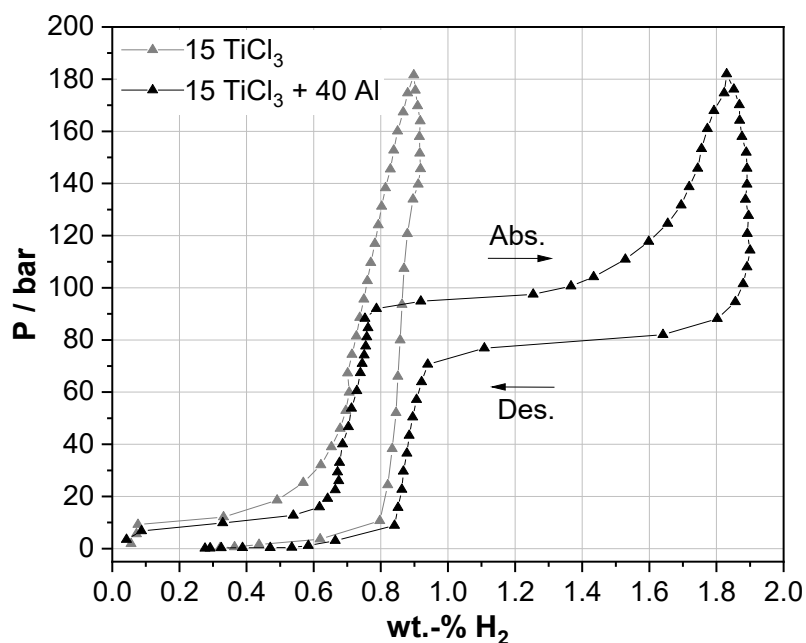
Figure 4.24 *The PCI curves for the sodium alanate samples with 15 mol% $TiCl_3$ and additional aluminum.*

Summarizing, the PCI measurements indicated the disappearance of the pressure plateau with the increase of the $TiCl_3$ dopant content. It was confirmed that

this effect is due to the lack of Al in the system caused by the formation of Al-rich-Ti phases. The addition of pure aluminum to the system has led to the appearance of the second plateau and to an increase of the hydrogen storage capacity. The performed experiments and calculations can be used to estimate the possible Al-Ti phase composition and deficiency of Al to complete hydrogenation. The experimental data agree well with the theoretically calculated values (Fig. 4.20), for 10 mol% TiCl$_3$-doped NaAlH$_4$, 27 mol% of extra Al was not enough to compensate the lack of Al, in contrast, 66 mol% was already over the optimal level. However, the PCI data can not clarify why 51 mol% of Al showed the highest hydrogen storage capacity. Therefore, to get more insights into the hydrogen sorption behavior of the samples with additional aluminum, high-pressure differential scanning calorimetry (HP-DSC) measurements were performed.

4.3.3 High-pressure DSC study of hydrogen sorption properties of doped sodium alanate system

The slow kinetics of sodium alanate makes the investigation of the hydrogen release and uptake pathways complicated and time-consuming. Therefore, in addition to PCI measurements, the investigation of the (de)hydrogenation processes in the Ti-doped NaAlH$_4$ system with Al addition was performed by means of HP-DSC. This analysis allows the correct determination and comparison of the temperatures and enthalpies of the (de)hydrogenation reactions. Moreover, the advantage of this method is that the effects of the additive on the hydrogen absorption/desorption properties can be investigated relatively quickly. The characterization of the doped sodium alanate system with the help of HP-DSC was published only by a few groups[361,362]. In this work, the investigation of the high TiCl$_3$ dopant level for sodium alanate will be shown for the first time.

Based on the optimized measuring procedure performed in collaboration with K. Burkmann in terms of his bachelor work[363], the HP-DSC traces were mainly measured between room temperature and 350 ºC with constant heating and cooling rates (2 ºC/min) under isobaric condition (150 bar). Figure 4.25 shows the DSC curves with a linear temperature scan for doped/undoped sodium alanate samples.
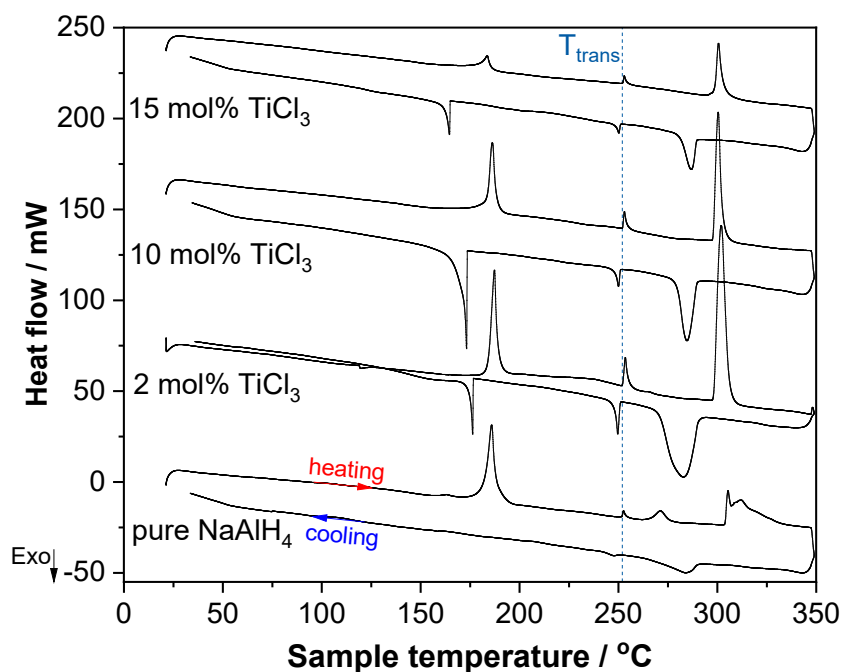
Figure 4.25 High-pressure DSC traces for doped/undoped NaAlH$_4$ measured at 150 bar.

Several signals are observed during heating and cooling. During heating, the signals are identified as follows: the first endothermic peak is attributed to the decomposition of NaAlH$_4$, the second peak is generally ascribed to the structural transformation of Na$_3$AlH$_6$ – the phase transition from the monoclinic α-Na$_3$AlH$_6$ to the orthorhombic β-Na$_3$AlH$_6$; the third signal assigned to the decomposition of Na$_3$AlH$_6$ to NaH. Owing to the reversibility of the hydrogenation reaction of doped sodium alanate, the peaks observed during cooling are related to the formation of NaAlH$_4$. The melting and decomposition of NaAlH$_4$ should deliver during DSC measurement two separate DSC signals based on the thermodynamic calculations at p(H$_2$) = 150 bar (at 182 ºC - melting, at 198 ºC - decomposition), whereas the experiments show only one signal at the predicted temperature of 182 ºC for melting.

The diagram shows the slow decomposition of pure alanate and demonstrates the advantage of using TiCl$_3$ as a dopant. The decomposition peaks for Ti-doped sodium alanate slightly shifted to a lower temperature (Table 4.4), compared to pure sodium alanate. However, the increase of the TiCl$_3$ dopant level has no strong effect on the (de)hydrogenation temperatures, but clearly improves the kinetics, in particular rehydrogenation reactions in comparison to pure sodium alanate. The first desorption step is more strongly influenced by the slow kinetics than the second, which can be concluded from the fact that the equilibrium has not been reached. Considering the slow reaction kinetics, equilibrium is unlikely to be reached in dynamic measurements

carried out by temperature variations. In comparison to dehydrogenation reactions, the hydrogenation reactions are clearly slower. The exothermic peaks during hydrogenation of the samples with higher Ti additive content become narrower, due to the faster kinetics of the hydrogen absorption, compared to the pure NaAlH$_4$ case in which hydrogen does not absorb under these conditions. It is important to note, that no evidence for the additional formation of the "unstable" hydride (titanium alanate) was found, which was expected to result from increasing the Ti content.

Table 4.4 *Relation between decomposition temperature and dopant content in sodium alanate measured under isobaric condition at 150 bar.*

TiCl$_3$ content	Onset temperature, °C		
	T$_{1\ des}$	T$_{trans}$	T$_{2\ des}$
15 mol%	179.6	252.3	298.8
10 mol%	183.9	252.3	298.5
2 mol%	184.2	252.2	298.4
pure	182.5	251.9	304.1

Overall, it must be noted that the onset temperatures (see Table 4.4) hardly depend on the additive amount. There are two possible reasons for this. The temperature of about 181°C[364] corresponds to the melting temperature of NaAlH$_4$. The melting is thermodynamically unstable at the chosen pressures and temperature, so this temperature effect is associated with the melting and simultaneous decomposition of NaAlH$_4$. The constancy of the second effect is associated with the phase transformation of sodium alanate. The third effect may again be associated with the melting of Na$_3$AlH$_6$ analogous to the interpretation of the first effect. There are no data on the melting of this compound, but the order of magnitude of this temperature is physically reasonable. The second explanation can be based on Scheme 4.5. During the milling of the starting components, NaCl and Al-Ti phase are already formed in addition to the target component NaAlH$_4$. Both by-products show no reactions with hydrogen under the selected reaction conditions, they are in principle inert. Therefore, the observed effects correspond only to the hydrogen sorption behavior of pure NaAlH$_4$. Both justifications also play a role in the discussion of the experiments as a function of pressure.

The effect of pressure on the (de)hydrogenation behavior of 15 mol% doped NaAlH$_4$ is shown in Figure 4.26.
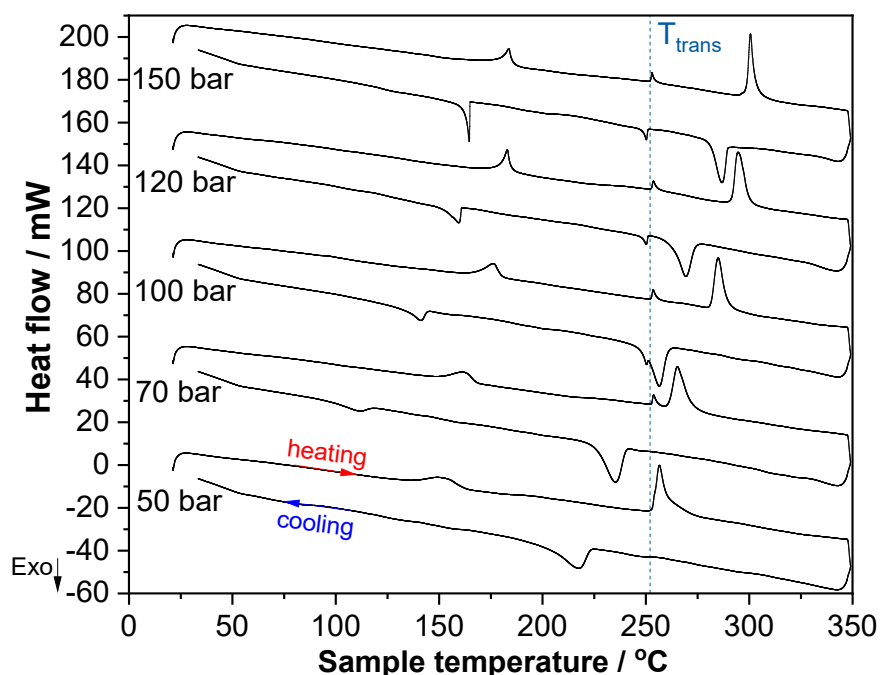
Figure 4.26 *High-pressure DSC plots for 15 mol% TiCl₃ doped NaAlH₄ measured at different pressures.*

With the increase of pressure, the decomposition/hydrogenation peaks became narrower, due to the increased reaction rate. The effect of pressure is clear, the rate of reaction is improved by increasing the driving force. The hydrogenation peaks at low pressures are broad and indistinct, and indicate the incomplete hydrogenation of the sample. By increasing the pressure, the dehydrogenation temperatures (Fig. 4.27; Appendix C, Table C.3) are shifted to higher values, and at lower pressure, this effect is more pronounced. The phase transition of Na_3AlH_6 was not influenced by the pressure change. The change of desorption temperature with the pressure change was observed only until 150 bar. Above $p(H_2)=150$ bar, the theoretical decomposition temperature of $NaAlH_4(s)$ is greater than 180°C, thus greater than the melting temperature of $NaAlH_4$. Above 150 bar, therefore, the almost constant decomposition temperature is again related to the melting temperature of $NaAlH_4$. An analogous interpretation can also be provided for the pressure dependence of the decomposition of Na_3AlH_6. Looking at Fig. 4.27, the melting temperature should be about 300°C. The slight increase of the onset temperature above the melting temperature can be explained in both cases by the pressure dependence of the melting temperature, since the molar volume of $NaAlH_4(liq) > NaAlH_4(s)$ or of $\beta\text{-}Na_3AlH_6(liq) > \beta\text{-}Na_3AlH_6(s)$ and follows with the equation of Clausius-Clapeyron:

$$\frac{dT}{dp} = \frac{\Delta_F H}{T \cdot \Delta_F V} \quad \Delta_F H > 0 \text{ and } \Delta_F V > 0, \text{ and thus } \frac{dT}{dP} > 0 \tag{4.22}$$
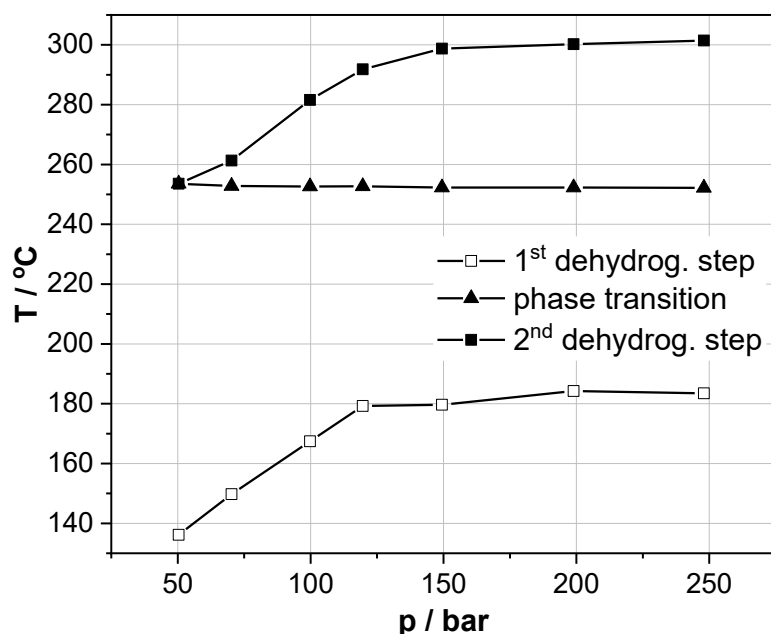
Figure 4.27 *Dependence of the desorption temperature from the pressure change for 15 mol% TiCl₃ doped NaAlH₄.*

From HP-DSC experiments, the thermodynamic parameters for NaAlH$_4$ can be obtained from the Van't Hoff equation by determining the temperature dependence of the equilibrium pressure:

$$p_{eq} = \frac{\Delta H}{RT} - \frac{\Delta S}{R}$$

(4.23)

In this way, from the linear fit of reciprocal temperature versus equilibrium pressure (Fig. 4.28; Appendix C, Table C.4), the reaction enthalpy and reaction entropy were determined.
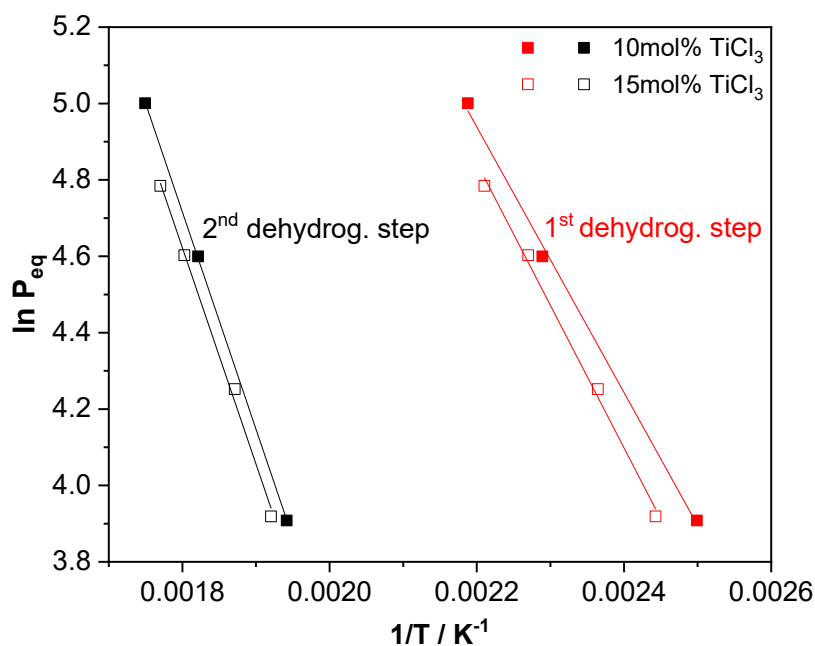
Figure 4.28 *Van´t Hoff plots of 10 and 15 mol% TiCl₃ doped NaAlH₄.*

The slight change of the reaction entropy in the solid phase by the addition of different titanium amounts makes this quantity less characteristic for this system than the reaction enthalpy (Table 4.5).

Table 4.5 *The values of reaction enthalpies and entropies of Ti-doped NaAlH₄.*

TiCl₃ content	$\Delta_R H^o_{1\ des.}$ kJ/mol H₂	$\Delta_R H^o_{2\ des.}$ kJ/mol H₂	$\Delta_R S^o_{1\ des.}$ J/K·mol H₂	$\Delta_R S^o_{2\ des.}$ J/K·mol H₂
15 mol%	31.0 ± 1.3	47.1 ± 2.0	108.5 ± 3.1	123.2 ± 3.7
10 mol%	28.9 ± 1.3	47.4 ± 0.4	104.7 ± 3.1	124.3 ± 0.7
4 mol% (HP-DSC)[361]	28.4 ± 1.5	51.9 ± 1.2	-	-
2 mol% (PCI)[58]	37	47	-	-

With an increase of the dopant content, slight increases of the reaction enthalpies for the first decomposition step were observed. However, the calculated enthalpies may deviate from the real value, because it is hard to attain an equilibrium of the system, and therefore the true enthalpy value is expected to be between the ones derived for absorption and desorption from the Van't Hoff plot:

$T_{eq}(abs.) < T_{eq} < T_{eq}(des.)$

$\Delta_R H^o(abs.) < \Delta_R H^o < \Delta_R H^o(des.)$

Moreover, at low pressures, the onset temperature is affected by the slow hydrogenation kinetics, and therefore were not taken for the calculation of the enthalpy. The obtained enthalpies for the first and second dehydrogenation steps of Ti-doped NaAlH₄ were compared with the literature data (Table 4.5). The enthalpy values obtained for the first step agree well with the data obtained by Rongeat et al.[361], in contrast, the values for the second step are in good agreement with the ones experimentally obtained from PCI measurements by Bogdanović et al.[58]. At high temperatures in HP-DSC measurements, the kinetics is faster and the reaction enthalpy can be calculated more precisely. The fact that obtained values are close to the literature data confirms that the onset temperatures obtained from HP-DSC measurements are precise enough to estimate the reaction enthalpy for the complex metal hydrides with slow kinetics.

Furthermore, the influence of the Al addition on the change of the thermodynamic parameters of Ti-doped NaAlH₄ was investigated. Figure 4.29 shows the isobaric hydrogen desorption/absorption behavior of different composite materials, with and without aluminum addition.
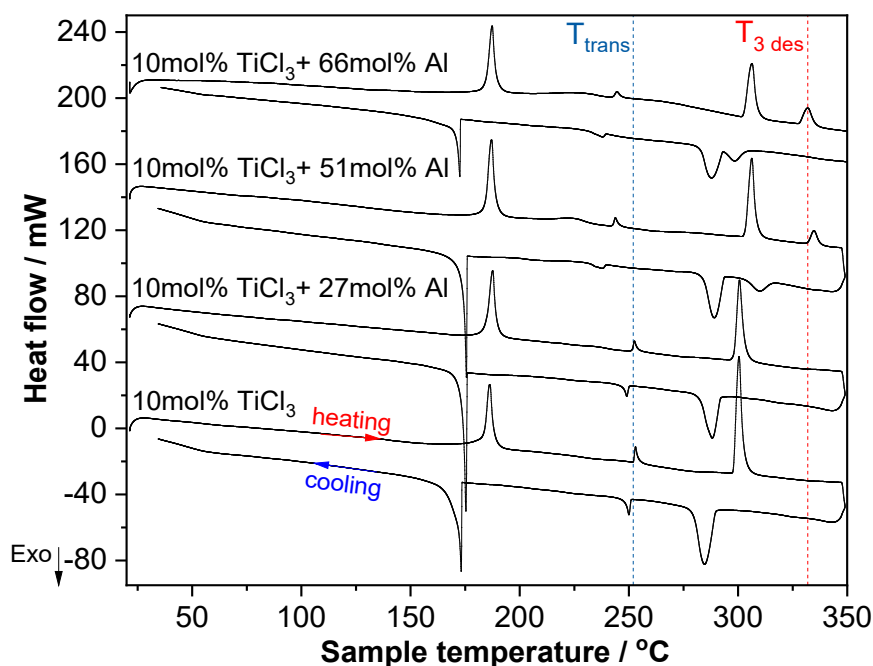
Figure 4.29 High-pressure DSC plots (150 bar) of 10 mol% TiCl$_3$ doped NaAlH$_4$ with/without Al addition.

The first decomposition peaks appear at nearly the same temperatures (Table 4.6) for all measured samples (under the same conditions 150 bar H$_2$ and 2 ºC/min heating rate). For the samples with very high Al content (51 and 66 mol%) two other signals, namely, structural transformation and second decomposition step were influenced. It is important to point out that the samples with 51 and 66 mol% of Al in 10 mol% TiCl$_3$ doped sodium alanate reveal the additional reversible effect which takes place around 330 °C (at the hydrogen pressure of 150 bar). The measured traces for doped sodium alanate samples showed good reproducibility (Appendix C, Fig. C.6 and C.7).

Table 4.6 The onset temperatures (at 150 bar) during decomposition of 10 mol% TiCl$_3$ doped NaAlH$_4$ with different Al content.

Additives	Onset temperature, ºC			
	T$_{1\,des}$	T$_{trans}$	T$_{2\,des}$	T$_{3\,des}$
10 mol% TiCl$_3$ + 66 mol% Al	184.5	242.9	302.8	328.2
10 mol% TiCl$_3$ + 51 mol% Al	184.2	242.7	303.3	332.0
10 mol% TiCl$_3$ + 27 mol% Al	184.5	251.6	298.3	-
10 mol% TiCl$_3$	183.9	252.3	298.5	-

The decomposition temperature of the new signal for both cases (with 51 and 66 mol% of extra Al) is above 300 °C and is pressure dependent (Table 4.7).

Considering that this process is reversible, the dependence of the temperature at which this effect is observed on the hydrogen pressure indicates the existence of a hydride.

Table 4.7 *Dependence of the decomposition temperatures from pressure for 10 mol% TiCl₃ with 66 mol% Al-doped NaAlH₄.*

Pressure, bar	Onset temperature, ºC			
	$T_{1\ des}$	T_{trans}	$T_{2\ des}$	$T_{3\ des}$
100	179.8	242.8	280.8	307.7
120	182.1	242.2	290.4	318.6
150	184.5	242.9	302.8	328.2
200	186.4	-	339.5	351.8

The calculated values of the reaction enthalpy and entropy based on the Van´t Hoff plot are presented in Table 4.8. The reaction enthalpy of the second step was not influenced by the aluminum addition. Interestingly, the value of the reaction enthalpy for the third event is close to the value for the reaction enthalpy of sodium hydride - 56.4 kJ/mol H_2[289]. However, it is very unlikely that the decomposition of NaH can occur at a temperature as low as the temperature of the third event since NaH is very stable and has a decomposition temperature of about 475 ºC[365].

Table 4.8 *The values of reaction enthalpies and entropies for Ti-doped NaAlH₄ with extra aluminum.*

Additive	$\Delta_R H^0_{2\ des.}$ kJ/mol H_2	$\Delta_R H^0_{3\ des.}$ kJ/mol H_2	$\Delta_R S^0_{2\ des.}$ J/K·mol H_2	$\Delta_R S^0_{3\ des.}$ J/K·mol H_2
10 mol%TiCl₃ + 66 mol%Al	47.1 ± 6.6	55.6 ± 3.1	123.5 ± 11	133.9 ± 5.3
10 mol%TiCl₃ + 51 mol%Al	47.6 ± 1.4	57.6 ± 1.5	124.0 ± 2.5	136.7 ± 2.5

In worth noting, that the new effect occurs only with the addition of a high amount of aluminum. The pressure dependence of the reaction and the value of the reaction entropy of about 135 J/(K·mol H_2) suggests that it is a decomposition of a hydride. Since the decomposition temperature is lower than that of pure NaH, an unknown Na-Al or Na-Al-Ti alloy must form. This assumption was made based on the similar behavior of LiH in the presence of Al[366]. Therefore, the observed effect at a relatively lower temperature compared to the pure NaH suggests the possibility that the release of hydrogen resulted from a reaction between NaH and Al rather than from the decomposition of NaH itself. However, no Na-Al compound is known to date.[367].

To gain more insight into the role of the aluminum and to study the decomposition path of the mixture with only aluminum and sodium alanate, a series of HP-DSC

measurements were performed. The HP-DSC measurement of the 66 mol% Al-doped NaAlH$_4$ sample also showed the third effect at about 330 ºC (Fig. 4.30).
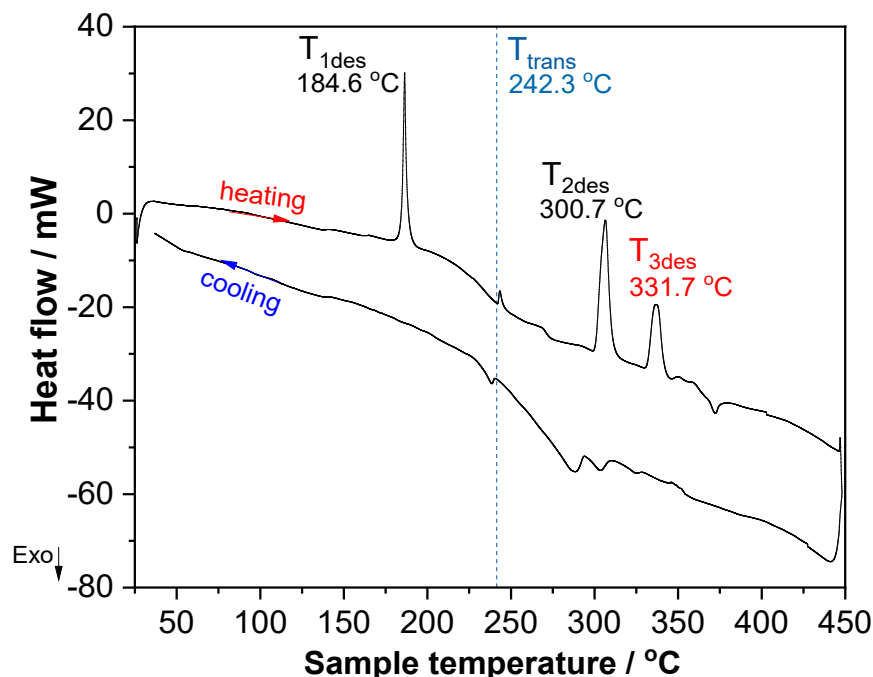
Figure 4.30 *HP-DSC plot measured at 150 bar for 66 mol% Al doped NaAlH$_4$.*

The Na$_3$AlH$_6$ phase transition was also affected and was found at the same temperature as for the previous samples with TiCl$_3$ and Al addition (Table 4.6). The system with added aluminum only displays very slow kinetics compared to the system with TiCl$_3$ addition. However, the kinetics was improved if only aluminum was added to sodium alanate in contrast to pure sodium alanate case.

Furthermore, in order to investigate the structural changes in the sample during decomposition, the dehydrogenation cycle was stopped at 320 ºC, before reaching the temperature of the new event. The hydrogen pressure of 150 bar was reduced immediately to atmospheric pressure and the system was allowed to cool down to 20 ºC. Afterward, the XPRD analysis was carried out to evaluate the structural changes in the sample (Fig. 4.31). Despite the noisy diffraction pattern (probably due to inhomogeneities in the sample), it was possible to distinguish the presence of NaH, Al, and other structurally unidentified material causing new reflections, especially one with high intensity at around 34º 2θ, which was also found in other samples with high Al content in TiCl$_3$-doped NaAlH$_4$ (Fig. 4.21 and 4.22). Thus, it was clarified that the new effect appears not due to the formation of Al-Ti phases, but due to Al addition and probably results from the formation of the metastable Na-Al phase.
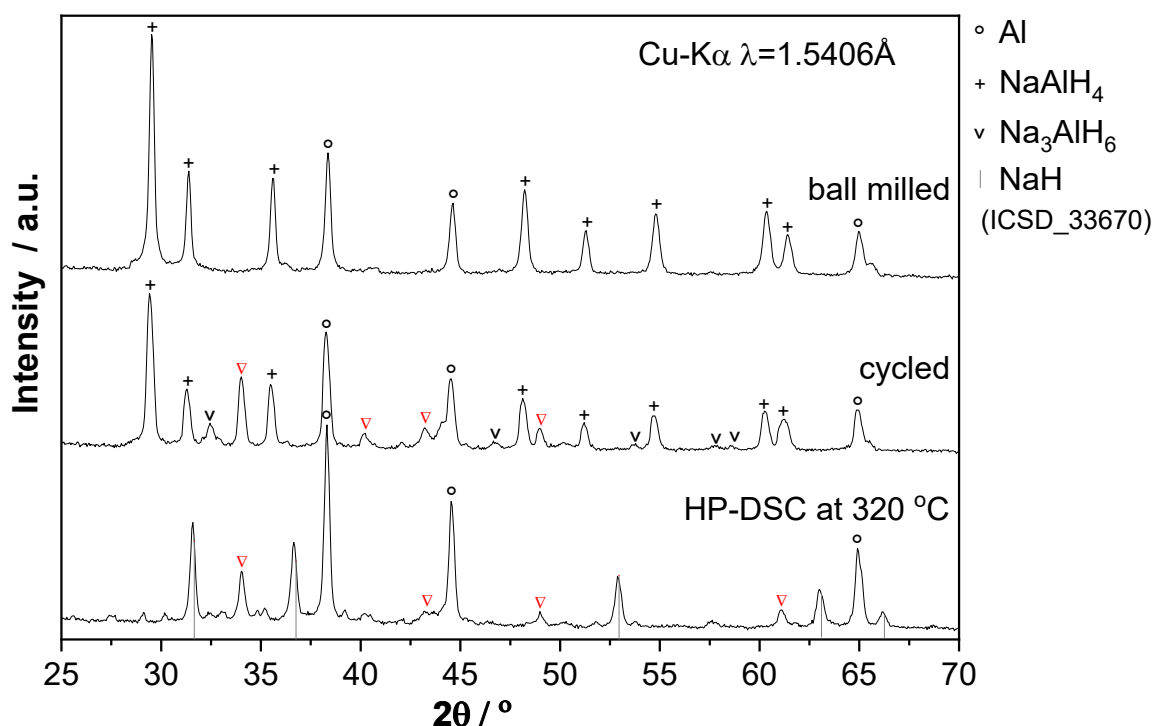
Figure 4.31 *XRPD patterns for 66 mol% Al doped NaAlH₄ ball milled (top), cycled in Sieverts apparatus (middle), and after HP-DSC measurement (bottom).*

From this investigation, it can be concluded that aluminum, but not an Al-Ti-phase as it was suggested previously, exerts a beneficial influence on the properties of doped sodium alanate for hydrogen cycling. However, it is still not clear whether Al forms an additional phase with Na, or facilitates the decomposition of NaH. Additional measurements of the decomposition behavior of NaH with Al would help to clarify this ambiguity.

In summary, the results obtained from PCI measurements combined with the ones of HP-DSC allowed a more comprehensive analysis of the (de)hydrogenation processes to be carried out, resulting in additional information regarding the role of the TiCl₃ and Al additives in the hydrogenation characteristics of the investigated sodium alanate composites.

4.3.4 Conclusions

In the introduction part, a detailed discussion about the properties of sodium alane was presented. Despite the low cost and weight, high hydrogen content, and auspicious operating conditions, several challenges and severe problems, associated with the properties of this material, as the hydrogen carrier were emphasized. Among others, the slow kinetics and the high enthalpy of hydrogen sorption/desorption are particularly prominent. This shows the need for new strategies to tune the properties

of the sodium alanate-based system in order to develop the composite material with favorable properties. The doping of $NaAlH_4$ with additives, such as $TiCl_3$, can significantly improve the hydrogenation/dehydrogenation kinetics and can influence the thermodynamics of the system. However, at the same time, it reduces significantly the hydrogen storage capacity, due to the additional weight of the dopant and the formation of undesirable by-products.

With the goal to develop a practical hydride composite based on sodium alanate, the hydrogen sorption properties were studied to gain a better understanding of the cycling behavior of a simple model system where sodium alanate doped with a small amount of the Ti additive. Further, the content of the catalyst was increased in order to form an Al-Ti-phase, which was expected to increase the dissociation pressure of the sodium alanate system, which is the chosen design target for a high-pressure hybrid tank. Therefore, samples containing relatively high amounts of the dopant (10 and 15 mol% of $TiCl_3$) were investigated in detail.

PCI curves recorded for Ti-doped $NaAlH_4$ confirmed that with the increase of the dopant content the hydrogenation/dehydrogenation rates increase and the gravimetric storage capacity decreases. Furthermore, the experimental results showed that already at 15 mol% of $TiCl_3$ the absorbed amount was significantly lower than theoretically calculated. Therefore, it was assumed that $NaAlH_4$ was consumed for the formation of $Al_{(1-y)}Ti_y$ phases ($y < 0.25$). In order to confirm this assumption, measurements with the addition of pure Al powder were performed. The obtained results clearly indicated that the excess of Al in the Ti-doped $NaAlH_4$ system increases the amount of cyclable hydrogen. These results also evidenced that the Al content is the limiting factor for the second hydrogenation step ($Na_3AlH_6 \rightarrow NaAlH_4$) since some of Al is consumed for the formation of the Al-rich-Ti-phase.

In order to gain more information about the effect of Al addition in Ti-doped sodium alanate, the (de)hydrogenation behavior of this system was studied using pressure differential calorimetry. From the Van't Hoff plot, the enthalpies for the first and second dehydrogenation steps of 10 mol%-doped $NaAlH_4$ were estimated to be 28.9 ± 1.3 kJ/mol H_2 and 47.4 ± 0.4 kJ/mol H_2, respectively. The measurements with added Al to Ti-doped $NaAlH_4$ samples showed an additional heat effect, the origin of which is not fully understood. This new event appears to be reversible in respect to temperature and pressure variations displaying a reaction enthalpy of about 56 kJ/mol H_2. Aiming at understanding the dehydrogenation reaction path, the XRPD analysis of the dehydrogenated and hydrogenated mixture of Al and $NaAlH_4$ was

carried out. A more detailed investigation of this system revealed that this effect appears most probably due to the formation of a metastable Na-Al phase.

Thus, the present study contributed to a better understanding of the hydrogen sorption chemistry in sodium alanate doped with a high content of additives and the influence of the addition of aluminum to the system.

5 SUMMARY AND CONCLUSIONS

In the introduction part of this thesis, the hydrogen absorption/desorption behavior of different complex hydride systems, with the emphasis on the perspective of light element containing hydrides developed in the last years, was discussed. There is a substantial amount of research done on modification of the properties of complex hydrides, for instance on tri- and multi-metal hydrides, to achieve the practical hydrogen storage system. Unfortunately, despite decades of extensive research, no material has been found which can combine all properties required for commercial applications. Therefore, the main task of this work was to search for Al-based material that can store hydrogen reversibly under mild conditions. In order to achieve this goal, the main efforts in this work were focused on two directions: the synthesis and design of new targeted materials and the development of already existing materials with specific properties.

The primary goal of the work on the submitted dissertation was to investigate the potential of Al-N–based compounds for solid-state hydrogen storage. In order to find suitable aminoalanes for hydrogen storage, several heterocyclic amines were examined. However, the numerous hydrogenation experiments with variants of the group of these compounds indicate that aminoalanes can not uptake hydrogen at pressure up to 1000 bar in the solid state. Several modifications of the synthesis procedure were made to generate novel aminoalanes with properties advantageous for rehydrogenation. Finally, it was concluded that aminoalanes can not uptake hydrogen in the solid state due to their high stability largely resulting from the oligomerization/polymerization process. Further studies showed that aminoalanes can be rehydrogenated in solution. Therefore, the first chapter of this work was mainly focused on the synthesis and investigation of Al-N-based compounds for reversible hydrogenation in the presence of a solvent. The perspective approach for reversible hydrogenation applying activated aluminum and secondary amine was proposed. By changing the reaction parameters and doping agent for aluminum, aminoalane with the desired properties was developed. In particular, it has been shown that:

1. The main factor that enables hydrogenation in the investigated system is the activation of aluminum by a transition metal additive. A selection of transition metal compounds has been investigated as additives for producing TM-activated aluminum (TM = Ti, Zr, Hf, and Y). It has been shown that Ti, Zr, and Hf can efficiently promote the activation of aluminum for its hydrogenation. The experiments performed showed

that the TM activity for the piperidinoalane formation decreases in the order Zr > Hf > Ti > Y.

2. The properties of triethylenediamine alane and piperidinoalane were investigated in detail. As the result of the structural and spectroscopic characterization, two crystal structures, $[pip_2AlH]_2$ and $[pip_3Al]_2$ (pip = 1 - piperidinyl, $C_5H_{10}N$) were discovered. Both structures possess dimers with $[AlN]_2$ units as central elements.

3. By using multinuclear NMR spectroscopy, the reversibility of the piperidinoalane-based system has been evidenced, demonstrating a potential pathway for hydrogen storage in aminoalanes. After the investigation of the main reaction variables, the optimal conditions for the reversible hydrogenation in this system ($[pip_2AlH]_2 \leftrightarrow [pipAlH_2]_2$) were defined: hydrogen uptake at 35 ºC and 80 bar of H_2 and hydrogen release at 120 ºC, in THF solution. Furthermore, the mechanism of aluminum hydrogenation in the presence of piperidine was proposed.

Despite the fact, that piperidinoalane cannot become a practical system, due to its low hydrogen storage capacity, it can open new possibilities for the application of other aminoalanes with more favorable properties for hydrogen storage. The simplicity and versatility of the proposed pathway could be suitable for the synthesis of other alane-based compounds. Thus, aminoalanes could become more available for a multitude of applications, such as the reduction of certain organic compounds, where Al could be reused. For potential practical applications of aminoalane as the hydrogen storage media, the identification of high hydrogen weight percentage systems with fast reversible hydrogenation kinetics will be a prerequisite.

The second part of this work was related to the modification of the properties of sodium alanate-based system in order to develop a composite useful for application in high-pressure hybrid tanks. In regard to meet the challenges to use sodium alanate-based systems as hydrogen storage material, several improvements were achieved by the addition of high amounts of transition metal salt and aluminum. In contrast to previous investigations, the additives were not meant to fulfill the role of catalysts but also to work as reactants changing thermodynamic properties. Based on the performed experiments the following conclusions were made:

1. With an increase of the $TiCl_3$ content, an enormous change of the hydrogen pressure plateau in Ti-doped $NaAlH_4$ was detected. The PCI curve showed the disappearance of the second hydrogenation step ($Na_3AlH_6 \rightarrow NaAlH_4$) for 15 mol% $TiCl_3$ doped $NaAlH_4$.

2. The hydrogen storage capacity of $NaAlH_4$ by adding high amounts of $TiCl_3$ decreased drastically, compared to the theoretically expected reduction. The unexpected relationship between dopant content and stored hydrogen amount was explained by the formation of metastable $Al_{(1-y)}Ti_y$ phases (y < 0.25).

3. It was assumed, that the consumption of aluminum for the formation of Al-Ti phases leads to the "depletion" of free aluminum in the system, and thus lowers the hydrogen storage capacity. In particular, for the dopant content up to 15 mol% of $TiCl_3$, this depletion affects only the second hydrogenation step ($Na_3AlH_6 \rightarrow NaAlH_4$). The good agreement between experimental and calculated data showed, that for a critical dopant content above ~14.3 mol% (for suggested $Al_{0.85}Ti_{0.15}$ phase), this step will be completely suppressed.

4. The analysis of PCI data clearly showed that after the addition of Al to Ti-doped samples the hydrogen storage capacity was noticeably increased. For 10 mol% Ti-doped $NaAlH_4$ the reversible hydrogen content was increased by 0.77 wt.- %, when 51 mol% of Al was added. It was assumed that extra Al addition facilitates the formation of $NaAlH_4$ from Na_3AlH_6, and as a result, increases the hydrogen storage capacity of Ti-doped $NaAlH_4$ system.

5. The optimum amount of Al addition as a function of Ti content in the assumed Al-Ti phase was calculated and showed good agreement with experimentally obtained data. The performed calculations can be used to estimate the possible Al-Ti phase composition and the deficiency of Al in Ti-doped $NaAlH_4$ system.

6. The addition of the high amounts of Al leads to an additional thermal signal during the HP-DSC measurement which takes place at around 330 ºC (at 150 bar). This event was reversible and pressure dependent, and occurs with a reaction enthalpy of about ~56 kJ/mol H_2. The temperatures of the structural transformation and decomposition of Na_3AlH_6 were also affected by the aluminum addition, compared to the sample with $TiCl_3$ addition, only.

7. To gain more insight into the role of aluminum in this composite, the mixture with only aluminum and sodium alanate was investigated. The HP-DSC measurements of the 66 mol% Al-doped $NaAlH_4$ sample also showed the signal at about 330 ºC (at 150 ºC). Thus, it was confirmed that the new effect is not related to the Al-Ti phase, but appears due to the decomposition of an unknown hydride phase.

The present study contributes to the understanding of the (de)hydrogenation behavior of Al-based systems with perspectives being applicable to other related materials.

RECOMMENDATIONS AND OUTLOOK

Many lessons that have been learned from the $NaAlH_4$ system may open up different possibilities for achieving the goals required for a practical hydrogen storage system. All these findings should be summarized for the extrapolation of this knowledge to other possible alanate-based hydrogen storage materials. On the other hand, a sodium alanate system, which cannot satisfy completely the requirements of the automotive industry, can be useful for stationary applications. Novel battery materials, solar heat storage, low-power small-scale units could be possible applications of sodium alanate. Thus, there is still some commercial interest in sodium alanate, even if originally it was envisaged for other applications.

The safety of a hydride-based storage system is an issue with respect to practical implementation as well. Sodium alanate, especially when loaded with titanium, is a very reactive solid, which can ignite with air or moisture. Strategies that reduce this problem have to be developed. Solving problems step by step may lead to hydrogen storage systems that could meet these requirements.

Many other Al-based complex hydrides have been not yet explored. The structures and thermodynamic properties of different Al-N-based complexes are still unknown. The main reason is that they are difficult to synthesize in crystalline form, but are often obtained as amorphous solids. Systematic investigations of these systems may reveal the material that matches simultaneously the thermodynamic and hydrogen capacity requirements.

Taking into account the results of this work, future activities should include:

1. A systematic study of aminoalane preparation from aluminum and amine via the mechanochemical approach under hydrogen pressure.

2. Optimization of the TM additive content in the activation procedure of aluminum. Investigation of other suitable additives for aluminum activation.

3. *In situ* experiments to clarify the role of TM additive for reversible hydrogenation of aluminum in the presence of an amine.

4. Further investigation of the nature of titanium species in Ti-doped $NaAlH_4$ to extend the knowledge about the mechanism of Ti action.

5. Identification of the new phase and effect that appear during Al addition to $NaAlH_4$. The HP-DSC measurement of NaH with the addition of Al, in order to compare the decomposition temperatures with pure NaH.

6. Modification of properties of other alanate-based complexes by aluminum addition.

Parallel to laboratory studies, the search for alternative hydrogen storage materials by computational methods should be pursued. The thermodynamic calculations may predict the dehydrogenation enthalpy of different complex hydrides and thereby be useful for identifying those compounds suitable for hydrogen storage.

REFERENCES

[1]   J. Verne, *Mysterious island*, Wordsworth **2010**.

[2]   S. Niaz, T. Manzoor, A. H. Pandith, *Renewable and Sustainable Energy Reviews* **2015**, *50*, 457.

[3]   M. A. Rosen, S. Koohi-Fayegh, *Energ. Ecol. Environ.* **2016**, *1*, 10.

[4]   A. Züttel, A. Borgschulte, L. Schlapbach, *Hydrogen as a Future Energy Carrier*, Wiley-VCH Verlag GmbH & Co. KGaA, Weinheim, Germany **2008**.

[5]   E. Anderson, F. Mitlitsky, T. Molter, *201st electrochemical society meeting Philadelphia,* **2002**.

[6]   D. Stolten (Ed.), *Hydrogen and Fuel Cells. Fundamentals, Technologies and Applications*, Wiley-VCH-Verl., Weinheim **2010**.

[7]   G. Karim, *Int. J. Hydrog. Energy* **2003**, *28*, 569.

[8]   G. Thomas, *US DOE Hydrogen Program 2000 Annual Review, May 9-11, 2000 San Ramon, California*.

[9]   X. Cheng, Z. Shi, N. Glass, L. Zhang, J. Zhang, D. Song, Z.-S. Liu, H. Wang, J. Shen, *J. Power Sources* **2007**, *165*, 739.

[10]   M. Fichtner, *Adv. Eng. Mater.* **2005**, *7*, 443.

[11]   U. Eberle, M. Felderhoff, F. Schuth, *Angew. Chem. Int. Ed. Engl.* **2009**, *48*, 6608.

[12]   *DOE Technical Targets for Onboard Hydrogen Storage for Light-Duty Vehicles*, (n.d.). Retrieved 03.06.2017, from https://www.energy.gov/eere/fuelcells/doe-technical-targets-onboard-hydrogen-storage-light-duty-vehicles.

[13]   F. Schüth, B. Bogdanović, M. Felderhoff, *Chem. Commun.* **2004**, 2249 – 2258

[14]   Materials-Based Hydrogen Storage, (n.d.). Retrieved 03.06.2017, from https://www.energy.gov/eere/fuelcells/materials-based-hydrogen-storage.

[15]   M. Dornheim, Ed. J. C. M. Piraján, *eBook* **2011,** ISBN: 978-953-307-563-1, DOI: 10.5772/21662.

[16]   K. T. Møller, A. S. Fogh, M. Paskevicius, J. Skibsted, T. R. Jensen, *Phys. Chem. Chem. Phys.* **2016**, *18*, 27545.

[17]   *Hydrogen Storage*, (n.d.). Retrieved 03.06.2017, from https://www.energy.gov/eere/fuelcells/hydrogen-storage.

[18]   D. Stolten, Grube, Thomas /Autors:Urbanczyk, R., D. Bathen, M. Felderhoff, J. Burfeind (Eds.), *18th World Hydrogen Energy Conference 2010 - WHEC 2010: Proceedings*, Forschungszentrum IEF-3, Jülich **2010**.

[19]   Y. Sun, C. Shen, Q. Lai, W. Liu, D.-W. Wang, K.-F. Aguey-Zinsou, *Energy Storage Mater.* **2018**, *10*, 168.

[20]   A. D. Lueking, R. T. Yang, N. M. Rodriguez, R. T. K. Baker, *Langmuir* **2004**, *20*, 714.

[21]   C. Liu, *Science* **1999**, *286*, 1127.

[22]   R. Ströbel, J. Garche, P. T. Moseley, L. Jörissen, G. Wolf, *J. Power Sources* **2006**, *159*, 781.

[23]   Q. Hu, Y. Lu, G. P. Meisner, *J. Phys. Chem. C* **2008**, *112*, 1516.

[24]   M. G. Nijkamp, J. E. M. J. Raaymakers, A. J. van Dillen, K. P. de Jong, *Appl Phys A* **2001**, *72*, 619.

[25]   H. W. Langmi, A. Walton, M. M. Al-Mamouri, S. R. Johnson, D. Book, J. D. Speight, P. P. Edwards, I. Gameson, P. A. Anderson, I. R. Harris, *J. Alloys Compd.* **2003**, *356-357*, 710.

[26]   S. H. Jhung, J. W. Yoon, J. S. Lee, J.-S. Chang, *Chemistry (Weinheim an der Bergstrasse, Germany)* **2007**, *13*, 6502.

[27]   G. Férey, M. Latroche, C. Serre, F. Millange, T. Loiseau, A. Percheron-Guégan, *Chem. Commun.* **2003**, *27*, 2976.

[28]   N. Rosi, J. Eckert, M. Eddaoudi, D. Vodak, J. Kim, M. Keffee, et al., *Science* **2003**, *300*, 1127.

[29]   Y. J. Choi, J. W. Lee, J. H. Choi, J. K. Kang, *Appl. Phys. Lett.* **2008**, *92*, 173102.

[30]   S. S. Han, H. Furukawa, O. M. Yaghi, W. A. Goddard, *J. Am. Chem. Soc.* **2008**, *130*, 11580.

[31]   E. Klontzas, E. Tylianakis, G. E. Froudakis, *J. Phys. Chem. C* **2008**, *112*, 9095.

[32]   E. Klontzas, E. Tylianakis, G. E. Froudakis, *Nano Lett.* **2010**, *10*, 452.

[33]   H. Lee, J.-won Lee, D. Y. Kim, J. Park, Y.-T. Seo, H. Zeng, I. L. Moudrakovski, C. I. Ratcliffe, J. A. Ripmeester, *Nature* **2005**, *434*, 743.

[34]   T. A. Strobel, C. A. Koh, E. D. Sloan, *Fluid Phase Equilibr.* **2007**, *261*, 382.

[35]   V. V. Struzhkin, B. Militzer, W. L. Mao, H.-K. Mao, R. J. Hemley, *Chemical reviews* **2007**, *107*, 4133.

[36]   R. B. Gupta, *Hydrogen fuel: Production, transport, and storage*, CRC Press, Boca Raton **2008**.

[37]   J. F. Stampfer Jr., C. E. Holley Jr., and J. F. Suttle, *J. Am. Chem. Soc.* **1960**, *82*, 3504.

[38]   L. Pasquini, E. Callini, M. Brighi, F. Boscherini, A. Montone, T. R. Jensen, C. Maurizio, M. Vittori Antisari, E. Bonetti, *J. Nanopart. Res.* **2011**, *13*, 5727.

[39]   G. Liang J. Huot S. Boily A. Van Neste R. Schulz, *J. Alloy. Compd.* **1999**, *292*, 247.

[40]   K. Zeng, T. Klassen, W.Oelerich, R. Bormann, *J. Alloy. Compd.* **1999**, *283*, 213.

[41]   E. Ivanov, I. Konstanchuk, A. Stepanov, V. Boldyrev, *J. Less-Common Met.* **1987**, *131*, 25.

[42]   G. Liu, F. Qiu, J. Li, Y. Wang, L. Li, C. Yan, L. Jiao, H. Yuan, *Int. J. Hydrog. Energy* **2012**, *37*, 17111.

[43]   F. M. Brower, N. E. Matzek, P. F. Reigler, H. W. Rinn, C. B. Roberts, D. L. Schmidt, J. A. Snover, K. Terada, *J. Am. Chem. Soc.* **1976**, *98*, 2450.

[44]   J. Graetz, J. J. Reilly, *J. Phys. Chem. B* **2005**, *109*, 22181.

[45]   J. Graetz, J. J. Reilly, *J. Alloys Compd.* **2006**, *424*, 262.

[46]   J. Graetz, J. J. Reilly, J. G. Kulleck, R. C. Bowman, *J. Alloy. Compd.* **2007**, *446-447*, 271.

[47]   S. Orimo, Y. Nakamori, T. Kato, C. Brown, C. M. Jensen, *Appl. Phys. A* **2006**, *83*, 5.

[48]   J. Graetz, S. Chaudhuri, Y. Lee, T. Vogt, J. T. Muckerman, J. J. Reilly, *Phys. Rev. B* **2006**, *74*, 27.

[49]   B. Baranowski, M. Tkacz, *Z. Phys. Chem* **1983**, *135*, 27-38.

[50]   R. Zidan, B. L. Garcia-Diaz, C. S. Fewox, A. C. Stowe, J. R. Gray, A. G. Harter, *Chem. Commun.* **2009**.

[51]   J. Graetz, S. Chaudhuri, J. Wegrzyn, Y. Celebi, J. R. Johnson, W. Zhou, J. J. Reilly, *J. Phys. Chem. C* **2007**, *111*, 19148.

[52]   P. Mauron, F. Buchter, O. Friedrichs, A. Remhof, M. Bielmann, C. N. Zwicky, A. Züttel, *J. Phys. Chem. B* **2008**, *112*, 906.

[53]   P. Martelli, R. Caputo, A. Remhof, P. Mauron, A. Borgschulte, A. Züttel, *J. Phys. Chem. C* **2010**, *114*, 7173.

[54]   K. Miwa, M. Aoki, T. Noritake, N. Ohba, Y. Nakamori, S.-i. Towata, A. Züttel, S.-i. Orimo, *Phys. Rev. B* **2006**, *74*, 1.

[55]   K. Chłopek, C. Frommen, A. Léon, O. Zabara, M. Fichtner, *J. Mater. Chem.* **2007**, *17*, 3496.

[56] H. I. Schlesinger, R. T. Sanderson, and A. B. Burg, *J. Am. Chem. Soc.* **1939**, *61*, 536.

[57] J. Block, A. P. Gray, *Inorg. Chem.* **1965**, *4*, 304.

[58] B. Bogdanović, R. A. Brand, A. Marjanović, M. Schwickardi, J. Tölle, *J. Alloys Compd.* **2000**, *302*, 36.

[59] H. Morioka, K. Kakizaki, S.-C. Chung and A. Yamada, *J. Alloys Compd.* **2003**, *353*, 310.

[60] J. R. Ares, K.-F. Aguey-Zinsou, F. Leardini, I. J. Ferrer, J.-F. Fernandez, Z.-X. Guo, C. Sánchez, *J. Phys. Chem. C* **2009**, *113*, 6845.

[61] M. Mamatha, B. Bogdanović, M. Felderhoff, A. Pommerin, W. Schmidt, F. Schüth, C. Weidenthaler, *J. Alloys Compd.* **2006**, *407*, 78.

[62] T. Ichikawa, S. Isobe, N. Hanada, H. Fujii, *J. Alloys Compd.* **2004**, *365*, 271.

[63] S. Isobe, T. Ichikawa, K. Tokoyoda, N. Hanada, H. Leng, H. Fujii, Y. Kojima, *Thermochim. Acta* **2008**, *468*, 35.

[64] P. Chen, Z. Xiong, J. Luo, J. Lin, K. L. Tan, *Nature* **2002**, *420*, 302.

[65] A. W. Titherley, *J. Chem. Soc., Dalton Trans.* **1894**, *65*, 504.

[66] S. Yamaguchi, H. Miyaoka, T. Ichikawa, Y. Kojima, *Int. J. Hydrog. Energy* **2017**, *42*, 5213.

[67] H. Y. Leng, T. Ichikawa, S. Hino, N. Hanada, S. Isobe, H. Fujii, *J. Phys. Chem. B* **2004**, *108*, 8763.

[68] A. Züttel, S. Rentsch, P. Fischer, P. Wenger, P. Sudan, P. Mauron, C. Emmenegger, *J. Alloys Compd.* **2003**, *356-357*, 515.

[69] M. Paskevicius, L. H. Jepsen, P. Schouwink, R. Černý, D. B. Ravnsbæk, Y. Filinchuk, M. Dornheim, F. Besenbacher, T. R. Jensen, *Chem. Soc. Rev.* **2017**, *46*, 1565.

[70] L. Li, C. Xu, C. Chen, Y. Wang, L. Jiao, H. Yuan, *Int. J. Hydrog. Energy* **2013**, *38*, 8798.

[71] J. J. Vajo, S. L. Skeith, F. Mertens, *J. Phys. Chem. B* **2005**, *109*, 3719.

[72] S. S. Muir, X. Yao, *Int. J. Hydrog. Energy* **2011**, *36*, 5983.

[73] O. Zavorotynska, A. El-Kharbachi, S. Deledda, B. C. Hauback, *Int. J. Hydrog. Energy* **2016**, *41*, 14387.

[74] G. Severa, E. Rönnebro, C. M. Jensen, *Chem. Commun.* **2010**, *46*, 421.

[75] E. G. Bardají, N. Hanada, O. Zabara, M. Fichtner, *Int. J. Hydrog. Energy* **2011**, *36*, 12313.

[76] C. Sugai, S. Kim, G. Severa, J. L. White, N. Leick, M. B. Martinez, T. Gennett, V. Stavila, C. Jensen, *ChemPhysChem* **2019**.

[77] I. Saldan, R. Campesi, O. Zavorotynska, G. Spoto, M. Baricco, A. Arendarska, K. Taube, M. Dornheim, *Int. J. Hydrog. Energy* **2012**, *37*, 1604.

[78] B. von Colbe, José M, M. Felderhoff, B. Bogdanović, F. Schüth, C. Weidenthaler, *Chem. Commun.* **2005**.

[79] B. Bogdanovic and M. Schwickardi, *J. Alloys Compd.* **1997**, *253-254*, 1.

[80] J. Gao, P. Adelhelm, M. H. W. Verkuijlen, C. Rongeat, M. Herrich, P. J. M. van Bentum, O. Gutfleisch, A. P. M. Kentgens, K. P. de Jong, P. E. de Jongh, *J. Phys. Chem. C* **2010**, *114*, 4675.

[81] M. H. W. Verkuijlen, J. Gao, P. Adelhelm, P. J. M. van Bentum, P. E. de Jongh, A. P. M. Kentgens, *J. Phys. Chem. C* **2010**, *114*, 4683.

[82] F. E. Pinkerton, *J. Alloys Compd.* **2011**, *509*, 8958.

[83] D. L. Anton, *J. Alloys Compd.* **2003**, *356-357*, 400.

[84] T. Sun, B. ZHOU, H. WANG, M. Zhu, *Int. J. Hydrog. Energy* **2008**, *33*, 2260.

[85] J. Mao, Z. Guo, H. Liu, *RSC Adv* **2012**, *2*, 1569.

[86]   M. P. Pitt, P. E. Vullum, M. H. Sørby, H. Emerich, M. Paskevicius, C. E. Buckley, J. C. Walmsley, R. Holmestad, B. C. Hauback, *J. Phys. Chem. C* **2012**, *116*, 14205.

[87]   J. A. Dilts and E. C. Ashby, *Inorg. Chem.* **1972**, *11*.

[88]   A. Andreasen, *J. Alloys Compd.* **2006**, *419*, 40.

[89]   Y. Kojima, Y. Kawai, M. Matsumoto, T. Haga, *J. Alloys Compd.* **2008**, *462*, 275.

[90]   D. Blanchard, H.W. Brinks, B.C. Hauback, P. Norby, *Mat. Sci. Eng. B* **2004**, *108*, 54.

[91]   J. Graetz, J. Wegrzyn and J. J. Reilly, *J. Am. Chem. Soc.* **2008**, *130*, 17790.

[92]   X. Liu, G. S. McGrady, H. W. Langmi, C. M. Jensen, *J. Am. Chem. Soc.* **2009**, *131*, 5032.

[93]   R. U. E. Wiberg, *Z. Naturforschg.* **1951**.

[94]   M. E. Kost, A. L. Golovanova, *Russ Chem Bull* **1975**, *24*, 905.

[95]   W. E. Reid, Jr., J. M. Bish, and A. Brenner, *J. Electrochem. Soc.* **1957**, *104*, 21.

[96]   W. M. Mueller, J. P. Blackledge, G. G. Libowitz, *Metal Hydrides*, Elsevier **1968**.

[97]   Z. Cao, L. Ouyang, H. Wang, J. Liu, M. Felderhoff, M. Zhu, *J. Mater. Chem. A* **2017**, *5*, 6042.

[98]   Y. Yan, H.-W. Li, T. Sato, N. Umeda, K. Miwa, S.-i. Towata, S.-i. Orimo, *Int. J. Hydrog. Energy* **2009**, *34*, 5732.

[99]   L. H. Rude, T. K. Nielsen, D. B. Ravnsbaek, U. Bösenberg, M. B. Ley, B. Richter, L. M. Arnbjerg, M. Dornheim, Y. Filinchuk, F. Besenbacher, T. R. Jensen, *Phys. Status Solidi A* **2011**, *208*, 1754.

[100]   K. E. Lamb, M. D. Dolan, D. F. Kennedy, *Int. J. Hydrog. Energy* **2019**, *44*, 3580.

[101]   A. Karkamkar, S. M. Kathmann, G. K. Schenter, D. J. Heldebrant, N. Hess, M. Gutowski, T. Autrey, *Chem. Mater.* **2009**, *21*, 4356.

[102]   M. G. Hu, R. A. Geanangel, W. W. Wendlandt, *Thermochim. Acta* **1978**, *23*, 249.

[103]   F. Baitalow, J. Baumann, G. Wolf, K. Jaenicke-Rößler, G. Leitner, *Thermochim. Acta* **2002**, *391*, 159.

[104]   C. R. Miranda, G. Ceder, *J. Chem. Phys.* **2007**, *126*.

[105]   A. D. Sutton, A. K. Burrell, D. A. Dixon, E. B. Garner, J. C. Gordon, T. Nakagawa, K. C. Ott, J. P. Robinson, M. Vasiliu, *Science (New York)* **2011**, *331*, 1426.

[106]   S. Hausdorf, F. Baitalow, G. Wolf, F. O.R.L. Mertens, *Int. J. Hydrog. Energy* **2008**, *33*, 608.

[107]   L. H. Jepsen, M. B. Ley, Y. Filinchuk, F. Besenbacher, T. R. Jensen, *ChemSusChem* **2015**, *8*, 1452.

[108]   L. H. Jepsen, M. B. Ley, Y.-S. Lee, Y. W. Cho, M. Dornheim, J. O. Jensen, Y. Filinchuk, J. E. Jørgensen, F. Besenbacher, T. R. Jensen, *Mater. Today* **2014**, *17*, 129.

[109]   Y. Guo, H. Wu, W. Zhou, X. Yu, *J. Am. Chem. Soc.* **2011**, *133*, 4690.

[110]   Z. Tang, F. Yuan, Q. Gu, Y. Tan, X. Chen, C. M. Jensen, X. Yu, *Acta Mater.* **2013**, *61*, 3110.

[111]   E. Roedern, T. R. Jensen, *Inorg. Chem.* **2015**, *54*, 10477.

[112]   X. Chen, X. Yu, *J. Phys. Chem. C* **2012**, *116*, 11900.

[113]   S. Hino, H. Grove, T. Ichikawa, Y. Kojima, M. H. Sørby, B. C. Hauback, *Int. J. Hydrog. Energy* **2015**, *40*, 16938.

[114]   I. Dovgaliuk, L. H. Jepsen, D. A. Safin, Z. Łodziana, V. Dyadkin, T. R. Jensen, M. Devillers, Y. Filinchuk, *Chem. Eur. J.* **2015**, *21*, 14562.

[115]   Y. Guo, Y. Jiang, G. Xia, X. Yu, *Chem. Comm.* **2012**, *48*, 4408.

[116]   I. Dovgaliuk, *Doctoral dissertation* **2015**, *Louvain-la-Neuve*.

[117] I. Dovgaliuk, C. S. Le Duff, K. Robeyns, M. Devillers, Y. Filinchuk, *Chem. Mater.* **2015**, *27*, 768.

[118] G. Xia, Y. Tan, X. Chen, Z. Guo, H. Liu, X. Yu, *J. Mater. Chem. A* **2013**, *1*, 1810.

[119] Y. Nakagawa, Y. Ikarashi, S. Isobe, S. Hino, S. Ohnuki, *RSC Adv* **2014**, *4*, 20626.

[120] T. Tsumuraya, T. Shishidou, T. Oguchi, *Phys. Rev. B* **2008**, *77*.

[121] F. E. Pinkerton, *J. Alloys Compd.* **2005**, *400*, 76.

[122] H. M. Jin, P. Wu, *Appl. Phys. Lett.* **2005**, *87*, 181917.

[123] Z. Xiong, J. Hu, G. Wu, P. Chen, W. Luo, K. Gross, J. Wang, *J. Alloys Compd.* **2005**, *398*, 235.

[124] G. Amica, S. Enzo, P. A. Larochette, F. C. Gennari, *Phys. Chem. Chem. Phys.* **2018**, *20*, 15358.

[125] G. M. Sheldrick, *Acta Crystallogr. A* **2008**, *64*, 112.

[126] G. M. Sheldrick, *Acta Crystallogr. C* **2015**, *71*, 3.

[127] Q.-L. Zhu, Q. Xu, *Energy Environ. Sci.* **2015**, *8*, 478.

[128] N. Kariya, A. Fukuoka, M. Ichikawa, *Appl. Catal. A* **2002**, *233*, 91.

[129] A. S. Kesten, *US Patent 4567033A* **1984**.

[130] E. Newson, Th. Haueter, P. Hottinger, F. Von Roth, G.W.H. Scherer, Th.H. Schucan, *Int. J. Hydrog. Energy* **1998**, *23*, 905.

[131] S. Hodoshima, H. Nagata, Y. Saito, *Appl. Catal. A* **2005**, *292*, 90.

[132] H. Liu, C. Liu, C. Yin, B. Liu, X. Li, Y. Li, Y. Chai, Y. Liu, *Catal. Today* **2016**, *276*, 46.

[133] L. M. Kustov, A. L. Tarasov, B. P. Tarasov, *Int. J. Hydrog. Energy* **2013**, *38*, 5713.

[134] C. Fellay, P. J. Dyson, G. Laurenczy, *Angew. Chem. Int. Ed. Engl.* **2008**, *47*, 3966.

[135] C. Reller, M. Pöge, A. Lißner, F. O. R. L. Mertens, *Environ. Sci. Technol.* **2014**, *48*, 14799.

[136] J. J. Verendel, P. Dinér, *ChemCatChem* **2013**, *5*, 2795.

[137] Y. Okada, E. Sasaki, E. Watanabe, S. Hyodo, H. Nishijima, *Int. J. Hydrog. Energy* **2006**, *31*, 1348.

[138] J. W. Makepeace, T. He, C. Weidenthaler, T. R. Jensen, F. Chang, T. Vegge, P. Ngene, Y. Kojima, P. E. de Jongh, P. Chen, W. I.F. David, *Int. J. Hydrog. Energy* **2019**, *44*, 7746.

[139] E. Clot, O. Eisenstein, R. H. Crabtree, *Chem. Commun.* **2007**.

[140] A. Moores, M. Poyatos, Y. Luo, R. H. Crabtree, *New J. Chem.* **2006**, *30*, 1675.

[141] G. P. Pez at el., *US patent 7101530* **2006**.

[142] G. P. Pez et al., *US patent 7351395* **2008**.

[143] F. Sotoodeh, K. J. Smith, *Can. J. Chem. Eng.* **2013**, *91*, 1477.

[144] R. H. Crabtree, *Energy Environ. Sci.* **2008**, *1*, 134.

[145] P. G. Campbell, L. N. Zakharov, D. J. Grant, D. A. Dixon, S.-Y. Liu, *J. Am. Chem. Soc.* **2010**, *132*, 3289.

[146] W. Luo, P. G. Campbell, L. N. Zakharov, S.-Y. Liu, *J. Am. Chem. Soc.* **2011**, *133*, 19326.

[147] Y. Cui, S. Kwok, A. Bucholtz, B. Davis, R. A. Whitney, P. G. Jessop, *New J. Chem.* **2008**, *32*, 1027.

[148] R. H. Crabtree, *ACS Sustainable Chem. Eng.* **2017**, *5*, 4491.

[149] J. Oh, H. B. Bathula, J. H. Park, Y.-W. Suh, *Commun. Chem.* **2019**, *2*, 972.

[150] J. Oh, K. Jeong, T. W. Kim, H. Kwon, J. W. Han, J. H. Park, Y.-W. Suh, *ChemSusChem* **2018**, *11*, 661.

[151] Y. Dong, M. Yang, Z. Yang, H. Ke, H. Cheng, *Int. J. Hydrog. Energy* **2015**, *40*, 10918.

[152] L. Li, M. Yang, Y. Dong, P. Mei, H. Cheng, *Int. J. Hydrog. Energy* **2016**, *41*, 16129.

[153] K.-i. Fujita, Y. Tanaka, M. Kobayashi, R. Yamaguchi, *J. Am. Chem. Soc.* **2014**, *136*, 4829.

[154] F. Sotoodeh, K. J. Smith, *Ind. Eng. Chem. Res.* **2010**, *49*, 1018.

[155] K. M. Eblagon, D. Rentsch, O. Friedrichs, A. Remhof, A. Zuettel, A. J. Ramirez-Cuesta, S. C. Tsang, *Int. J. Hydrog. Energy* **2010**, *35*, 11609.

[156] J. Oh, T. W. Kim, K. Jeong, J. H. Park, Y.-W. Suh, *ChemCatChem* **2018**, *10*, 3892.

[157] P. G. Campbell, A. J. V. Marwitz, S.-Y. Liu, *Angew. Chem. Int. Ed. Engl.* **2012**, *51*, 6074.

[158] P. G. Campbell, J. S. A. Ishibashi, L. N. Zakharov, S.-Y. Liu, *Aust. J. Chem.* **2014**, *67*, 521.

[159] L. Winner, W. C. Ewing, K. Geetharani, T. Dellermann, B. Jouppi, T. Kupfer, M. Schäfer, H. Braunschweig, *Angew. Chem. Int. Ed. Engl.* **2018**, *57*, 12275.

[160] E. C. Ashby, G. J. Brendel, H. E. Redman, *Inorg. Chem.* **1963**, *Vol. 2*, 499.

[161] Z. Jiang, R. A. Dougal, S. Liu, S. A. Gadre, A. D. Ebner, J. A. Ritter, *J. Power Sources* **2005**, *142*, 92.

[162] D. Teichmann, W. Arlt, P. Wasserscheid, R. Freymann, *Energy Environ. Sci.* **2011**, *4*, 2767.

[163] E. Wiberg and A. May, *Z. Naturforsch.* **1955**, *10 b*, 239.

[164] J. L. Atwood, K. W. Butz, M. G. Gardiner, C. Jones, G. A. Koutsantonis, C. L. Raston, K. D. Robinson, *Inorg. Chem.* **1993**, *32*, 3482.

[165] R. Ehrlich, A. R. Young, B. M. Lichstein, D. D. Perry, *Inorg. Chem.* **1964**, *3*, 628.

[166] N. M. Alpatova, T. N. Dymova, Y. M. Kessler and O. R. Osipov, *Russ. Chem. Rev.* **1968**, *37*.

[167] F. R. Bennett, F. M. Elms, M. G. Gardiner, G. A. Koutsantonis, C. L. Raston and N. K. Roberts, *Organometallics* **1992**, *11*, 1457.

[168] C. Jones, G. A. Koutsantonis and C. L. Raston, *Polyhedron* **1993**, *12*, 1829.

[169] F. M. Elms, M. G. Gardiner, G. A. Koutsantonis, C. L. Raston, J. L. Atwood and K. D. Robinson, *J. Organomet. Chem.* **1993**, *449*, 45.

[170] I. B. Gorrell, P. B. Hitchcock and J. D. Smith, *J. Chem. Soc., Chem. Commun.* **1993**, http://pubs.rsc.org/en/content/articlepdf/1993/c3/c39930000189.

[171] M. G Gardiner and C. L. Raston, *Coord. Chem. Rev.* **1997**, *166*, 1.

[172] J. K. Ruff and M. F. Hawthorne, *J. Am. Chem. Soc.* **1960**, *82 (9)*, 2141.

[173] J. K. Ruff, *J. Am. Chem. Soc.* **1961**, *83*, 1798.

[174] J. K. Ruff, *J. Am. Chem. Soc.* **1961**, *83*, 2835.

[175] S. J. Schauer and G. H. Robinson, *J. Coord. Chem.* **1993**, *30*, 197.

[176] T. Belgardt, S. D. Waezsada, H. W. Roesky, H. Gornitzka, L. Häming and D. Stalke, *Inorg. Chem.* **1994**, *33*, 6247.

[177] A. Storr, B. S. Thomas and A. D. Penland, *J. Chem. Soc., Dalton Trans.* **1972**.

[178] K. M. Waggoner, M. M. Olmstead and P. P. Power, *Polyhedron* **1990**, *9*, 257.

[179] C. L. Raston, *J. Organomet. Chem.* **1994**, *475*, 15.

[180] P. J. Brothers, R. J. Wehmschulte, M. M. Olmstead, K. Ruhlandt-Senge, S. R. Parkin and P. P. Power, *Organometallics* **1994**, *13*, 2792.

[181] P. C. Andrews, M. G. Gardiner, C. L. Raston and V.-A. Tolhurst, *Inorg. Chim. Acta* **1997**, *259*, 249.

[182] T. D. Humphries, K. T. Munroe, A. Decken, G. S. McGrady, *Dalton Trans.* **2013**, *42*, 6953.

[183] C. W. Heitsch, C. E. Nordman, R. W. Parry, *norg. Chem.* **1963**, *2*, 508.

[184] T. D. Humphries, P. Sirsch, A. Decken, G. Sean McGrady, *J. Mol. Struct.* **2009**, *923*, 13.

[185] C. J. Harlan, S. G. Bott and A. R. Barron, *J. Chem. Crystallogr* **1998**, *28*, 649.

[186] J. L. Atwood, F. R. Bennett, F. M. Elms, C. Jones, C. L. Raston and K. D. Robinson, *J. Am. Chem. Soc.* **1991**, *113*, 8183.

[187] U. Dümichen, T. Gelbrich, J. Sieler, *Z. Anorg. Allg. Chem.* **2001**, *627*.

[188] C. Klein, H. Nöth, M. Tackeand and M. Thomann, *Angew. Chem. Int. Ed. Engl.* **1993**, *32*, 886.

[189] T. Bernert, M. B. Ley, J. Ruiz-Fuertes, M. Fischer, M. Felderhoff and C. Weidenthaler, *Acta Crystallogr. B* **2016**, *72 (2)*, 232.

[190] A. J. Downs, D. Duckworth, J. C. Machellc and C. R. Pulham, *Polyhedron* **1992**, *11*, 1295.

[191] K. M. Waggoner and Philip P. Power, *J. Am. Chem. Soc.* **1991**, *113*.

[192] E. Wiberg, H. Graf, M. Schmidt, R. Uson, *Z. Naturforsch., B: Chem. Sci.* **1952**, *7*, 578.

[193] A. R. Young, R. Ehrlich, *J. Am. Chem. Soc.* **1964**, *86*, 5359.

[194] J. K. Ruff, *Inorg. Chem.* **1962**, *1*, 612.

[195] R. A. Kovar and E. C. Ashby, *Inorg. Chem.* **1971**, *10*, 893.

[196] E. C. Ashby, *J. Am. Chem. Soc.* **1964**, *86*, 1882.

[197] H. D. Murib J, *US patent 3,642,853* **1972**.

[198] T. H. Baum, C. E. Larson and R. L. Jackson, *Appl. Phys. Lett.* **1989**, *55*, 1264.

[199] A. T. S. Wee, A. J. Murrell, N. K. Singh, D. O'Hare and J. S. Foord, *J. Chem. Soc., Chem. Commun.* **1990**.

[200] La H. Dubois, B. R. Zegarski, M. E. Gross and R. G. Nuzzo, *Surf. Sci.* **1991**, *244*, 89.

[201] D. M. Frigo, G. J. M. van Eijden, P. J. Reuvers and C. J. Smit, *Chem. Mater.* **1994**, *6*, 190.

[202] E. M. Marlett and W. S. Park, *J. Org. Chem.* **1990**, *55*, 2968.

[203] J. S. Cha and H. C. Brown, *J. Org. Chem.* **1993**, *58*, 3974.

[204] E. Wiberg und A. May, *Z. Naturforschg* **1955**, *10 b*, 229.

[205] D. Lacina, J. Wegrzyn, J. Reilly, Y. Celebi and J. Graetz, *Energy Environ. Sci.* **2010**, *3*, 1099.

[206] D. Lacina, J. Reilly, Y. Celebi, J. Wegrzyn, J. Johnson and J. Graetz, *J. Phys. Chem. C* **2011**, *115*, 3789.

[207] C. Ni, J. E. Wegrzyn, W. Zhou, Y. Celebi and J. Graetz, *Int. J. Hydrog. Energy* **2013**, *38*, 9779.

[208] C. Ni, L. Yang, J. T. Muckerman and J. Graetz, *J. Phys. Chem. C* **2013**, *117*, 14983.

[209] B. M. Wong, D. Lacina, I. M. B. Nielsen, J. Graetz and M. D. Allendorf, *J. Phys. Chem. C* **2011**, *115*, 7778.

[210] T. Q. Hua, R. K. Ahluwalia, *Int. J. Hydrog. Energy* **2011**, *36*, 15259.

[211] C. Ni, L. Yang, J. T. Muckerman and J. Graetz, *J. Phys. Chem. C* **2013**, *117*, 2628.

[212] D. Lacina, J. Reilly, J. Johnson, J. Wegrzyn and J. Graetz, *J. Alloys Compd.* **2011**, *509*, S654-S657.

[213] J. A. Hatnean, J. W. Thomson, P. A. Chase and D. W. Stephan, *Chem. Comm.* **2014**, *50*, 301.

[214] F. Habermann, *Bachelorarbeit* **2017**, *TU Freiberg*, 134.

[215] T. Belgardt, J. Storre, A. Klemp, H. Gornitzka, L. Haming, H.-G. Schmidt and H. W. Roesky, *J. CHEM. SOC. DALTON TRANS.* **1995**.

[216] C. Y. Tang, A. J. Downs, T. M. Greeneb and S. Parsons, *Dalton Trans.* **2003**.

[217] D. D. Tanner, C. M. Yang, *J. Org. Chem.* **1993**, *58*, 1840.

[218] W. J. Bailey, F. Marktscheffe, *J. Org. Chem.* **1960**, *25*, 1797.

[219] B. Birkmann, T. Voss, S. J. Geier, M. Ullrich, G. Kehr, G. Erker, D. W. Stephan, *Organometallics* **2010**, *29*, 5310.

[220] H. E. Redman, Patent US 2885314 **1959**.

[221] J. Ortmeyer, A. Bodach, L. Sandig-Predzymirska, B. Zibrowius, F. Mertens and M. Felderhoff, *Chem. Phys. Chem.* **2019**, *20*, 1360.

[222] H. Flores-Segura, L. A. Torres, *J. Struct. Chem.* **1997**, *8*, 227.

[223] M. M. Andrianarison, M. C. Ellerby, I. B. Gorrell, P. B. Hitchcock, J. D. Smith and D. R. Stanley, *J. Chem. Soc., Dalton. Trans.* **1996**.

[224] J. S. Silverman, C. J. Carmalt, D. A. Neumayer, A. H. Cowley, B. G. McBurnett and A. Decken, *Polyhedron* **1998**, *17*, 977.

[225] H. Li, M. J. Meziani, A. Kitaygorodskiy, F. Lu, C. E. Bunker, K. A. S. Fernando, E. A. Guliants and Y-P. Sun, *J. Phys. Chem. C* **2010**, *114*, 3318.

[226] T. D. Humphries, K. T. Munroe, A. Decken and G. S. McGrady, *Dalton Trans.* **2013**, *42*, 6965.

[227] F. C. Sauls, C. L. Czekaj and L. V. Interrante, *Inorg. Chem.* **1990**, *29*, 4688.

[228] T. J. Frankcombe, *Chem. Rev.* **2012**, *112*, 2164.

[229] Z. O. Kocabas Atakli, E. Callini, S. Kato, P. Mauron, S.-I. Orimo and A. Zuttel, *Phys. Chem. Chem. Phys.* **2015**, *17*, 20932.

[230] K. J. Gross, S. Guthrie, S. Takara and G. Thomas, *J. Alloys Compd.* **2000**, *297*, 270.

[231] R. T. Walters and J. H. Scogin, *J. Alloys Compd.* **2004**, *379*, 135.

[232] M. Felderhoff and B. Zibrowius, *Phys. Chem. Chem. Phys.* **2011**, *13*, 17234.

[233] R. Xiong, G. Sang, G. Zhang, X. Yan, P. Li, Y. Yao, D. Luo, C. Chen and T. Tang, *Int. J. Hydrog. Energy* **2017**, *42*, 6088.

[234] C. Reller, *Angew. Chem. Int. Ed. Engl.* **2012**, *51*, 11731.

[235] C. Reller and F. O. R. L. Mertens, *Eur. J. Inorg. Chem.* **2014**, *2014*, 450.

[236] J. Wang, A. D. Ebner, J. A. Ritter, *Adsorption* **2005**, *11*, 811.

[237] B. Bogdanovic and M. Schwickardi **1997**.

[238] M. Termtanun, P. Rangsunvigit, B. Kitiyanan, S. Kulprathipanja, W. Tanthapanichakoon, *Sci. Technol. Adv. Mater.* **2005**, *6*, 348.

[239] PubChem, *Periodic Table of Elements, (n.d.).* Retrieved 04.02.2020, from https://pubchem.ncbi.nlm.nih.gov/periodic-table/.

[240] R. D. Shannon, *Acta Cryst.* **1976**, *A32*, 751.

[241] J. Graetz, B. C. Hauback, *MRS Bull.* **2013**, *38*, 473.

[242] G. G. Libowitz, H. F. Hayes, and T. R. P. Gibb Jr., *J. Phys. Chem.* **1958**, *62*, 76.

[243] H. H. van Mal, K.H.H. Buschow, A. R. Miedema, *J. Less-Common Met.* **1974**, *35*, 65.

[244] M. Hirscher, *Handbook of Hydrogen Storage*, Wiley-VCH Verlag GmbH & Co. KGaA, Weinheim, Germany **2010**.

[245] P. Chen, M. Zhu, *Materials Today* **2008**, *11*, 36.

[246] J. J. Reilly Jr. and R. H. Wiswall Jr., *Inorg. Chem.* **1968**, *7*, 2254-2256.

[247] T. Takasaki, T. Mukai, N. Kitamura, T. Sakai, *Studies in Sci. and Techn.* **2014**, *3*, 39.

[248] D. Kyoi, T. Sato, E. Rönnebro, N. Kitamura, A. Ueda, M. Ito, S. Katsuyama, S. Hara, D. Noréus, T. Sakai, *J. Alloys Compd.* **2004**, *372*, 213.

[249] D. Kyoi, T. Sato, E. Rönnebro, Y. Tsuji, N. Kitamura, A. Ueda, M. Ito, S. Katsuyama, S. Hara, D. Noréus, T. Sakai, *J. Alloys Compd.* **2004**, *375*, 253.

[250] V. M. Skripnyuk, E. Rabkin, *Int. J. Hydrog. Energy* **2012**, *37*, 10724.

[251] T. Z. Si, J. B. Zhang, D. M. Liu, Q. A. Zhang, *J. Alloys Compd.* **2013**, *581*, 246.

[252] T. Si, Y. Cao, Q. Zhang, D. Sun, L. Ouyang, M. Zhu, *J. Mater. Chem. A* **2015**, *3*, 8581.

[253] Y. Song, Z. X. Guo, R. Yang, *Phys. Rev. B* **2004**, *69*, 217.

[254] E. A. Nickels, M. O. Jones, W. I. F. David, S. R. Johnson, R. L. Lowton, M. Sommariva and P. P. Edwards, *Angew. Chem. Int. Ed. Engl.* **2008**, *47*, 2817.

[255] R. Černý, G. Severa, D. B. Ravnsbæk, Y. Filinchuk, V. D'Anna, H. Hagemann, D. Haase, C. M. Jensen, T. R. Jensen, *J. Phys. Chem. C* **2009**, *114*, 1357.

[256] N. Eigen, U. Bösenberg, J. Bellosta von Colbe, T. R. Jensen, Y. Cerenius, M. Dornheim, T. Klassen, R. Bormann, *J. Alloys Compd.* **2009**, *477*, 76.

[257] O. Friedrichs, J. W. Kim, A. Remhof, F. Buchter, A. Borgschulte, D. Wallacher, Y. W. Cho, M. Fichtner, K. H. Oh, A. Züttel, *Phys. Chem. Chem. Phys.* **2009**, *11*, 1515.

[258] A. Remhof, O. Friedrichs, F. Buchter, P. Mauron, J. W. Kim, K. H. Oh, A. Buchsteiner, D. Wallacher, A. Züttel, *J. Alloys Compd.* **2009**, *484*, 654.

[259] Y. Zhang, Q. Tian, J. Zhang, S.-S. Liu, L.-X. Sun, *J. Phys. Chem. C* **2009**, *113*, 18424.

[260] G. Barkhordarian, T. Klassen, M. Dornheim, R. Bormann, *J. Alloys Compd.* **2007**, *440*, L18-L21.

[261] S.-A. Jin, Y.-S. Lee, J.-H. Shim, Y. W. Cho, *J. Phys. Chem. C* **2008**, *112*, 9520.

[262] J.-H. Shim, J.-H. Lim, S.-u. Rather, Y.-S. Lee, D. Reed, Y. Kim, D. Book, Y. W. Cho, *J. Phys. Chem. Lett.* **2010**, *1*, 59.

[263] J.-H. Shim, Y.-S. Lee, J.-Y. Suh, W. Cho, S. S. Han, Y. W. Cho, *J. Alloys Compd.* **2012**, *510*, L9-L12.

[264] D. M. Liu, W. J. Huang, T. Z. Si, Q. A. Zhang, *J. Alloys Compd.* **2013**, *551*, 8.

[265] S. Bouaricha, J. P. Dodelet, D. Guay, J. Huot, S. Boily, R. Schulz, *J. Alloy. Compd.* **2000**, *297*, 282.

[266] A. Andreasen, *Int. J. Hydrog. Energy* **2008**, *33*, 7489.

[267] L. Pranevicius, D. Milcius, L.L. Pranevicius, G. Thomas, *J. Alloys Compd.* **2004**, *373*, 9.

[268] G. Streukens, B. Bogdanović, M. Felderhoff, F. Schüth, *Phys. Chem. Chem. Phys.* **2006**, *8*, 2889.

[269] A. E. Finholt, G. D. Barbaras, G. K. Barbaras, G. Urry, T. Wartik and H. I. Schlesinger, *J. Inorg. Nucl. Chem.* **1955**, *1*, 317.

[270] H. Clasen, *Angew. Chem.* **1961**, *73*, 322.

[271] L. I. Zakharkin, V. V. Gavrilenko, *Dokl. Akad. Nauk SSSR* **1962**, *145*, 793.

[272] E. C. Ashby and P. Kobetz, *Inorg. Chem.* **1966**, *5*, 1615.

[273] B. Bogdanović, M. Felderhoff, M. Germann, M. Härtel, A. Pommerin, F. Schüth, C. Weidenthaler, B. Zibrowius, *J. Alloys Compd.* **2003**, *350*, 246.

[274] T. N. Dymova, N. G. Eliseeva, S. I. Bakum, Y. M. Dergachev, *Dok. Akad. Nauk USSR* **1974**, *215*, 1369.

[275] T. N. Dymova, Y. M. Dergachev, V. A. Sokolov, N. A. Grechanaya, *Dok. Akad. Nauk USSR* **1975**, *224*, 591.

[276] A. Peles, J. A. Alford, Z. Ma, L. Yang, M. Y. Chou, *Phys. Rev. B* **2004**, *70*, 683.

[277] J. W. Lauher, D. Dougherty, P. J. Herley, *Acta Crystallogr. B Struct. Sci.* **1979**, *35*, 1454.

[278] T. J. Frankcombe, *J. Phys. Chem. C* **2013**, *117*, 8150.

[279] E. Rönnebro, D. Noréus, K. Kadir, A. Reiser, B. Bogdanovic, *J. Alloys Compd.* **2000**, *299*, 101.

[280] J. P. Bastide, B. Bonnetot, J. M. Létoffé, P. Claudy, *Mat. Res. Bull.* **1981**, *16*, 91-96.

[281] C. E. Messer, L. G. Fasolino, C. E. Thalmayer, *J. Am. Chem. Soc.* **1955**, *77*, 4524.

[282] M. B. Smith, G. E. Bass Jr., *J. Chem. Eng. Data* **1963**, *8*, 342.

[283] P. Claudy, B. Bonnetot, G. Chahine, J. M. Letoffe, *Thermochim. Acta* **1980**, *38*, 75.

[284] P. Claudy, J.-M. Letoffe, G. Chahine, B. Bonnetot, *Thermochim. Acta* **1984**, *78*, 323.

[285] B. Bonnetot, G. Chahine, P. Claudy, M. Diot, J. M. Letoffe, *J. Chem. Thermodyn.* **1980**, *12*, 249.

[286] S. M. Opalka, D. L. Anton, *J. Alloys Compd.* **2003**, *356-357*, 486.

[287] W. Grochala, P. P. Edwards, *Chem. Rev.* **2004**, *104*, 1283.

[288] C. Qiu, S. M. Opalka, G. B. Olson, D. L. Anton, *Int. J. Mat. Res.* **2006**, *97*, 845.

[289] B.-M. Lee, J.-W. Jang, J.-H. Shim, Y. W. Cho, B.-J. Lee, *J. Alloys Compd.* **2006**, *424*, 370.

[290] C. Qiu, S. M. Opalka, G. B. Olson, D. L. Anton, *Int. J. Mat. Res.* **2006**, *97*, 1484.

[291] J. Yang, A. Sudik, C. Wolverton, D. J. Siegel, *Chem. Soc. Rev.* **2010**, *39*, 656.

[292] L. Schlapbach, A. Züttel, *Nature* **2001**, *414*, 353.

[293] B. von Colbe, José M., W. Schmidt, M. Felderhoff, B. Bogdanović, F. Schüth, *Angew. Chem. Int. Ed. Engl.* **2006**, *45*, 3663.

[294] M. Martin, C. Gommel, C. Borkhart, E. Fromm, *J. Alloys Compd.* **1996**, *238*, 193.

[295] H. Yang, A. Ojo, P. Ogaro, A. J. Goudy, *J. Phys. Chem. C* **2009**, *113*, 14512.

[296] C. Jensen, *Int. J. Hydrog. Energy* **1999**, *24*, 461.

[297] K. J. Gross, E. H. Majzoub, S. W. Spangler, *J. Alloys Compd.* **2003**, *356-357*, 423.

[298] B. Bogdanović, M. Schwickardi, *Appl. Phys. A* **2001**, *72*, 221.

[299] B. Bogdanović, M. Felderhoff, A. Pommerin, F. Schüth, N. Spielkamp, A. Stark, *Journal of Alloys and Compounds* **2009**, *471*, 383.

[300] A. J. Maeland, B. Hauback, H. Fjellvåg, M. Sørby, *Int. J. Hydrog. Energy* **1999**, *24*, 163.

[301] V. P. Balema, J. W. Wiench, K. W. Dennis, M. Pruski, V. K. Pecharsky, *J. Alloy. Compd.* **2001**, *329*, 108.

[302] L. Zaluski, A. Zaluska, J. O. Ström-Olsen, *J. Alloys Compd.* **1999**, *290*, 71.

[303] A. Züttel, C. Nützenadel, P. Sudan, P. Mauron, C. Emmenegger, S. Rentsch, L. Schlapbach, A. Weidenkaff, T. Kiyobayashi, *J. Alloys Compd.* **2002**, *330-332*, 676.

[304] H. W. Brinks, C. M. Jensen, S. S. Srinivasan, B. C. Hauback, D. Blanchard, K. Murphy, *J. Alloys Compd.* **2004**, *376*, 215.

[305] C. P. Baldé, B. P. C. Hereijgers, J. H. Bitter, K. P. de Jong, *J. Am. Chem. Soc.* **2008**, *130*, 6761.

[306] T. Kiyobayashi, S. S. Srinivasan, D. Sun, C. M. Jensen, *J. Phys. Chem. A* **2003**, *107*, 7671.

[307] E. H. Majzoub, K. J. Gross, *J. Alloys Compd.* **2003**, *356-357*, 363.

[308] Z. Fang, Z. Jing, J. Zhu, G. Chen, D. Sun, Dalin, B. He, Z. Wei, W. Zheng and S. Wei, *J. Phys. Chem. C* **2007**, *111*, 3476.

[309] X. Xiao, L. Chen, X. Wang, Q. Wang and C. Chen, *Int. J. Hydrog. Energy* **2007**, *32*, 2475.

[310] R. A. Zidan, S. Takara, A. G. Hee, C. M. Jensen, *J. Alloys Compd.* **1999**, *285*, 119.

[311] G. Sandrock, K. Gross, G. Thomas, C. Jensen, D. Meeker, S. Takara, *J. Alloys Compd.* **2002**, *330-332*, 696.

[312] J. Wang, A. D. Ebner, R. Zidan, J. A. Ritter, *J. Alloys Compd.* **2005**, *391*, 245.

[313] X. Xiao, L. Chen, X. Wang, S. Li, C. Chen, Q. Wang, *Int. J. Hydrog. Energy* **2008**, *33*, 64.

[314] B. Bogdanović, M. Felderhoff, A. Pommerin, F. Schüth and N. Spielkamp, *Adv. Mater.* **2006**, *18*, 1198.

[315] D. Pukazhselvan, M. SterlinLeo Hudson, O. N. Srivastava, *Int. J. Hydrog. Energy* **2012**, *37*, 3697.

[316] X. Fan, X. Xiao, L. Chen, S. Li, H. Ge, Q. Wang, *J. Phys. Chem. C* **2011**, *115*, 2537.

[317] A. Zaluska, L. Zaluski, J. O. Ström-Olsen, *J. Alloys Compd.* **2000**, *298*, 125.

[318] H. Raghubanshi, M. S. L. Hudson, O. N. Srivastava, *Int. J. Hydrog. Energy* **2011**, *36*, 4482.

[319] Y. Liu, Z. Ren, X. Zhang, N. Jian, Y. Yang, M. Gao, H. Pan, *Energy Technol.* **2018**, *6*, 487.

[320] Q. J. Fu, A. J. Ramirez-Cuesta, S. C. Tsang, *J. Phys. Chem. B* **2006**, *110*, 711.

[321] A. Borgschulte, A. Züttel, P. Hug, G. Barkhordarian, N. Eigen, M. Dornheim, R. Bormann and A. J. Ramirez-Cuesta, *Phys. Chem. Chem. Phys.* **2008**, *10*, 4045.

[322] G. K. P. Dathar, D. S. Mainardi, *J. Phys. Chem. C* **2010**, *114*, 8026.

[323] C. M. Araújo, R. Ahuja, J. M. Osorio Guillén, P. Jena, *Appl. Phys. Lett.* **2005**, *86*, 251913.

[324] O. Palumbo, R. Cantelli, A. Paolone, C. M. Jensen, S. S. Srinivasan, *J. Phys. Chem. B* **2005**, *109*, 1168.

[325] A. Peles, Van de Walle, Chris G., *Phys. Rev. B* **2007**, *76*, 1.

[326] A. Marashdeh, J.-W. I. Versluis, Á. Valdés, R. A. Olsen, O. M. Løvvik, G.-J. Kroes, *J. Phys. Chem. C* **2013**, *117*, 3.

[327] S. Chaudhuri, J. Graetz, A. Ignatov, J. J. Reilly, J. T. Muckerman, *J. Am. Chem. Soc.* **2006**, *128*, 11404.

[328] S. Singh, S. W. H. Eijt, J. Huot, W. A. Kockelmann, M. Wagemaker, F. M. Mulder, *Acta Mater.* **2007**, *55*, 5549.

[329] B. Bogdanović, U. Eberle, M. Felderhoff, F. Schüth, *Scr. Mater.* **2007**, *56*, 813.

[330] A. Léon, O. Kircher, H. Rösner, B. Décamps, E. Leroy, M. Fichtner, A. Percheron-Guégan, *J. Alloys Compd.* **2006**, *414*, 190.

[331] O. M. Løvvik, S. M. Opalka, *Phys. Rev. B* **2005**, *71*, 1.

[332] D. Sun, T. Kiyobayashi, H. T. Takeshita, N Kuriyama, C. M. Jensen, *J. Alloys Compd.* **2002**, *337*, L8-L11.

[333] J. Graetz, A. Y. Ignatov, T. A. Tyson, J. J. Reilly, J. Johnson, *Appl. Phys. Lett.* **2004**, *85*, 500.

[334] G. Sandrock, K. Gross, G. Thomas, *J. Alloys Compd.* **2002**, *339*, 299.

[335] P. Wang, X.-D. Kang, H.-M. Cheng, *J. Phys. Chem. B* **2005**, *109*, 20131.

[336] S. Chaudhuri, J. T. Muckerman, *J. Phys. Chem. B* **2005**, *109*, 6952.

[337] K. Bai, P. Wu, *Appl. Phys. Lett.* **2006**, *89*, 201904.

[338] P. E. Vullum, M. P. Pitt, J. C. Walmsley, B. C. Hauback, R. Holmestad, *J. Alloys Compd.* **2011**, *509*, 281.

[339] M. Oehring, T. Klassen, R. Bormann, *J. Mater. Res.* **1993**, *8*, 2819.

[340] F. Zhang, L. Lu, M.O. Lai, *J. Alloys Compd.* **2000**, *297*, 211.

[341] M. Schoenitz, X. Zhu, E. L. Dreizin, *JMNM* **2004**, *20-21*, 455.

[342] M. E. J. Braun, *Metall. Mater. Trans. A* **2001**, *32*, 1037.

[343] J. C. Schuster, M. Palm, *JPED* **2006**, *27*, 255.

[344] H. W. Brinks, B. C. Hauback, S. S. Srinivasan, C. M. Jensen, *J. Phys. Chem. B* **2005**, *109*, 15780.

[345] M. P. Pitt, P. E. Vullum, M. H. Sørby, M. P. Sulic, C. M. Jensen, J. C. Walmsley, R. Holmestad, B. C. Hauback, *Acta Mater.* **2008**, *56*, 4691.

[346] A. G. Haiduc, H. A. Stil, M. A. Schwarz, P. Paulus, J.J.C. Geerlings, *Journal of Alloys and Compounds* **2005**, *393*, 252.

[347] X. D. Kang, P. Wang, X. P. Song, X. D. Yao, G. Q. Lu, H. M. Cheng, *Journal of Alloys and Compounds* **2006**, *424*, 365.

[348] M. P. Pitt, P. E. Vullum, M. H. Sørby, H. Emerich, M. Paskevicius, C. E. Buckley, E.M. Gray, J. C. Walmsley, R. Holmestad, B. C. Hauback, *Philosophical Magazine* **2013**, *93*, 1080.

[349] M. P. Pitt, P. E. Vullum, M. H. Sørby, H. Emerich, M. Paskevicius, C. E. Buckley, E. M. Gray, J. C. Walmsley, R. Holmestad, B. C. Hauback, *J. Alloys Compd.* **2012**, *521*, 112.

[350] M. P. Pitt, M. Paskevicius, C. J. Webb, M. H. Sorby, S. Delleda, T. R. Jensen, B. C. Hauback, C. E. Buckley, E. MacA. Gray, *Int. J. Hydrog. Energy* **2011**, *36*, 8403.

[351] X. Fan, X. Xiao, L. Chen, K. Yu, Z. Wu, S. Li, Q. Wang, *Chem. Commun.* **2009**.

[352] M. P. Pitt, P. E. Vullum, M. H. Sørby, H. Emerich, M. Paskevicius, C. E. Buckley, E. M. Gray, J. C. Walmsley, R. Holmestad, B. C. Hauback, *J. Alloys Compd.* **2012**, *527*, 16.

[353] G. Streukens, *Doctoral dissertation, Ruhr Universität Bochum* **2007**.

[354] E. W. Lemmon, M. L. Huber, J. W. Leachman, *J. Res. Natl. Inst. Stan* **2008**, *113*, 341.

[355] P. S. Rudman, J. J. Reilly, R. H. Wiswall, *Ber. Bunsenges. Phys. Chem.* **1977**, *81*, 76.

[356] K. J. Gross, G. J. Thomas, E. Majzoub, G. Sandrock, *Proceedings U.S. DOE Hydrogen Program Review,* **2001**.

[357] K. Hashi, K. Ishikawa, K. Suzuki, K. Aoki, *Journal of Alloys and Compounds* **2002**, *330-332*, 547.

[358] C. Weidenthaler, A. Pommerin, M. Felderhoff, B. Bogdanović, F. Schüth, *Phys. Chem. Chem. Phys.* **2003**, *5*, 5149.

[359] H. W. Brinks, M. Sulic, C. M. Jensen, B. C. Hauback, *J. Phys. Chem. B* **2006**, *110*, 2740.

[360] P. S. Rudman, J. J. Reilly, R. H. Wiswall, *J. Less. Common Met.* **1978**, *58*, 231.

[361] C. Rongeat, I. Llamas-Jansa, S. Doppiu, S. Deledda, A. Borgschulte, L. Schultz, O. Gutfleisch, *J. Phys. Chem. B* **2007**, *111*, 13301.

[362] L. Li, F. Qiu, Y. Wang, G. Liu, Y. Xu, C. An, Y. Wang, L. Jiao, H. Yuan, *J. Mater. Chem.* **2012**, *22*, 13782.

[363] K. Burkmann, *Studienarbeit, TU Freiberg* **2018,** *64*.

[364] P. Adelhelm, J. Gao, M. H. W. Verkuijlen, C. Rongeat, M. Herrich, P. J. M. van Bentum, O. Gutfleisch, A. P. M. Kentgens, K. P. de Jong, P. E. de Jongh, *Chem. Mater.* **2010**, *22*, 2233.

[365] J. Šubrt, K. Tobola, *Journal of Thermal Analysis* **1976**, *10*, 5.

[366] S. Aronson, F. J. Salzano, *Inorg. Chem.* **1969**, *8*, 1541.

[367] J. L. Murray, *J. Phase Equilib.* **1983**, *4*, 407.

[368] J. P. Campbell, W. L. Gladfelter, *Inorg. Chem.* **1997**, *36*, 4094.

Appendix A

Preparation of aminoalanes

Synthesis routes for aminoalanes preparation:

1. *Direct reaction between aluminum hydride and amine:*

- *AlH_3 and amine in THF solution*

In this synthesis approach, first, γ-AlH_3 was prepared by the reaction of lithium alanate and aluminum chloride according to the reaction described by Brower et al.[43] In the second step, the solid alane was dissolved in THF and this solution was added to the reaction flask that contained THF suspension of amine. The reaction mixture was usually cooled to -78 ºC (isopropanol/dry ice) and then slowly warmed up until room temperature and stirred until hydrogen evolution has stopped. The solid product was collected from the resulting suspension by filtration, washed with THF, and dried for several hours in vacuum.

- *AlH_3 ethereal solution and amine*

In this synthesis route, two steps were involved: in the first stage, the solution of AlH_3 was generated by the reaction of $LiAlH_4$ and $AlCl_3$ in Et_2O; in the second step, the formed solution was directly treated with the amine solution in Et_2O at -78 ºC. This reaction mixture was allowed to heat up slowly to room temperature. The reaction was finished when the hydrogen evolution has stopped. The solid product was collected from the resulting mixture by solvent extraction under vacuum.

2. *Direct reaction between alkyl aluminum and amine:*

The solution of diisobuthylaluminum hydride (DIBAL) or trimethylaluminum (TMAL) in hexane (or toluene) was added to the amine solution at 0 ºC. The reaction mixture was allowed to reach room temperature.

3. *Synthesis via chloramine (trichlormelamine):*

The formation of aminoalane succeeded by the simple addition of the $LiAlH_4$ solution in Et_2O (or hexane, toluene) to chloramine solution at -78 ºC. The precipitated LiCl was filtered off after the reaction mixture reached room temperature.

4. *Cascade reaction with aluminum chloride, lithium alanate and amine:*

This approach was developed for the amines, which were insoluble in common organic solvents. In order to obtain the soluble intermediate, the amine was reacting with an ethereal solution of $AlCl_3$, the further reaction with $LiAlH_4$ finally give aminoalane.

5. *Salt reaction between lithium alanate and amine hydrochloride:*

In the common procedure, $LiAlH_4$ was dissolved in Et_2O, and then was mixed with a precooled (to -78 ºC) solution of amine hydrochloride in Et_2O. After reaching room temperature, the reaction mixture was filtrated in order to remove LiCl.

6. Transamination reaction:

In this synthesis approach, first, trimethylamine alane was prepared as described in method (5). The obtained powder was dissolved in diethyl ether and was added to diethyl ether suspension of amine.

7. Direct hydrogenation of activated aluminum and amine:

This reaction path requires prior preparation of the activated aluminum powder developed by Graetz et al.[51] The hydrogenation of amine with activated aluminum in the presence of solvent (THF or Et$_2$O) took place in the autoclave reactor under hydrogen pressure up to 100 bar.

Caution: Aluminum hydride and its derivatives are air- and moisture-sensitive and are pyrophoric. Some aminoalanes can lead to spontaneous, violent reactions upon contact with the air (e.g. 2-Picolylamine alane) or upon mechanical impact (e.g. Triazine alane).

Table A.1 Starting conditions for aminoalanes preparation and the yield of the formed product (in grey - the product cannot be purified from LiCl).

N	Amine			Solvent		Aluminum source			T, ºC	Yield	
		m, g	n, mmol		mL		m, g	n, mmol		m, g	%
1. Direct reaction between aluminum hydride and amine											
1	Melamine	0.77	6.1	THF	50	AlH$_3$	1.1	36.7	-78/RT	1.3	78
2	Melamine	0.5	4.0	Et$_2$O	50	AlH$_3$	0.71	23.7	-78/RT	0.84	77
3	Melamine	0.5	4.0	THF	50	AlH$_3$	0.36	12.0	0/RT	0.67	91
4	Melamine	0.5	4.0	THF	50	AlH$_3$	0.12	4.0	0/RT	0.5	102
5	Melamine	1.0	7.9	Et$_2$O	50	AlH$_3$	0.71	23.7	RT	1.74	120
6	Triaminopyrimidine	1.0	8.0	THF	90	AlH$_3$	0.72	24.0	-78/RT	2.23	130
7	Triaminopyrimidine	1.0	8.0	Hexane	90	AlH$_3$	0.72	24.0	0/RT	1.34	78
8	Triazine	0.5	6.2	THF	50	AlH$_3$	0.8	26.7	0/RT	0.36	34
9	Triazine	0.5	6.2	THF	50	AlH$_3$	0.555	18.5	-78/RT	1.08	102
10	Diaminotriazole	0.5	5.0	THF	50	AlH$_3$	0.15	5.0	RT	0.58	-
11	Diaminotriazole	0.5	5.0	THF	50	AlH$_3$	0.3	10.0	RT	0.41	-
12	Diaminotriazole	0.5	5.0	Et$_2$O	50	AlH$_3$	0.3	10.0	RT	0.53	-
13	Diaminotriazole	0.5	5.0	THF	50	AlH$_3$	0.454	15.1	RT	0.85	90
14	Triazole	0.5	7.2	Et$_2$O	50	AlH$_3$	0.217	7.2	-78/RT	0.51	-
15	2-Picolylamine	2.57ml	25.0	Hexane	20	AlH$_3$	0.75	25.0	-78/RT	2.2	64
16	2-Picolylamine	1.3ml	12.6	THF	20	AlH$_3$	0.375	12.5	-78/RT	1.65	95
17	2-Picolylamine	2 ml	19.4	Et$_2$O	40	AlH$_3$	0.58	19.4	-78/RT	2.8	104
18	Pyrrole	1.67	25	THF	20	AlH$_3$	0.75	25.0	-78/RT	1.41	58
19	Triethylendiamine	1	8.9	THF	40	AlH$_3$	0.3	10.0	-78/RT	1.08	85
20	Triethylendiamine	1	8.9	Et$_2$O	50	AlH$_3$	0.27	9.0	-78/RT	1.0	79
21	Pyridine	1 ml	12.4	THF	25	AlH$_3$	0.372	12.4	-40/RT	0.8	60
22	Pyridine	1 ml	12.4	THF	25	AlH$_3$	0.372	12.4	-40/RT	1.1	81
23	Pyridine	1 ml	12.4	Et$_2$O	25	AlH$_3$	0.372	12.4	-78/RT	1.27	94
24	Pyridine	20ml	248	-	-	LiAlH$_4$	0.38	12.7	RT	1.45	105
25	Pyrazine	0.5	6.2	Hexane	50	AlH$_3$	0.187	6.2	-78/RT	0.18	-
26	Pyrazine	0.5	6.2	THF	50	AlH$_3$	0.187	6.2	-78/RT	0.79	115
27	Pyrazine	0.5	6.2	THF	50	AlH$_3$	0.374	12.5	-78/RT	1.1	126
28	Pyrazine	0.5	6.2	Et$_2$O	30	AlH$_3$	0.187	6.2	-78/RT	0.55	80
29	Pyrazine	0.5	6.2	Et$_2$O	30	AlH$_3$	0.374	12.5	-78/RT	0.6	67
30	Aniline	0.83ml	9.0	C$_6$H$_6$	40	AlH$_3$	0.27	9.0	RT	0.27	24
31	Aniline	1 ml	10.9	THF	40	AlH$_3$	0.315	10.5	-78/RT	1.87	140
32	Aniline	1.5ml	16.4	Et$_2$O	40	AlH$_3$	0.5	16.7	-78/RT	2.3	114

33	Tetramethyl-piperidine	1 ml	5.9	Et$_2$O	40	AlH$_3$	0.178	6.0	-78/RT	0.91	90
34	Tetramethyl-piperidine	2 ml	11.9	Et$_2$O	40	AlH$_3$	0.178	6.0	-78/RT	0.95	47
35	Piperidine	1 ml	10.1	Et$_2$O	40	AlH$_3$	0.303	10.1	-78/RT	1.0	87
36	Piperidine	2 ml	20.2	Et$_2$O	40	AlH$_3$	0.303	10.1	-78/RT	1.65	72
37	Piperidine	3.5ml	35.4	Et$_2$O	40	AlH$_3$	0.303	10.1	-78/RT	2.32	68
38	Piperidine	1ml	10.1	Et$_2$O	40	AlH$_3$	0.607	20.2	-78/RT	0.87	75
39	Piperazine	1	11.6	Et$_2$O	50	AlH$_3$	0.348	11.6	-78/RT	1.14	85
40	Piperazine	1	11.6	Et$_2$O	50	AlH$_3$	0.696	23.3	-78/RT	1.24	73
41	Pyrrole	1 ml	14.4	Et$_2$O	45	AlH$_3$	0.43	14.3	-78/RT	0.84	60
42	Pyrrole	2 ml	28.8	Et$_2$O	45	AlH$_3$	0.43	14.3	-78/RT	oil	-
43	Pyrrole	3 ml	43.2	Et$_2$O	45	AlH$_3$	0.43	14.3	-78/RT	3.46	83
44	Pyrrolidine	1 ml	12.2	Et$_2$O	45	AlH$_3$	0.365	12.2	-78/RT	0.88	71
45	Pyrrolidine	2 ml	24.4	Et$_2$O	45	AlH$_3$	0.365	12.2	-78/RT	oil	-
46	Pyrrolidine	3 ml	36.6	Et$_2$O	45	AlH$_3$	0.365	12.2	-78/RT	2.25	61
47	Pyrrolidine	1 ml	12.2	Et$_2$O	45	AlH$_3$	0.73	24.3	-78/RT	0.84	68

2. Direct reaction between alkyl aluminum and amine (DIBAH - AlHBu$_2$ (1M in hexane), TMA - AlMe$_3$ (2M in hexane/toluene)

48	Melamine	1	7.9	Hexane	20	TMA	12 ml	24	0/RT	1.99	-
49	Triaminopyrimidine	1	8.0	Hexane	20	TMA	12 ml	24	0/RT	1.05	-
50	2-Picolylamine	2.57 ml	25	Hexane	5	TMA	12.5 ml	25	0/RT	4.2	102
51	3-Picolylamine	0.815 ml	8.0	Hexane	5	TMA	4 ml	8.0	0/RT	1.3	98
52	Pyrrole	1.73ml	25	Hexane	20	TMA	12.89 ml	25	0/RT	2.91	84
53	Pyrazine	0.5	6.2	Hexane	45	TMA	6.24 ml	12.5	-78/RT	1.31	94
54	Aniline	0.98ml	10.7	Hexane	15	TMA	5.37 ml	10.5	0/RT	1.6	90
55	Aniline	0.98ml	10.7	Hexane	10	DIBAH	10.74 ml	10.7	0/RT	2.07	82
56	Acetonitrile	0.64 ml	12.2	Toluene	20	DIBAH	12.2 ml	12.2	0/RT	oil	-
57	Acetonitrile	1 ml	19.1	Toluene	10	TMA	9.57 ml	19.1	0/RT	2.11	97

3. Synthesis via chloramine (trichlormelamine)

58	Trichloromelamine	1.0	4.4	THF	60	LiAlH$_4$	0.496	13.1	-78/RT	2.66	280
59	Trichloromelamine	1.0	4.4	Et$_2$O	60	LiAlH$_4$	0.496	13.1	-78/RT	1.92	202

4. Cascade reaction with aluminum chloride, lithium alanate and amine

60	Melamine	0.5	4.0	Et$_2$O	60	LiAlH$_4$/ AlCl$_3$	0.91/ 0.79	24.0/ 6.0	0/RT	1.6	131
61	Melamine	0.5	4.0	Et$_2$O	60	AlCl$_3$/ LiAlH$_4$	0.79/ 0.91	6.0/ 24.0	0/RT	1.1	90
62	Melamine	0.5	4.0	Et$_2$O	40	AlCl$_3$/ LiAlH$_4$	0.529/ 0.45	4.0/ 11.9	0/RT	1.43	117
63	Melamine	0.5	4.0	Et$_2$O	60	AlCl$_3$/ LiAlH$_4$	1.057/ 0.91	8.0/ 24.0	0/RT	1.54	126
64	Melamine	0.5	4.0	Et$_2$O	90	AlCl$_3$/ LiAlH$_4$	1.586/ 1.354	12.0/ 35.7	0/RT	1.8	147
65	Melamine	0.5	4.0	THF	60	AlCl$_3$/ LiAlH$_4$	3.17/ 0.91	23.8/ 24.0	0/RT	2.7	221
66	Melamine	0.5	4.0	Et$_2$O	60	AlCl$_3$/ LiAlH$_4$	3.17/ 0.91	23.8/ 24.0	0/RT	1.25	102
67	Melamine	0.5	4.0	Et$_2$O	60	AlCl$_3$/ LiAlH$_4$	3.17/ 0.9	23.8/2 4.0	RT/RT	1.96	131
68	Melamine	0.5	4.0	Et$_2$O	60	LiAlH$_4$/ AlCl$_3$	0.91/ 3.17	24.0/ 23.8	RT/RT	1.31	107
69	Melamine	0.5	4.0	Et$_2$O	130	AlCl$_3$/ LiAlH$_4$	3.17/ 2.7	23.8/ 71.1	0/RT	1.8	147
70	Triaminopyrimidine	1.0	8.0	THF	90	LiAlH$_4$/ AlCl$_3$	0.91/ 1.07	24.0/ 8.0	0/RT	3.5	203

| 71 | Triaminopyrimidine | 1.0 | 8.0 | THF | 90 | AlCl$_3$/ LiAlH$_4$ | 1.07/ 0.91 | 8.0/ 24.0 | 0/RT | 3.79 | 220 |
| 72 | Triazine | 0.5 | 6.2 | Et$_2$O | 60 | AlCl$_3$/ LiAlH$_4$ | 2.47/ 0.7 | 18.5/ 18.5 | -78/RT | 2.05 | 193 |

5. Salt reaction between lithium alanate and amine hydrochloride

73	Dimethylamine hydrochloride	1.0	9.1	Et$_2$O	70	LiAlH$_4$	0.7	18.4	-78/RT	0.5	74
74	Dimethylamine hydrochloride	1.72	15.7	Et$_2$O	50	LiAlH$_4$	1.0	26.4	-78/RT	0.72	62
75	Trimethylamine hydrochloride	1.0	7.3	Et$_2$O	60	LiAlH$_4$	0.28	7.3	-78/RT	0.71	74
76	Piperidine hydrochloride	1.0	8.2	Et$_2$O	40	LiAlH$_4$	0.312	8.2	-78/RT	0.78	83
77	Piperidine hydrochloride	1.5	12.3	Et$_2$O	40	LiAlH$_4$	0.234	6.2	-78/RT	0.81	87

6. Transamination reaction (with (CH$_3$)$_3$NAlH$_3$ = TMAA)

| 78 | Melamine | 0.471 | 3.7 | Toluene | 50 | TMAA | 1.0 | 11.2 | -40/RT | 0.6 | 76 |
79	Tetramethyl-piperidine	2.5ml	14.8	Toluene	20	TMAA	0.6	6.7	-40/RT	0.78	31
80	Tert-butylamine	0.59ml	5.6	Toluene	50	TMAA	0.5	5.6	-40/RT	oil	-
81	3,5-Dimethylaniline	0.7ml	5.6	Toluene	50	TMAA	0.5	5.6	-40/RT	oil	-
82	Aniline	0.49ml	5.6	Toluene	50	TMAA	0.5	5.6	-40/RT	oil	-
83	3-Picolylamine	0.57ml	5.6	Toluene	50	TMAA	0.5	5.6	-40/RT	0.91	120

Pyridine alane complex

The reaction of pyridine with aluminum hydride was tested with different ratios of pyridine to alane. In the case of the molar ratio (1:1) between pyridine and alane, the amorphous product was detected (Figure A.1). In case of molar ratio (2:1) between pyridine and alane, crystalline and partly amorphous solid was obtained.
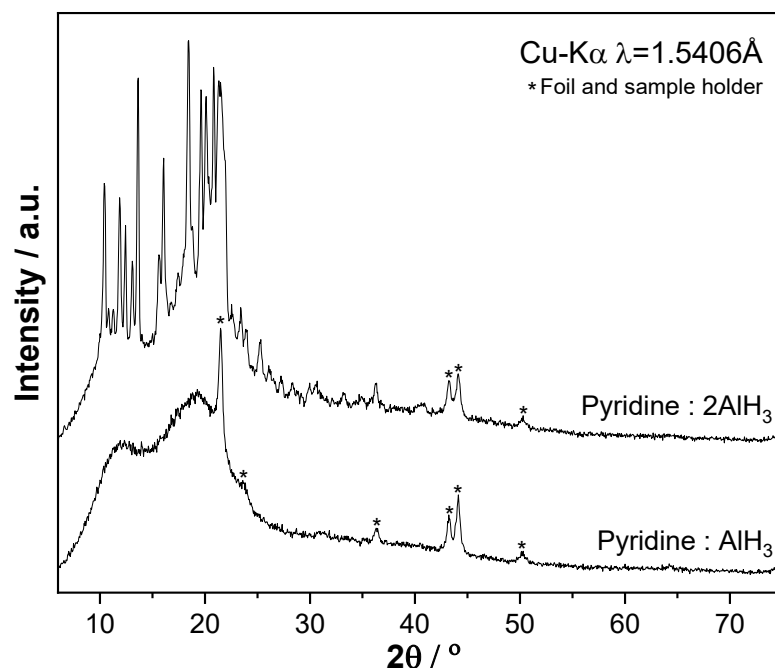
Figure A.1 *XRPD patterns of the product obtained after the reaction between pyridine and alane in different ratios.*

The formation of the amorphous solid can be attributed to the transfer of the hydrogen from AlH$_3$ to the pyridine ring by forming dihydropyridine structure, where

hydrogen can be attached to the different carbon atoms in the ring forming the mixture of the different isomers (Scheme A.1). Similar behavior was observed when pyridine was reacting with lithium alanate and resulted in five isomers[217].
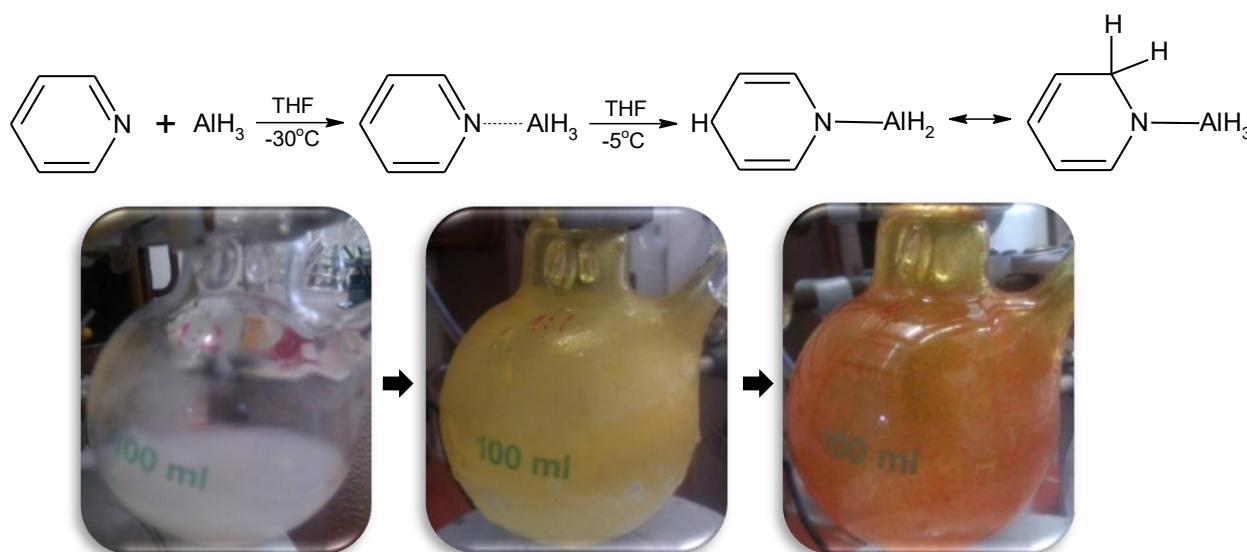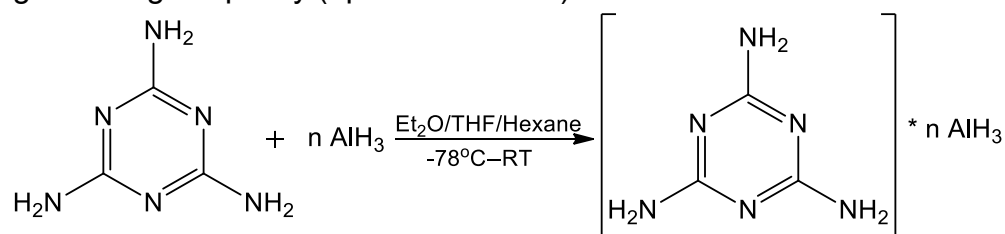

Scheme A.1 *Proposed reaction scheme of the pyridine alane formation with the depiction of the color change of the reaction mixture.*

Table A.2 *Practical and theoretical elemental composition of the formed pyridine alanes.*

	Ratio	Elemental analysis			ICP-OES
	Pyridine:AlH$_3$	N	C	H	Al
Calculated	1:1	12.72	54.54	8.24	24.50
	2:1	14.73	63.14	7.95	14.18
Found	1:1	8.99	40.14	7.25	19.74
	2:1	7.11	41.40	6.68	12.86

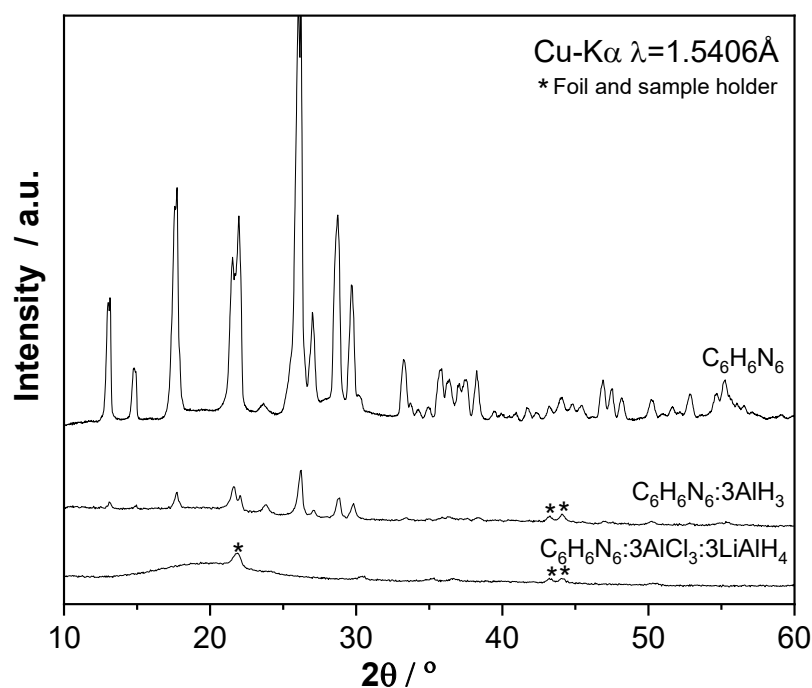## *Melamine alane complex*

The melamine alane is one of the investigated amines with a high potential hydrogen storage capacity (up to 7.44 wt.-%).

Scheme A.2 *Proposed reaction between melamine and alane.*

The obtained insoluble solid product was amorphous (Fig. A.2) independent of the preparation method.

***Figure A.2*** *XRPD patterns of the product obtained after the reaction between melamine and alane.*

As shown in Table A.3 the theoretical calculation of the elemental composition of the formed product was not in agreement with the found values. The found C content was higher than expected. The possible explanation is the presence of the solvent fragments incorporated in the structure, which can also lead to the low N content in the final material.

Table A.3 *Calculated and found elemental composition of melaminealane.*

|	Ratio	Elemental analysis			ICP-OES
		N	C	H	Al
Calculated	$C_3H_6N_6$:AlH$_3$=(1:1)	54.53	23.38	4.58	17.51
	$C_3H_6N_6$:AlH$_3$=(1:2)	46.15	19.79	4.43	29.63
	$C_3H_6N_6$:AlH$_3$=(1:3)	40.00	17.15	4.32	38.53
Found	$C_3H_6N_6$:AlH$_3$=(1:3)	16.57	36.6	6.31	31.49

Pyrazine alane complex

Solid-state NMR analysis of pyrazine alane complex showed high content of CH_2 groups in the range of 10-50 ppm (Fig. A.3). The presence of different signals in the CH_2 range could indicate the hydrogenation of pyrazine ring, cleavage of the solvent and its incorporation to the structure (but not free solvent). The solvent cleavage and its further complexation with Lewis base pair were already mentioned in the literature[219,368]. Such a tendency was observed for most investigated aromatic heterocycle amines.
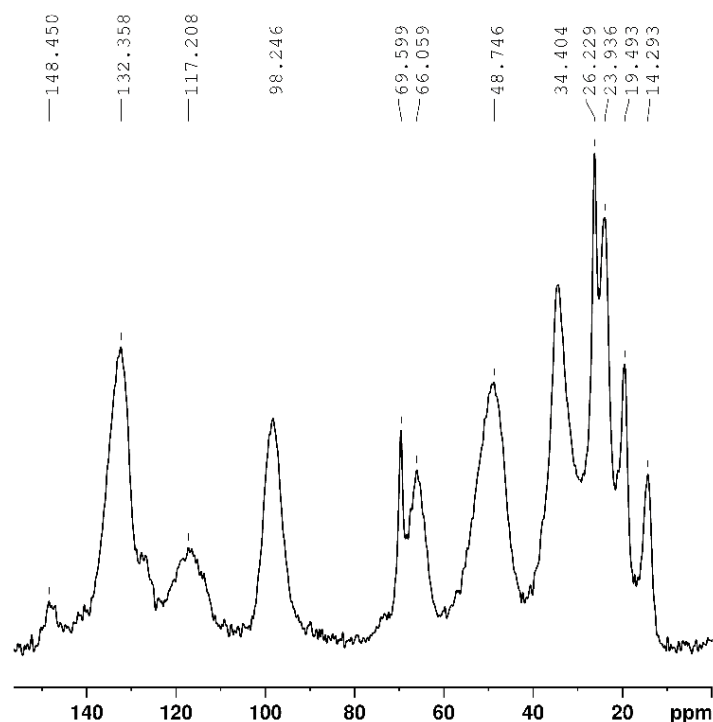
Figure A.3 *Solid-state ^{13}C NMR spectra of pyrazine alane complex synthesized by the wet chemical synthesis with AlH₃-ethereal solution.*

Imine hydrogenation with alkyl aluminum hydride

Crystalline compound (4-bromobenzyl(phenyl)amino di-isobutyl aluminum) was synthesized as described by Hatnean at el.[213] The subsequent reaction of the Al-amide with H_2 proceeds to regenerate the Al–H bond, liberating amine (Scheme A.3). This hydrogenolysis of the Al–N bond is thought to be facilitated by elevated temperatures by effecting dissociation of the Al-amide dimer. The monomeric form can then interact with H_2 affording the transient formation of the amine-alane adduct. Thermal dissociation liberates DIBAH and frees the product amine.
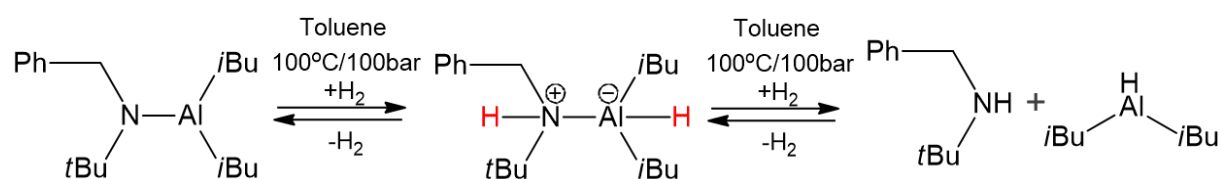
Scheme A.3 *Proposed hydrogenation pathway in imines-alkyl aluminum system.*

In Figure A.4 hydrogen uptake by the reaction mixture compared to the blank measurement is shown. After subtracting the pressure drop due to dissolution of H_2 (2.3 bar), the obtained pressure uptake in both cases was close to the theoretically calculated.
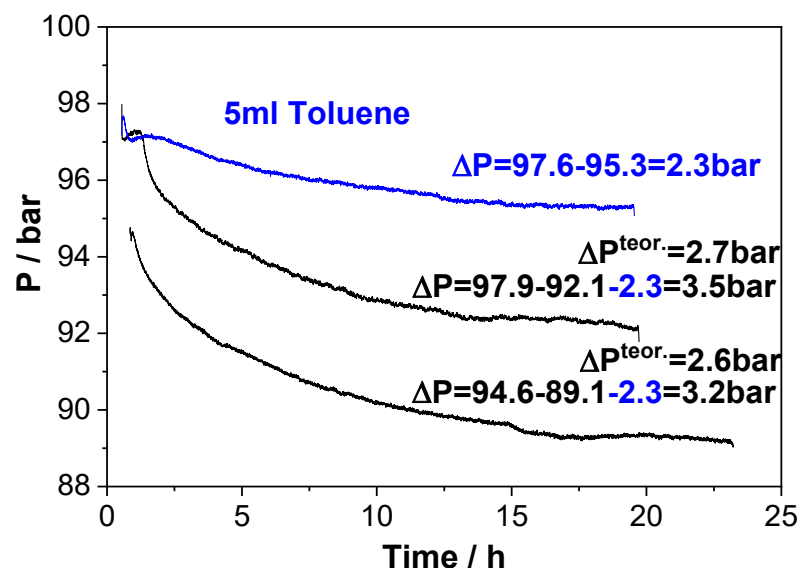
Figure A.4. *Reactor pressure during the initial hydrogenation of 5 ml of solvent (top) and 4-bromobenzyl(phenyl)amino di-isobutyl aluminum in toluene (middle and bottom).*

Liquid proton NMR showed duplet at 3.7 ppm (CH_2 group) and singlet at 3.25 ppm (NH group), thus proved that synthesis was made successful.

The synthesized alkylaminoalanenes were also tested for hydrogen uptake in the Sieverts apparatus in the solid-state (Table A.4), no hydrogen uptake was detected.

Sieverts apparatus

The main equipment for testing of hydrogen sorption properties of synthesized materials in the pressure range up to 1000 bar was constructed by Dr. Seidel and M. Piller (Fig. A.5). For the investigation of the hydrogen uptake, the high-pressure apparatus (compressor PMHP 50-1000-V2) was built. A thermocouple was used to monitor the external temperature, and the gas pressure in the reactor was measured using a pressure sensor (±0.05 bar). The sample holder was loaded with synthesized material in the glove box and then attached to the apparatus. After evacuation, the volumetric measurement with helium, to evaluate the effective volume was performed. The hydrogenation experiment was started from 50 bar with the 50 bar step at 0 ºC, RT, 50 ºC, and 100 ºC.

After completing this equipment few unexpected problems appeared:

- ball valves are not in agreement with technical properties (not tight up to 1000 bar) → they were changed to needle valves;

- the absorbed amount of hydrogen was in the range of measuring error → the filter volume was reduced;

- high-pressure measurements are highly sensitive to changes of the surrounding temperature → the special climate control is needed;

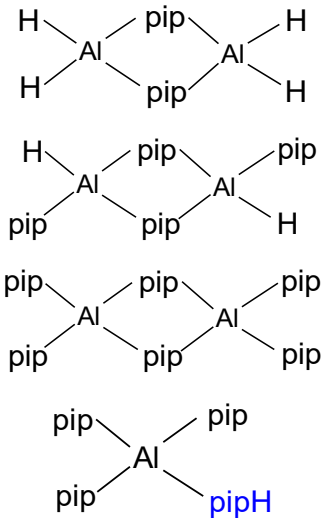- the manual control of each hydrogenation step → automatization is needed.
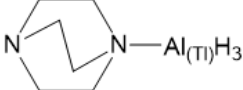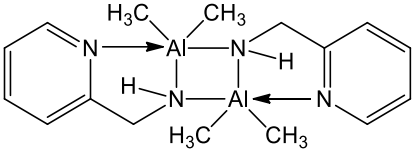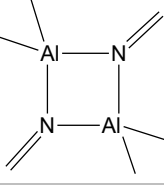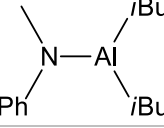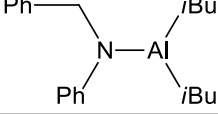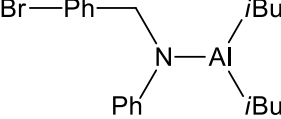
Figure A.5 *Homemade Sievert's apparatus and the high-pressure compressor up to 1000 bar.*

The aminoalanes, which were obtained in a pure form, were systematically investigated under hydrogen pressure (Table A.4). No hydrogen uptake was observed.

Table A.4. *Hydrogenation experiments carried out with solid aminoalanes at 50-1000 bar at different temperatures (0, RT, 50, 100 ᵒC).*

	Aminoalanes	Formula
1.	**Tert-Butylaminoalane (Mülheim group**): - Dimeric form - Tetrameric forms	$R_1 = CH_3, R_2 = CH_2CH_3$ $R_1 = CH_2CH_3, R_2 = CH_2CH_3$ $R_1 = H, R_2 = C(CH_3)_3$ $\quad R_1 = C(CH_3)_3$
2.	**Pyridine alane:** - Pyridine·AlH_3 - Pyridine·$2AlH_3$ - Pyridine·$AlCl_3$ - Pyridine·$LiAlH_4$	

3.	**Piperidinoalanes:** - Piperidine·AlH$_3$ - Piperidine·2AlH$_3$ - Piperidine·3AlH$_3$ - Ti-doped - Zr-doped	
4.	**Triethylanediamine:** - TEDA with Ti-activated aluminum	
5.	**2-Picolylamine dimethylaluminum**	
6.	**Acetonitril·Al(CH$_3$)$_3$**	
7.	**Benzyl(methyl)amino di-isobutyl aluminum** (RT and 100 ºC)	
8.	**Benzyl(phenyl)amino di-isobutyl aluminum** (RT and 100 ºC)	
9.	**4-bromobenzyl(phenyl)amino di-isobutyl aluminum** (RT and 100 ºC)	

The performed hydrogenation experiments showed that none of the investigated aminoalanes can uptake hydrogen in a solid-state under the used conditions. It was concluded, that the formed strong dimers or trimers are thermodynamically stable to allow rehydrogenation. Only in one case the hydrogenation was achieved, however, the reproducibility of the experiment was not showed, therefore it would require further investigation. Complex synthesized via direct reaction of piperidine with Al*(Zr) was hydrogenated in the solid-state with the addition of Zr-doped Al. The final product was confirmed to be the composition of compounds (**1**) and (**2**) as shown in Fig. A.6, suggesting the next hydrogenation pathway:
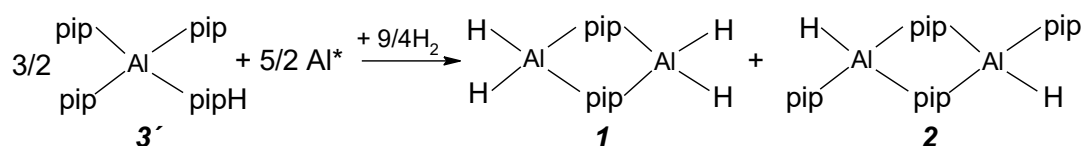
Scheme A.4 *Proposed hydrogenation pathway in piperidinoalane system.*
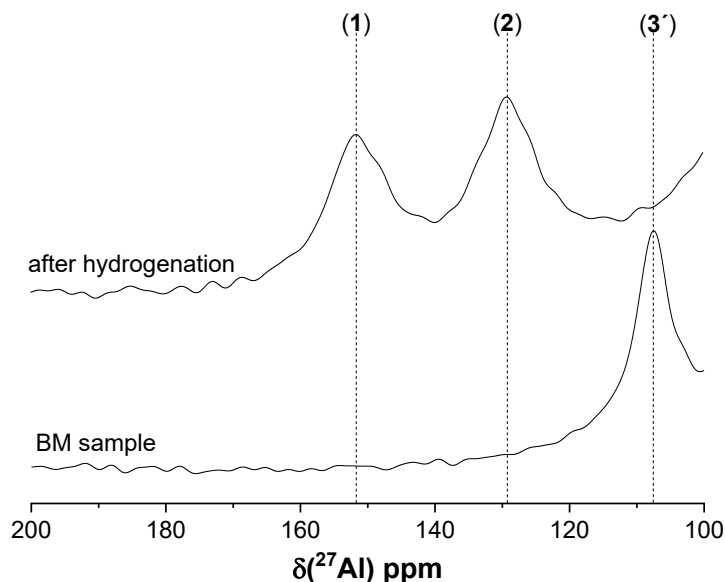
Figure A.6 *^{27}Al NMR spectra of piperidinoalane (formed from direct hydrogenation of Al*(Zr) with piperidine within 6 h) before and after hydrogenation in the solid-state.*

Therefore, it was suggested that the aminoalane that can exist in a monomeric form could be hydrogenated in the solid-state.

Autoclave reaction with activated aluminum and amine

Table A.5 *Starting conditions for hydrogenation reaction of activated aluminum and amine.*

N	Amine	Al*(TM)	Solvent	P, bar	T, ºC	Time, h
1.	TEDA	Al*(Ti)	THF	34.7	27	70
2.	TEDA	Al*(Ti)	THF	36.9	28	86
3.	TEDA	Al*(Zr)	THF	36.6	28	91
4.	TEDA	Al*(Zr)_BM	THF	38.4	23	94
5.	TEDA	Al*(Hf)	THF	34.5	23	92
6.	TEDA	Al*(Y)	THF	36.4	25	91
7.	TEDA	Al	THF	35.6	35	90
8.	Pyridine	Al*(Ti)	THF	58.6	29	120
9.	Pyridine	Al*(Ti)	THF	92.5	32	67
10	Pyrazine	Al*(Ti)	THF	97.6	32	89
11.	Pyrrole	Al*(Ti)	Et$_2$O	92.1	25	20
12.	Pyrrole	Al*(Ti)	THF	90.7	35	22
13.	Pyrrole	Al*(Zr)	THF	87.8	28	21
14.	Pyrrole	Al*(Hf)	THF	92.6	29	23
15.	Pyrrolidine	Al*(Ti)	THF	106	27	18

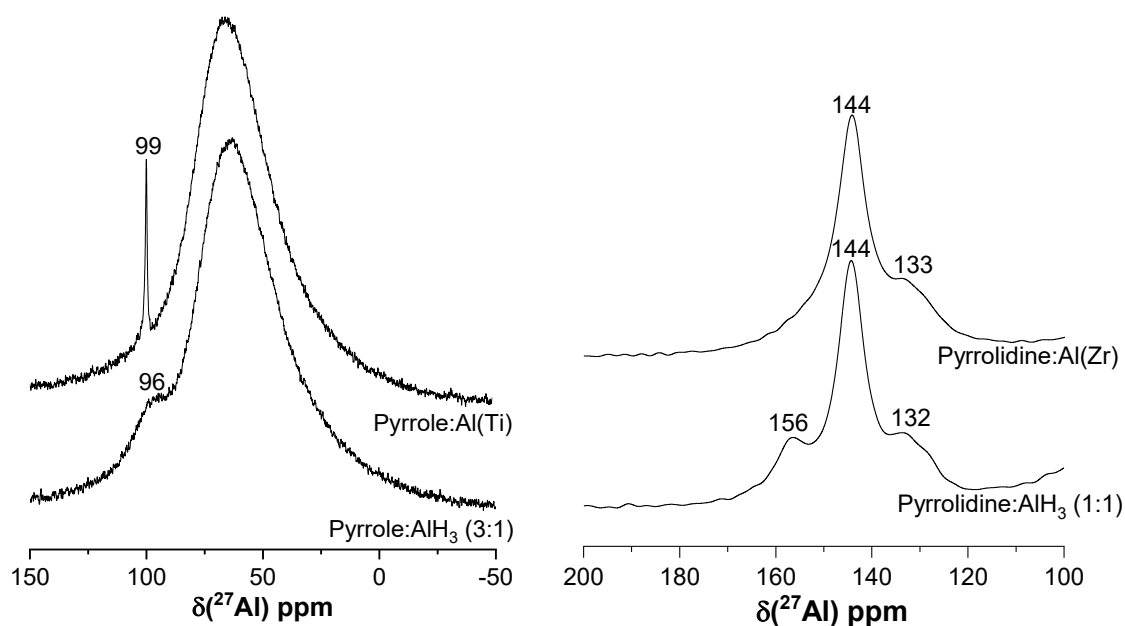| 16.	Pyrrolidine	Al*(Zr)	THF	82.2	22	24
17.	Tetramethylpiperidine	Al*(Ti)	Et$_2$O	102	23	27
18.	Piperidine	Al*(Ti)	Et$_2$O	90.2	33	54
19.	Piperidine	Al*(Ti)	Et$_2$O	99.7	23	27
20.	Piperidine	Al*(Ti)	Benzene	103.6	32	18
21.	Piperidine	Al*(Ti)	Benzene	105.1	35	15
22.	Piperidine	Al*(Ti)	THF	97.8	22	24
23.	Piperidine	Al*(Zr)	Et$_2$O	93	23	21
24.	Piperidine	Al*(Zr)	Benzene	88.7	27	18
25.	Piperidine	Al*(Zr)	THF	76.2	25	24
26.	Piperidine	Al*(Zr)_BM	THF	101.2	23	23
27.	Piperidine	Al*(Hf)	THF	100.4	22	24
28.	Piperidine	Al*(Y)	THF	92.9	26	25
29.	Piperidine	Al	Et$_2$O	94.8	27	22

Pyrrole alane complex

^{1}H NMR spectrum of pyrrole (Fig. A.7) in d-benzene shows two quartets centered at 6.37 ppm (C-H(B)) and 6.29 ppm (C-H(C)) and a very broad triplet (N-H(A)) from spin-spin interactions between ^{1}H and ^{14}N at ca.7 ppm. By observing the spectrum of the molecule dissolved in d-benzene (Fig. A.6) N-H group was more affected by medium effects than C-H. The more pyrrole is diluted in d-benzene, the shorter becomes the distance between quartets (for 0.1 ml – 0.08 ppm, 0.3ml – 0,11ppm, 0.5ml – 0.13 ppm) in ^{1}H NMR spectra. Similar shifts behavior was observed in ^{13}C NMR. During the investigation of the pyrrole alane complexes, the experiments revealed that pyrrole-alane can exist in three species ([(C$_4$H$_4$N)$_n$AlH$_{3-n}$]$_2$, where n = 1, 2, 3). ^{27}Al NMR spectra showed signals at 135 ppm, 114 ppm, and 96 ppm for 1, 2, and 3 respectively.

Figure A.7 ^{1}H NMR spectra of pyrrole diluted in d-benzene.

Pure species were not obtained, because pyrrole-alane complexes are unstable. Three types of doped Al* with Ti-, Zr- and Hf- additives were used, in order to find out which species could be formed from the direct hydrogenation of Al with pyrrole. No Al signal was detected by ^{27}Al NMR after synthesis with Al*(Zr), and only a small amount of product was detected with Al*(Hf). The successful synthesis was conducted only with Al*(Ti) with a yield of 75 %. ^{27}Al NMR spectra showed (Fig. A.8) the presence of dehydrogenated species only.

Figure A.8 ^{27}Al *NMR spectra of the pyrrole alane (left) and pyrrolidine alane (right) complexes.*

Appendix B

Data information for crystal structure of [pip₂AlH]₂ (2)

Table B.1 *Crystal data and structure refinement for [pip₂AlH]₂ (2)*

Moiety composition	C20 H42 Al2 N4
Empirical formula	C20 H42 Al2 N4
Formula weight	392.53
Temperature	160(2) K
Wavelength	0.71073 Å
Crystal system	Orthorhombic
Space group	Pbca
Unit cell dimensions	a = 12.5724(5) Å α = 90°
	b = 17.8509(8) Å β = 90°
	c = 20.6212(10) Å γ = 90°
Volume	4628.0(4) Å³
Z	8
Density (calculated)	1.127 Mg/m³
Absorption coefficient	0.137 mm⁻¹
F(000)	1728
Crystal size	0.500 x 0.300 x 0.100 mm³
Theta range for data collection	2.798 to 25.996°
Index ranges	-13<=h<=15, -22<=k<=22, -24<=l<=25

|	
Reflections collected	28952
Independent reflections	4533 [R(int) = 0.0453]
Observed reflections [I>2sigma(I)]	3403
Completeness to theta = 25.996°	99.8 %
Absorption correction	Integration
Max. and min. transmission	0.9948 and 0.9365
Refinement method	Full-matrix least-squares on F^2
Data / restraints / parameters	4533 / 42 / 478
Goodness-of-fit on F^2	1.102
Final R indices [I>2sigma(I)]	R1 = 0.0473, wR2 = 0.1129
R indices (all data)	R1 = 0.0681, wR2 = 0.1216
Extinction coefficient	n/a
Largest diff. peak and hole	0.196 and -0.227 e.Å^{-3}

Data information for crystal structure of [pip₃Al]₂ (3)

***Table B.2** Crystal data and structure refinement for [pip₃Al]₂ (3)*

|		
Moiety composition	C30 H60 Al2 N6	
Empirical formula	C30 H60 Al2 N6	
Formula weight	558.80	
Temperature	160(2) K	
Wavelength	0.71073 Å	
Crystal system	Triclinic	
Space group	$P\bar{1}$	
Unit cell dimensions	a = 8.6112(9) Å	α = 95.138(8)°
	b = 8.8513(9) Å	β = 90.659(8)°
	c = 10.9777(10) Å	γ = 108.065(8)°
Volume	791.60(14) Å^3	
Z	1	
Density (calculated)	1.172 Mg/m^3	
Absorption coefficient	0.121 mm^{-1}	
F(000)	308	
Crystal size	0.300 x 0.200 x 0.100 mm^3	
Theta range for data collection	2.887 to 27.000°.	
Index ranges	-10<=h<=10, -11<=k<=10, -13<=l<=14	
Reflections collected	10488	
Independent reflections	3419 [R(int) = 0.0387]	

Observed reflections [I>2sigma(I)]	2618
Completeness to theta = 27.000°	99.5 %
Absorption correction	Integration
Max. and min. transmission	0.9916 and 0.9696
Refinement method	Full-matrix least-squares on F^2
Data / restraints / parameters	3419 / 0 / 172
Goodness-of-fit on F^2	1.050
Final R indices [I>2sigma(I)]	R1 = 0.0417, wR2 = 0.1006
R indices (all data)	R1 = 0.0638, wR2 = 0.1124
Extinction coefficient	n/a
Largest diff. peak and hole	0.304 and -0.264 e.Å^{-3}

Formation of piperidinoalanes without applying hydrogen pressure

In the glove box, the reactants (0.55 g (20.3 mmol) of Al*(Zr), 2 mL (20.2 mmol) of piperidine) were weighted and dissolved in 25 mL of THF in an autoclave reactor. The reactor was sealed, removed from the glove box and connected to the pressure sensor and thermocouple. The reaction mixture was stirred for ~24 h. The pressure increase up to 7.5 bar was observed until ~21 h (Fig. B.1, left). After ~24 h reactor was removed in the glove box and the sample was taken for NMR analysis. Conversion of Al*(Zr) was 55%. The ^{27}Al NMR spectra of the obtained product shown in Fig. B.1 (right) revealed the formation of **2** and **3´**.
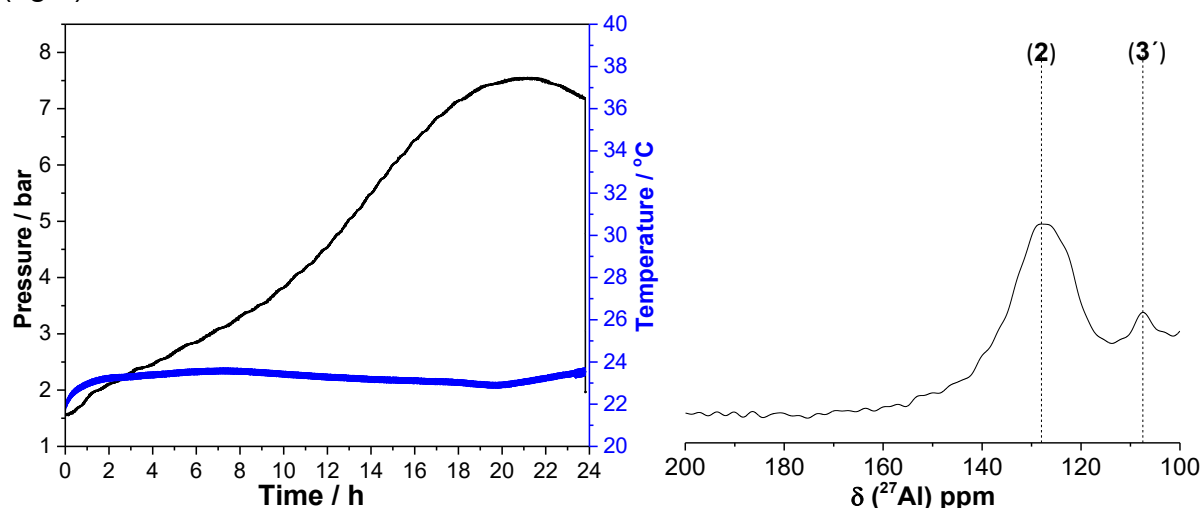

Figure B.1 *Reactor pressure during reaction of Al*(Zr) with piperidine in THF (left), ^{27}Al NMR spectra of the formed product after ~24 h (right).*

Piperidinoalane
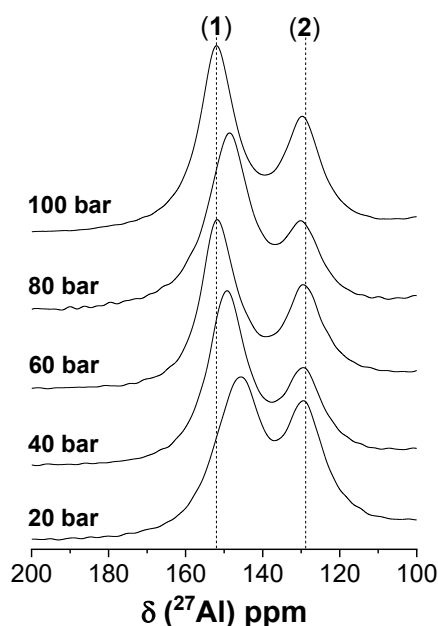
Figure B.2 *^{27}Al NMR spectra of the products obtained after direct hydrogenation (under different pressures) of Al*(Zr) supported by piperidine.*

Figure B.2 shows the comparison of the ^{27}Al NMR spectra recorded for the products obtained after the syntheses under the different hydrogen pressures. For ^{27}Al NMR spectra, the quantitative evaluation of the signal is possible. The deconvolution of the spectra was performed with the help of dmfit2015 program. The product composition in % can be calculated directly from the ratios of the percentages of the total area under their absorption curve. For the simulation of the spectra, the Gaussian/Lorentzian model was chosen and four peaks were manually fitted: two for the signal for the measuring glass tube (found in all NMR spectra) and the other two for the obtained product.

From the percent values obtained for the products, the correlation between compounds **1** and **2** was calculated. As an example of the simulation, the deconvolution of the ^{27}Al NMR spectra recorded for the product obtained after synthesis under 80 bar is shown in Figure B.3.
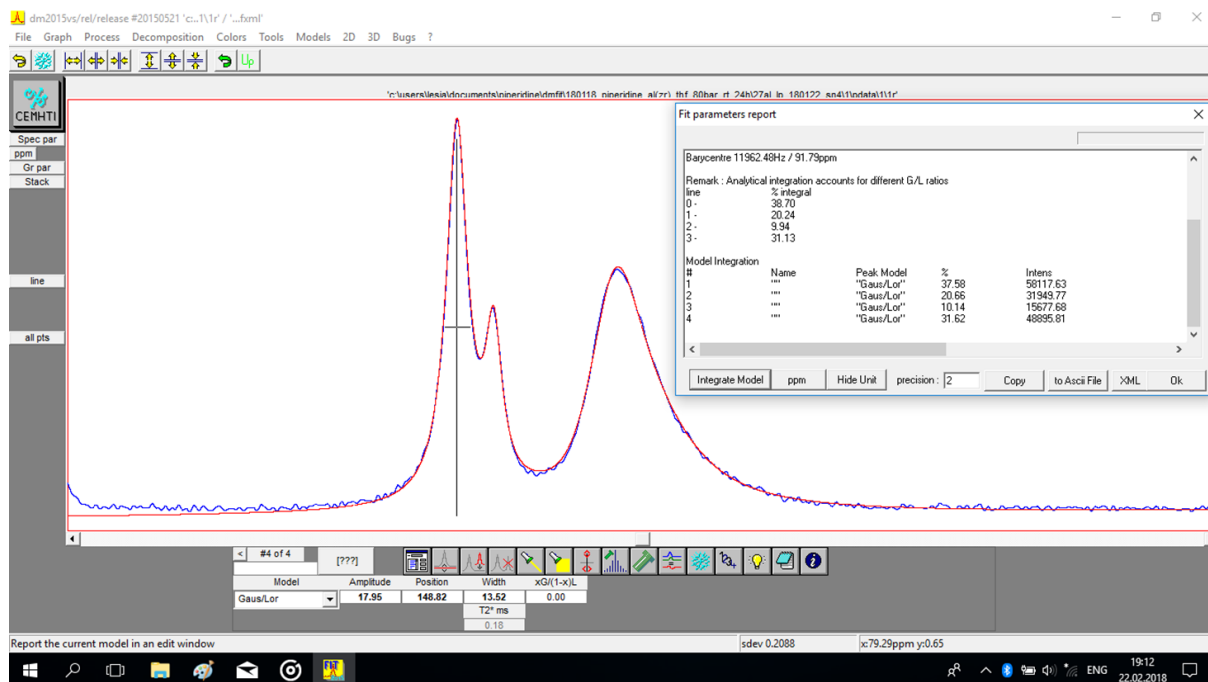
Figure B.3 *The view of the dmfit program during deconvolution of the ^{27}Al NMR spectra recorded for the product obtained from the direct hydrogenation of Zr-activated aluminum with piperidine at 80 bar and room temperature within 24 h.*

The results of the simulation are summarized in Table B.3.

Table B.3 *The data obtained from the simulation of the ^{27}Al NMR spectra of the product obtained under the different hydrogen pressures.*

| Pressure, bar	Peak number	Origin of the peak	% of the total area	% of the product area
20 bar	1	NMR tube	36.52	-
	2	NMR tube	26.41	-
	3	Compound **2**	15.69	42
	4	Compound **1**	21.38	58
40 bar	1	NMR tube	31.51	-
	2	NMR tube	34.44	-
	3	Compound **2**	12.52	37
	4	Compound **1**	21.52	63
60 bar	1	NMR tube	38.03	-
	2	NMR tube	31.85	-
	3	Compound **2**	11.80	39
	4	Compound **1**	18.32	61
80 bar	1	NMR tube	37.58	-
	2	NMR tube	20.66	-
	3	Compound **2**	10.14	24
	4	Compound **1**	31.62	76
100 bar	1	NMR tube	22.27	-
	2	NMR tube	37.59	-
	3	Compound **2**	14.94	37
	4	Compound **1**	25.20	63

Appendix C

TiH$_2$ addition to NaAlH$_4$
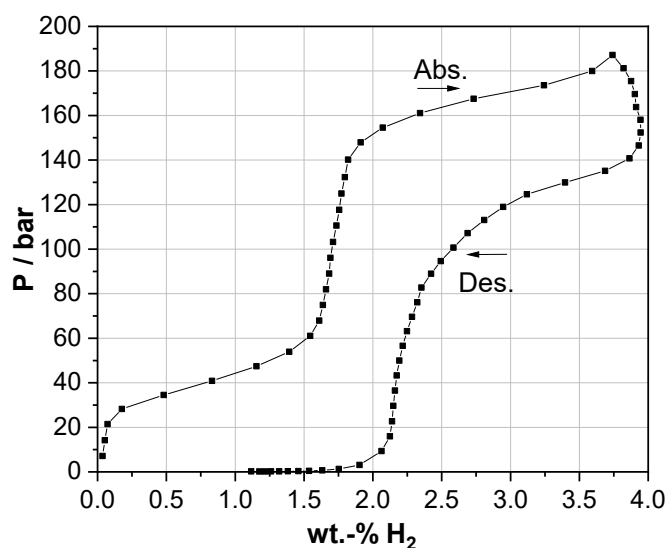
Figure C.1 *The PCI curves for the 10 mol% TiH$_2$ doped NaAlH$_4$ measured at 200 ºC.*

The PCI curves measured at a lower temperature than 200 ºC did not show any distinguishable pressure plateaus.

Influence of the waiting time on the hydrogen storage capacity

The time given to the system to reach the equilibrium (for 2 mol% TiCl₃ doped NaAlH₄ sample) was varied from 30 min, 2 h, and 5 h (Fig. C.2). With the increase of the waiting time, first, hysteresis decreases, and second, the amount of absorbed hydrogen increases. Even with the long time given to the system to equilibrate the equilibrium was not reached. The increase of absorbed hydrogen amount only was observed for the second hydrogenation step. Consequently, the second hydrogenation step ($Na_3AlH_6 \rightarrow NaAlH_4$) is the rate-limiting step. The slow kinetics of hydrogenation is probably the reason why the full storage capacity was not attained.
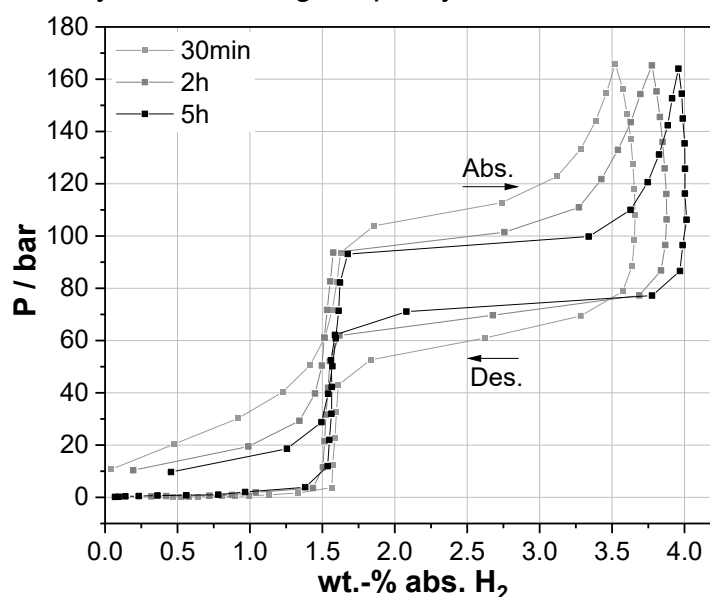
Figure C.2 *PCI curves measured at 160 ºC for 2 mol% TiCl₃ doped NaAlH₄.*

Calculated theoretical hydrogen storage capacity

The uncertainty in the theoretical hydrogen storage capacity calculated by different groups could arise from the performed calculation of the molar mass of the investigated composites. The middle molar mass calculated by Streukens et al.[268] for the sample obtained after ball milling of sodium alanate with the TiCl₃ was calculated as a mole fraction:

$$M_1 = (1 - y) \cdot M(NaAlH_4) + y \cdot M(TiCl_3)$$

However, in the PhD work of Streukens[353], was mentioned, that the mole percentage of added TiCl₃ was not referred to the total amount of the sample (in the case of molar fraction) but to the amount of sodium alanate. Thus, in this case, the middle molar mass should be calculated as follows:

$$M_2 = M(NaAlH_4) + y \cdot M(TiCl_3)$$

In Table C.1 results for these both cases are compared. The notable difference appears at the higher amount of the TiCl₃ in NaAlH₄.

Table C.1 *Dependence of the theoretical hydrogen storage capacity on the dopant content in TiCl₃-doped NaAlH₄.*

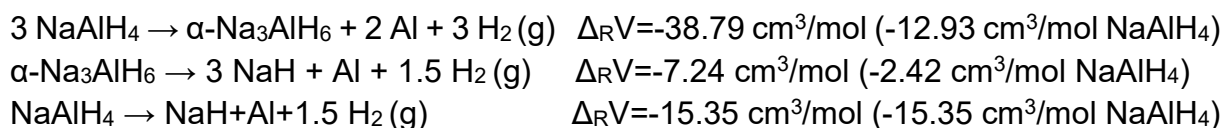| TiCl₃	wt.-% H₂	Middle molar mass M₁	wt.-% H₂	Middle molar mass M₂	wt.-% H₂
mol%	*Streukens[353]*	*g/mol*	*calculated*	*g/mol*	*calculated*
0	5.60	54.00	5.60	54.00	5.60
0.5	5.42	54.50	5.46	54.77	5.44
2	5.04	56.00	5.08	57.08	4.98
4	4.55	58.00	4.59	60.17	4.42
10	3.28	64.01	3.31	69.41	3.05
17.5	1.99	71.51	2.01	80.96	1.77
25	0.95	79.01	0.96	92.51	0.82
33.333	0.00	87.35	0.00	105.35	0.00

Hydrogen sorption behavior of Pd powder

The calculated amount of absorbed hydrogen is 0.6 wt.-% H_2, the measured value was 0.53 wt.-% H_2.
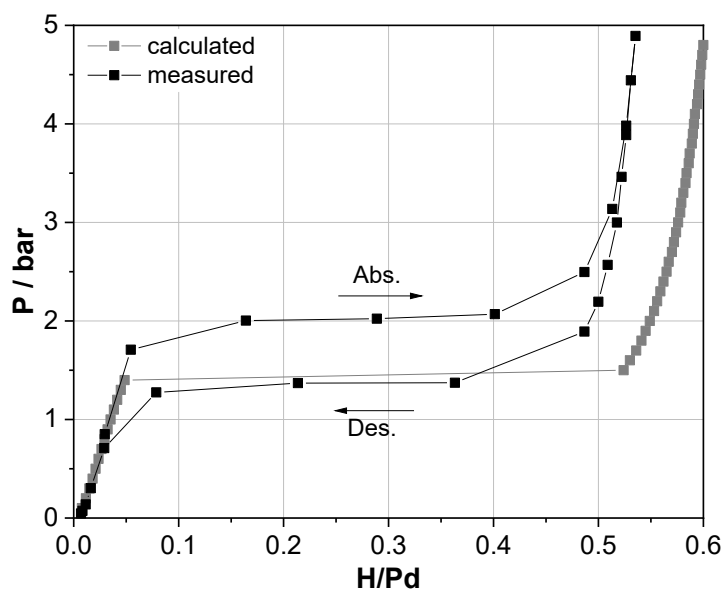
Figure C.3 *PCI measurement at 160 ºC for Pd powder.*

Volume change during hydrogen sorption of NaAlH₄

Table C.2 *Properties of the investigated materials.*

Compound	Molar mass M, g/mol	Density D, g/cm³	Volume V, cm³/mol
NaAlH₄	54.00	1.27	42.52
α-Na₃AlH₆	102.00	1.48	68.79
NaH	23.99	1.396	17.18
Al	26.98	2.7	9.99

3 NaAlH$_4$ → α-Na$_3$AlH$_6$ + 2 Al + 3 H$_2$ (g) Δ_RV=-38.79 cm^3/mol (-12.93 cm^3/mol NaAlH$_4$)
α-Na$_3$AlH$_6$ → 3 NaH + Al + 1.5 H$_2$ (g) Δ_RV=-7.24 cm^3/mol (-2.42 cm^3/mol NaAlH$_4$)
NaAlH$_4$ → NaH+Al+1.5 H$_2$ (g) Δ_RV=-15.35 cm^3/mol (-15.35 cm^3/mol NaAlH$_4$)

These calculations indicated that the volume change during dehydrogenation reaction will reach 36.1 %, this could influence significantly the effective volume determine from the calibration with the helium gas. However, the experiments with the measuring of the effective volume before the dehydrogenation and after did not show significant difference. For 10 mol% TiCl$_3$ doped sodium alanate sample:

1. Before dehydrogenation of NaAlH$_4$: V_e = 2.8261 ml
2. After dehydrogenation of NaAlH$_4$: V_e = 2.8453 ml

The volume change ΔV_e = 0.0192 ml was less than one percent (0.68%). Thus, it concluded that the volume change does not have an influence on the total absorbed hydrogen amount.

Thermodynamic calculation of the influence of Al addition

In order to explain the positive influence of Al addition, it is necessary to assume the formation of a stable Al$_3$Ti phase and Al-Ti phase in which Al content is larger than that in Al$_3$Ti. For the simple thermodynamic modeling two limit states can be assumed:

1. Formation of a solid solution of Ti in Al. The description is made following the laws of mixed-phase thermodynamics, assuming ideal behavior, the enthalpy of mixing is zero and the entropy of mixing is determined by the statistical distribution of Ti in Al.

2. Formation of A-rich compound. For the calculation, the composition of Al$_{0.85}$Ti$_{0.15}$ was assumed.

For thermodynamic modeling TiCl$_3$ content of 0.1 mol / 1 mol NaAlH$_4$ and the addition of 0.27 mol Al / 1 mol NaAlH$_4$ was assumed.

In the first case (Fig. C.5, left) the resulting relationship between hydrogenation pressure and hydrogen content at T = 160 °C is shown.
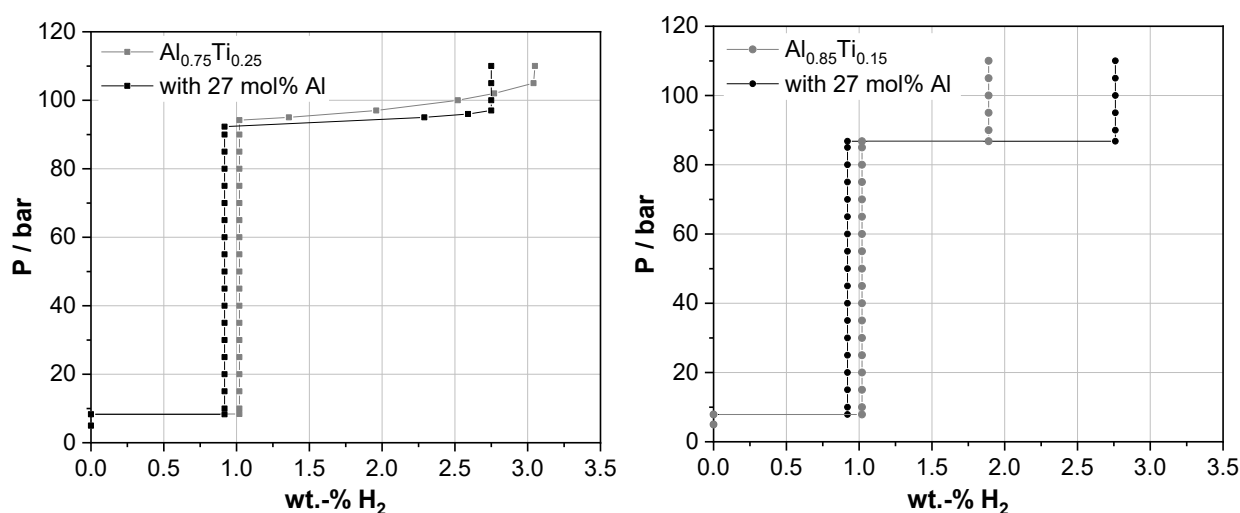

Figure C.4 *Predicted influence of 27 mol% Al addition to 10 mol% TiCl$_3$ doped NaAlH$_4$ on the hydrogen storage properties: PCI curve at 160 ºC for the predicted Al$_3$Ti phase (left) and for Al$_{0.85}$Ti$_{0.15}$ phase (right).*

The difference in the hydrogen content (Fig. C.5, left) results only from the reference to different masses: 69.41 g/mol without Al and 76.70 g/mol with Al, i.e. the addition of Al has no effect on the hydrogen capacity, especially if the stable compound Al_3Ti was formed. Deviations occur with respect to the equilibrium pressures. If Al_3Ti is formed, a slight increase of the second plateau ($Na_3AlH_6 \rightarrow NaAlH_4$) was observed.

The second case suggests the formation of irreversible $Al_{0.85}Ti_{0.15}$ phase, so that there is a deficiency of Al for the second hydrogenation step. In Figure C.5 (right) the hydrogenation isotherms at T = 160 °C for 10 mol% $TiCl_3$ doped $NaAlH_4$ with/without Al additive (27 mol%) are demonstrated. The calculations showed the positive influence of Al addition on the second hydrogenation step, so the lack of free aluminum was fulfilled.

Influence of aluminum addition

The sample with an additional 66 mol% of aluminum didn't improve the hydrogen storage capacity of 10 mol% $TiCl_3$ doped $NaAlH_4$ sample, compared to the samples with lower aluminum content (Fig. C.5).
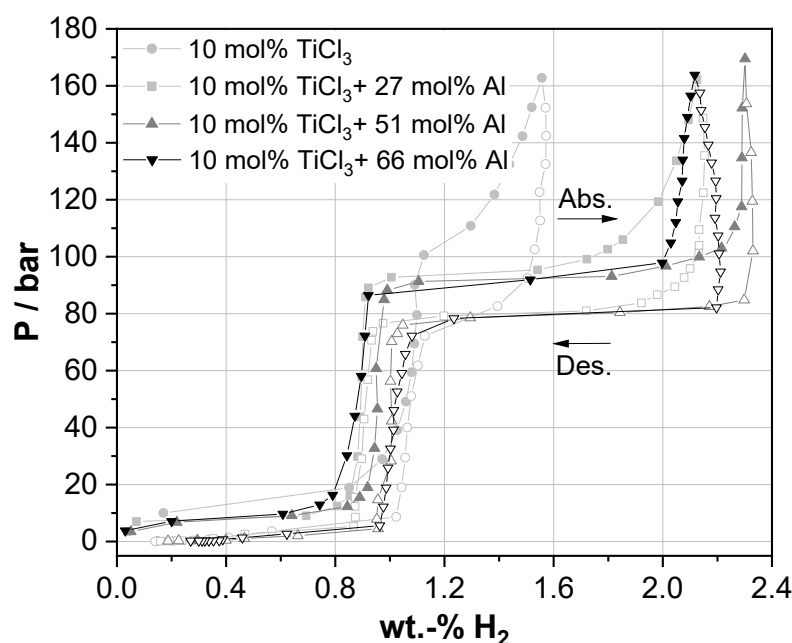
Figure C.5 *The PCI curves for the sodium alanate samples with 10 mol% $TiCl_3$ and additional aluminum measured at 160 ºC.*

HP-DSC data for $TiCl_3$ doped $NaAlH_4$ samples

Table C.3 *Dependence of the dehydrogenation temperature of 15 mol% doped $NaAlH_4$ from the pressure.*

| Pressure, bar	Onset temperature, ºC		
	$T_{1 des}$	T_{trans}	$T_{2 des}$
250	183.5	252.2	301.4
200	184.3	252.3	300.2
150	179.6	252.3	298.8
120	179.3	252.7	291.8
100	167.4	252.6	281.6

70	149.8	252.8	261.3
50	136.2	253.5	253.5

Table C.4 *Equilibrium pressures and temperatures for the samples with 10 mol% and 15 mol% TiCl$_3$ doped NaAlH$_4$.*

| Additive content	P$_{eq}$, bar	T$_{eq}$, ºC	
		1 step	**2 step**
10 mol % TiCl$_3$	49.8	126.99	241.84
	99.45	163.68	275.91
	148.5	183.93	298.47
15 mol % TiCl$_3$	50.34	136.18	247.55
	70.36	149.76	261.28
	99.78	167.42	281.59
	119.64	179.26	291.81

The equilibrium temperature at 200 bar for 10 mol% TiCl$_3$ doped NaAlH$_4$ was not taken for the calculation of the reaction enthalpy and entropy, as the temperature for the first dehydrogenation step appears together with the melting point.
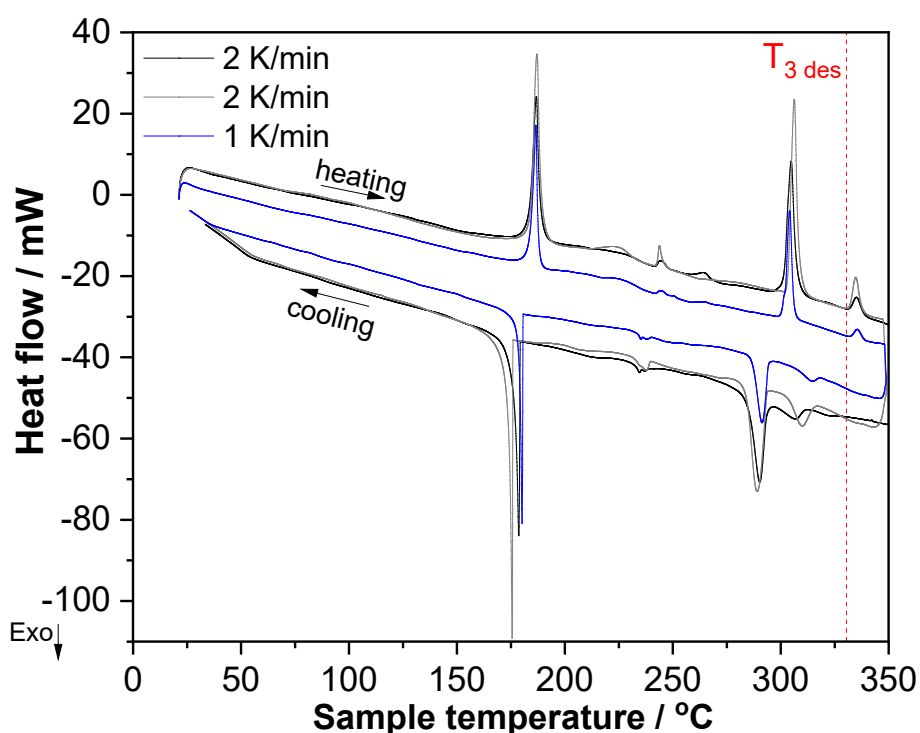
Figure C.6 *HP-DSC plots for 10 mol% TiCl$_3$ and 51 mol% Al-doped NaAlH$_4$ measured at 150 bar with the different heating rates.*
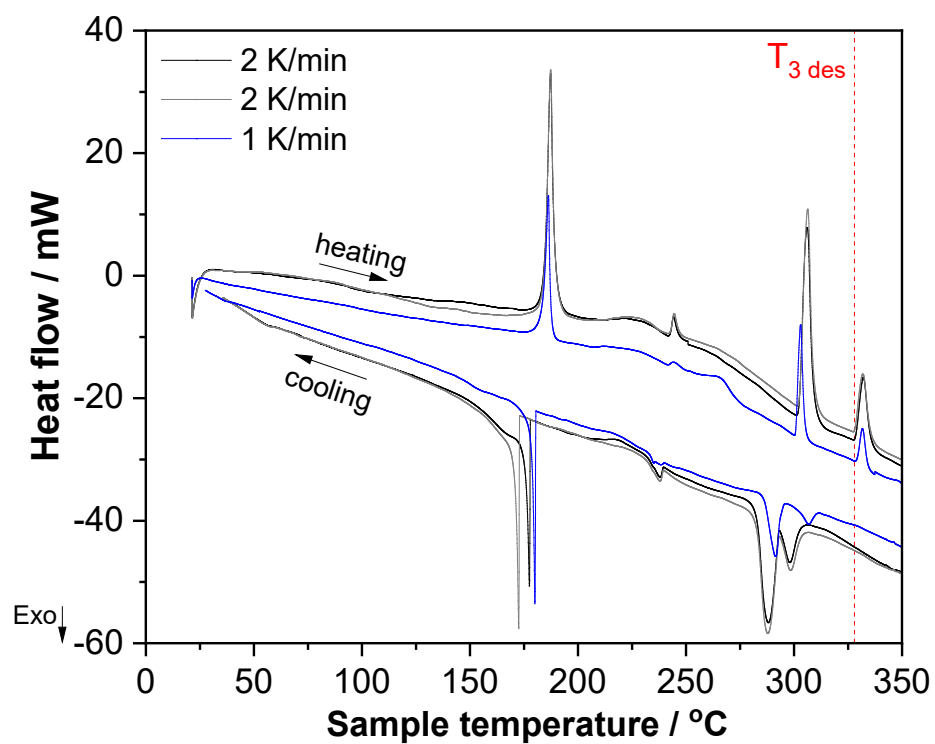
Figure C.7 *HP-DSC plots for 10 mol% TiCl₃ and 66 mol% Al-doped NaAlH₄ measured at 150 bar with the different heating rates.*

Publications

Papers:

1. J. Ortmeyer, A. Bodach, **L. Sandig-Predzymirska**, B. Zibrowius, F. Mertens, M. Felderhoff, A mechanochemical approach to synthesize the triethylenediamine · AlH$_3$ adduct, ChemPhysChem 2019, 20(10), pp. 1360-1368. DOI: 10.1002/cphc.201801093.

2. **L. Sandig-Predzymirska**, J. Ortmeyer, J. Wagler, E. Brendler, F. Habermann, M. Anders, M. Felderhoff, F. Mertens, The direct and reversible hydrogenation of activated aluminium supported by piperidine, Dalton Transactions 2020, DOI: 10.1039/D0DT03175E.

3. F. O. Mertens, M. Anders, A. Schwarzer, E. Brendler, R. Pollex, E. Schumann, **L. Sandig-Predzymirska**, S. Kaiser, Bis-(triphanylphosphane) aluminum hydride – a simple way to provide, store, and use non-polymerized alane for synthesis, ChemPlusChem, (accepted), DOI: 10.1002/cplu.202100287

Conference with oral contribution:

1. **L. Sandig-Predzymirska**, K. Burkmann, J. Seidel, F. Mertens, High-pressure DSC study of hydrogen sorption/desorption properties of doped sodium alanate, 12-14.06.2019, Braunschweig, Germany.

Poster presentation:

1. **L. Sandig-Predzymirska**, K. Burkmann, J. Seidel, F. Mertens, Influence of the aluminum addition on the hydrogenation/dehydrogenation behavior of doped sodium alanate, 12-14.06.2019, Braunschweig, Germany.

Abstract:

1. C. Reller, M. Anders, **L. Predzymirska**, F. Mertens Recycling of spent ammonia borane and ammonia alazane related compounds, MH2016 - Interlaken, Switzerland, 2016.